

KIT SCIENTIFIC REPORTS 7664

# Annual Report 2013

Institute for Nuclear Waste Disposal  
Institut für Nukleare Entsorgung

H. Geckeis, M. Altmaier, S. Fanghänel, P. Kaden (eds.)



H. Geckeis, M. Altmaier, S. Fanghänel, P. Kaden (eds.)

## Annual Report 2013

Institute for Nuclear Waste Disposal  
Institut für Nukleare Entsorgung

### Cover illustration

- left:* 3D porous media representation based on  $\mu$ CT measurements showing the influence of pore scale celestite precipitation (white grains) on the Laplace field in the direction of diffusion.
- middle:* ESEM image of amorphous technetium(IV)-oxide surrounded by needle like magnesium-oxychlorid crystals, field of view 40  $\mu$ m. Artificial view with pseudocolors by combination of secondary electron and backscattered electron images.
- right:* High-resolution TEM image: lattice fringes of plutonium(IV)-oxide colloids deposited onto a carbon film, field of view 7.5 nm.

Karlsruhe Institute of Technology  
**KIT SCIENTIFIC REPORTS 7664**

# Annual Report 2013

Institute for Nuclear Waste Disposal  
Institut für Nukleare Entsorgung

by

H. Geckeis, M. Altmaier, S. Fanghänel, P. Kaden (eds.)

## Report-Nr. KIT-SR 7664

The Institute for Nuclear Waste Disposal, INE, (Institut für Nukleare Entsorgung) belongs to the KIT Energy Center. The KIT Energy Center with its 1100 employees is one of the largest energy research centers in Europe. It bundles the energy research activities of the KIT, the merger of the former Forschungszentrum Karlsruhe and Universität Karlsruhe and reknown cooperation partners. By this, it crosses the lines between disciplines and combines fundamental and applied research in all relevant energies for industry, household, service and mobility. The involved institutes and research groups conduct the research work on their own authority. The joining of subjects, the interdisciplinary collaboration of scientists, and the common use of high-end devices and installations, develops a new quality of research and teaching. The KIT Energy Center develops solutions in energy technology from a single source and acts as a highly valuable consultancy institution for politics, business, and society in all questions of energy. (<http://www.energy.kit.edu/>)

### Impressum



Karlsruher Institut für Technologie (KIT)  
KIT Scientific Publishing  
Straße am Forum 2  
D-76131 Karlsruhe

KIT Scientific Publishing is a registered trademark of Karlsruhe Institute of Technology. Reprint using the book cover is not allowed.

[www.ksp.kit.edu](http://www.ksp.kit.edu)



*This document – excluding the cover – is licensed under the  
Creative Commons Attribution-Share Alike 3.0 DE License  
(CC BY-SA 3.0 DE): <http://creativecommons.org/licenses/by-sa/3.0/de/>*



*The cover page is licensed under the Creative Commons  
Attribution-No Derivatives 3.0 DE License (CC BY-ND 3.0 DE):  
<http://creativecommons.org/licenses/by-nd/3.0/de/>*

Print on Demand 2015

ISSN 1869-9669





## Table of contents

<b>1</b>	<b>Introduction to the Institute for Nuclear Waste Disposal (INE)</b> .....	<b>1</b>
<b>2</b>	<b>Education and training</b> .....	<b>5</b>
<b>3</b>	<b>National and international cooperation, conferences and workshops</b> .....	<b>7</b>
<b>4</b>	<b>Fundamental Studies: Process understanding on a molecular scale</b> .....	<b>11</b>
4.1	Chemistry and thermodynamics of actinides and fission products in aqueous solution.....	11
4.2	Sorption on mineral surfaces .....	17
4.3	Multitracer (HTO, <sup>36</sup> Cl, <sup>85</sup> Sr) diffusion in Cu(en) <sub>2</sub> -illite and Cu(en) <sub>2</sub> -montmorillonite .....	21
4.4	Retention of radionuclides by secondary phase formation .....	24
<b>5</b>	<b>Applied studies: radionuclide retention in the multi-barrier system</b> .....	<b>29</b>
5.1	Highly radioactive waste forms .....	29
5.2	Non-heat producing waste forms and barrier materials .....	35
5.3	Colloid impact on radionuclide migration .....	38
5.4	Thermo-mechanical-hydraulic (TMH) modeling .....	42
5.5	Impact of fracture heterogeneity on bentonite erosion rates .....	45
5.6	Reactive transport modeling .....	48
<b>6</b>	<b>Separation of long-lived minor actinides</b> .....	<b>51</b>
<b>7</b>	<b>Vitrification of High-Level Radioactive Waste</b> .....	<b>55</b>
7.1	VPC Project .....	55
7.2	Research work for immobilization of high active solid waste .....	58
<b>8</b>	<b>Development of actinide speciation methods</b> .....	<b>59</b>
8.1	R&D projects conducted at the INE-Beamline for Actinide Research at ANKA and at external synchrotron radiation sources .....	59
8.2	Laser spectroscopy .....	65
8.3	Characterisation at the nanoscale by TEM and XPS .....	68
8.4	NMR spectroscopy – covalence in actinide complexes .....	71
8.5	Computational Chemistry .....	74
<b>9</b>	<b>Radiochemical and Elemental Analysis</b> .....	<b>79</b>
<b>10</b>	<b>Radiation Protection Research</b> .....	<b>85</b>
<b>11</b>	<b>Publications</b> .....	<b>89</b>



# 1 Introduction to the Institute for Nuclear Waste Disposal (INE)

The Institute for Nuclear Waste Disposal, **INE**, (Institut für Nukleare Entsorgung) at the Karlsruhe Institute of Technology **KIT** performs R&D focusing on

- (i) **long term safety research for nuclear waste disposal,**
- (ii) **immobilization of high level radioactive waste (HLW),**
- (iii) **separation of minor actinides from HLW, and**
- (iv) **radiation protection.**

All R&D activities of KIT-INE are integrated into the program Nuclear Safety Research within the KIT-Energy Center. INE contributes to German provident research for the safety of nuclear waste disposal, which is the responsibility of the Federal Government.

Following the decision taken by Germany to phase out the use of nuclear energy, the safe disposal of long-lived nuclear waste remains as a key topic of highest priority. Projections based on scheduled operation times for nuclear power plants (Amendment to German Atomic Energy Act, August 2011) in Germany, indicate that about a total of 17,770 tons of spent nuclear fuel will be generated. About 6,670 tons have been shipped to France and the UK up until 2005 for reprocessing, to recover plutonium and uranium. Consequently, two types of high level, heat producing radioactive waste have to be disposed of safely: spent fuel and vitrified high level waste from reprocessing (HLW glass). The disposal of low- and intermediate level waste present in much larger quantities likewise needs to be addressed.

Over the last decades, a consensus within the international scientific/technical community was established, clearly emphasizing that storage in deep geological formations is the safest way to dispose of high level, heat producing radioactive waste. Disposal concepts with strong inherent passive safety features ensure the effective protection of the population and the biosphere against radiation exposure over very long periods of time. The isolation and immobilization of nuclear waste in a repository is ensured by the appropriate combination of redundant barriers (multi-barrier system).

**Long term safety research for nuclear waste disposal** at KIT-INE establishes geochemical expertise and models to be used in the disposal Safety Case, focusing primarily on the detailed scientific description of aquatic radionuclide chemistry in the geochemical environment of a repository. Work concentrates on the disposal of spent fuel and HLW-glass in the relevant potential host rock formations currently considered: rock salt, clay and crystalline rock formations. Actinides and long-lived fission products play a central role, as they dominate HLW radiotoxicity over long periods of time. Long-lived anionic fission prod-

ucts are likewise investigated as significant contributors to the maximum radiation dose projected for relevant scenarios.

Relevant long term scenarios for nuclear repositories in deep geological formations have to take into account possible radionuclide transport via the groundwater pathway. Thermomechanical studies are performed at INE, in order to describe the evolution of the constructed repository after closure. Possible groundwater intrusion into emplacement caverns is assumed to cause waste form corrosion and eventually radionuclide release. Radionuclide mobility is then determined by the various geochemical reactions in complex aquatic systems: i.e. dissolution of the nuclear waste form (HLW glass, spent fuel), radiolysis phenomena, redox reactions, complexation with inorganic and organic ligands, colloid formation, surface reactions at mineral surfaces, precipitation of solid phases and solid solutions.

Prediction and quantification of all these processes require fundamental thermodynamic data and comprehensive process understanding at the molecular scale. Radionuclide concentrations in relevant aqueous systems typically lie in the nano-molar range, which is exceedingly small in relation to main groundwater components. Quantification of chemical reactions occurring in these systems require the application and development of advanced sophisticated methods and experimental approaches, to provide insight into the chemical speciation of radionuclides at trace concentrations. Innovative laser and X-ray spectroscopic techniques are continuously developed and applied to this end. A specialized working group performing state-of-art theoretical quantum chemical calculations for actinide chemistry support both interpretation of experimental results and optimized experiment design.

The long-term safety of a nuclear waste repository must be demonstrated by application of modelling tools on real natural systems over geological time scales. Geochemical models and thermodynamic databases are developed at INE as basis for the description of radionuclide geochemical behaviour in complex natural aquatic systems. The prediction of radionuclide migration in the geosphere necessitates coupled modelling of geochemistry and transport. Transferability and applicability of model predictions are examined by designing dedicated laboratory experiments, field studies in underground laboratories and by studying natural analogue systems. This strategy allows to identify and analyze key uncertainties and continuously optimize the developed models.

Within the R&D topic **immobilization of high level radioactive waste**, INE contributes to the decommissioning of nuclear facilities. The core process technology for the Vitrification Plant (VEK) on the site of the former Karlsruhe Reprocessing Plant (WAK; located at KIT Campus North) has been developed by INE.

INE was involved in functional testing of process systems, as well as in the performance of the cold test operation and played a leading role in the highly successful hot operation of the VEK plant. The vitrification technology developed at INE is highly competitive on an international level. This is evidenced by the strong interest of countries like China or the Russian Federation in establishing technology transfer.

The Partitioning & Transmutation (P&T) strategy is pursued and developed in many international research programs. INE research activities in P&T are focused on the partitioning step, i.e. **separation of minor actinides from HLW**. The R&D aims to develop efficient separation processes for minor actinides for subsequent transmutation into short-lived or stable fission products. INE develops highly selective extracting agents and performs experiments to derive kinetic and thermodynamic data to assess and optimize extraction reactions. R&D spans experimental, analytical and theoretical work, dedicated to understanding extraction ligand selectivity on a molecular scale.

The R&D topic **radiation protection** at INE focuses on the assessment of radiation exposures on man by estimating doses either from external radiation fields or from incorporation of radionuclides. The strategy driving this work is to provide techniques and models for an individualized dosimetry, which goes beyond the current approach of applying reference models in dose assessments. Both the specific anatomical and physiological features of the exposed individual and the specific effective radiation fields are considered in the frame of an individualized dosimetry. Work is performed in close cooperation with the KIT safety management KSM.

**INE laboratories** are equipped with all necessary infrastructures to perform radionuclide/actinide research, including hot cells, alpha glove boxes, inert gas alpha glove boxes and radionuclide laboratories. State-of-the-art analytical instruments and methods are applied for analysis and speciation of radionuclides and radioactive materials. Advanced spectroscopic tools exist for the sensitive detection and analysis of radionuclides. Trace element and isotope analysis is made by instrumental analytical techniques such as X-ray fluorescence spectroscopy (XRF), atomic absorption spectroscopy (AAS), ICP-atomic emission spectroscopy (ICP-AES) and ICP-mass spectrometry (Quadrupole-ICP-MS and high resolution ICP-MS).

Methods available for surface sensitive analysis and characterisation of solid samples include X-ray diffraction (XRD), atomic force microscopy (AFM) and laser-ablation coupled with ICP-MS. A modern X-ray photoelectron spectrometer (XPS) and an environmental scanning electron microscope (ESEM) are installed. INE has direct access to a TEM instrument on the KIT Campus North site (Institut für Angewandte Materialien). Laser spectroscopic techniques are developed and applied for sensitive actinide and fission product speciation such as time-resolved laser fluorescence spectroscopy (TRLFS), laser photo acoustic spectroscopy (LPAS), laser-induced breakdown detection (LIBD) and Raman spectroscopy. A tuneable optical parametric oscillator (OPO) laser system with TRLFS-detection is used for high resolution spectroscopy at liquid helium temperature. Structural insight into actinide species is obtained by extended X-ray fine structure (EXAFS) spectroscopy at the INE-Beamline at the Karlsruhe synchrotron source ANKA. The INE-Beamline, in the direct vicinity of INE hot laboratories and in combination with the other analytic methods, represents a world-wide unique experimental and analytic infrastructure, which both profits from and contributes to INE's leading expertise in the field of actinide chemistry and spectroscopy. Quantum chemical calculations are performed on INE's computing cluster which is equipped with 17 nodes and 76 processors. A 400 MHz-NMR spectrometer adapted to measuring radioactive liquid samples adds to the analytical and speciation portfolio of INE. Additional facilities at INE include a glass lab for development of glass matrices for immobilization of highly radioactive waste. The INE CAD workstations enable construction and planning of hardware components, process layout and flow sheets for HLLW vitrification facilities. The institute workshop is equipped with modern machine tools to manufacture components for specific experimental and analytical devices in hot laboratories.

In 2013 the **Institute for Nuclear Waste Disposal** had **115 employees** working in the seven departments, which reflect the R&D and organizational tasks of the institute (Fig. 1): (i) safety of nuclear waste disposal, (ii) geochemistry, (iii) radiochemistry, (iv) actinide speciation, (v) vitrification of high level waste, (vi) radiation protection research and (vii) scientific/technical coordination and analytical chemistry.

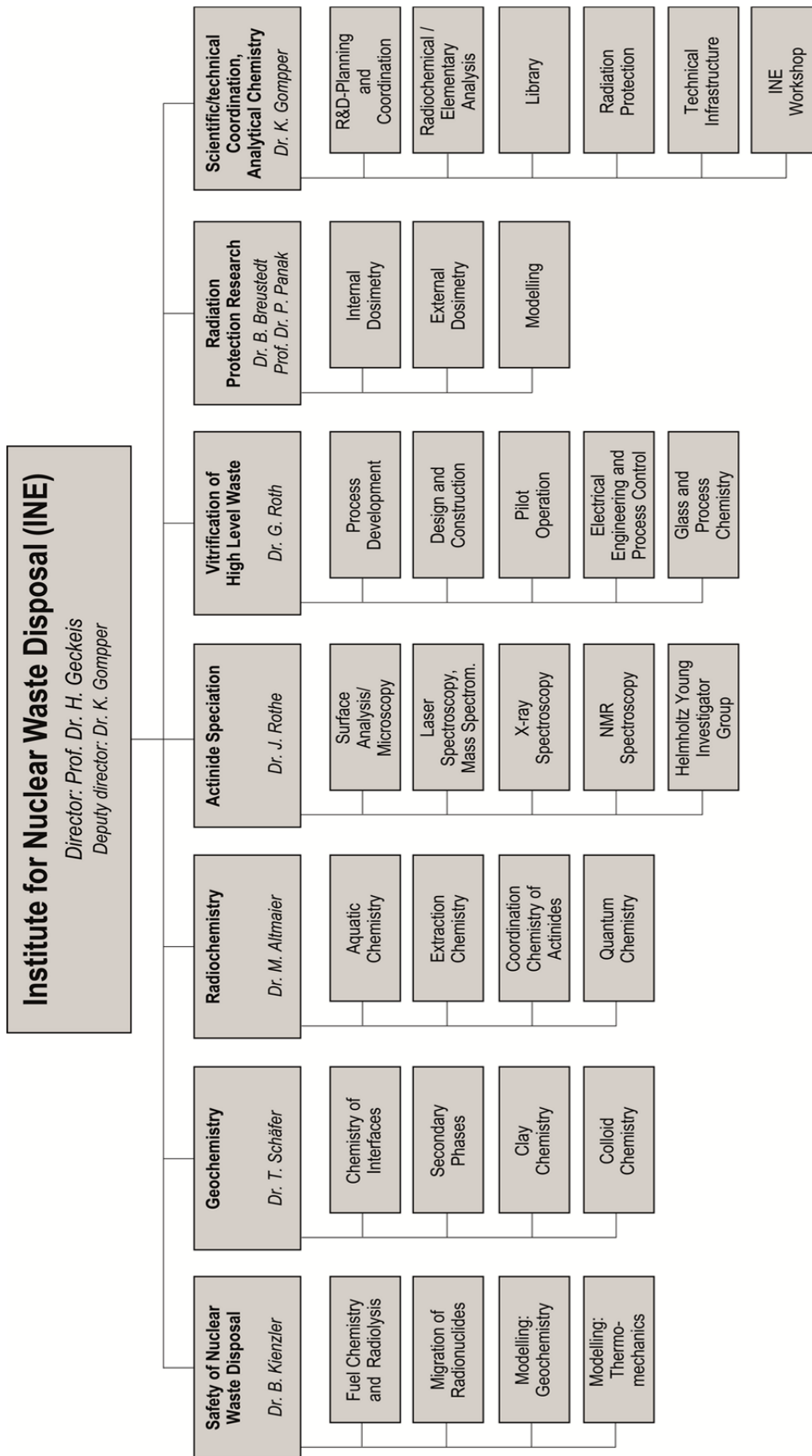


Fig. 1: Organisational chart of the Institute for Nuclear Waste Disposal (INE).



## 2 Education and training

Teaching of students and promotion of young scientists is of fundamental importance to ensure high level competence and to maintain a leading international position in the fields of nuclear and radiochemistry. INE scientists are strongly involved in teaching at KIT Campus South and the Universities of Heidelberg, Berlin, Jena and Mainz.

Prof. Dr. **Horst Geckeis**, director of INE, holds a professorship for radiochemistry at KIT Campus South, Department Chemistry and Biosciences. He teaches fundamental and applied radiochemistry for chemistry students in bachelor, master and diploma courses. A radiochemistry module consisting of basic and advanced lectures on nuclear chemistry topics and laboratory courses has been set up for diploma and master students in Karlsruhe.

Prof. Dr. **Petra Panak**, heading a working group on actinide speciation at INE, holds a professorship of radiochemistry at the University of Heidelberg. A basic course in radiochemistry is offered for bachelor and/or master students. An advanced course comprised of chemistry of f-elements and medical applications of radionuclides is also offered. The advanced radiochemistry lectures are supplemented by scientific internships at the INE radioactive laboratories.

Nearly 35 students from Karlsruhe and Heidelberg participated in two 3-week radiochemistry laboratory courses in 2013 held at KIT-CN in the FTU radiochemistry and hot laboratories at INE. Some students are intensifying their knowledge in nuclear/radiochemistry topics during scientific internships at INE. Obviously students became interested in nuclear chemistry topics and appreciate the various semester courses.

Dr. **Andreas Bauer** is lecturing Clay Mineralogy at the University of Jena. His lecture deals with mineralogical characterization of these fine materials and the importance of quantifying surface reactions. In the second part of the lectures sound, practical advice on powder X-ray diffraction in general is provided, as well as a useful set of step-by step instructions for the novice.

Lectures and practical units taught by Dr. **Thorsten Schäfer** at the Freie Universität Berlin, Institute of Geological Sciences, Department of Earth Sciences, focused in 2013 on a master degree course on laboratory and field methods in hydrogeology, including performance and analysis of tracer tests using conservative, weakly sorbing tracers and colloids, pumping tests and determination of hydraulic parameters (Applied Hydrogeology III).

Dr. **Thorsten Stumpf** gave lectures at the KIT Campus South, Department Chemistry and Biosciences, in the field of chemistry of f-elements and inorganic chemistry and Dr. **Tonya Vitova** gave lectures in the field of instrumental analytics.

Dr. **Bastian Breustedt** gave a lecture on biokinetics of radionuclides as well as a lecture on physiology and anatomy at KIT Campus South, Department Electrical Engineering and Information Technology. Moreover he organized the EURADOS WG7 - KIT Training Course on Monte Carlo Methods for calibration of body counters, November 25-27, 2013 at KIT.

Dr. **Frank Becker** gave lectures at the Baden-Wuerttemberg Cooperative State University (DHBW). The lectures comprised principles of statistics and measurements, atomic physics and nuclear physics.

*Others:*

- **Bernd Schimmelpfennig, Robert Polly, Peter Kaden**, ACTINET-I3: The ThUL Spring School in Actinide Chemistry, KIT, January 14-18, 2013
- **Horst Geckeis, Petra Panak**, The 7th Summer School on Actinide Science, KIT, July 16-19, 2013

Through this close cooperation with universities, students are educated in the field of nuclear and actinide chemistry, which most universities can no longer offer. Hence, INE makes a vital contribution to the intermediate and long perspective of maintaining nuclear science competence.

*PhD-students*

In 2013 24 students worked at INE on their doctoral dissertations; seven of them were awarded their doctorate. Topics of the theses are:

- Investigation of solubility and redox chemistry of Neptunium and Plutonium
- Complexation of partitioning relevant N-donor ligands – water soluble BTP ligands for the i-SANEX process
- Development of anthropomorphic models for *in-vivo* measurements in radiation protection.
- Incorporation of elements with low solubility in alkaline borosilicate glasses for the immobilization of high-radioactive liquid waste
- Comparative NMR-Studies of extraction agents for the separation of trivalent actinides
- Interaction of human serum transferrin with actinides and lanthanides
- Structural study on Cm(III) and Eu(III) complexes with ligands relevant to partitioning
- Sorption of trivalent actinides on iron oxides
- Technetium redox processes and Tc(IV) solubility studies Redox-speciation of repository relevant and redox-sensitive elements in aqueous solutions by capillary electrophoresis coupled to ICP-MS

- Release and speciation of actinides by the fabrication and dissolution of Mo- and Zr-based nuclear fuel oxides
- Study of repository relevant carbon compounds and their influence on the  $^{14}\text{C}$ -respectively actinide immobilization
- Investigation of the solubility and complexation of trivalent actinides: hydrolysis and complexation with organic ligands
- Influence of anions on the lanthanide/actinide interaction with mineral surfaces
- Characterization of actinide species in systems relevant for safety assessment of a nuclear waste repository by high-resolution X-ray emission/absorption spectroscopy
- Characterization of bonding differences by high-resolution X-ray emission and inelastic X-ray scattering techniques
- Description of radionuclide sorption at high ionic strength
- Effect of supersaturation index and precipitation kinetics on the incorporation of trivalent actinides/lanthanides in sulfate/carbonate minerals and CSH phases
- The effects of Porosity Clogging on Transport Properties of Porous Materials under Geochemical Perturbation
- Advanced spectroscopic and microscopic structural investigations of nuclear waste glass forms
- Bentonite erosion and colloid mediated radionuclide transport in advection controlled systems
- Investigation of solubility and complexation of Plutonium and Neptunium in highly reducing aquatic systems
- Tc migration in advection/diffusion controlled natural systems: Influence of ferrous iron pool
- Investigation of the retention of actinides, lanthanides and long-lived fission products on stable solid phases within the system  $\text{Mg} - \text{Na} \pm \text{Cl} \pm \text{CO}_2 - \text{H}_2\text{O}$

### 3 National and international cooperation, conferences and workshops

INE R&D involves numerous national and international collaborations and projects. These are described in the following.

#### **National**

INE is involved in various bi- and multilateral collaborations with national research centers, universities and industrial partners on different topics. The projects are partly supported by the German Federal Ministry for Economics and Technology (BMW), the Federal Ministry for Education and Research (BMBF), the Federal Ministry for the Environment, Nature Conservation, Building and Nuclear Safety (BMUB), the German Research Foundation (DFG) and the Helmholtz Association (HGF).

Primary goal within the collaborative project **VESPA** with partners GRS, HZDR-IRE and FZJ-IEK 6 is to reduce the conservatism in the assumptions currently made in performance assessment calculations concerning the radionuclides  $^{14}\text{C}$ ,  $^{79}\text{Se}$ ,  $^{129}\text{I}$  and  $^{99}\text{Tc}$ . There is reasonable evidence that sorption values for radionuclides on organics, clay surfaces, layered double hydroxides or steel corrosion products are significantly higher than currently used in modeling approaches. This could, in “what if” scenarios, lead to significantly lower radionuclide release rates than currently predicted. The project VESPA focuses on the reduction of these uncertainties.

Within the national **THEREDA** project, INE generates a centrally managed and administered database of evaluated thermodynamic parameters in cooperation with the GRS, HZDR-IRE, TU-BAF and AF-Consult Switzerland Ltd., Baden (Switzerland). Thermodynamic data are required for environmental applications in general and radiochemical issues in particular. This database is to be developed to a national (reference) standard and will be the basis for performance assessment calculations for a national nuclear waste repository. More information about this project can be obtained from the web page: [www.thereda.de](http://www.thereda.de).

The National **HATT** project focuses on the migration of radionuclides in natural clay formations and in bentonite, considered as technical barrier. Within this project not only the mechanism of radionuclide sorption onto clay is studied, but also the influence of organic matter naturally occurring in the clay stone on the radionuclide migration is a matter of interest. Here, the interaction of actinides with humic substances and small organic molecules are examined. Additionally, the influence of borate, a component of the high-radioactive waste, on the solubility of actinides is one important issue of the project. Besides INE, the members of this collaborative project are GRS, HZDR-IRE, University of Mainz, University of Potsdam, Technical University of Munich, University of Dresden and University of Saarland.

The bilateral GRS-INE project **KOLLORADO-e** started in March 2013 with a duration of three years as a successor of the KOLLORADO-2 project, focusing on the erosion stability of compacted bentonite (geotechnical barrier) as a function of the contact water chemistry/hydraulics and the formation of near-field colloids/nanoparticles as potential carriers for actinides/radionuclides. Both, a detailed experimental program quantifying the bentonite erosion and investigating the influence of surface roughness/charge heterogeneity on nanoparticle mobility and actinide bentonite nanoparticle sorption reversibility, as well as approaches to implement the acquired process understanding in reactive transport modeling codes comprise the project activities.

The general aim of the BMW Joint Project on “**Improvement of tools for the safety assessment of underground repositories**” is directed towards reliable constitutive models for predicting correctly relevant deformation phenomena in rock salt. Benchmark calculations on various influencing processes increase the confidence in the models and numerical simulations and thereby enhance the acceptance of results. Another aim is to identify possibilities for further model developments and improvements.

In the BMBF-project **Radiation and Environment II**, INE is responsible for the work package “Efficiency calibration of *in-vivo* counters with anthropomorphic models adapted to individuals”. In this work package, the influence of different anatomies on the calibration of *in-vivo* counters and subsequent dosimetry measurements are studied and quantified. By modifying the models, a better agreement between the geometries of measurement and calibration shall be reached. Different biometric parameters of the individual are measured and used in the adaption of the models.

The BMBF funded joint research project **ImmoRad** (Fundamental investigations for the immobilization of long-lived radionuclides through interaction with secondary mineral phases in deep geological nuclear waste repositories) started in February, 2012. ImmoRad concentrates on application-based fundamental research on retention processes in deep geological environments. Within this project, structural incorporation/entrapment or formation of solid solutions of radionuclides into host minerals in aquatic environments is studied. National (KIT-INE, HZDR, University Frankfurt, University of Bonn) and international partners (PSI-LES; Switzerland and University Oviedo; Spain) collaborate within this project. For more information please visit <http://www.immorad.eu/>.

The project “**Untersuchungen zum grundlegenden Verständnis der selektiven Komplexierung von f-Elementen (f-Kom)**“ funded by the German Federal

Ministry of Research and Education in the field of Basic Energy Research 2020+ aims at establishing a fundamental understanding of the separation of long-lived radionuclides from nuclear waste. The participating project partners from KIT-INE, KIT-CS, Universität Erlangen, Universität Heidelberg and Forschungszentrum Jülich are combining their expertise and activities in synthesis, spectroscopy, technology and theory, in order to be able to describe and ultimately predict and optimize liquid-liquid extraction separation processes for actinides at the molecular scale. The project includes a strong component of education and training of young scientists in research topics related to nuclear waste disposal and promotes their networking in the European research landscape.

The BMWi funded project “Disposal options for radioactive residues: Interdisciplinary analyses and development of evaluation principles (**ENTRIA**)” aims to develop evaluation principles for three options for management of highly radioactive waste: prolonged surface storage, emplacement in deep geological formations without retrievability measures and with monitoring retrievability measures, respectively. A major goal of ENTRIA is the strong interaction between young and senior scientists of various disciplines (civil engineering, law, natural sciences, philosophy, and social sciences). Within the project, KIT-INE is responsible for work packages on developing radionuclide source terms and developing individual dosimetry for personnel with respect to the three options. Detailed information about ENTRIA can be found on the webpage: <http://www.entria.de/>.

The Helmholtz young investigator group (HYIG) “**Advanced synchrotron-based systematic investigations of actinide (An) and lanthanide (Ln) systems to understand and predict their reactivity**” started July 2011 and will systematically investigate *in-situ* the electronic and coordination structure of actinides and chemical homologue lanthanide systems with novel synchrotron-based high resolution X-ray emission/inelastic scattering techniques. The experimental results are supported by theoretical calculations and simulations with quantum chemical codes. These investigations will improve our understanding of actinide/lanthanide reactivity in repository systems and waste matrices on a molecular scale and thereby support the reliability of evaluation of repository long-term safety. The elucidation of electronic and coordination structures of, e.g., actinide/lanthanide extraction ligand complexes will find application in optimization of separation technologies of lanthanide cations from minor actinides (partitioning), while at the same time provide basic insight into structure-reactivity relationships of actinide elements, which is a present scientific frontier.

#### **International**

Two international projects focus on the stability of the bentonite buffer/backfill in contact with water conducting features and the influence of colloids on radionuclide migration in crystalline host rock: the Colloid Formation and Migration (**CFM**) experiment, coordi-

nated by NAGRA (National Cooperative for the Disposal of Radioactive Waste, Switzerland), and the **Colloid Project**, initiated by SKB (Swedish Nuclear Fuel and Waste Management Co., Sweden). Both projects are currently jointly working together using the experimental set-up in the controlled zone at the Grimsel Test Site (Switzerland). Additional partners involved are from Japan (JAEA, AIST, CRIEPI), South Korea (KAERI), Finland (POSIVA Oy and Helsinki University), Switzerland (NAGRA, PSI-LES), Spain (CIEMAT), Sweden (SKB, KTH), United Kingdom (NDA RWMD) and United States (LANL). INE plays a decisive role in the laboratory program of both projects and is also mainly carrying out the field activities.

#### **EURATOM 7th Framework Program**

The 7<sup>th</sup> framework Collaborative Project (CP) “Cation diffusion in clayrocks” (**CatClay**) began in June 2010 and continued this year. The aim of CatClay is to improve understanding of the phenomena governing migration of radionuclides in clayrocks as potential host rocks for the deep geological disposal of nuclear waste. The project focuses on the diffusion-driven transport of cationic species,  $\text{Sr}^{2+}$ ,  $\text{Zn}^{2+}$ ,  $\text{Co}^{2+}$  and  $\text{Eu}^{3+}$ , which are more or less strongly sorbed on clay mineral surfaces. CatClay, coordinated by CEA, combines model and experimental developments from the partners, ANDRA, BRGM, CEA, SCK-CEN, PSI-LES, Appelo Hydrochemical Consultant and KIT-INE.

INE continues to be a core member in **TALISMAN** (Transnational Access to Large Infrastructure for a Safe Management of Actinide), the follow-up project to the European “Network of Excellence for Actinide Sciences” (ACTINET-I3) which will run until January 2016. TALISMAN aims to reinforce networking and facilitating the use of existing European infrastructures in actinide sciences in order to keep a leading position in the field of nuclear energy. TALISMAN pooled facilities are accessible as a multi-site user facility for selected joint research activities (JRP). The pooled facilities offer includes: CEA (France), CHALMERS (Sweden), EC-JRC-ITU (EU), HZDR-IRE, KIT-INE (both Germany), Micro-XAS beamline at the Swiss Light Source, PSI, Paul-Scherrer-Institut (Switzerland) and NNL, National Nuclear Laboratory (United Kingdom). These pooled facilities are laboratories licensed and equipped with infrastructure and know-how for handling radioactive material at various levels of activity and under controlled conditions, with access to analytical techniques and characterization methods.

TALISMAN pooled facilities are the sites of JRP’s proposed by European institutions and organizations. These research projects potentially address all the major fields of basic actinide sciences, keeping in mind the potential applications for the production of nuclear fission energy and the safety of nuclear waste disposal, and include:

- Actinide separation chemistry
- Actinides in the geological environment
- Actinide materials

Further, these activities are complemented by two so-called Joint Research Activities (JRA). The objective of these JRA is to improve the quality of the services offered to the Users. One JRA is dedicated to the implementation of spectroscopic databases giving each user access to reference data. The second JRA is continuing to develop the fundamental understanding of actinides in order to give more elaborated modeling based tools for the analyses and the understanding of experimental results acquired within the JRPs (ThUL; Theoretical User Laboratory).

Detailed information about this project can be found on the webpage <http://www.talisman-project.eu/>.

The **EURACT-NMR** project is a 32 month coordination and support action starting in February 2011 and is established to provide transnational access to the Karlsruhe Actinide NMR Center of Excellence with state-of-the-art nuclear magnetic resonance facilities at the KIT-INE and JRC Institute for Transuranium Elements (ITU). These institutes have two 400 MHz NMR spectrometers, which have been adapted to allow advanced nuclear magnetic resonance experiments on radioactive solid and liquid materials. The aim of EURACT-NMR is to open up unique and newly available actinide nuclear magnetic resonance facilities to nuclear researchers across Europe and EC associated countries. Additionally it will help to nurture nuclear magnetic resonance expertise and awareness amongst the European nuclear research community, in order to develop new experimental validation methods for complex models of the behaviour in nuclear materials and processes. End of June 2013 the program ended with a final workshop in Karlsruhe bringing together beneficiaries of the EURACT-NMR program and researchers in the field from Europe and beyond. During three days with four sessions and a poster section the results of the numerous research projects of the EURACT-NMR program were presented and a link to theoretical calculations in the field was established in an own dedicated session.

Activities of the collaborative project **SKIN** (Slow processes in close-to-equilibrium conditions for radionuclides in water/solid systems of relevance to nuclear waste management) began upon its establishment in February 2011. Solid/liquid chemical equilibrium hypotheses (sorption, solubility, solid-solution formation) are key concepts in the assessment of nuclear waste safety. The project intends to assess the use/misuse of solubility data of sparingly soluble tetravalent actinides, to understand the coupling of major and trace element chemistry in radionuclide migration behaviour considering the extremely large exchange pool of natural minerals present in the disposal sites and to include irreversibility in models on the mobility of radionuclides in the repository environment. Ultimately, the goal is to assess to what degree the ignorance/non-inclusion of these studied slow processes leads, in performance assessment (PA), to over-conservative, or in few cases, even too optimistic evaluations.

The Collaborative Project Crystalline Rock Retention Processes (**CROCK**) which was coordinated by

KIT-INE was established with the overall objective to develop a methodology for decreasing the uncertainty in the long-term prediction of the radionuclide migration in the crystalline rock repository far-field. The project (January 2011 – June 2013, duration: 30 months) is implemented by a consortium of 10 beneficiaries consisting on 5 large European Research Institutions, 2 Universities and 3 small and medium enterprises from six different countries with dedicated crystalline host-rock disposal programs and particular competence in this field. National Waste Management organizations (WMO) also participate in the project contributing with co-funding to beneficiaries, infrastructures, knowledge, information and reviewing the work program. WMO participate together with National Regulators to guidance with respect to application of the project to the disposal Safety Case. A compilation of the outcome of the project is documented in the two workshop proceedings: KIT Scientific Reports 7629 and 7656. Detailed information can also be found on the webpage: <http://www.crockproject.eu/>.

The **BOOSTER** project (BiO-dOSimetric Tools for triagE to Responders) addresses the requirement of effective management of an incident involving exposure of large numbers of people to radioactive material. BOOSTER is a capability project designed to research and develop new bio-dosimetric tools, in order to quickly evaluate the level of potential casualties, determine by appropriate sensors their consequences, allow an efficient triage of exposed people, integrate a useful and usable toolbox, train civil protection operators and define commercial exploitation potentialities.

Within the EURATOM 7<sup>th</sup> FP, INE coordinates the Collaborative Project “Fast / Instant Release of Safety Relevant Radionuclides from Spent Nuclear Fuel (CP **FIRST-Nuclides)**”. The CP was started in January 2012. Quantification and understanding of the release mechanisms of gaseous and readily soluble radionuclides from high burn-up UO<sub>2</sub> fuel is investigated experimentally. Furthermore, models will be developed to predict the time-dependent mobilization of the different radionuclides on the fuel rod/fuel element scale as function of the time period between disposal and canister failure.

**ASGARD** (Advanced fuelS for Generation IV reActors: Reprocessing and Dissolution; 1/2012–12/2015) is a EURATOM FP7 Large Scale Integrated Project focusing on advanced/novel nuclear fuels fabrication and their respective reprocessing issues. ASGARD seeks integration between reactor, fuel and recycling communities, which today is lacking. In some cases this results in discrepancies between the reactor design on one hand, and the technological feasibility of fabricating, dissolving and reprocessing the selected fuel on the other hand. ASGARD is an integrated effort of 16 institutions from 9 European countries. It is coordinated by Chalmers Technical University.

**SACSESS** (Safety of ACTinide SEparation proceSSes; 3/2013–2/2016) is a EURATOM FP7 Collaborative Project dealing with safety aspects of hydrometallurgical and pyrometallurgical actinide separation pro-

cesses developed in previous EURATOM projects. SACSESS provides a structured framework to enhance the fuel cycle safety associated to P&T. In addition, safety studies are performed to identify weak points to be further studied. These data are used to optimise flowsheets and process operation conditions. 26 Partners from 10 countries (plus JRC-ITU and Japan) contribute to SACSESS. The project is coordinated by CEA; KIT is in charge of the hydro-metallurgy domain.

Recent safety assessments of nuclear waste repositories in crystalline formations have shown that the formation and stability of colloids may have a direct impact on the overall performance of the repository. The main aim of the 7<sup>th</sup> framework collaborative project **BELBaR** is to increase the mechanistic understanding of the processes that control bentonite erosion, clay colloid stability, and ability to transport radionuclides. The final outcome is to examine how colloids and related phenomena can be considered in the long-term safety case and to make recommendations on the quantitative and qualitative approaches that a safety case could pursue to adequately address this potentially very significant issue. BELBaR coordinated by SKB consists of a consortium of 14 partners from Sweden, Finland, Spain, Czech Republic, Great Britain, Russia and Germany with KIT-INE leading WP3 on "Colloid radionuclide & host rock interaction".

The 7<sup>th</sup> FP Collaborative Project (CP) "CAST (Carbon-14 Source Term)" was started in 2013. The CP is coordinated by NDA (UK) and has a duration of 54 months. 33 research and waste management organisations contribute to the CP which is structured in 7 work packages. KIT-INE participates in 3 work packages: "Steels", "Zircaloy" and "Dissemination". INE's contribution to the project covers the determination of the inventory of <sup>14</sup>C in irradiated stain-less steel and zircaloy-4 as well as the analysis of the speciation of <sup>14</sup>C compounds which may be released from these materials in contact with aqueous solutions.

#### *Conferences and workshops*

INE has organized a series of workshops and conferences or has contributed significantly to the organization:

- ABC-Salt Workshop III, Actinide Brine Chemistry, Santa Fe, USA, April 15-17, 2013
- EURACT NMR workshop, Karlsruhe, Germany, July 17-19, 2013
- ACTINIDES 2013, Karlsruhe, Germany, July 21-26, 2013
- Migration 2013, Brighton, UK, September 8-13, 2013

## 4 Fundamental Studies: Process understanding on a molecular scale

Fundamental studies on radionuclide chemistry and geochemistry ensure a detailed understanding and reliable quantitative prediction of aqueous chemistry. In order to allow a comprehensive assessment of radionuclide behaviour and mobility in aquatic systems relevant for nuclear waste disposal, studies with actinides and long-lived fission products are performed. The investigated aqueous systems cover from dilute solutions to highly saline salt brine systems and establish essential site-independent data and process understanding. Work is focusing both on detailed experimental investigations using the unique facilities available at KIT-INE and subsequently developing reliable chemical models and consistent thermodynamic data. This combined approach allows a systematic and reliable evaluation of key processes such as radionuclide solubility, radionuclide speciation, radionuclide retention and transport processes in relevant near- and far-field scenarios. The work summarized in this section is related to the (i) chemistry and thermodynamics of actinides and fission products in aqueous solution, (ii) radionuclide sorption on mineral phases, (iii) radionuclide diffusion in clays, and (iv) retention of radionuclides by secondary phase formation. The studies aim at identifying relevant radionuclide retention/retardation mechanisms on a molecular level and their robust thermodynamic quantification in support of the Nuclear Waste Disposal Safety Case. Fundamental studies on aqueous radionuclide chemistry are giving support to the applied studies (see Chapter 6) performed at KIT-INE.

### 4.1 Chemistry and thermodynamics of actinides and fission products in aqueous solution

*M. Altmaier, N. L. Banik, A. Baumann, M. Böttle, K. Dardenne, D. Fellhauer, D. R. Fröhlich, X. Gaona, M. Herm, K. Hinz, M. Lagos, P. Lindqvist-Reis, M. Maiwald, R. Marsac, P.J. Panak, J. Rothe, J. Runke, J. Schepperle, A. Skerencak-Frech, Th. Rabung, E. Yalcintas*

In co-operation with:

*B. Baeyens<sup>a</sup>, Th. Fanghänel<sup>b,c</sup>, R. Janicki<sup>d</sup>, M. Marques Fernandes<sup>a</sup>, T. Wiss<sup>b</sup>*

<sup>a</sup> Paul Scherrer Institut, Villigen, Switzerland; <sup>b</sup> JRC-ITU, European Commission, Karlsruhe, Germany, <sup>c</sup> Heidelberg University, Heidelberg, Germany; <sup>d</sup> Faculty of Chemistry, University of Wrocław, Wrocław, Poland

#### Introduction

A detailed knowledge on the aquatic chemistry and thermodynamics of actinides and fission products is mandatory for the safety and performance assessment of repositories for nuclear waste disposal. Several thermodynamic databases are developed and maintained worldwide with this aim (e.g. NAGRA-TDB, ThermoChimie, JAEA-TDB, THEREDA), most of them strongly relying on the thermochemical database project of the Nuclear Energy Agency (NEA-TDB). Fundamental research in this field is needed to derive comprehensive chemical, thermodynamic and activity models of specific, relevant systems. These models provide the basis for a good reliability of these databases and resulting thermodynamic calculations.

In 2013, the scientific research developed at KIT-INE in this field focused on actinides solubility, redox behaviour, hydrolysis and complexation with strong ligands (e.g. carbonate, oxalate). Further attention was dedicated to long-lived fission products and investigating the effect of temperature on aqueous actinide chemistry, research activities which will be intensified at KIT-INE in the coming years. Furthermore, formation of “weak complexes” and the challenge of their thermodynamic interpretation were tackled within a comprehensive experimental approach for the system  $\text{Ln}^{\text{III}}/\text{An}^{\text{III}}\text{-OH-NO}_3$ .

Reflecting its expertise and high international reputation in the field of aquatic chemistry and thermodynamics, KIT-INE participates in a number of NEA-TDB activities. INE is co-initiator of the state-of-the-art report on “Pitzer Modelling of Aquatic Chemistry in Saline Systems” and of the “Update Book on the Chemical Thermodynamics of Actinides and Fission Products”. In 2014, KIT-INE organizes the 16<sup>th</sup> *International Symposium on Solubility Phenomena and Related Equilibrium Processes (ISSP-16)* in Karlsruhe within ongoing IUPAC activities.

#### Solubility of Tc(IV) in dilute to concentrated NaCl, MgCl<sub>2</sub> and CaCl<sub>2</sub> solutions

<sup>99</sup>Tc is a  $\beta$ -emitting fission product highly relevant for the safety assessment of nuclear waste repositories due to its significant inventory in radioactive waste, long half-life ( $t_{1/2} \sim 211.000$  a) and redox sensitivity. Due to the very reducing conditions expected under repository conditions, an appropriate knowledge of the Tc(IV) solubility and aqueous speciation in dilute to concentrated NaCl, MgCl<sub>2</sub> and CaCl<sub>2</sub> solutions is required in the context of nuclear waste disposal.

A Tc(VII) stock solution was electrochemically reduced in 1.0 M HCl and precipitated as  $\text{TcO}_2 \cdot x\text{H}_2\text{O}$  at pH~12 in 5 mM Na<sub>2</sub>S<sub>2</sub>O<sub>4</sub>. After an aging time of two

months, about 5 mg of Tc from the resulting solid phase were added to each independent batch sample pre-equilibrated in (0.5 M – 5.0 M) NaCl, (0.25 M – 4.5 M) MgCl<sub>2</sub> and (0.25 M – 4.5 M) CaCl<sub>2</sub> with  $2 \leq \text{pH}_c \leq 14$ . Na<sub>2</sub>S<sub>2</sub>O<sub>4</sub>, SnCl<sub>2</sub> or Fe powder were used to maintain reducing conditions. Tc concentration, pH<sub>c</sub> and E<sub>h</sub> were monitored with time. After reaching equilibrium conditions, solid phases of selected samples were characterized by XRD, SEM-EDS and quantitative chemical analysis.

Tc(IV) solubility data obtained in NaCl ( $t \leq 350$  days) and MgCl<sub>2</sub>/CaCl<sub>2</sub> ( $t \leq 300/180$  days) are shown in Figure 1a and 1b, respectively. Experimentally measured solubility in dilute NaCl and MgCl<sub>2</sub> solutions agree very well with thermodynamic calculations considering the speciation scheme and log \*K° values selected by the NEA-TDB [1].

In the acidic pH range, a very significant increase in the solubility is observed with increasing ionic strength for all considered salt systems. In concentrated alkaline NaCl solutions, the same speciation as for diluted systems is retained (e.g. predominance of TcO(OH)<sub>3</sub><sup>-</sup>), although a decrease in solubility compared to dilute systems takes place due to ion interaction processes. In concentrated MgCl<sub>2</sub> and CaCl<sub>2</sub>

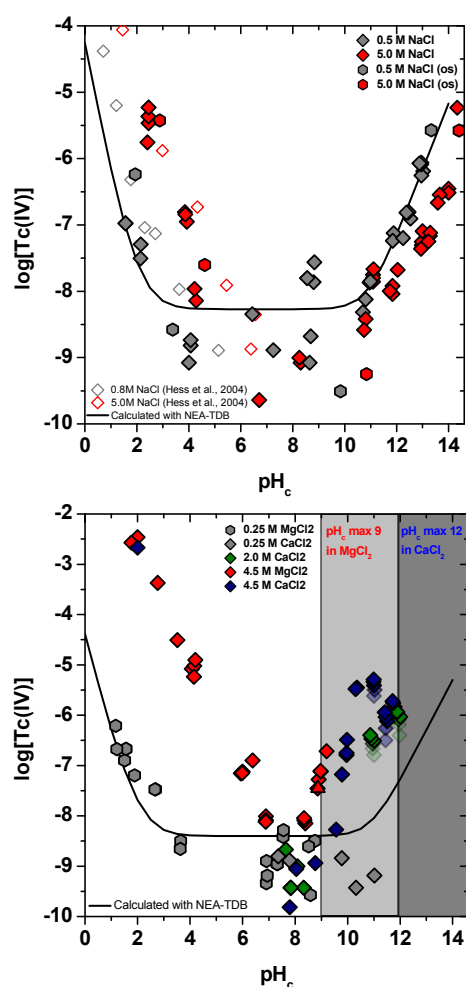


Fig. 1: (a) Solubility of Tc(IV) in 0.5 M and 5.0 M NaCl. (b) Solubility of Tc(IV) in 0.25 M – 4.5 M MgCl<sub>2</sub> and 0.25 M – 4.5 M CaCl<sub>2</sub>.

solutions, a steep increase of solubility with slope +2 takes place at  $\text{pH}_c \geq 8$ . This increase is attributed to the formation of the ternary species  $\text{Mg}_x[\text{TcO}(\text{OH})_y]^{2x-2-y}$  and  $\text{Ca}_x[\text{TcO}(\text{OH})_y]^{2x-2-y}$ , similar to those ternary species previously reported for An(IV) and Zr(IV) [2]. XRD, SEM-EDS and chemical analysis confirm that  $\text{TcO}_2 \cdot x\text{H}_2\text{O}(\text{s})$  is the solid phase controlling the solubility of Tc(IV) in NaCl and MgCl<sub>2</sub> systems. Longer equilibration time and solid phase characterization are needed for CaCl<sub>2</sub> system at  $\text{pH}_c \geq 11$ . Chemical, thermodynamic and activity models (SIT, Pitzer) will be derived for the system  $\text{Tc}^{4+} - \text{H}^+ - \text{Na}^+ - \text{Mg}^{2+} - \text{Ca}^{2+} - \text{OH}^- - \text{Cl}^- - \text{H}_2\text{O}$  based upon the newly generated experimental solubility data.

### Investigation of the Np(V) / Np(IV) redox equilibrium in aqueous solutions

One of the major characteristic of the early actinide elements (U to Am) in aqueous solution is their complex redox chemistry: within the thermodynamic stability field of water, up to four An oxidation states An(III) to An(VI) can exist or even co-exist. All of them show a markedly different behavior regarding the basic chemical reactions in solution e.g. solubility equilibria, complex formation, sorption processes etc. The An oxidation state distribution and speciation is thermodynamically a function of pH value and redox potential pe ( $\text{pe} = 16.9 E_h$  for  $T = 25^\circ\text{C}$ ) and can therefore be calculated for a system with defined redox conditions  $\text{pe} + \text{pH}$ . In the present study we systematically investigated the redox behavior of Np in redox-neutral to reducing aqueous solutions as function of the redox potential pe and pH value, and compared the results to thermodynamic calculations.

Batch experiments were performed with <sup>237</sup>Np in 0.1 M NaCl solutions under Ar atmosphere and at room temperature. The pH in the sample solutions were fixed to values of 4 to 10 using pH buffers. The redox potentials pe were controlled by additions of 1-3 mM of chemically different organic or inorganic (homogenous and heterogeneous) reducing agents: hydroquinone, 9,10-anthraquinone / anthrahydroquinone-2,6-disulfonate (AQDS/AH<sub>2</sub>QDS), FeCl<sub>2</sub>/FeCl<sub>3</sub>, synthetic magnetite, Fe powder, Na<sub>2</sub>S<sub>2</sub>O<sub>4</sub>. The inactive matrix solutions were spiked with aliquots of a 3 mM <sup>237</sup>NpO<sub>2</sub><sup>+</sup> stock solution to obtain  $[\text{Np}]_{\text{tot}} = (4 \pm 1) \cdot 10^{-5}$  M (oversaturation approach). In four additional samples approx. 2 mg of NpO<sub>2</sub>(am) was added initially (undersaturation experiments). The samples were analyzed for pH, pe, and aqueous Np concentration after 10 kD (~ 2 nm) ultrafiltration by LSC and HR-ICPMS as function of time (typically for ~100 d; partly up to five years). Under the pH conditions investigated Np(V) is quantitatively soluble whereas Np(IV) forms sparingly soluble NpO<sub>2</sub>(am) with a solubility of  $\log [\text{Np}] = -9 \pm 1$ . The redox equilibrium Np(V)/Np(IV) can therefore be monitored by the concentration of dissolved Np in solution.

In presence of AQDS/AH<sub>2</sub>QDS, Fe powder, Na<sub>2</sub>S<sub>2</sub>O<sub>4</sub> and FeCl<sub>2</sub>/FeCl<sub>3</sub> (for pH > 6), the initial Np(V) was quantitatively reduced to sparingly soluble NpO<sub>2</sub>(am)

within 1 to 200 d. This observation is in agreement with thermodynamic considerations: the redox conditions  $pe+pH$  of all these samples (red symbols in Figure 2) are in the thermodynamic  $pe+pH$  region, where the Np solubility is expected to be controlled by the equilibrium reaction



The corresponding  $\text{Np}(\text{IV})(\text{aq})$  equilibrium concentration was successfully determined by high-resolution ICPMS ( $\log [\text{Np}] = -9.5 \pm 0.5$ ). A reliable value for the equilibrium constant for reaction (a) was evaluated which confirms the recommended value from NEA-TDB [1] and reduces the reported uncertainties.

In the samples with more positive redox potentials (hydroquinone,  $\text{FeCl}_2/\text{FeCl}_3$   $\text{pH} < 6$ ; green symbols in Figure 2), the reduction of the initial  $\text{Np}(\text{V})$  (oversaturation approach) was covered by very slow kinetics. Within the time of investigation (partly up to 5 years), no steady state was reached. In the analogue samples with initial  $\text{NpO}_2(\text{am})$  instead of  $\text{Np}(\text{V})$  (undersaturation approach; blue symbols in Figure 2), the equilibration processes were faster: partial oxidation of the initial  $\text{NpO}_2(\text{am})$  to aqueous  $\text{Np}(\text{V})$  was observed, and an equilibrium was attained within approx. two years. The final level of dissolved  $\text{Np}(\text{V})$  was directly correlated to the redox potential  $pe$  in the systems, as expected for the thermodynamic equilibrium



The equilibrium constant derived for reaction (b) is in very good agreement with previous work by Rai et al. [3].

The behaviour of Np in redox-neutral and reducing aqueous solutions investigated in this study clearly can accurately be understood and quantitatively be described in terms of equilibrium thermodynamics. Constants for the two most relevant Np equilibrium reactions under these conditions were evaluated, which support the recommended values and reduces

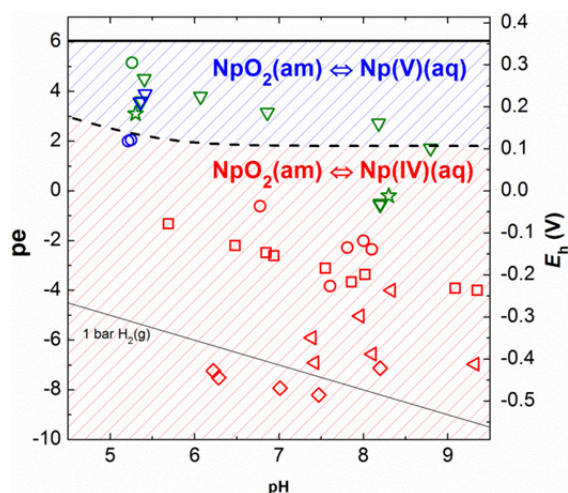


Fig. 2: Experimental  $(pe+pH)$ -values in the different Np redox samples. Red and blue symbols indicate samples where equilibrium (a) and (b) were attained, respectively. In samples marked with green symbols no equilibrium state has been reached.

uncertainties. For some redox systems the equilibration between  $\text{Np}(\text{V})$  and  $\text{Np}(\text{IV})$  was found to be very slow indicating that for a comprehensive description of the aqueous Np redox behaviour the consideration of kinetic aspects might be necessary for certain scenarios.

### Solubility and hydrolysis of U(VI) at 80°C under acidic to hyperalkaline conditions

Temperature is one of the parameters that will vary during the different phases of operation of a high level radioactive waste (HLW) repository. Elevated temperature conditions (up to 200°C depending on hostrock system and repository concept) will affect actinide chemistry in the near-field of a HLW repository. The hydrolysis of U(VI) has been thoroughly studied at 25°C. The thermodynamic data selection resulting from the NEA-TDB reviews is thus very complete (as  $\log K^\circ$ ,  $\Delta_f G^\circ_m$  or  $\Delta_f G^\circ_m$ ) and includes most of the hydrolysis species expected to form from very acidic to hyperalkaline pH conditions [1]. On the contrary, a very limited number of studies is dedicated to assess the effect of temperature on the hydrolysis of U(VI), which results in enthalpy and entropy data selection in the NEA-TDB being restricted to  $\text{UO}_2\text{OH}^+$ . Regarding solid phases, enthalpy, entropy and  $C^\circ_{p,m}$  data are selected in the NEA-TDB for  $\text{UO}_3 \cdot 2\text{H}_2\text{O}(\text{cr})$  based on calorimetric studies. No data are selected for ternary Na-U(VI)-OH solids reported to control the solubility of U(VI) in alkaline conditions [1].

Undersaturation solubility experiments were conducted with  $\text{UO}_3 \cdot 2\text{H}_2\text{O}(\text{cr})$  and  $\text{Na}_2\text{U}_2\text{O}_7 \cdot \text{H}_2\text{O}(\text{cr})$  solid phases synthesized and characterized in a previous solubility study at 25°C [4]. All samples were prepared in an inert gas ( $\text{N}_2$ ) glovebox under exclusion of  $\text{O}_2$  and  $\text{CO}_2$ . U(VI) solid phases were distributed in several independent batch experiments (4–5 mg solid per sample), arranged in two series of 0.5 M NaCl-NaOH solutions with  $4 \leq \text{pH}_m \leq 7$  ( $\text{UO}_3 \cdot 2\text{H}_2\text{O}(\text{cr})$ ) and  $8 \leq \text{pH}_m \leq 12$  ( $\text{Na}_2\text{U}_2\text{O}_7 \cdot \text{H}_2\text{O}(\text{cr})$ ) and stored in an oven at 80°C (in a  $\text{N}_2$  glovebox). Samples were equilibrated for ~1 year and monitored at regular time intervals for dissolved uranyl, [U], and  $\text{pH}_m$ . Triplicate aliquots (supernatant, 0.1  $\mu\text{m}$  filtration and 10 kD ultrafiltration) were taken for the quantification of [U] by ICP-MS. After reaching equilibrium conditions, solid phases of selected samples were characterized by XRD, SEM-EDS and chemical analysis.

The results shown in Figure 3 indicate that the solubility of U(VI) under weakly acidic conditions slightly decreases (~0.5 log-units) at 80°C compared to similar solubility experiments at 25°C. XRD, SEM-EDS and chemical analysis confirm the transformation of  $\text{UO}_3 \cdot 2\text{H}_2\text{O}(\text{cr})$  into a Na-bearing solid phase with Na:U ~0.5. No solid phase transformation takes place for  $\text{Na}_2\text{U}_2\text{O}_7 \cdot \text{H}_2\text{O}(\text{cr})$  under alkaline to hyperalkaline conditions. For this solid phase, a significant increase in solubility (1–2 log units) is observed at 80°C above  $\text{pH}_m = 9.5$ . Similar to 25°C, the solubility

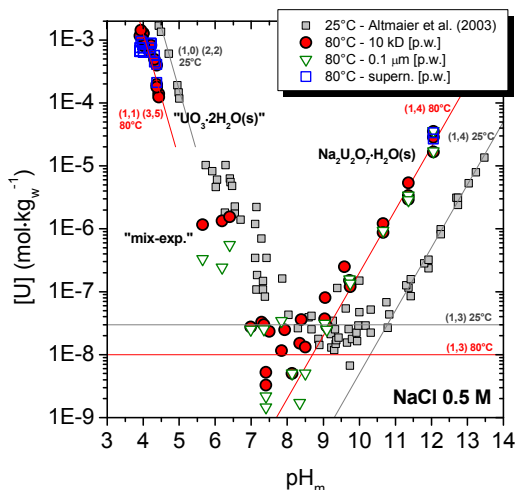


Fig. 3: Solubility of U(VI) in 0.5 M NaCl at  $T = 25^\circ\text{C}$  [4] and  $T = 80^\circ\text{C}$  [p.w.].

of U(VI) as a function of pH shows a well-defined slope of +1 in the  $\text{pH}_m$  region 9–12, corresponding to the equilibrium  $0.5 \text{Na}_2\text{U}_2\text{O}_7 \cdot \text{H}_2\text{O}(\text{cr}) + 2 \text{H}_2\text{O} \Leftrightarrow \text{Na}^+ + \text{UO}_2(\text{OH})_4^{2-} + \text{H}^+$ . This observation is consistent with the expected increase of hydrolysis of metal ions with increasing temperature as a result of the increase of  $K_w$  of  $\text{H}_2\text{O}$ .

The combination of slope analysis with accurate solid phase characterization (XRD, SEM–EDS, chemical analysis) allows the development of a thermodynamic model for the system  $\text{UO}_2^{2+} - \text{H}^+ - \text{Na}^+ - \text{OH}^- - \text{Cl}^-$  at  $80^\circ\text{C}$  valid within  $4 \leq \text{pH}_m \leq 12$ .

### Solubility and TRLFS study of An<sup>III</sup>/Ln<sup>III</sup> in Na–Mg–Ca–Cl–NO<sub>3</sub> solutions

In repositories containing waste from nuclear fuel reprocessing, high concentrations of nitrate ( $\geq 1 \text{M}$ ) and slow nitrate reduction kinetics may affect the aqueous speciation of radionuclides and thus impact their mobilization into the biosphere. In this context, the solubility and speciation of Nd(III) and Cm(III) as chemical analogues of Am(III) and Pu(III) in dilute to concentrated NaCl–NaNO<sub>3</sub>, MgCl<sub>2</sub>–Mg(NO<sub>3</sub>)<sub>2</sub> and CaCl<sub>2</sub>–Ca(NO<sub>3</sub>)<sub>2</sub> mixed solutions were investigated under repository-relevant pH conditions and  $22 \pm 2^\circ\text{C}$ .

Samples were prepared and stored in Ar glove boxes. Batch solubility experiments were performed from undersaturation with Nd(OH)<sub>3</sub>(am) (6–12 mg) in 0.1–6.02 m NaCl–NaNO<sub>3</sub>, 0.25–5.2 m MgCl<sub>2</sub>–Mg(NO<sub>3</sub>)<sub>2</sub> and 2.91/4.02 m CaCl<sub>2</sub>–Ca(NO<sub>3</sub>)<sub>2</sub> background electrolytes. Samples were monitored for  $\text{pH}_m$  and  $m_{\text{Nd(III)}}$ . Solid phases were characterized using XRD and SEM–EDX. Nd–L<sub>III</sub> EXAFS spectra were recorded in fluorescence mode at the INE beamline at ANKA. Cm(III)–TRLFS measurements were performed with  $\sim 10^{-7} \text{M}$  Cm(III) per sample in 5.61/6.02 m NaCl–NaNO<sub>3</sub>, 0.25/4.1 m MgCl<sub>2</sub>–Mg(NO<sub>3</sub>)<sub>2</sub> and 4.02 m CaCl<sub>2</sub>–Ca(NO<sub>3</sub>)<sub>2</sub>.

Figure 4 shows exemplarily the solubility of Nd(OH)<sub>3</sub>(am) in 4.06/4.02 m Mg–Ca–Cl–NO<sub>3</sub> mixtures. No significant enhancement in Nd(OH)<sub>3</sub>(am) solubility occurs in CaCl<sub>2</sub>–Ca(NO<sub>3</sub>)<sub>2</sub> and NaCl–NaNO<sub>3</sub> (data not shown) mixtures compared to nitrate-free systems [5]. On the contrary, a clear increase in solubility occurs for MgCl<sub>2</sub>–Mg(NO<sub>3</sub>)<sub>2</sub> mixtures with  $m_{\text{Mg}^{2+}} \geq 2.83 \text{m}$ ,  $m_{\text{NO}_3^-} \geq 1.13 \text{m}$  and  $\text{pH}_m = 8\text{--}9$ . Provided the solubility control exerted by Nd(OH)<sub>3</sub>(am) (confirmed by XRD and SEM–EDX in all systems with  $m_{\text{Cl}^-} \leq 5.82 \text{m}$ ), the slope analysis of the experimental data in MgCl<sub>2</sub>–Mg(NO<sub>3</sub>)<sub>2</sub> mixtures indicates the formation of aqueous species Mg–Nd–OH–NO<sub>3</sub> with stoichiometries Nd:OH 1:1 ( $\text{pH}_m \leq 8.3$ ) and Nd:OH 1:2 ( $\text{pH}_m > 8.3$ ).

Cm(III)–TRLFS and EXAFS data reveals the formation of aquatic “An<sup>III</sup>/Ln<sup>III</sup>–OH–NO<sub>3</sub>” species under weakly alkaline  $\text{pH}_m$  conditions only in MgCl<sub>2</sub>–Mg(NO<sub>3</sub>)<sub>2</sub> systems, thus hinting towards the participation of Mg<sup>2+</sup> in the complex formation reaction.

The combination of slope analysis, solid phase characterization, EXAFS and Cm(III)–TRLFS observations confirms the relevance of the equilibrium reactions  $\text{An}^{\text{III}}/\text{Ln}^{\text{III}}(\text{OH})_3(\text{am}) + 2\text{H}^+ + \text{NO}_3^- + \text{Mg}^{2+} \Leftrightarrow \text{Mg}[\text{An}^{\text{III}}/\text{Ln}^{\text{III}}(\text{OH})\text{NO}_3]^{3+} + 2\text{H}_2\text{O}$  and  $\text{An}^{\text{III}}/\text{Ln}^{\text{III}}(\text{OH})_3(\text{am}) + \text{H}^+ + \text{NO}_3^- + \text{Mg}^{2+} \Leftrightarrow \text{Mg}[\text{An}^{\text{III}}/\text{Ln}^{\text{III}}(\text{OH})_2\text{NO}_3]^{2+} + \text{H}_2\text{O}$  in concentrated nitrate-bearing Mg-systems and permits to further extend the chemical, thermodynamic and activity models described in [5] for Ln(III) and An(III) to  $\text{Ln}^{3+}/\text{An}^{3+} - \text{H}^+ - \text{Na}^+ - \text{Mg}^{2+} - \text{Ca}^{2+} - \text{OH}^- - \text{Cl}^- - \text{NO}_3^-$  systems.

The development of thermodynamic and activity models based on the chemical model proposed above using both SIT and Pitzer approaches is under way.

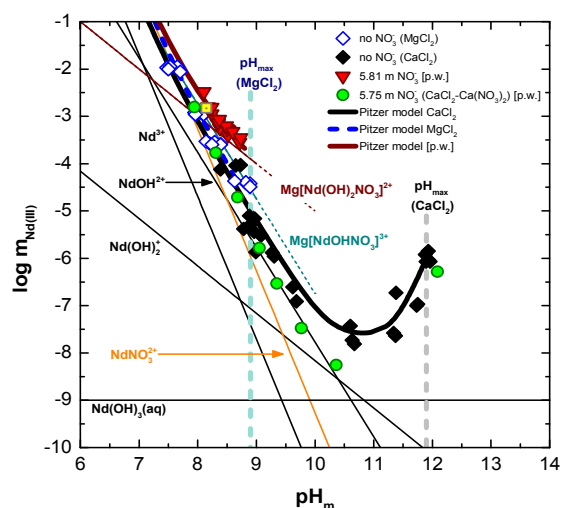


Fig. 4: Solubility and aqueous speciation of Nd(OH)<sub>3</sub>(am) in 4.06 m MgCl<sub>2</sub>–Mg(NO<sub>3</sub>)<sub>2</sub> and 4.02 m CaCl<sub>2</sub>–Ca(NO<sub>3</sub>)<sub>2</sub> mixtures with 5.81/5.75 m NO<sub>3</sub><sup>−</sup>. Reference data [5] in nitrate-free solutions included for comparison. Yellow square indicates the sample used for Nd–L<sub>III</sub> EXAFS.

## Structure and Spectroscopy of Eu(III) and Cm(III) tetracarboxylates

Carbonate is an important inorganic anion in natural ground waters, which can play a central role as *O*-donor ligand to actinide(III) ions upon water intrusion to a nuclear waste repository. A comprehensive understanding of An(III)-carbonate interactions is therefore required. Here, we report recent studies on Eu(III) and Cm(III) carbonate complexation in aqueous solution at different concentrations of potassium carbonate, metal concentrations, as well as the ionic strength, using absorption and luminescence spectroscopies. Particularly, we addressed the unsettled question whether the limiting complex  $[M(\text{CO}_3)_n]^{2n+3}$  ( $n = 1-4$ ;  $M = \text{Eu}, \text{Cm}$ ) is a tri- or tetracarboxylate complex [6-8].  $[\text{C}(\text{NH}_2)_3]_5[\text{Gd}(\text{CO}_3)_4(\text{H}_2\text{O})] \cdot 2\text{H}_2\text{O}$  (**1**) and  $[\text{C}(\text{NH}_2)_3]_5[\text{Y}(\text{CO}_3)_4] \cdot 2\text{H}_2\text{O}$  (**2**) doped with Eu and Cm were used as structure models for the tetracarboxylate complexes in solution at high carbonate concentration. Emission spectra and lifetimes of Cm(III) and Eu(III) in **1** and **2** were compared with the corresponding data of the solutions. We present here selected data on the limiting Eu(III)/Cm(III) carbonate complexes at  $\sim 2 \text{ M K}_2\text{CO}_3$ .

A detailed picture about the nature of the limiting species and its equilibrium species was obtained from the hypersensitive  ${}^7\text{F}_0 \rightarrow {}^5\text{D}_2$  and  ${}^5\text{D}_0 \rightarrow {}^7\text{F}_2$  transitions and by comparison of the oscillator strengths of the former transition. The intensities of these transitions are 4-5 times larger for **2** than for **1**, while those of the solution are between these values (Figure 5). In addition, the center-of-gravity of the  ${}^5\text{D}_2$  level in **1** is blue-shifted compared to the solution. These studies indicate that the tetracarboxylate complex at high carbonate concentration may be attributed to a  $[\text{Eu}(\text{CO}_3)_4]^{5-}$  complex and not  $[\text{Eu}(\text{CO}_3)_4(\text{H}_2\text{O})]^{5-}$ . Although only minor changes were observed in the  ${}^7\text{F}_0 \rightarrow {}^5\text{D}_2$  and  ${}^5\text{D}_0 \rightarrow {}^7\text{F}_2$  spectra at elevated carbonate concentrations, by comparing these transitions with those in **2** the molar fraction of  $[\text{Eu}(\text{CO}_3)_4]^{5-}$  was estimated to  $\sim 20\%$ . According to solubility studies the main species in these solutions is probably a tricarbonate com-

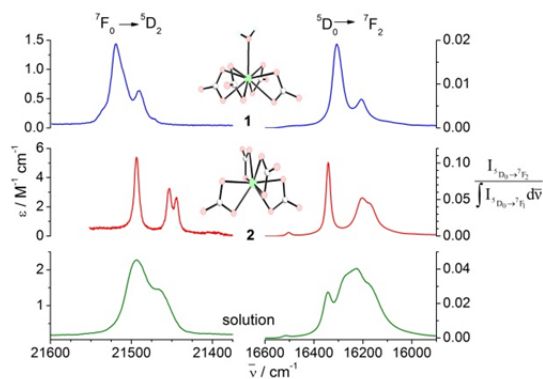


Fig. 5: Vis-absorption and emission spectra of the  ${}^7\text{F}_0 \rightarrow {}^5\text{D}_2$  and  ${}^5\text{D}_0 \rightarrow {}^7\text{F}_2$  transitions, respectively, of **1**, **2**, and  $0.0185 \text{ M Eu(III)}$  in  $2.045 \text{ M K}_2\text{CO}_3$ .

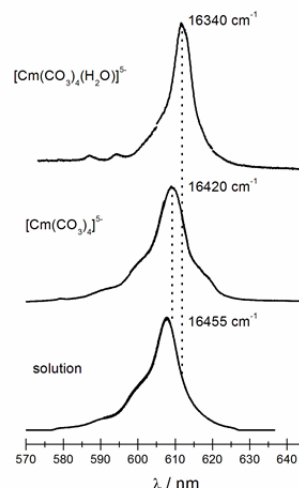


Fig. 6: Luminescence spectra of the  ${}^6\text{D}_{7/2} \rightarrow {}^8\text{S}_{7/2}$  transition of Cm(III) in  $2 \text{ M K}_2\text{CO}_2$  and in **1** and **2**.

plex, which points to an equilibrium between tri- and tetracarboxylate complexes.

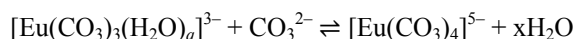


Figure 6 shows the emission spectra of Cm(III) in  $2 \text{ M K}_2\text{CO}_2$  and in **1** and **2**. The peak maxima of the spectra of the crystals are red-shifted compared to the solution; though the difference in the peak positions between the  $[\text{Cm}(\text{CO}_3)_4]^{5-}$  complex in **2** and the solution is small. It is not possible to compare the intensity of the bands, thus no quantitative conclusions can be made. Nevertheless, the marked similarities between the spectra suggest the presence of both tri- and tetracarboxylate complexes in concentrated carbonate solution, as shown by Fanghanel et al. [9]. In summary, in concentrated aqueous carbonates solutions, Eu(III) and Cm(III) form limiting tetracarboxylate species of  $[\text{Eu}(\text{CO}_3)_4]^{5-}$ ,  $[\text{Cm}(\text{CO}_3)_4]^{5-}$  and/or  $[\text{Cm}(\text{CO}_3)_4(\text{H}_2\text{O})]^{5-}$ .

### Thermodynamics of $[\text{Cm}(\text{Ox})_n]^{3-2n}$ complexes at $T = 20 - 90^\circ\text{C}$

The formation of  $[\text{Cm}(\text{Ox})_n]^{3-2n}$  ( $n = 1, 2, 3, 4$ ) complexes is studied by TRLFS at different ligand concentrations ( $[\text{Ox}^{2-}]_{\text{tot}} = 5 \cdot 10^{-4} - 1 \cdot 10^{-2} \text{ m}$ ) and different ionic strengths ( $I_m = 1.0 - 4.0 \text{ (NaCl)}$ ) as a function of the temperature ( $T = 20 - 90^\circ\text{C}$ ). The total proton concentration is fixed at  $[\text{H}^+]_{\text{tot}} = 9.3 \cdot 10^{-3} \text{ m}$ . The experiments are conducted in a quartz cuvette which is embedded in a temperature controlled copper block.

At room temperature three different complexed species are formed with increasing ligand concentration. Using slope analysis, the species are identified as  $[\text{Cm}(\text{Ox})_n]^{3-2n}$  ( $n = 1, 2, 3$ ) complexes. The emission bands of the different components are located at  $596.5 \text{ nm}$  ( $[\text{Cm}(\text{Ox})]^{3+}$ ),  $598.9 \text{ nm}$  ( $[\text{Cm}(\text{Ox})_2]^{1+}$ ) and  $601.3 \text{ nm}$  ( $[\text{Cm}(\text{Ox})_3]^{3-}$ ) (Figure 7). For all samples a shift of the speciation towards the higher complexed species is observed with increasing temperature. Also, a fourth species appears at  $604.7 \text{ nm}$  at higher temperatures. According to the slope analysis, this species is a  $[\text{Cm}(\text{Ox})_4]^{5-}$  complex. No complexes of Cm(III)

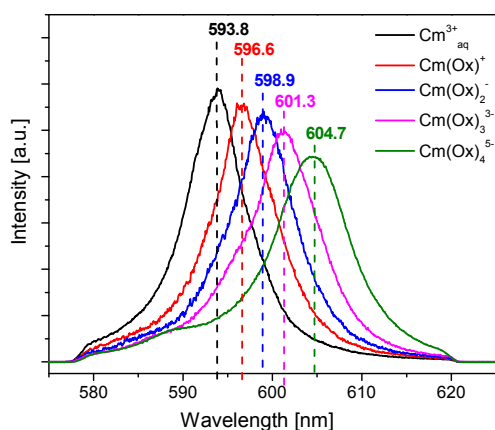


Fig. 7: Emission bands of the  $[Cm(Ox)_n]^{3-2n}$  ( $n = 1, 2, 3, 4$ ) complexes

with  $H_2Ox$ ,  $HOx^-$  and  $NaOx^-$  are found under the present experimental conditions. The conditional stability constants ( $\log K^n(T)$ ) are calculated according to the law of mass action and extrapolated to zero ionic strength with the specific ion interaction theory (SIT). At 25°C, values of  $\log K^0_1(25^\circ C) = 6.78 \pm 0.20$ ,  $\log K^0_2(25^\circ C) = 4.45 \pm 0.38$  and  $\log K^0_3(25^\circ C) = 2.34 \pm 0.35$  are determined. These results are in very good agreement with the analogous values for Am(III) oxalate complexes [10]. The individual  $\log K^n(T)$  values show different behavior with increasing temperature. The  $\log K^0_1(T)$  decreases slightly by 0.1 logarithmic units. Contrary to this, the  $\log K^0_2(T)$  and  $\log K^0_3(T)$  values increase with temperature. While  $\log K^0_2(T)$  increases by approximately 0.5 logarithmic units, the  $\log K^0_3(T)$  values show a distinctively stronger temperature dependency. It increases by about 1.4 orders of magnitude in the studied temperature range. Additionally, for the  $[Cm(Ox)_4]^{5-}$  complex a value of  $\log K^0_4(90^\circ C) = 1.31 \pm 0.35$  is determined. The thermodynamic stability constants are linearly correlated with the reciprocal temperature. Thus, the

temperature dependent change of the standard reaction enthalpy ( $\Delta_r H^0_m$ ) is negligible and the  $\log K^n(T)$  values are fitted by the integrated van't Hoff equation over the entire studied temperature range. The results of the thermodynamic data of the individual complexation steps show a small negative value for the standard reaction enthalpy of the  $[Cm(Ox)]^+$  complex ( $\Delta_r H^0_{m,1} = -7.54 \pm 3.98$  kJ/mol). In contrast to this, the formation of the 1:2 and 1:3 complexes is endothermic ( $\Delta_r H^0_{m,2} = 21.74 \pm 3.98$  kJ/mol;  $\Delta_r H^0_{m,3} = -7.54 \pm 3.98$  kJ/mol). This indicates a different coordination mode of the second and third oxalate ligand compared to the first one. Furthermore, the stepwise complexation reactions show positive and successively increasing standard reaction entropies ( $\Delta_r S^0_{m,1} = 106.3 \pm 11.9$  J/mol·K;  $\Delta_r S^0_{m,2} = 157.6 \pm 10.5$  J/mol·K;  $\Delta_r S^0_{m,3} = 176.5 \pm 21.0$  J/mol·K).

## References

- [1] R. Guillaumont et al., *Chemical Thermodynamics Vol. 5*, Elsevier, Amsterdam, (2003).
- [2] M. Altmaier et al., *Radiochimica Acta*, **96**, 541-550, (2008).
- [3] D. Rai et al., *Radiochimica Acta*, **42**, 35-41 (1987).
- [4] M. Altmaier et al., *Migration Conference, Gyeongju (Korea)*, (2003).
- [5] Neck, V. et al., *Pure Appl. Chem.*, **81**: 1555 (2009).
- [6] Fanghänel, Th. et al., *J. Sol. Chem.*, **28**: 447 (1999)
- [7] Vercouter, T. et al., *Inorg. Chem.*, **44**: 5833 (2005)
- [8] Janicki, R. et al., *Eur. J. Inorg. Chem.*, 3601 (2011)
- [9] Fanghänel, Th. et al., *Radiochim. Acta.*, **82**: 47 (1998)
- [10] W. Hummel, et al., *Comptes Rendus Chimie*, **10**, 948-958, (2007).

## 4.2 Sorption on mineral surfaces

A. Schnurr, N.L. Banik, K. Dardenne, A. Diascorn, H. Geckeis, T. Kupcik, J. Lützenkirchen, C. Marquardt, R. Marsac, T. Rabung, J. Rothe, T. Schäfer, D. Schild

### Introduction

Radionuclide retention onto mineral surfaces is a key aspect which has to be considered in performance safety calculations for nuclear waste repositories. In this respect, fundamental studies are essential to understand the (sorption) reactions and mechanisms at the mineral-water interface. In this annual report, we want to especially highlight the work regarding An/Ln retention onto clay minerals.

Besides pure and well defined laboratory systems also natural and site specific samples have to be studied. By combination of a top down / bottom up approach and a quantitative description of sorption reactions by the means of thermodynamic constants relevant sorption data can be provided for performance assessment.

### Trivalent actinide and lanthanide sorption onto clay minerals under saline conditions

Due to their high sorption capacity, their swelling properties and their low water permeability in the compacted state, clay minerals are of great interest as suitable components of geotechnical and geological barriers. Illite, smectite and illite/smectite mixed layers are the most important components of the proposed claystone host rocks and often amount up to 50 or more wt. % of the material [1]. Previous detailed sorption studies were typically carried out up to  $I = 0.1$  molar ([1-4]). Nevertheless, clay rock pore water chemistry can also be characterized by high salinity up to  $\sim 5$  molal [5] as e.g. in the Jurassic and lower Cretaceous clay rock in Northern Germany.

Saline conditions are not only restricted to the presence of rock salt formations. For instance, in Canada sedimentary rocks in contact with brine solutions up to 6.5 M are considered as potentially suitable host rock formations for high level waste. In all cases, detailed sorption investigations are necessary under

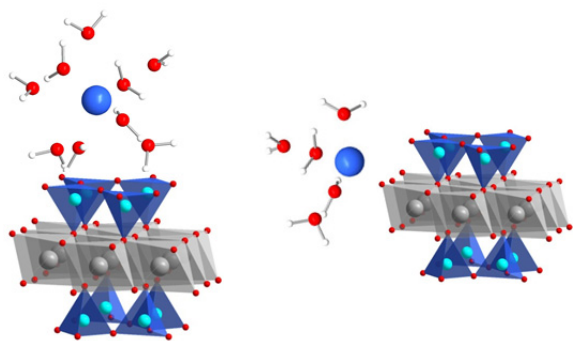


Fig. 1: Trivalent actinide/lanthanide sorption mechanism onto TOT clay minerals. Outer-sphere sorption at the basal planes (left) and inner-sphere sorption at the edges (right).

the prevailing (saline) conditions.

Illite and montmorillonite (smectite) are layered aluminosilicates with a repetition of TOT (tetrahedral-octahedral-tetrahedral) layers. Isomorphous substitutions within the lattice cause a permanent negative charge. In illite, which has a higher negative layer charge compared to smectites, the charge compensation is mainly induced by facile desolvating potassium cations located in the inter-layers. As a consequence the swelling properties in pure illite are completely absent and a lower cation exchange capacity compared to smectites is measured. Both types of clay are characterized by permanently negatively charged basal planes and pH dependent protonated or deprotonated hydroxyl groups on the edge planes. As a consequence, cations are predominately bound on the basal planes as outer-sphere complexes (Fig. 1 left) via cation exchange reactions at low pH and low ionic strength. By increasing pH, prevailing inner-sphere complexation (Fig. 1 right) at the edges is clearly verified by spectroscopic methods ([6], [7]).

A frequently applied model to describe the interactions of various radionuclides with clay minerals has been developed by Bradbury and Baeyens ([2], [8]). This quasi mechanistic 2 site protolysis non-electrostatic surface complexation and cation exchange (2SPNE SC/CE) model was developed to describe titration, sorption edge and sorption isotherm data over a wide pH range (3-12) up to background electrolyte concentrations of about 0.1 molar (monovalent salt).

The non-electrostatic nature of the surface complexation part avoids one of the potential complications arising with high salinity. Therefore, one of the aims of the present work is to test the applicability of the 2SPNE SC/CE model at highly saline conditions.

Batch sorption edge experiments were carried out with three different background electrolytes (NaCl, CaCl<sub>2</sub> and MgCl<sub>2</sub>) at different ionic strengths ([NaCl] up to 4.4 mol/kg, [CaCl<sub>2</sub>] and [MgCl<sub>2</sub>] up to 2.1 mol/kg), at fixed metal concentration ([Eu]<sub>total</sub> =  $2 \times 10^{-7}$  M, spiked with <sup>152</sup>Eu for  $\gamma$ -counting and at constant solid to liquid ratios (S:L = 2 g/L purified illite du Puy and SWy-2) over a wide pH<sub>m</sub> range (3-12).

In the case of illite (Figs. 2 and 3), the extent of Europium uptake approaches > 99.5% at pH<sub>m</sub> > 8 for all investigated electrolyte solutions. The same has been observed in other systems, i.e. the high salt content clearly does not suppress the strong uptake of trivalent metal cations.

In general, sorption edges shift to higher pH<sub>m</sub>-values with increasing ionic strength up to a pH<sub>m</sub> value where the ionic strength dependency is no longer

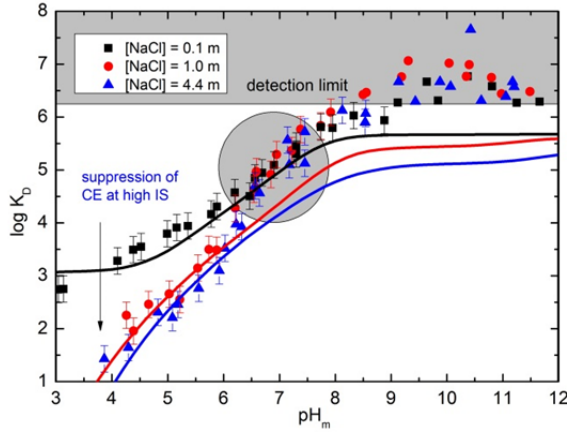


Fig. 2: Sorption edges for Eu ( $m_{Eu\ total} \sim 2 \times 10^{-7}$  mol/kg), S:L 2 g/L onto Illite du Puy as a function of  $pH_m$  against logarithm of distribution ratio at different NaCl concentrations. The solid lines represent the calculations using the 2SPNE SC/CE model considering the Pitzer approach for the activity coefficient calculations.

obvious ( $pH_{mNaCl} \sim 6.5$ ,  $pH_{mMg/CaCl_2} \sim 8$ ). In presence of divalent cations, however, actinide/lanthanide sorption is much stronger suppressed than observed for NaCl solutions.

A possible explanation for this might be the stronger competition of divalent cations with actinide/lanthanide sorption to cation exchange sites but maybe also to inner sphere sorption sites at the edges of the clay particles.

The present work clearly demonstrates that clay minerals represent strong retardation barriers for trivalent metal ions even under highly saline conditions.

### Neptunium redox speciation at the surface of illite

Neptunium (Np) is an important element in the context of high level radioactive waste disposal. Under oxidizing conditions, Np exists in its pentavalent oxidation state as the neptunyl ion ( $NpO_2^+$ ), which is rather weakly sorbed to minerals surfaces and is, as a consequence, considered as rather mobile. Under reducing conditions, Np(IV) prevails and is considered as rather immobile because of its strong sorption to minerals and its low solubility [7].

Most of the studies on Np sorption onto clay minerals were performed under aerobic conditions, where the Np(V) oxidation state is dominant, or under inert atmosphere but without monitoring or controlling the redox potential [9]. However, slightly oxidizing to reducing conditions are frequently found in soil or natural clay rocks, where Np(V) reduction to Np(IV) is relevant.

The present study is dedicated to  $NpO_2^+$  sorption to purified illite du Puy (reference material used within the CP CatClay project) under inert (Argon) atmosphere, which is expected to lead to slightly reducing conditions. Classical batch experiments are performed in 0.1 M NaCl, 2 g/L of illite, at various pH (4-10), total Np concentrations ( $[Np]_{tot} = 3 \times 10^{-8} - 3 \times 10^{-4}$  M) and reaction times (2-63 days). The  $E_h$  is monitored. X-ray

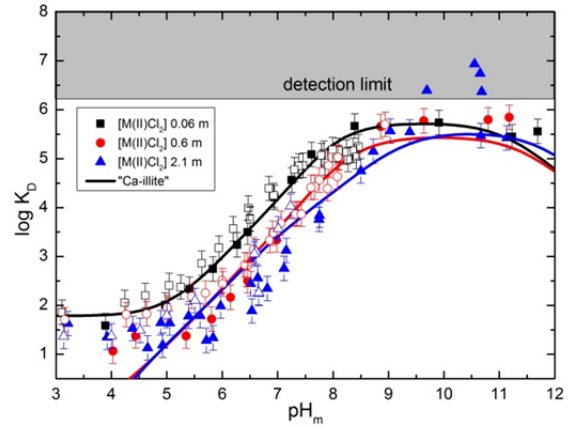


Fig. 3: Sorption edges for Eu ( $m_{Eu\ total} \sim 2 \times 10^{-7}$  mol/kg), S:L 2 g/L onto Illite du Puy as a function of  $pH_m$  against logarithm of distribution ratio at different Mg(open)/Ca(closed) $Cl_2$  concentrations. Solid lines are calculated with the 2SPNE SC/CE model with some slight modifications for the surface complexation constants.

absorption near edge structure spectroscopy (XANES) is applied to determine the Np redox state at the illite surface. Finally, Np sorption and redox speciation are described using a surface complexation model.

The total amount of Np sorption to illite does not increase after 7 days reaction time showing a relatively fast uptake process. Figure 4a compares the present Np-illite pH-edge for  $[Np]_{tot} = 3 \times 10^{-8}$  M under anaerobic conditions ( $\log K_D$  versus pH) with literature pH-edges for Np-illite under aerobic conditions [9] and Th(IV)-illite [10]. Measured partition coefficients ( $K_D$ ) are intermediate, though, which suggests a partial reduction of Np(V) to Np(IV) in our experiments.

Significant differences in white line intensity and the first post-edge oscillation with the Np(V) reference support the presence of a significant amount of Np(IV). Np L3-edge XANES obtained on a wet paste at  $pH=7.4$ , 20 g/L of illite and  $[Np]_{tot} = 3 \times 10^{-4}$  M is compared with literature Np(V) and Np(IV) references [11] in figure 4b.

The XANES spectrum is analysed by a linear combination fit of the two references and based on this 14% of the sorbed Np would be Np(IV).

Given the experimental  $E_h$  ( $0.40 \pm 0.05$  V) and according to the Nernst equation, the redox potential of the Np(V)/Np(IV) couple at the surface (at equal concentrations of Np(V) and Np(IV)) for  $pH=7.4$  is equal to  $0.35 \pm 0.05$  V, i.e. approximately 0.25 V above the corresponding one in solution.

The unknown Np(IV)-illite surface complexation constants for the 2 SPNE SC/CE model [10] are fitted to our results using PhreePlot [12]. Np(IV) surface complexation constants are consistent with the established linear free energy relationship [10]. A  $pH(E_h)$  diagram for Np is plotted on figure 4c using our data. The diagram distinguishes Np redox speciation in solution (black) and at the surface of illite (grey). It shows that, although Np(V) is the dominant state in solution, relatively high  $K_D$  values are meas-

ured because Np(IV) is thermodynamically favoured at the surface of illite.

Clay adsorbed or structural Fe(II) is known as an efficient redox partner for actinides [13], which might explain the fast surface mediated reduction of Np(V). However, both sorption data and XANES analysis point to a limited amount of available Fe(II) in our illite with respect to Np(V) reduction (~1% of the total Fe(II) content). Further studies are required to elucidate the role of Fe(II).

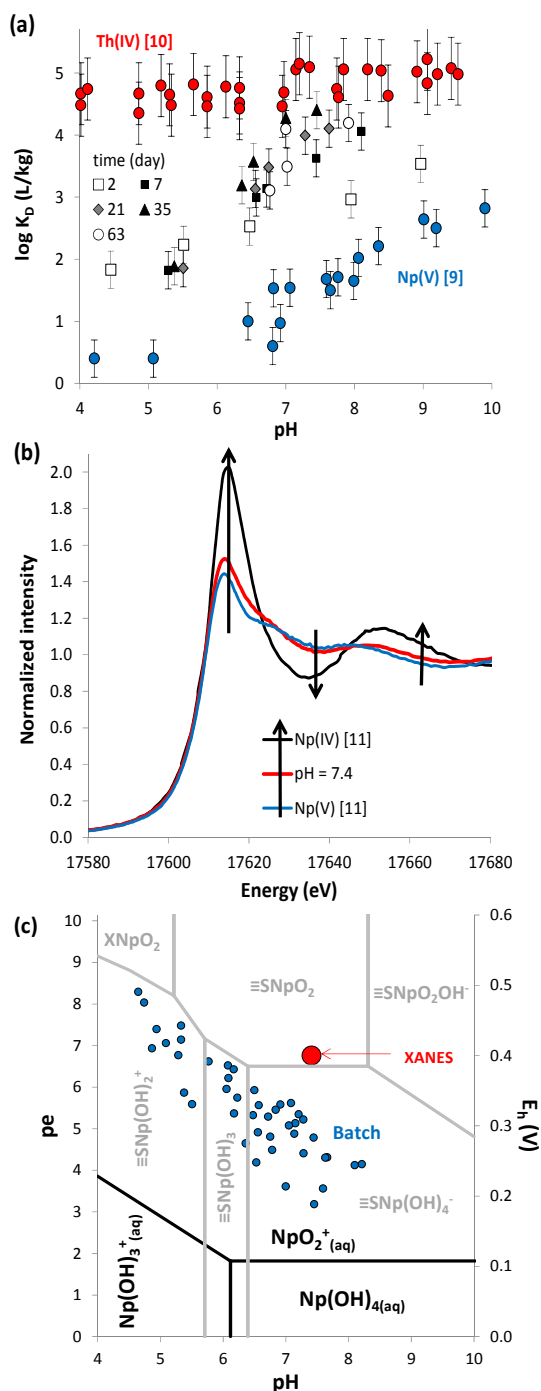


Fig. 4: (a) Np sorption to illite ( $K_D$ ) versus pH and reaction time, compared with literature Np(V) [9] and Th(IV) [10] data. (b) Np-illite XANES for pH=7.4 compared with Np(V) and Np(IV) references [11]. (c) Np pH-pe( $E_h$ ) diagram in solution (black) and at the surface of illite (grey), with the experimental results (black symbols).

The present findings have important consequences concerning Np mobility in the environment, since surface complexation reactions enlarge the stability field of the rather immobile Np(IV). Our interpretation might be applicable to other elements as well as other adsorbing phases.

### Hexavalent actinide sorption onto clay minerals under saline conditions

In the present work, hexavalent uranium (U(VI)) sorption onto illite (illite du Puy) under saline conditions and exclusion of carbon dioxide (glove box) was studied. Batch sorption edge measurements were carried out in three different background electrolytes (NaCl, CaCl<sub>2</sub> and MgCl<sub>2</sub>) at different ionic strengths (varied up to [NaCl] = 4.37 mol/kg and [M(II)Cl<sub>2</sub>] = 2.11 mol/kg), at fixed metal concentration ([U]<sub>total</sub> ~ 4x10<sup>-7</sup> mol/kg) and at constant solid to liquid ratio (S:L = 2 g/L) over a wide pH range (3-12). At pH > 11, uranium (VI) sorption decreases due to competition with negatively charged aqueous uranium(VI) hydroxide species (Fig. 5).

The pH<sub>m</sub> dependent sorption of uranium onto illite is presented in Fig. 6 at different NaCl background electrolyte concentrations. Unlike previous studies on trivalent actinide sorption onto clay minerals under saline conditions there is only a very small or even no impact of the NaCl concentration on the uranium sorption behaviour. The variation of the NaCl content between 0.1 and 4.37 mol/kg does not significantly change the distribution ratio of uranium. Also the variation of the initial uranium concentration by one order of magnitude from ~ 1.0 – 10.0 x10<sup>-7</sup> mol/kg does not have a significant effect and indicates that the experiments are performed in the ideal sorption range. Small differences are within the range of the experimental uncertainty.

It is important to note that in the pure NaCl system there is a high uptake (>99.5%) of uranium sorbed onto the illite du Puy in the environmentally most relevant pH range (6.5 < pH < 11.0).

The same observation is found for CaCl<sub>2</sub> and MgCl<sub>2</sub> solutions. The comparison between 1:1 and 2:1 back-

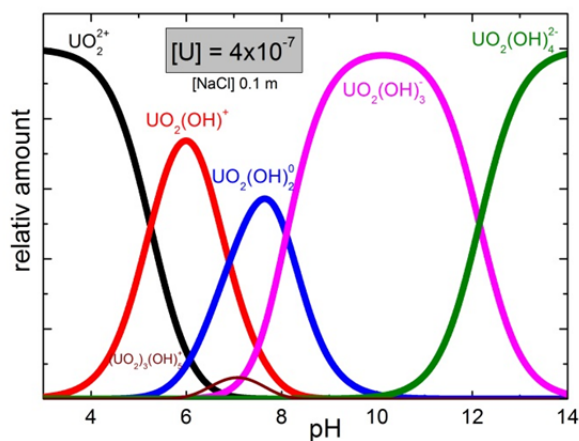


Fig. 5: Calculated aqueous speciation of U ( $m_{U, total} \sim 4.0 \cdot 10^{-7}$  mol/kg), as a function of pH<sub>m</sub> against the relative amount of each species in 0.1 mol/kg NaCl.

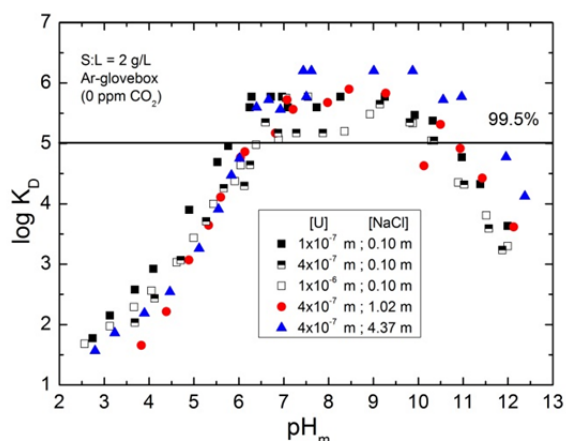


Fig. 6: Sorption edges for U ( $m_{U, total} \sim 1.0, 4.0$  and  $10.0 \cdot 10^{-7}$  mol/kg), S:L 2 g/L, on Illite du Puy as a function of  $pH_m$  against logarithm of distribution ratio at different NaCl concentrations.

ground electrolytes exhibits slightly lower sorption in  $CaCl_2$  and  $MgCl_2$  solutions and a small dependence on 2:1 electrolyte total concentration might be derived from experimental data. (Fig.7). Nevertheless, considering the experimental uncertainties, this effect is not very pronounced.

In the pH range from 7 – 11 there is also in the pure  $CaCl_2$  and  $MgCl_2$  system an almost quantitative retardation (>99.5) of U(VI) onto the clay mineral similar as has been found for the NaCl system. At very high pH values (>11.0) uranium sorption decreases again in all investigated systems.

The general pH dependent trend for uranium sorption can be explained considering the calculated uranium aqueous speciation (Fig. 5). Up to pH values < 8 positively charged or neutral complexes dominate the uranium speciation. The strong sorption of the formally negatively charged  $UO_2(OH)_3^-$  complex dominating the speciation between pH 8.1 and 12.1 could be explained by the increased effective charge of uranium due to its linear oxo-complex structure. For the  $UO_2^{2+}$

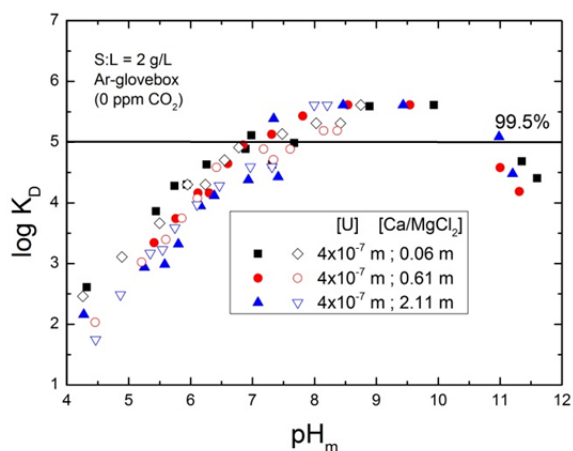


Fig. 7: Sorption edges for U ( $m_{U, total} \sim 4.0 \cdot 10^{-7}$  mol/kg), S:L 2 g/L, on Illite du Puy as a function of  $pH_m$  against logarithm of distribution ratio at different Mg(open)/Ca(closed) $Cl_2$  concentrations between 0.06 and 2.11 mol/kg.

ion an effective charge in the equatorial plane of +3.3 is documented. The presence of 3 additional hydroxide ligands might therefore not completely compensate this charge. At higher pH ( $pH > 11$ ) the negatively charged tetrahydroxo complex predominates the speciation and subsequently uranium sorption decreases.

The present work clearly demonstrates that clay minerals represent strong retardation barriers for hexavalent metal ions even under highly saline conditions.

## References

- [1] Bradbury, M.H. and Baeyens, B., *Geochim. Cosmochim. Acta*, **73**, 990-1003 (2009).
- [2] Poinssot, C. et al., *Geochim. Cosmochim. Acta*, **63**, 3217-3227 (1999).
- [3] Baeyens, B. and Bradbury, M.H., *Clay. Clay. Miner.*, **52**, 421-431 (2004).
- [4] Bradbury, M.H. and Bayens, B., *Geochim. Cosmochim. Acta*, **66**, 2325-2334 (2002).
- [5] Brewitz, W.: *Eignungsprüfung der Schachtanlage Konrad für die Endlagerung radioaktiver Abfälle. GSF-T136*, Neuherberg (1982).
- [6] Geckeis, H. and Rabung, T., *J. Contam. Hydrol.* **102**, 187-195 (2008).
- [7] Geckeis, H. et al., *Chem. Rev.* **113**, 1016-1062 (2013).
- [8] Bradbury, M.H. and Baeyens, B., *J. Contam. Hydrol.* **27**, 223-248 (1997).
- [9] Gorgeon, L., *Ph.D. thesis*, Paris 6 University (1994).
- [10] Bradbury, M.H. and Baeyens, B., *Geochim. Cosmochim. Acta*. **73**, 1004-1013 (2009).
- [11] Gaona, X. et al., *Radiochim. Acta* **100**, 759-770 (2012).
- [12] Kinniburgh, D.G. and Cooper, D.M., <http://www.phreeplot.org> (2009).
- [13] Chakraborty, S. et al., *Environ. Sci. Technol.* **44**, 3779-3785 (2010).

## 4.3 Multitracer (HTO, $^{36}\text{Cl}$ , $^{85}\text{Sr}$ ) diffusion in $\text{Cu}(\text{en})_2$ -illite and $\text{Cu}(\text{en})_2$ -montmorillonite

T. Kupcik, M.A. Glaus<sup>a</sup>, L.R Van Loon<sup>a</sup>, B. Baeyens<sup>a</sup>, Th. Schäfer

<sup>a</sup> Laboratory for Waste Management, Paul Scherrer Institut, CH-5232 Villigen, Switzerland

### Introduction

Clay rich sedimentary formations are currently investigated in several European countries as potential host rocks for a radioactive waste repository: Callovo-Oxfordian argillite (F), Opalinus Clay (CH), Boom Clay (B), Boda Claystone (HU). In Germany, suitable (thick and homogeneous) claystone formations can be found both in Northern (Lower Cretaceous and the Middle and Lower Jurassic) and Southern Germany (Middle Jurassic) [1]. In general, clayrocks can be characterized as fine-grained porous materials, mainly composed of clay minerals (illite, smectite, kaolinite), carbonate phases (calcite, dolomite), together with accessory mineral phases (pyrite, feldspar, quartz) and organic matter [2]. Due to the small hydraulic conductivity ( $10^{-14} - 10^{-13}$  m/s) diffusion is the main transport mechanism for solute contaminants in argillaceous rocks. For neutral and charged tracers, the diffusive transport (i.e. the effective diffusion coefficient  $D_e$ ) was observed to decrease for cations > neutral species > anions [3-6]. The reduced diffusivity of anionic compared to neutral species is well understood and can be related to a repulsive interaction of anions with the negatively charged clay surfaces leading to a reduced accessibility of the total pore space (*anion exclusion*). In contrast, cationic species sorbing by cation exchange are able to move through the whole pore space. Although being electrostatically attracted to the negatively charged clay surfaces, cations retain their mobility and the higher effective diffusion coefficient compared to HTO can be related to their enrichment in the interlayer (*surface diffusion*). Values for  $D_e$  were observed to decrease for cationic and increase for anionic tracers with increasing ionic strength [5,6], thus indicating that an electrostatic shielding of the surface charge (by an increase in ionic strength) is affecting the diffusion properties of charged solutes. An interesting question related to this subject is, how these properties are altered if negative surface charge is occupied by a high selective index complex. Organic ligand-metal complexes such as copper-ethylenediamine  $\text{Cu}(\text{en})_2^{2+}$  are reported to block effectively the planar surface charge in montmorillonites and reduce considerably the access of alkaline-earth metals to these exchange sites [7,8]. Thus,  $\text{Cu}(\text{en})_2^{2+}$  exchanged montmorillonite and illite were prepared, the former representing low-charged clays capable of swelling, while the latter is taken as a model for high-charged clay minerals with collapsed interlayers not accessible for solutes. Subsequently multi-tracer (HTO,  $^{36}\text{Cl}^-$  and  $^{85}\text{Sr}^{2+}$ ) diffusion was performed in cooperation with the Laboratory for Waste Management (LES), Paul Scherrer Institute, Villigen PSI,

Switzerland within a delegation in the framework of the EU Project CP CatClay.

### Experimental

In case of illite, 13.5 mmol  $\text{CuSO}_4 \cdot 5\text{H}_2\text{O}$  were dissolved in 2 L Milli-Q- $\text{H}_2\text{O}$ . Subsequently 30 mmol ethylenediamine was added and the mixture stirred for 1 h. The solution was transferred in a 2 L Kautex bottle containing 100 g Na-illite (CEC= 225 meq/kg) and shaken end-over-end overnight. Hereafter, the supernatant was separated and discarded by a gentle centrifugation (2000 rpm for 1h) and the solid was suspended in a neutral Milli-Q- $\text{H}_2\text{O}$  (pH 7). This procedure was repeated until the solution was colourless. The fine grained material was obtained by freeze drying and sieving (< 63  $\mu\text{m}$ ). In case of montmorillonite the experimental procedure was adapted to the higher CEC of Na-montmorillonite (CEC= 850 meq/kg): 51.5 mmol Cu(II), 2 L MilliQ water, 112.2 mmol ethylenediamine. After compacting (bulk dry density  $\rho_{\text{db}} \sim 1700 \text{ kg m}^{-3}$ ) the samples were pre-equilibrated against 0.1 M  $\text{NaClO}_4$  /  $10^{-4}$  M  $\text{KCl}$  /  $5 \cdot 10^{-3}$  M MES solutions (pH 5) from both sides. After one month the solutions were replaced against new ones. The solution in one reservoir was spiked with HTO,  $^{36}\text{Cl}$  (both at  $\sim 1000 \text{ Bq/cm}^3$ ) and  $^{85}\text{Sr}$  ( $\sim 100 \text{ Bq/cm}^3$ ), while the other one contained the background electrolyte solely (representing the high (HCR)- and low-concentration (LCR) reservoir, respectively). The diffusion experiments were performed according to published procedures [9]. In deviation to [9], diffusion cells with advective flushed filters were used (for details see [10]).

### Results and Discussion

Fig. 1 shows the results for the diffusion of HTO (a),  $^{36}\text{Cl}^-$  (b) and  $^{85}\text{Sr}^{2+}$  (c) through  $\text{Cu}(\text{en})_2\text{-mnt.}$ , both as flux ( $\text{Bq} \cdot \text{d}^{-1} \cdot \text{cm}^{-2}$ ) and evolution of activity ( $\text{Bq} \cdot \text{g}^{-1}$ ) in the high concentration reservoir. The data are also representative for  $\text{Cu}(\text{en})_2\text{-il.}$  For HTO and  $^{36}\text{Cl}^-$  a steady state (indicated by a constant flux) is reached after  $\sim 8$  days, while for  $^{85}\text{Sr}^{2+}$  the flux is still increasing after 32 days. Due to a limited experimental time, the experiments were terminated after this period.

In case of a steady state (indicated by a constant flux), the effective diffusion coefficient  $D_e$  and the rock capacity factor  $\alpha$  can be calculated by an analytical method (for details see [9]).

The rock capacity factor is defined as

$$\alpha = \varepsilon + \rho \cdot K_d \quad (1)$$

with  $\varepsilon$  the porosity (-),  $\rho$  the bulk dry density ( $\text{kg} \cdot \text{m}^{-3}$ ) and  $K_d$  the sorption coefficient. For non-sorbing tracers (i.e. HTO and  $\text{Cl}^-$ )  $K_d$  equals 0 and  $\alpha = \varepsilon$ .

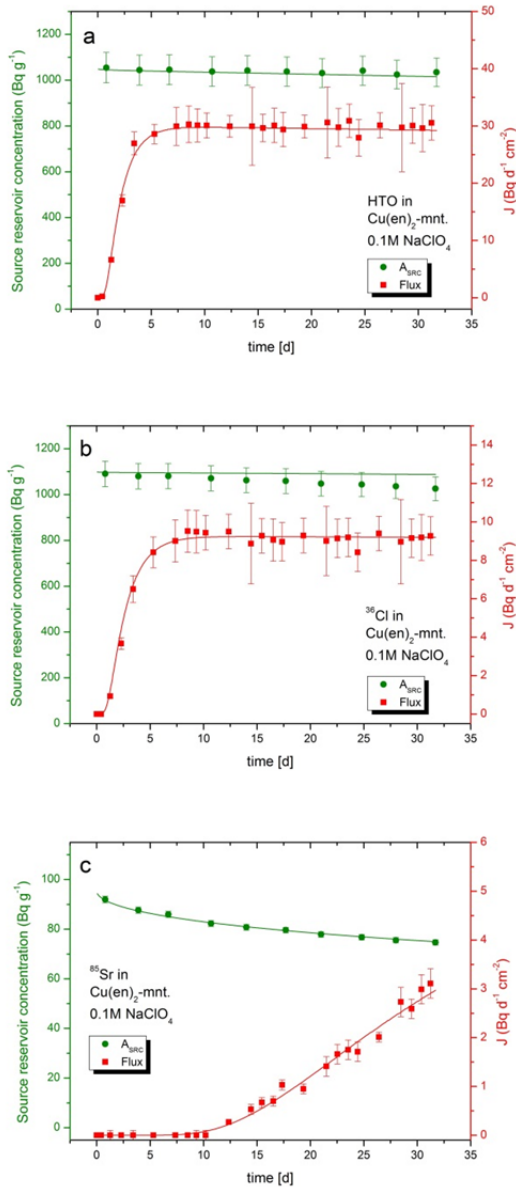


Fig. 7: Diffusion of HTO (a)  $^{36}\text{Cl}^-$  (b) and  $^{85}\text{Sr}^{2+}$  (c) through compacted  $\text{Cu}(\text{en})_2$ -montmorillonite (background electrolyte 0.1M  $\text{NaClO}_4$ ) as mass flux in the low concentration reservoir ( $J$ ) and evolution of the source reservoir concentration. The solid lines are the best fit parameter (Tab. 1).

Tab. 1: Summary of  $D_e$  ( $\text{m}^2 \cdot \text{s}^{-1}$ ) and  $\alpha$  (-) values for HTO,  $^{36}\text{Cl}^-$  and  $^{85}\text{Sr}^{2+}$  in  $\text{Cu}(\text{en})_2$ -illite and -montmorillonite at a bulk dry density ( $\rho_{\text{db}}$ ) of  $1700 \text{ kg} \cdot \text{m}^{-3}$ , together with literature data for the Na-exchanged clays.

Tracer	$\text{Cu}(\text{en})_2$ -illite		Na-illite		$\text{Cu}(\text{en})_2$ -mnt.		Na-mnt.	
	$D_e$	$\alpha$	$D_e$	$\alpha$	$D_e$	$\alpha$	$D_e$	$\alpha$
HTO	$1.76 \times 10^{-10}$	-0.42	$2.0 \pm 0.2 \times 10^{-10a}$	$0.43 \pm 0.20^a$	$2.1 \times 10^{-11}$	0.41	$3.8 \pm 0.7 \times 10^{-11b}$	$0.38 \pm 0.05^b$
	$1.86 \pm 0.19 \times 10^{-10}$	$0.44 \pm 0.13$			$3.35 \times 10^{-11}$	0.39		
$^{36}\text{Cl}$	$6.6 \times 10^{-11}$	0.33	$5.4 \times 10^{-11}$	0.20	$9.8 \times 10^{-12}$	0.14	$7.2 \pm 0.8 \times 10^{-14c}$	$0.019 \pm 0.002^c$
	$6.45 \pm 0.87 \times 10^{-11}$	$0.32 \pm 0.10$			$9.82 \times 10^{-12}$	0.14		
$^{85}\text{Sr}$	$1.56 \pm 0.61 \times 10^{-10}$	$40.9 \pm 20.0$	$1 \times 10^{-9a}$	$90^a$	$9.66 \pm 5.5 \times 10^{-11}$	$20.3 \pm 15.8$	-	-

Values in normal type have been calculated using an analytical method [9]. Values in italics are the best-fit parameter using the flux data. <sup>a</sup> [10],  $\rho_{\text{db}} = 1700 \text{ kg} \cdot \text{m}^{-3}$ ; <sup>b</sup> [11],  $\rho_{\text{db}} = 1564 \text{ kg} \cdot \text{m}^{-3}$ , salinity 1.0 M  $\text{NaClO}_4$ ; <sup>c</sup> [5]  $\rho_{\text{db}} = 1900 \text{ kg} \cdot \text{m}^{-3}$ , salinity 0.1 M  $\text{NaClO}_4$ .

Values for  $D_e$  and  $\alpha$  determined analytically are only robust, if the boundary conditions  $c_{\text{HCR}} \sim \text{const.}$  and  $c_{\text{LCR}} \sim 0$  are fulfilled throughout the experiment. For the present work, this is true in case of  $\text{Cu}(\text{en})_2$ -mnt., where the loss in activity in the high-concentration reservoir with respect to the initial activity was 1.9% for HTO and 0.6% for  $^{36}\text{Cl}^-$ . However, a decrease in activity of 13.4% and 5.9% (HTO and  $^{36}\text{Cl}^-$ , respectively) is observed for  $\text{Cu}(\text{en})_2$ -il., which can lead to biased values for  $D_e$  and  $\alpha$ . Therefore,  $D_e$  and  $\alpha$  were also determined by modelling the experimental data by numerical methods, where the above mentioned restrictions are not applicable (for details see [5]). The results for  $\text{Cu}(\text{en})_2$ -il. and  $\text{Cu}(\text{en})_2$ -mnt. together with literature data for Na-il. and Na-mnt. are summarized in Table 1.

For HTO, the values for the effective diffusion coefficient  $D_e$  and  $\alpha$  for both  $\text{Cu}(\text{en})_2$ -il. and  $\text{Cu}(\text{en})_2$ -mnt. are in good agreement with literature data on Na-il. and Na-mnt., indicating that the geometrical properties (i.e. tortuosity, constrictivity) were not altered by  $\text{Cu}(\text{en})_2^{2+}$ -exchange. In case of  $\text{Cu}(\text{en})_2$ -mnt., the effective diffusion coefficient as well as the porosity for  $^{36}\text{Cl}^-$  are significantly higher compared to the  $\text{Na}^+$ -exchanged mineral. While  $\epsilon$  increased by a factor of  $\sim 7$ ,  $D_e$  changed by two orders of magnitude. This effect is also apparent though less pronounced in case of  $\text{Cu}(\text{en})_2$ -il. For  $^{85}\text{Sr}^{2+}$ , an decrease in  $D_e$  of one order of magnitude is apparent in case of  $\text{Cu}(\text{en})_2$ -il., with a value similar to the one determined for neutral HTO. An analogous result is not observed in case of  $\text{Cu}(\text{en})_2$ -mnt., where  $D_e$  for  $^{85}\text{Sr}^{2+}$  is found to be higher than for HTO. Unfortunately, literature data on  $\text{Sr}^{2+}$  diffusion in homoionic montmorillonites are scarce, and not available for highly compacted systems to the best knowledge of the authors.

These results indicate a reduced influence of the negative surface charge, affecting the transport properties of cationic and anionic tracers. In detail,  $D_e$  and  $\alpha$  increase for  $^{36}\text{Cl}^-$ , as anions are no longer repelled from the vicinity of the clay surface. An inversed trend is apparent for  $^{85}\text{Sr}^{2+}$  in  $\text{Cu}(\text{en})_2$ -il., where  $D_e$  and  $\alpha$  decrease by  $\text{Cu}(\text{en})_2^{2+}$ -exchange, pointing to a distribution of cations in the whole pore space (as indicated by the lower  $\alpha$  values).

This effect is more apparent for montmorillonites, where diffusion properties of solutes are mainly influenced by interlayer water. As these interlayers are not accessible in case of illite, the diffusion only takes place in the external layer water and water present in the free pore space [12]. González Sánchez et al. [12] reported that the amount of water layers between two clay particles is smaller for Na-montmorillonite compared to Na-illite (~2 and ~9, respectively). Since only the water molecules in the first nanometres next to the clay surface (~2 water layers) are affected by the clay-water interface [13], the effect on  $\text{Na}^+ \leftrightarrow \text{Cu}(\text{en})_2^{2+}$ -exchange on the diffusion properties is more pronounced in case of montmorillonite compared to illite.

### Summary

Our results on the multi-tracer diffusion experiments in  $\text{Cu}(\text{en})_2$ -illite and -montmorillonite show a significant change of the transport parameter for charged solutes. The observed trends are in line with a (partially) neutralized clay surface.

### References

- [1] P. Hoth et al., *BGR-Bericht* 2007, p. 94.
- [2] Altmann, S. et al. *Applied Geochemistry*, 2012. **27(2)**: p. 463-478.
- [3] Wersin, P. et al., *Applied Geochemistry*, 2008. **23(4)**: p. 678-691.
- [4] Van Loon, L.R. et al., *Applied Geochemistry*, 2007. **22(11)**: p. 2536-2552.
- [5] Glaus, M.A. et al., *Environmental Science & Technology*, 2007. **41(2)**: p. 478-485.
- [6] Glaus, M.A. et al., *Geochim. Cosmochim. Acta*, 2010. **74(7)**: p. 1999-2010.
- [7] Maes, A. et al., *Journal of the Chemical Society, Faraday Transactions 1: Physical Chemistry in Condensed Phases*, 1978. **74(0)**: p. 182-189.
- [8] Maes, A. and Cremers, A., *Journal of the Chemical Society, Faraday Transactions 1: Physical Chemistry in Condensed Phases*, 1979. **75(0)**: p. 513-524.
- [9] Van Loon, L.R. et al., *Journal of Contaminant Hydrology*, 2003. **61**: p 73-83.
- [10] Glaus, M.A. et al., *Diffusion of moderately and strongly sorbing radionuclides in compacted illite*, 2012: [www.catclay.org](http://www.catclay.org).
- [11] Glaus, M.A. et al., *Environmental Science & Technology*, 2013. **47**: p. 11522-11527.
- [12] González Sánchez, F. et al., *Applied Geochemistry*, 2008. **23(12)**: p. 3840-3851.
- [13] Sposito, G. and Prost, R., *Chemical Reviews*, 1982. **82(6)**: p. 553-573.

## 4.4 Retention of radionuclides by secondary phase formation

S. Hofmann\*, L. Temgoua, N. Finck, K. Dardenne, T. Schäfer, H. Geckeis

In co-operation with:

M. Schmidt<sup>a</sup>, T. Stumpf<sup>a</sup>, P. Fenter<sup>b</sup>, J. Stubbs<sup>c</sup>, P. Eng<sup>c</sup>

<sup>a</sup> Institute for Resource Ecology, Helmholtz Center Dresden-Rossendorf (Germany), <sup>b</sup> Chemical Science and Engineering Division, Argonne National Laboratory, Argonne, IL (USA), <sup>c</sup> University of Chicago, Center for Advanced Radiation Sources, Chicago, IL 60637 (USA).

\* present address: Institute for Resource Ecology, Helmholtz Center Dresden-Rossendorf (Germany).

### Introduction

Secondary phases may form upon contact of the High Level nuclear Waste (HLW) matrix with ground water over geological time scales. Such alteration phases represent a significant retention potential for the radiotoxic and long-lived radionuclides (RNs), acting as an additional barrier to the migration of RN. The presence of RN released from the corroding waste matrix during the (co)precipitation of such neoformed phases in aqueous environment opens the possibility to structurally incorporate them in the bulk solid. The formation of such solid solutions may result in an effective long-term immobilization. The molecular scale incorporation mechanism of actinides and long-lived fission products in selected mineral phases is currently investigated at INE. The combination of advanced complementary spectroscopic techniques provides such molecular scale information. Together with quantum chemical calculations, the ultimate goal is to obtain a thermodynamic description of the solid solution formation.

### Structure of the calcite-water interface in presence of NaNO<sub>3</sub>

The interaction of trivalent lanthanides and actinides with the mineral phase calcite is of high importance for the safety assessment of deep geological repositories for high level nuclear waste (HLW). A strong influence of NaNO<sub>3</sub> upon calcite surfaces and hence their reactivity has been reported recently [1]. A soft surface layer, seen by high resolution AFM and SEM, is formed in presence of NaNO<sub>3</sub> even at trace concentrations. The formation of this surface layer governs surface reactions with Ln(III) and An(III). To further study the surface structure, *in situ* surface X-ray scattering techniques have been applied.

By means of high-brilliance X-ray beams from a synchrotron radiation facility, studies of solid/liquid interfaces can be conducted. Using crystal truncation rod (CTR) measurements, structural and electronic properties of surfaces can be obtained and changes due to ion adsorption or morphological transformations can be observed. For this experiment, natural calcite single crystals have been freshly cleaved and put into contact with calcite saturated solution containing 1 mM NaNO<sub>3</sub>. The crystals are fixed on a sample holder and measured after one, three, 30 and 330 hours of contact time. These studies are performed at beamline 13-IDC, Advanced Photon Source, Argonne National Laboratory.

The hydration structure of the calcite (104) solution interface in presence of NaNO<sub>3</sub> with increasing contact times is studied by specular CTR measurements. Reaction solutions contained 3 mM NaNO<sub>3</sub> and 10  $\mu$ M Y(NO<sub>3</sub>)<sub>3</sub>. The CTR data were collected by measuring X-ray reflectivity, the fraction of the incident X-ray beam reflected by the calcite (104) surface, as a function of vertical momentum transfer  $Q = 4\pi/\lambda \sin(2\theta/2)$ , where  $2\theta$  is the incident angle and  $\lambda$  is the wavelength of the monochromatic X-ray beam, at fixed photon energy ( $E$ ) [2].

The CTR data from the first three scans presented in Fig. 1 (red, black and blue data points) are very similar in shape and show no changes of intensity with increasing contact time within measurement accuracy. Intensity values vary up to 5 orders of magnitude with highest values close to corresponding Bragg reflections ( $Q = 2, 4, 6 \text{ \AA}^{-1}$ ). The similarities between these samples and calcite references from the literature [3] imply that the effect caused by NaNO<sub>3</sub> does not change surface reflectivity and hence the surficial structure significantly within 30 hours. However, after 330 hours (two weeks, green data points) contact time, the calcite (104) surface shows different reflectivity behavior. The flanks near the Bragg peaks, especially at  $Q \sim 2$  and  $4 \text{ \AA}^{-1}$ , drop off more rapidly which can be interpreted directly as an increase in surface roughness.

The interfacial structure is determined after normalization of the CTR data and consecutive fitting of the atomic structure of the surface. The resulting electron densities can be plotted as a function of atomic distances with sub- $\text{\AA}$  resolution. A representative electron density profile for the unchanged calcite surface is presented in Fig. 2. The data are fitted by surface relaxation of the first two calcite layers with only water adsorbed to the surface. This interfacial structure is in good agreement with the literature [3, 4].

The change in reflectivity after 330 hours corresponds to significant changes in the interfacial structure. We observe a broad surface species without internal structure. The layer thickness of  $\sim 8 \text{ \AA}$  is also in good agreement with AFM and SEM results. This approach results in a good fit to the data and consequently gives account of the non-crystalline surface layer whose formation is induced by the presence of NaNO<sub>3</sub>. It should be noted that the angles of the first CaCO<sub>3</sub> layer are somewhat distorted in comparison to the underlying layers of the calcite crystal, showing that stronger surface relaxation is necessary for con-

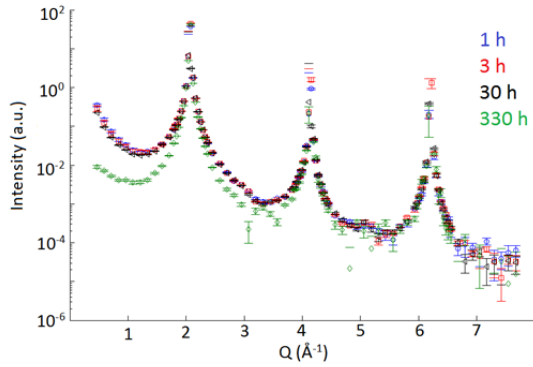


Fig. 1: Electron density profile of calcite in contact with  $\text{NaNO}_3$  for 1, 3, 30 and 330 h.

vergence of this system. This destabilisation might be the reason for the partial dissolution observed by microscopic techniques.

Trace amounts of  $\text{NaNO}_3$  have a significant influence on the calcite surface and hence its interactions with metal ions such as adsorption and incorporation. The effect seen by AFM in [1] has been reproduced by surface-sensitive X-ray measurements (CTR). Also the observation of frayed and rounded step edges, supposedly caused by a partial dissolution of the  $\text{CaCO}_3$  matrix, is supported by the necessity of strong surface relaxation for CTR fitting. Due to non-observable sorption of trivalent yttrium with this experimental setup, upcoming studies will concentrate upon the interaction of metal ions with the changed surficial structure including the location of e.g.,  $\text{Y}^{3+}$ ,  $\text{Am}^{3+}$  within the found surface layer. For this, resonant anomalous X-ray measurements (RAXR) will be performed providing more detailed and element-specific information.

### Factors influencing the nucleation kinetics of celestite

The nucleation of celestite ( $\text{SrSO}_4$ ) was studied for supersaturation ratios ( $\Omega$ ) ranging from 1.26 to 31.63, temperatures (T) between 278.15 and 348.15 K and ionic strength (I) up to 3 mol/l. Induction times ( $t_{\text{ind}}$ ) were determined by laser induced breakdown detection (LIBD). Interfacial tension,  $\gamma_{\text{s,hom}}$ , of 27 mJ/m<sup>2</sup>

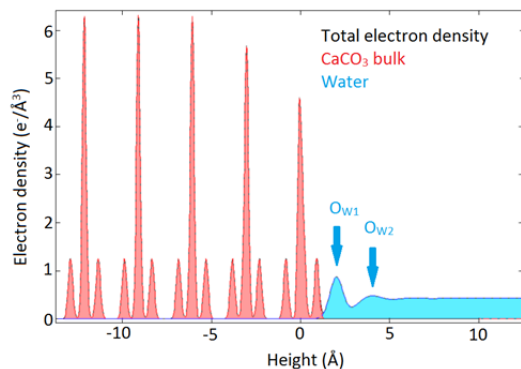


Fig. 2: Electron density profile of the sample in contact with  $\text{NaNO}_3$  for three hours. Ca, C and O in red and surface water structure in blue. Adsorbed first and second water layer indicated by arrows.

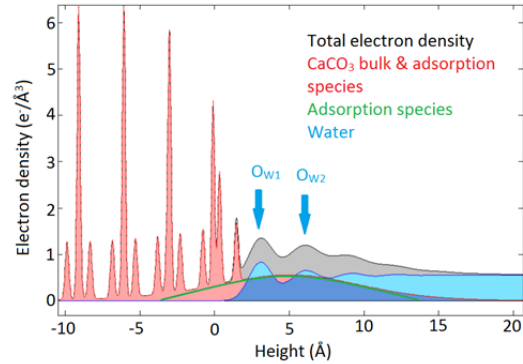


Fig. 3: Electron density profile of the sample in contact with  $\text{NaNO}_3$  for 330 hours. Adsorbed first and second water layer indicated by arrows.

was determined for the homogeneous nucleation of celestite.  $t_{\text{ind}}$  was shortened by the increase of supersaturation, ionic strength, temperature and by the presence of spherical glass particles as heterogeneous seed material. Contrarily, dissolved silicon acts as a nucleation inhibitor, thus contributing to the prolongation of induction times.

#### Effect of solution supersaturation

Experimental data show two different straight lines (Fig. 4). This behavior was also reported for the homogeneous precipitation of calcium carbonate [5], nickel ammonium sulfate [6] and strontium sulfate [7]. The change of slope at  $(\ln \Omega)^{-2} \sim 0.3$  corresponds to the threshold between homogeneous and heterogeneous nucleation [8].

At low  $\Omega$ , the nucleation is predominantly heterogeneous whereas at high  $\Omega$  homogeneous nucleation prevails. From literature data, it is known that  $\gamma$  decreases with decreasing  $\Omega$  (see Fig. 5). Our data expands the data found in the literature to lower supersaturations.

#### Effect of ionic strength

In general, for solutions with  $I < 0.1$  M, the effect of the background electrolyte depends only on the ionic strength and not on the nature of the electrolytes ions. At high ionic strength, this independence with respect to the nature of electrolytes disappears [9]. Factors contributing to the electrolyte effect derive from the

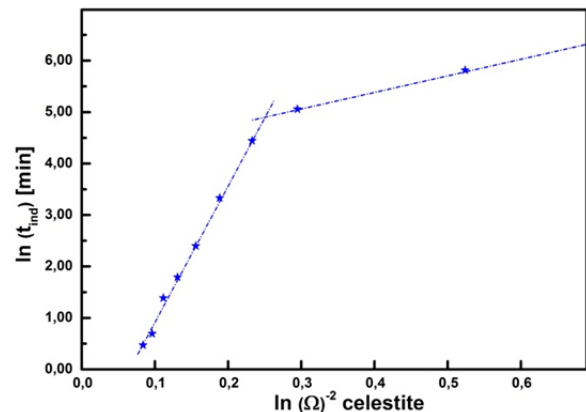


Fig. 4: Induction period as function of supersaturation at 22°C.

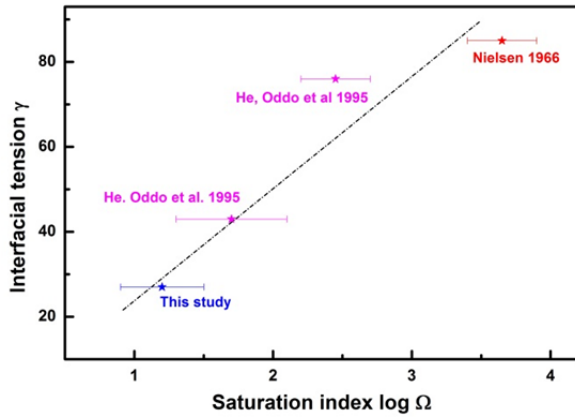


Fig. 5: Interfacial tensions calculated for celestite as a function of solution supersaturation.

electrostatic attractive and repulsive forces that exist between the ions of an electrolyte and the ions involved in an equilibrium. The direct consequence of these forces is the surrounding of each ion from the dissociated reactant by a shell of solution containing a slight excess of electrolyte ions of opposite charge.

At lower ionic strength, the induction times decrease with increasing ionic strength. This dependence is less pronounced at  $I > 1.0$  M sodium chloride. The morphology of precipitates is also influenced (Fig. 6). The characterization of the precipitates is ongoing.

#### Effect of temperature

The effect of temperature on the induction times of celestite nucleation was studied at  $\Omega = 7.94$ . Fig. 7 shows a linear relationship between the logarithms of  $t_{ind}$  and the inverse of the absolute temperature. The size of crystals increase with increasing temperature (Fig. 8).

#### Effect of dissolved silicon

The effect of dissolved silicon on the crystallization of

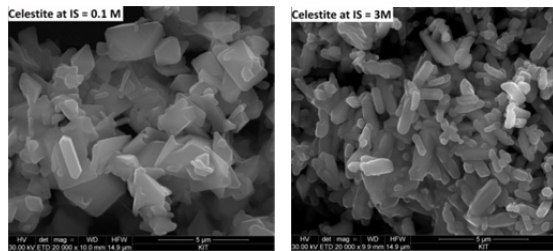


Fig. 6: SEM of celestite at  $I = 0.1$  M (left) shows orthorhombic crystals while peanut-like crystals are observed at 3.0 M (right).

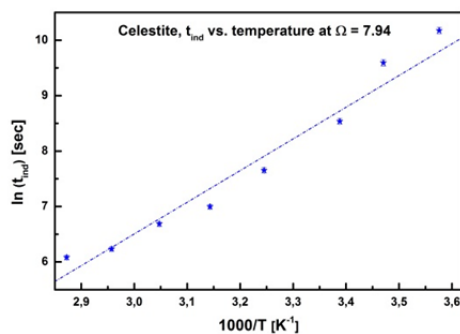


Fig. 7: Effect of temperature on  $t_{ind}$  of celestite.

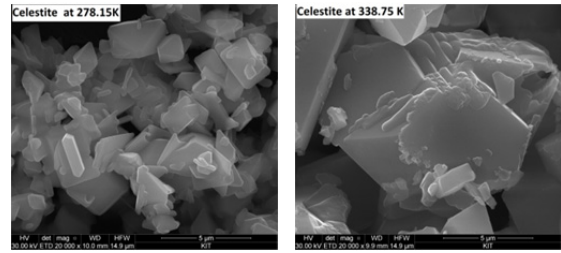


Fig. 8: SEM of homogeneously precipitated celestite at 278.15 K (left) and 338.15 K (right).

$\text{SrSO}_4$  was reported by Pina et al. [10]. In this study, we quantify the effect of dissolved silicon on the nucleation kinetics of  $\text{SrSO}_4$  for contents up to 1.5 ppm.

Results of the experiments are plotted in Fig. 9. At  $[\text{Si}] < 0.8$  ppm, the effect of dissolved silicon can be neglected. We observed an inhibition of nucleation at  $[\text{Si}] > 1$  ppm. In general, the inhibition of nucleation results from an increase in the interfacial crystal-solution free energy due to the modification of the crystal surface properties by the inhibiting agents. Such a modification can occur by adsorption of the inhibitors onto the crystal surfaces or by their incorporation into the crystal structure [10].

#### Effect of heterogeneous seeding

Different amounts of seeds were added to freshly prepared supersaturated solutions and the changes in induction times recorded. Experimental data are plotted in Fig. 10. A linear relationship is observed between  $t_{ind}$  and the surface of seeds. At lower  $\Omega$ , where the heterogeneous nucleation prevails, the promoting effect of seeding material on nucleation is more pronounced compared to areas where homogeneous nucleation plays an important role as can be seen from the slopes of the linear interpolations. Furthermore, the critical supersaturation state is lowered in the presence of glass particles.

#### Outlook

The experimental determination of induction times is the fundament to establish reliable predictive modeling hypotheses of secondary phases formation in pores media of the host rock in deep geological repositories for nuclear waste. The data determined experimentally can be implemented in codes for geochemical calcula-

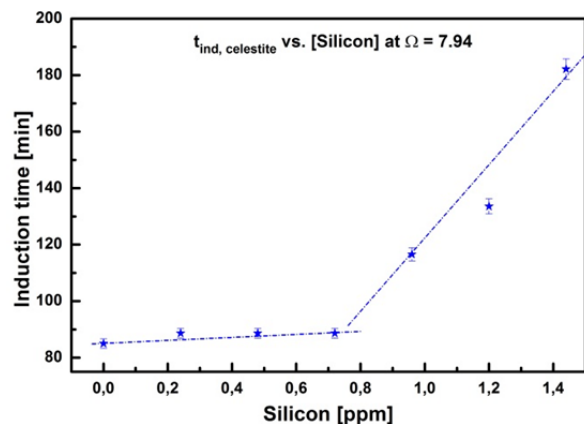


Fig. 9: Inhibition of celestite precipitation in the presence of dissolved silicon.

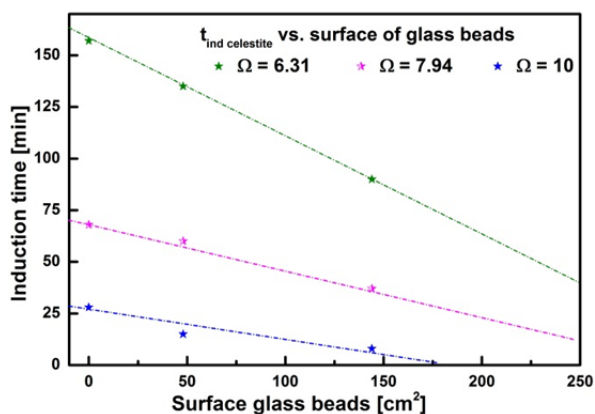


Fig. 10: Induction times of celestite as function of surface area of the heterogeneous seed material (glass beads).

tions (e.g. in the case of reactive transport modelling). Experimental results demonstrate that the mechanism of nucleation depends strongly on the supersaturation state of the solution. Further, the ionic strength, temperature increase and use of glass beads as seed was found to promote nucleation of celestite. However, many additives present in natural pore water, such as silicon, act as inhibitors thus increasing the induction times of nucleation.

### Yttrium retention by clay minerals: structural investigation

Clay minerals may play an important role in the safe disposal of HLW. Depending on the concept, the waste disposal site may be located in clay rock and the retention properties of the engineered barrier may be improved by using bentonite, which is mostly made of Al-rich smectite. Furthermore, hectorite, an Mg-rich smectite, has been identified in HLW glass corrosion experiments [11]. RN released from the waste matrix may be retained either by surface adsorption onto such secondary phases and/or by entrapment in the bulk structure.

The retention of yttrium by hectorite was investigated. Trivalent yttrium having a size between that of Lu(III) and Eu(III), was used as surrogate for trivalent actinides. Previous data showed that the smaller Lu(III) can occupy clay-like octahedral lattice site [12], and data for Eu(III) showed that very little amount can certainly enter the structure [13]. Yttrium adsorption and coprecipitation experiments were carried out and the samples were analyzed by XAS to elucidate the retention mode(s).

#### Experimental

Hectorite was crystallized from a brucite precursor [12] precipitated in the presence of Y(III) (sample YcopHec). Separately the aqua ions were adsorbed on pure hectorite (sample YadsHec) and a brucite precursor (YcopBru) was prepared under identical conditions as in YcopHec. XRD data indicated that the samples consist either of brucite (YcopBru) or smectite (YcopHec). These samples were prepared as oriented films to collect polarized Y K-edge XAS data [12] at various angles ( $\alpha$ ) between the layer plane and the electric field of the X-ray beam [12]. Powder XAS

data were collected for the references Y(III)<sub>aq</sub>, Y<sub>2</sub>O<sub>3</sub>, Y(OH)<sub>3</sub> and Ycarbo (synthesis adapted from [14]).

#### Results and discussion

The XANES (X-ray absorption near-edge structure) regime in a XAS experiment is dependent on the local environment (structure, geometry, valence...) and the features can be used as fingerprint. The data collected for the references (Fig. 11) exhibit all distinct features. These are also different from those of the samples under investigation, meaning that the samples do not contain any of the reference phases. Furthermore, the polarized data exhibit a significant angular dependence, pointing to an anisotropic Y chemical environment. This can be explained by the presence of several atomic shells having different orientation. This result also attests for the quality of the textured samples.

Accordingly, the Fourier transforms (FT) exhibit a significant angular dependence (Fig. 12). The amplitude and sometimes the position of the FT contribution varies with  $\alpha$ . This attests for the presence of several atomic shells having distinct orientations and corroborates the conclusions of the XANES data.

Information on the chemical environment was provided by the fits to the EXAFS data. Yttrium is 5- to 6-fold coordinated by O atoms in YcopBru and ~6 Mg atoms are detected as next nearest neighbors. The types of neighbors, the coordination numbers and the angular dependence strongly point to Y located in an octahedral brucite-like environment.

The Y chemical environment changed upon hectorite crystallization. The first shell consists in two O subshells and Mg atoms are detected at a distance

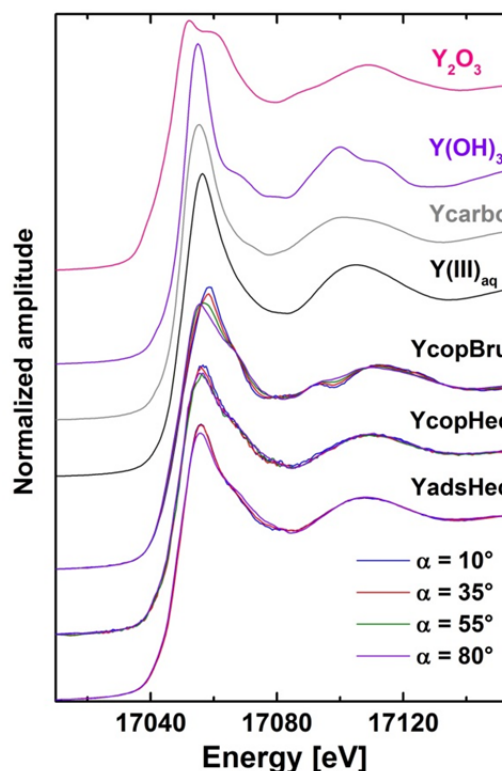


Fig. 11: Yttrium K-edge XANES of the reference compounds and of the samples collected at various angles.

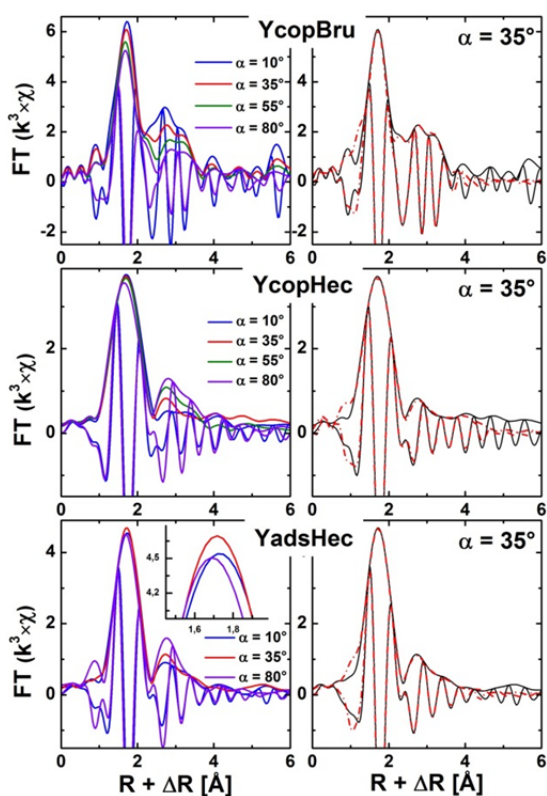


Fig. 12: Polarized Fourier transforms of the three samples (left) with the fit to the data collected at 35° (right).

similar as in brucite, but with lower coordination numbers. These data suggest a more constrained lattice site compared to brucite, and a Li(I) substitution for Mg(II) for local charge balance because Li is too light to be detected by XAS, respectively. Furthermore, the variation in Mg coordination number with  $\alpha$  suggests that Y is located in the octahedral sheet. In contrast, Y forms inner-sphere surface complexes at the platelet edges in YadsHec. The Y polyhedra share edges with Mg octahedra and are tilted off the clay median plane. This behavior is similar to what has been reported for Lu [12].

#### Conclusion – outlook

The present data show that Y(III) can be incorporated at clay octahedral sites. The actinides which are of similar size may then also be retained by structural retention in smectite secondary phases. Such information is of paramount importance for safety performance assessment because the strength of the (im)mobilization directly depends on the retention mode. However, the present data do not allow con-

cluding on the stability of such neoformed phases under repository relevant conditions. Nevertheless, data could show that Lu is still homogeneously distributed in the colloidal fraction mobilized from the “bulk” hectorite after two years of contact time [15]. The analysis of the colloidal fraction mobilized from YcopHec indicates that Y is also structurally retained in the hectorite nanoparticles (see Chapter 6.3 of this report). This indicates that the colloids correspond to miniatures of the bulk material.

#### References

- [1] Hofmann, S., et al., *Geochimica Et Cosmochimica Acta*, 2014. **125**(1): p. 528-538.
- [2] Fenter, P.A., *X-ray reflectivity as a probe of mineral-fluid interfaces: A user guide*, in *Applications of Synchrotron Radiation in Low-Temperature Geochemistry and Environmental Sciences*, P.A. Fenter, et al., Editors. 2002. p. 149-220.
- [3] Fenter, P. and Sturchio, N.C., *Calcite (1 0 4)–water interface structure, revisited. Geochimica Et Cosmochimica Acta*, 2012. **97**(0): p. 58-69.
- [4] Heberling, F., et al., *Structure and reactivity of the calcite–water interface. Journal of Colloid and Interface Science*, 2011. **354**(2): p. 843-857.
- [5] Söhnle, O. and Mullin, J.W., *Journal of Crystal Growth*, 1978. **44**(4): p. 377-382.
- [6] Mullin, J.W. and Ang, H.M., *Powder Technology*, 1974. **10**(3): p. 153-156.
- [7] Malollari, I.X. et al., *Journal of Crystal Growth*, 1995. **155**(3-4): p. 240-246.
- [8] Lacmann, R., *Chemie Ingenieur Technik*, 1998. **70**(11): p. 1468-1468.
- [9] IUPAC. 1994, 66 1077. *Compendium of chemical terminology*. 2nd ed. (the "Gold Book")
- [10] Pina, C.M. and Tamayo, Á., *Geochimica Et Cosmochimica Acta*, 2012. **92**(0): p. 220-232.
- [11] Jollivet, P., et al., *Journal of Nuclear Materials*, 2012. **420**(1-3): p. 508-518.
- [12] Finck, N. et al., *Environmental Science & Technology*, 2009. **43**(23): p. 8807-8812.
- [13] Finck, N. et al., *Mineralogical Magazine*, 2012. **76**(7): p. 2723-2740.
- [14] Philippini, V. et al., *Journal of Solid State Chemistry*, 2008. **181**(9): p. 2143-2154.
- [15] Bouby, M. et al., *Mineralogical Magazine*, 2012. **76**(7): p. 2709-2721.

## 5 Applied studies: radionuclide retention in the multi-barrier system

Radionuclide retention in the multi-barrier system requires a wide variety of investigations using specific materials, approaches, methods, analytical techniques and models. The investigations presented in the following chapter cover the quantification of radionuclide mobilization and immobilization from spent nuclear fuel, Zircaloy and irradiated metals, from vitrified high level waste, and from cemented waste forms. With respect to emergency measures for the Asse salt mine, retention of radionuclides onto Sorel based backfill materials was analyzed. Furthermore, sampling was organized to extend such studies for the overlying rocks of the Asse salt dome.

The colloidal impact on radionuclide migration was studied with respect to the stabilization of polynuclear Pu(IV) species by humic acids, and by model systems, such as synthetic nanoparticles from (yttrium co-precipitated hectorite). Measurements of interaction forces between nanoparticles and mineral surfaces under various pH and metal ion concentrations contribute to deeper understanding of sorption processes.

Modelling studies include the simulation of thermo hydro mechanic (THM) processes in the near-field of a HLW disposal in rock salt as well as the simulation of flow and transport phenomena in crystalline host rocks. Coupled reactive modelling was applied for evaluation of long-term leaching experiments in order to quantify the effect of solution composition on diffusion processes as well as on sorption and diffusion processes in porous illite media investigating the effect of its intrinsic heterogeneity.

### 5.1 Highly radioactive waste forms

*E. González-Robles, M. Herm, N. Müller, M. Böttle, E. Bohnert, V. Metz, B. Kienzler*

#### Corrosion behaviour of spent nuclear fuel in high pH solutions

In Belgium, Boom clay is considered as host rock for disposal of high level wastes. For spent nuclear fuel (SNF) and vitrified HAW, a specific engineered barrier system the so-called "Supercontainer" was developed. With respect to SNF disposal, the "Supercontainer" comprises of containers of fuel assemblies in carbon steel overpacks, which are surrounded by an overpack of a Portland cement concrete buffer and an outer stainless steel envelope [1,2,3].

After re-saturation of the engineered barriers, the pore water composition will be altered by interactions with concrete. The altered pore water is simulated by a "young cement water with calcium (YCWCa)" solution (pH of 13.5) that represents a certain degree of concrete alteration. The YCWCa is composed mainly by KOH and NaOH, and a minor concentration of Na<sub>2</sub>SO<sub>4</sub>, Ca(OH)<sub>2</sub> and CaCO<sub>3</sub>.

Due to the slow corrosion rate of the canister materials under highly alkaline conditions [4], the SNF could come in contact with the evolved highly alkaline solution. In parallel, a certain H<sub>2</sub> partial pressure is formed by steel corrosion processes. Consequently, the aim of the experimental work is to study the corrosion behaviour of the UO<sub>2</sub> matrix of SNF in YCWCa in presence of externally applied H<sub>2</sub> overpressure.

#### Studied spent nuclear fuel

The studied SNF was irradiated during four cycles in the Gösigen pressurised water reactor located in Switzerland. During irradiation the SNF achieved an average burn-up of 50.4 GWd/tHM. The SNF was discharged in May 1989 that implies a cooling time of 22 years prior to start of the experiments. More details about the SNF can be found elsewhere [5,6].

#### Sample preparation and pre-treatment

SNF fragments were obtained by decladding the clad-ded pellet K11 which was previously leached during two years. The complete process followed is described in references [5,7].

Five of the fragments obtained from pellet K11 were selected, and denoted as F1, F2, F3, F4 and F5. The fragments were weighted and their surface area was derived from optical microscope images (Table 1).

After physical characterisations and prior to the leaching experiments, the fragments were submitted to a careful sample pre-treatment to remove potentially adhering fine particles. In a first step, the five fragments were immersed in 200 mL of 1x10<sup>-3</sup> M HCl over about 2 days. Afterwards, the SNF fragments were rinsed with Milli-Q-water to remove HCl and washed with 200 mL Milli-Q-water during 3 days. In a final step, the fragments were washed using 200 mL of fresh Milli-Q-water over 1 day.

**Tab. 1:** Physical characterisation of used SNF fragments.

Sample	F1	F2	F3	F4	F5
m (g)	0.136	0.225	0.174	0.169	0.205
V (cm <sup>3</sup> )	0.013	0.022	0.017	0.016	0.020
S <sub>a</sub> (m <sup>2</sup> )	2x10 <sup>-5</sup>	3x10 <sup>-5</sup>	2x10 <sup>-4</sup>	3 x10 <sup>-5</sup>	2x10 <sup>-5</sup>
*S <sub>spec</sub> (m <sup>2</sup> /g)	4x10 <sup>-4</sup>	4x10 <sup>-4</sup>	4x10 <sup>-4</sup>	5 x10 <sup>-4</sup>	3x10 <sup>-4</sup>
**S <sub>spec</sub> (m <sup>2</sup> /g)	5x10 <sup>-4</sup>	5x10 <sup>-4</sup>	4x10 <sup>-4</sup>	6x10 <sup>-4</sup>	4x10 <sup>-4</sup>

\*corresponds to roughness factor of 3.

\*\*corresponds to roughness factor of 3.5.

#### Experimental procedure

Leaching experiments with the fragments were conducted in autoclaves. In a multi-sampling experiment with fragment F1, samples were taken at different

time steps during a static period. Single point experiments with fragments F2, F3, F4 and F5 were sampled solely at the end of the static leaching period.

### Pre-leaching in YCWCa

The five fragments were submitted to pre-leaching under Ar atmosphere. This so-called “wash cycle” was carried out with the main objective to reduce the quantity of an early contribution of Cs coming from open fresh grain boundaries. Each SNF fragment was placed together with a Ti plate in an autoclave, which was flushed with Ar for about 30 min to remove air out of the vessel. Under constant Ar flux, the autoclave was filled with ~100 mL of YCWCa using a syringe. Pre-leaching of the fragments was carried out for 15 to 41 days. After pre-leaching, the complete solution was removed and analysed. Characteristics of the wash cycle are reported in Table 2.

**Tab. 2:** Duration and solution mass change of the pre-leaching “wash cycle”.

Exp.	Duration (days)	<sup>a</sup> Solution (g)	<sup>a</sup> Solution recovery (g)
F1	15	109.955	105.796
F2	15	108.641	104.698
F3	17	103.994	101.684
F4	41	101.761	100.525
F5	41	102.419	100.756

<sup>a</sup> The uncertainty of the value is ( $\pm 0.001$ ).

### Static leaching experiments

After the wash cycle, each autoclave was refilled with ~200 mL of fresh YCWCa solution by using the procedure described above. In the static leaching period a gas atmosphere of 92% Ar and 8% H<sub>2</sub> with a total pressure of 40 bar was applied (i.e. p<sub>H<sub>2</sub></sub> = 3.2 bar). In the multi-sampling experiment F1, gas and solution samples were taken after 127, 180, 253, 341 and 425 days. After each sampling, the remaining gas was purged with Ar, and afterwards the 92% Ar / 8% H<sub>2</sub> atmosphere was re-established within the autoclave. Gas and solution samples were taken at the end of the single point experiments F2, F3, F4 and F5 after 341, 252, 182 and 59 days, respectively. Table 3 presents the initial and the final mass of the leachant at the end of the static period of the five autoclave experiments.

**Tab. 3:** Duration and solution mass change of the static leaching period.

Exp.	Duration (days)	<sup>a</sup> Initial solution (g)	<sup>a</sup> Final solution (g)
F1	440	205.025	126.827
F2	341	205.532	200.187
F3	252	204.681	200.573
F4	182	201.986	191.520
F5	59	203.819	198.665

<sup>a</sup> The uncertainty of the value is ( $\pm 0.001$ ).

### Rinsing of reaction vessel

After recovering of the SNF sample and the remaining solution at the end of each experiment the autoclave walls were rinsed. In a first step the autoclave was

rinsed with Milli-Q water during 1 day. Afterwards, a second rinse of the autoclave was carried out with 5 M HNO<sub>3</sub> solution during 1 day. Aliquots of both rinsed solution were analysed. Detailed descriptions of sampling and analytical procedures are given elsewhere [8].

### Results and discussion

Following radioisotopes were studied: <sup>90</sup>Sr, <sup>99</sup>Tc, <sup>134</sup>Cs, <sup>137</sup>Cs, <sup>154</sup>Eu, <sup>155</sup>Eu, <sup>238</sup>U, and <sup>241</sup>Am.

### Fraction of inventory in the aqueous phase

The fraction of inventory in aqueous phase (FIAP) was calculated to quantify how much of the initial inventory of the SNF sample was released to the solution. The FIAP is plotted in Fig. 3 as function of the contact time for the multi-sampling experiment and the four single point experiments.

A comparison of the single point experiments shows that after relatively high FIAP values at 59 days, the FIAP of <sup>134</sup>Cs, <sup>137</sup>Cs and <sup>238</sup>U remains virtually constant at 252 and 341 days (Fig. 1a). The high initial release of <sup>238</sup>U is attributed to the presence of a oxidated layer. The <sup>90</sup>Sr FIAP of the short term experiment F5 (59 days) is slightly lower than the <sup>90</sup>Sr FIAP of the three longer single point experiments, which indicate a constant <sup>90</sup>Sr FIAP between 182 and 341 days. The FIAP of <sup>99</sup>Tc seems to decrease after long leaching time, as indicated by the relatively low <sup>99</sup>Tc FIAP in the long term experiment F2 (341 days).

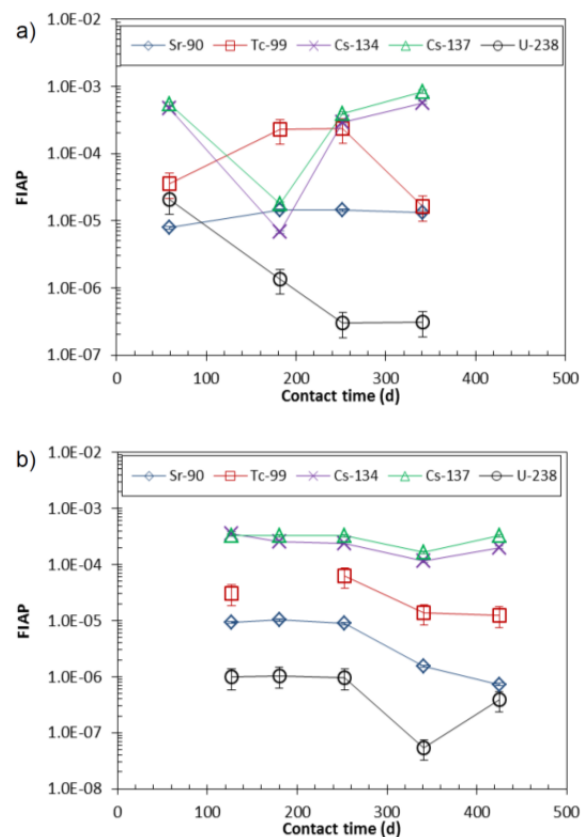


**Fig. 1:** FIAP as a function of contact time a) single point experiments F2, F3, F4, F5; b) multi-sampling experiment F1.

In the multi-sampling experiment F1, FIAP values of  $^{134}\text{Cs}$ ,  $^{137}\text{Cs}$  and  $^{238}\text{U}$  remain virtually constant over 440 days (Fig. 1b). In case of  $^{90}\text{Sr}$  and  $^{99}\text{Tc}$  the FIAP decrease after 253 days, which is attributed to sorption of these radionuclides onto the autoclave walls.

#### Sorption onto autoclave walls

Based on analyses of the solutions after rinsing of the autoclaves, amounts of radionuclides sorbed onto the vessel walls were determined. The amount of sorbed radionuclides (in %) relative to the total amount of released radionuclides (i.e. radionuclide inventories in leachant + radionuclide inventories in rinse solution) are given in Tab. 4. Since  $^{154}\text{Eu}$ ,  $^{155}\text{Eu}$  and  $^{241}\text{Am}$  concentrations in the leachant were below detection limit and they were determined solely in the rinse solution of the autoclave walls, the fraction of the sorbed fraction is 100%. Except the short term experiment F5, a considerable sorption of  $^{238}\text{U}$  (79 to 99%) and an increase of  $^{90}\text{Sr}$  sorption with time (4 to 82%) was observed in the experiments F1, F2, F3 and F4. Sorption values of  $^{99}\text{Tc}$  in the range of 11 to 56% scattered with time; relatively low sorption of  $^{134}\text{Cs}$  and  $^{137}\text{Cs}$  was observed (less than 11%).

The results suggest the necessity to take into account sorption for comparing the mobilized nuclides in the different experiments and for calculating the dissolution rate and fractional release rate.

**Tab 4:** Radionuclide sorption (%) onto the autoclave walls determined at the end of the experiments.

Exp.	F5	F4	F3	F2	F1
<sup>a</sup> Time (d)	100	223	269	356	440
$^{90}\text{Sr}$	10	4.1	8.2	44	82
$^{99}\text{Tc}$	56	31	26	46	11
$^{134}\text{Cs}$	0.29	<sup>a</sup> d.l.	0.35	0.25	7
$^{137}\text{Cs}$	0.40	1.5	0.16	0.70	10
$^{154}\text{Eu}$	—	100	100	100	100
$^{155}\text{Eu}$	—	—	—	100	100
$^{238}\text{U}$	45	93	79	97	99
$^{241}\text{Am}$	—	—	100	100	100

<sup>a</sup>The time is the sum of those given in Tables 2 and 3.

#### Dissolution and fractional release rates

Consequently, the fractional release rate (FRR) was calculated on basis of the fraction of radionuclides released into solution and the fraction of radionuclides sorbed on the autoclave walls. Figure 2 plots the fractional release per day as function of the contact time in the five leaching experiments.

The FRR of  $^{241}\text{Am}$  and the fission products are compared with the FRR of  $^{238}\text{U}$  to determine, whether they dissolve congruently with the  $\text{UO}_2$  fuel matrix. Since the ratio of the FRR of  $^{90}\text{Sr}$ ,  $^{155}\text{Eu}$  and  $^{241}\text{Am}$  versus the FRR of  $^{238}\text{U}$  are close to unity, it is concluded that these radionuclides dissolve congruently. Since the FRR values are relatively high for  $^{99}\text{Tc}$ ,  $^{134}\text{Cs}$  and  $^{137}\text{Cs}$  in comparison to  $^{238}\text{U}$ , it is concluded that these radionuclides were release faster and incongruently with  $^{238}\text{U}$ .

A molar release rate was calculated from the total amount (mol) of radionuclides dissolved in solution

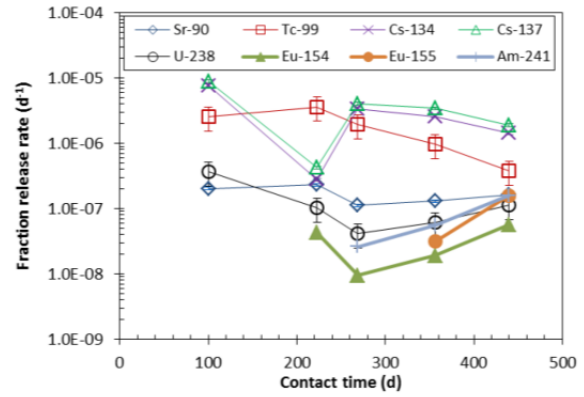


**Fig. 2:** Fractional release rate at the end of each experiment as a function of the contact time.

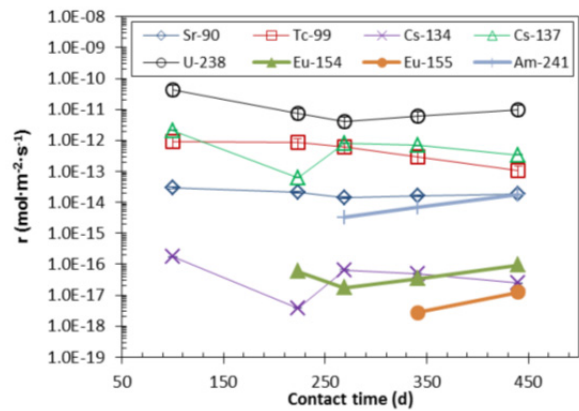


**Fig. 3:** Surface related release rate as a function of contact.

and radionuclides sorbed on the autoclave walls. For calculating the surface area related release rate (in terms of  $\text{mol}\cdot\text{m}^{-2}\cdot\text{s}^{-1}$ ), the specific surface area values  $S'_{\text{spec}}$  with a roughness factor of 3 was used (see Table 1). In Figure 3, the release rate of each radionuclide is plotted as a function of the contact time.

After 440 days the release rates in ( $\text{mol}\cdot\text{m}^{-2}\cdot\text{s}^{-1}$ ) are the following:

$$\begin{array}{ll}
 1.8 \cdot 10^{-14} & \text{for } ^{90}\text{Sr}, & 1.1 \cdot 10^{-13} & \text{for } ^{99}\text{Tc}, \\
 2.4 \cdot 10^{-17} & \text{for } ^{134}\text{Cs}, & 3.4 \cdot 10^{-13} & \text{for } ^{137}\text{Cs}, \\
 9.4 \cdot 10^{-17} & \text{for } ^{154}\text{Eu}, & 1.3 \cdot 10^{-17} & \text{for } ^{155}\text{Eu}, \\
 1.0 \cdot 10^{-11} & \text{for } ^{238}\text{U} & \text{and } 1.8 \cdot 10^{-14} & \text{for } ^{241}\text{Am}.
 \end{array}$$

#### Fission gas release under anoxic leaching of spent nuclear fuel

Within the 7<sup>th</sup> FP CP FIRST-Nuclides, the fast release (IRF) of radionuclides from SNF is investigated. The IRF is a result of segregation of parts of the radionuclide inventory to (i) the gap interface between the cladding and the pellet, (ii) the fractures as well as to (iii) grain boundaries. Relevant for IRF are fission gases (Kr and Xe), volatile elements ( $^{129}\text{I}$ ,  $^{137}\text{Cs}$ ,  $^{135}\text{Cs}$ ,  $^{36}\text{Cl}$  and  $^{79}\text{Se}$ ) and segregated metals ( $^{99}\text{Tc}$ ,  $^{107}\text{Pd}$  and  $^{126}\text{Sn}$ ) [9].

The degree of segregation of the various radionuclide is highly dependent on in-reactor fuel operating parameters (such as linear power rating, fuel temperature, burn-up, ramping processes) and interim storage

time. These effects cause diffusion of fission gases to grain boundaries, grain growth accompanied by grain boundary sweeping, gas bubble formation and interlinkage and intersection of gas bubbles by cracks in the fuel [10].

The aim of the present study is the quantification of instant release fraction from irradiated high burn-up  $\text{UO}_2$  during leaching of fuel pellets under anoxic condition in a diluted  $\text{NaCl-NaHCO}_3$  solution. As a first step, emphasis is given to the release of fission gases during the leaching experiments.

#### Sample preparation

From the spent nuclear fuel rod segment SBS1108-N0204 a clad fuel pellet was cut by JRC-ITU [11]. The procedure was carried out using a cutting machine equipped with a diamond wafering blade (Buehler Isomet® series 15HC). The dry cutting was performed slowly without any cooling liquid and under  $\text{N}_2$  atmosphere. The complete cutting procedure is described elsewhere [11].

In Figure 5, the clad fuel pellet selected to perform the leaching experiments under anoxic conditions is shown. The sample was weighed and its dimensions (length and diameter) were measured. The mass and dimension of the clad fuel pellet are given in Table 4.

#### Experimental procedure

A static leaching experiment was performed in a 250 ml stainless steel Ti-lined VA autoclave (Berghof Company, Eningen, Germany) equipped with 2 valves in the lid to allow solution and gas sampling.

The multi-sampling experiment was carried out under anoxic conditions in a gas atmosphere of 92% Ar and 8%  $\text{H}_2$  with a total pressure of 40 bar. To ensure that both sides of the clad pellet sample are in contact with the solution, the sample is mounted in specifically manufactured Ti sample holder (Fig. 6).

The holder with the sample was placed in the autoclave. The autoclave was closed and flushed with Ar to remove air out of the vessel. Using 50 ml syringes, the autoclave was filled with 220 mL of bicarbonate

**Tab. 4:** Mass and dimension of the SNF sample.

Parameter	Value
External diameter (mm)	$10.75 \pm 0.01$
Internal diameter (mm)	$9.35 \pm 0.01$
Length (mm)	$9.85 \pm 0.01$
Weight (g)	$7.770 \pm 0.001$
Weight of fuel (g)	$6.97 \pm 0.001$

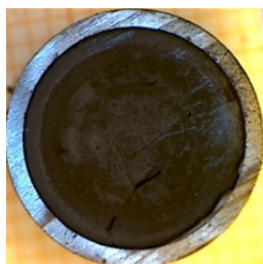


**Fig. 5:** Cross section of the clad fuel sample.

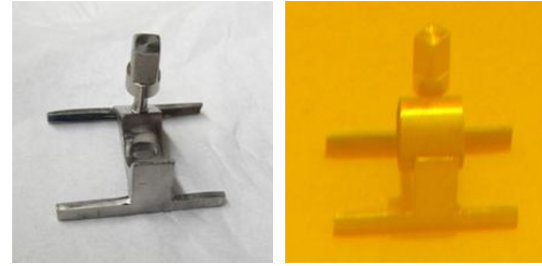


**Fig. 6:** a) sample holder used during the experiment; b) sample holder mounted with pellet before immersion into the solution.

water (19 mM  $\text{NaCl} + 1 \text{ mM NaHCO}_3$ ) under constant Ar flux to avoid air intrusion. After one day, a gas sample was taken and the solution was completely renewed. After this 1-day pre-leaching, the autoclave was refilled with 220 mL of the bicarbonate solution in the same way as described above.

In the consecutive static period of the leaching experiment, gas ( $50 \pm 1$ ) mL and liquid ( $15 \pm 1$ ) mL samples were taken at 1, 7, 21 and 56 days. After each sampling, the remaining gas was purged with Ar, and the 92% Ar / 8%  $\text{H}_2$  atmosphere was re-established within the autoclave. It is emphasized that the autoclave was not replenished with fresh solution to replace the sampled volume.

#### Results and discussion

The gas samples were analyzed using a gas mass spectrometer (GAM400, In Process Instruments, Bremen, Germany) equipped with a Faraday and SEV detector and a batch inlet system.

The measured amount (in terms of moles) of Kr and Xe are converted into cumulative fractions of the Kr and Xe inventories released into the gas phase (FIG<sub>c</sub>) and as fractional release rate of Kr and Xe (FRR per day).

The FIG<sub>c</sub> of Kr and Xe as a function of the cumulative contact time is plotted in Figure 7. It can be observed that the FIG<sub>c</sub> of Kr is significantly higher than FIG<sub>c</sub> of Xe. In the pre-leaching step (“wash cycle”), the fraction released was  $(1.8 \pm 0.2) \cdot 10^{-2}$  for Kr and  $(1.1 \pm 0.1) \cdot 10^{-3}$  for Xe. After 57 days of cumulative contact, the fraction of the inventory released in the gas phase was  $(2.0 \pm 0.1) \cdot 10^{-1}$  for Kr and  $(6.4 \pm 0.3) \cdot 10^{-2}$  for Xe. Therefore, 20% of the Kr

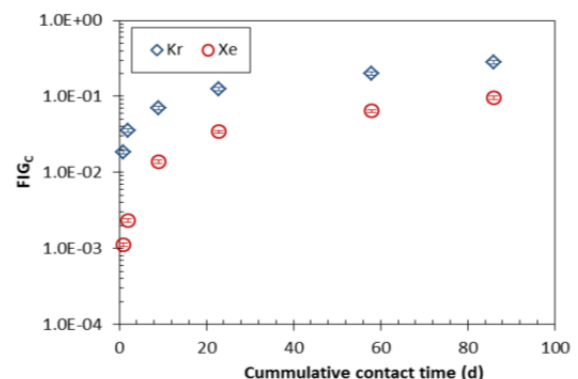


**Fig. 7:** Cumulative release fraction of Kr and Xe as function of the cumulative contact time.

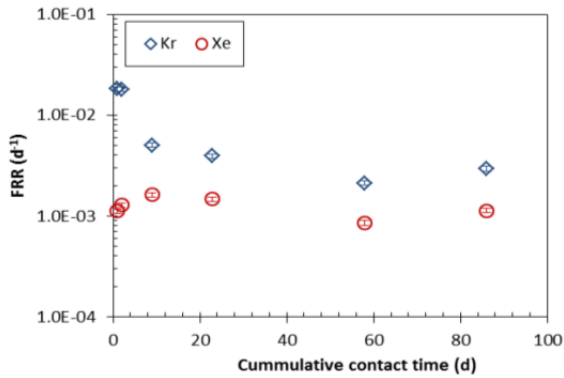


Fig. 8: Fractional release rate of Kr and Xe as function of the cumulative contact time.

inventory and 6.4% of the Xe inventory was released during the first 57 days of the leaching experiment.

The FRR of Kr and Xe as function of the contact time is plotted in Figure 8. It can be noted that after constant initial high fractional release rate of Kr  $(1.8 \pm 0.3) \cdot 10^{-2} \text{ d}^{-1}$ , the fractional release rate decreases one order of magnitude achieving a value of  $(2.1 \pm 0.2) \cdot 10^{-3} \text{ d}^{-1}$  after two months. The fractional release rate of Xe seems to be virtually constant during the first 4 samplings. Afterwards, the fractional release rate drops reaching a value of  $(8.5 \pm 0.7) \cdot 10^{-4} \text{ d}^{-1}$  after a cumulative contact time of 57 days.

### Quantification and speciation of <sup>14</sup>C from an irradiated UO<sub>2</sub> fuel rod segment

<sup>14</sup>C is one of the radionuclides important in safety assessments of spent nuclear fuel (SNF) disposal due to its assumed mobility and its half-life of 5730 a. Upon contact with water, <sup>14</sup>C-bearing species are expected to be released from the fuel rods into aqueous solution and to some extent into the gas phase as inorganic and/or organic compounds. Solubility, sorption behavior and distribution of <sup>14</sup>C in solution and gas depends strongly on the chemical form of <sup>14</sup>C. In this study we determine the inventory and speciation of <sup>14</sup>C of a SNF pellet, Zircaloy cladding (Zry-4/DX ELS 0.8) and a plenum stainless steel spring (X 7 CrNiAl 17 7). The investigated materials are sampled from the fuel rod segment SBS1108-N0204 and underwent the same history as the spent nuclear fuel samples described in the previous sub-section. Details on the sample properties are given in reference [6].

<sup>14</sup>C is an activation product formed in parts of fuel assemblies by neutron capture reactions of <sup>14</sup>N, <sup>17</sup>O and <sup>13</sup>C. <sup>14</sup>N is the main naturally occurring nitrogen isotope (99.63%), whereas <sup>13</sup>C (1.10%) and <sup>17</sup>O (0.038%) are low abundance naturally occurring carbon and oxygen isotopes. A very small amount of <sup>14</sup>C is also formed by ternary fission in the fuel. Nitrogen and carbon are present as impurities in fuel, Zircaloy cladding and structural parts of light water reactor (LWR) fuel assemblies.

Since <sup>14</sup>C is mainly formed by a <sup>14</sup>N(n,p)<sup>14</sup>C reaction, estimations of the <sup>14</sup>C inventories in the studied

materials of the SNF fuel rod segment are calculated based on published nitrogen impurities in PWR fuel (10 ppm), Zircaloy-4 (40 ppm) and stainless steel (500 ppm) [12,13]. For PWR assemblies with an average BU of  $\sim 50 \text{ GWd/t}_{\text{HM}}$ , <sup>14</sup>C inventories of 27200, 30000 and 80000 Bq/g are estimated for irradiated fuel, Zircaloy-4 and stainless steel, respectively [12,13]. Possible reaction partners of <sup>14</sup>C, after formation, are among others, U, O, Zr, Fe, Cr and Ni and it is potentially present in the fuel or structural parts of the fuel assemblies as oxide or carbide. Corrosion of these materials leads to formation of volatile and/or dissolved compounds like carbonates or hydrocarbons.

For determining the inventory/chemical form of <sup>14</sup>C, dissolution experiments with a clad fuel pellet, Zircaloy-4 without fuel and a stainless steel spring of the N0204 segment are performed in autoclaves under reducing conditions at room temperature in the INE shielded box line.

We are currently setting up a method that allows the separation and quantification of inorganic and organic <sup>14</sup>C species in gaseous and aqueous samples derived from these particular dissolution experiments (Fig. 9). The analytical separation procedure involves several steps (i.e. acid stripping and wet oxidation) during which the inorganic and organic carbon fractions are extracted and converted into CO<sub>2</sub> which is then absorbed in washing bottles containing 2 M NaOH. A catalytic furnace between two sets of washing bottles ensures oxidation of reduced compounds like CO or CH<sub>4</sub>. The content of <sup>14</sup>C (weak β<sup>-</sup> emitter) in the NaOH solutions will be finally determined by LSC (Fig. 10). Tests performed with inorganic and organic <sup>14</sup>C reference materials indicate that the chemical yield of the separation method is > 88% for both the inorganic as well as the organic <sup>14</sup>C fractions. The efficiency of the catalytic furnace was successfully tested using CH<sub>4</sub> with a yield of  $\sim 99\%$  for the conversion of methane to CO<sub>2</sub>.

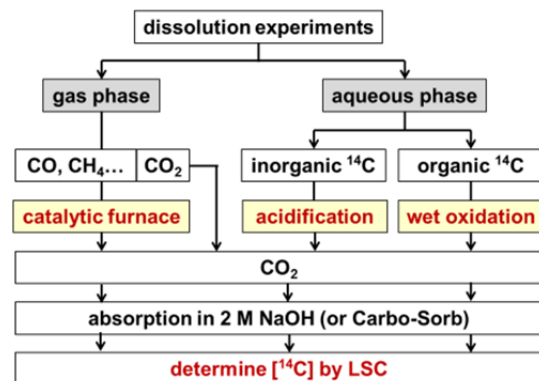


Fig. 9: Scheme of the <sup>14</sup>C extraction procedure.

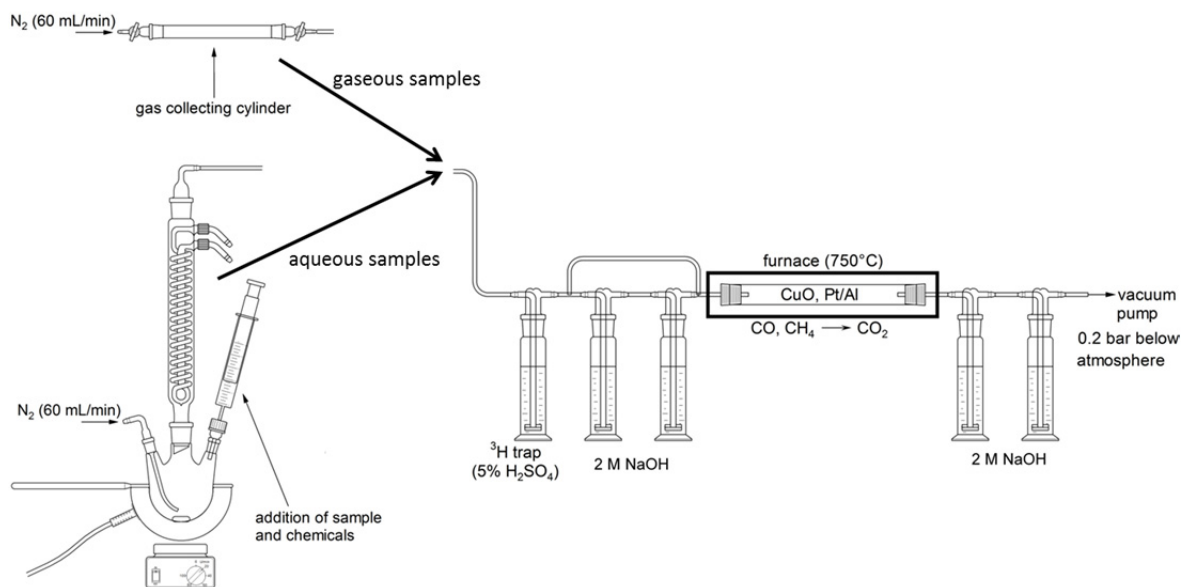


Fig. 10: Experimental design for  $^{14}\text{C}$  extraction of gaseous and aqueous samples.

## References

- [1] Bel, J. et al., *10th Int'l Conf. on Environm. Remed. Radioactive Waste Managem. ICM 2005*, Glasgow, UK, p. 1339 (2005)
- [2] Gens, R., et al., *J. Phys. IV (Proceedings)*, **136**, 13-23 (2006).
- [3] Bennett, D.G., Gens, R, *J. Nucl. Mater.* **379**, 1 (2008)
- [4] Kursten, B. et al., *6th Int'l Conf. on Managem. and Disposal of Radioactive Waste*, Luxembourg, 428-453 (2004).
- [5] Loida, A. et al., *Mat. Res. Soc. Symp. Proc.*, **1193**, 597-604 (2010).
- [6] Metz, V. et al., *FIRST-Nuclides 2<sup>nd</sup> Annual Workshop proceedings*, Antwerp, Belgium (2013).
- [7] Geckeis, H., et al., *Annual Report 2012. KIT scientific reports 7655* (2012)
- [8] Grambow, B. et al., *Forschungszentrum Karlsruhe, FZKA report 5702* (1996).
- [9] Johnson, L., et al., *J. Nucl. Mater.*, **346**, 56-65 (2005).
- [10] Johnson, L., Shoesmith, D.W. *Spent Fuel in Radioactive Waste Forms for the Future*. W. Lutze and R.C. Ewing, Eds. (North-Holland, Amsterdam) 635-698 (1988).
- [11] Wegen, D.H., et al., *KIT Scientific Reports 7639*, 193-199 (2012).
- [12] Sakuragi, T. et al., *Proceedings of the ASME 2013, ICM2013*, Brussels, Belgium (2013).
- [13] Kienzler, B. et al., *FIRST-Nuclides 2<sup>nd</sup> Annual Workshop proceedings*, Antwerp, Belgium (2013).

## 5.2 Non-heat producing waste forms and barrier materials

*E. Bohnert, C. Borkel, N. Finck, B. Kienzler, V. Metz, V. Montoya Garcia, T. Rabung, M. Schlieker, M. Wiedemann*

### Retention of Cm(III) and Eu(III) by brucite in the system Mg-Na-Cl-H<sub>2</sub>O

For the isolation of radioactive waste from the biosphere, a reliable description of actinide retention mechanisms in the near-field is necessary in long-term safety analyses for the disposal in deep geological formations, e.g. rock salt. Under reducing conditions, which develop after closure of a deep underground repository, actinides are expected to prevail in tri- and tetravalent redox states. There is currently a strong interest in developing engineered barrier materials, which provide favourable chemical conditions with respect to low actinide solubility and significant actinide retention capacities. For decades, a combination of Mg-oxychloride Mg<sub>2</sub>(OH)<sub>3</sub>Cl·4H<sub>2</sub>O(s), so-called Sorel phase, and brucite Mg(OH)<sub>2</sub>(s) is used as building material in conventional salt mines and currently discussed in concepts for sealing of radioactive waste repositories in rock salt [1,2]. At 25°C brucite and Mg-oxychloride are the thermodynamically stable solid phases in the system Mg<sup>2+</sup>-Na<sup>+</sup>-Cl<sup>-</sup>-OH<sup>-</sup>-H<sub>2</sub>O, besides halite NaCl(s) and bischofite MgCl<sub>2</sub>·6H<sub>2</sub>O(s) [2,3]. For the Asse II salt mine (Lower Saxony, Germany) and the Waste Isolation Pilot Plant (New Mexico, USA), where low level and intermediate level radioactive waste products are emplaced, brucite / Sorel based materials and MgO are used as sealing materials and engineered buffer, respectively. In contact with NaCl or MgCl<sub>2</sub> dominated salt brines, these materials buffer the pH<sub>m</sub> at 8–9, and scavenge CO<sub>2</sub> potentially produced by microbial degradation of organic waste constituents [1]. The present study focus on the retention mechanisms of Cm(III) and Eu(III) by brucite at a wide range of ionic strength (I = 0.15–5.2 molal), at room temperature. Recrystallization experiments were prepared with MgCl<sub>2</sub> ± NaCl ± NaClO<sub>4</sub> solutions as background electrolytes in a disposal relevant range of 9.0 ≤ pH<sub>m</sub> ≤ 9.3 and doped with [Cm(III)] = 10<sup>-7</sup> molal. The formation of the Cm(III) sorption species were investigated by kinetic studies with time-resolved laser fluorescence spectroscopy (TRLFS). The chemical environment of Eu(III) in brucite samples, recovered from co-precipitation experiments at high ionic strength (I = 1.2 and 5.2 molal), was determined by extended X-ray absorption fine structure (EXAFS). The aim of this work is to combine spectroscopic and macroscopic approaches by using co-precipitation and recrystallization experiments to obtain a better understanding of the sorption / incorporation mechanism.

Synthetic Mg(OH)<sub>2</sub>:Eu was prepared by co-precipitation of 0.4 molal MgCl<sub>2</sub> solution (+ 4 molal NaCl solution) with 2 molal NH<sub>4</sub>OH solution and 700 ppm of a 0.1 molal Eu(III) stock solution. Fluka

brucite (BioUltra ≥ 99%) was used for a recrystallization treatment in MilliQ water for 2 weeks. Recrystallized and co-precipitated brucite were characterized using TGA-DSC (Netzsch STA409C/CD), SEM-EDX (Quanta 650 ESEM, Fei) and XRD (AXS D8 Advanced diffractometer, Bruker). The molal H<sup>+</sup> concentration (pH<sub>m</sub> = -log[m(H<sup>+</sup>)]) of the suspensions was determined with combination pH electrodes (Orion Ross, Thermo Scientific). To convert the operational measure “pH<sub>exp</sub>” values, the approach of Altmaier et al. [3] was applied. Cm(III) fluorescence spectra were collected using a Nd:YAG laser (Surelite II, Continuum; 10 Hz) pumping a dye laser (Narrowscan Dye Laser, Radiant Dyes). Europium L<sub>3</sub>-edge EXAFS spectra were recorded at the INE-Beamline for actinide science at the ANKA synchrotron light source [4].

Kinetic series, investigated with TRLFS, of Cm(III) / brucite / brine recrystallization experiments show the formation of two consecutive Cm(III) sorption species on brucite within the first 20 hours (Fig. 1). At lower ionic strength (I ≤ 1.2 molal) the fluorescence peaks are strongly red-shifted suggesting an incorporated species. With increasing ionic strength, a significant weaker red shift is observed corresponding to a favoured inner-sphere coordination of the Cm(III) complex on brucite. Further TRLFS kinetic studies will be carried out to determine the life-times of both species.

EXAFS investigation of the co-precipitated Mg(OH)<sub>2</sub>:Eu samples indicated the incorporation of Eu(III) into the octahedral structure of brucite (Fig. 2). The first FT contributions of both samples are related to O atoms bound to Eu and are fitted using two O atoms at different distances. Due to the larger ionic radius of Eu(III) the substitution of Mg resulted in a structural distortion of the MgO<sub>6</sub> octahedra. This very likely leads to cancellation effects and thus low numbers of detected neighbors. Contributions at longer distances are modelled using Mg atoms. It is concluded that Eu substitutes, at least partly, for Mg in brucite and the next nearest Mg shell splits into two subshells in order to accommodate this large cation.

The observed retention of Cm(III) and Eu(III) by brucite at ionic strengths of 0.15–5.2 molal demonstrated the suitability of brucite based materials as engineered buffer with respect to trivalent actinides under a wide range of saline conditions. In experimental studies in diluted solutions, an incorporation of Eu(III) into the octahedral brucite structure was determined by Finck et al. [5]. Further TRFLS studies with Cm(III) / Eu(III) / brucite / brine suspensions at low temperatures are planned.

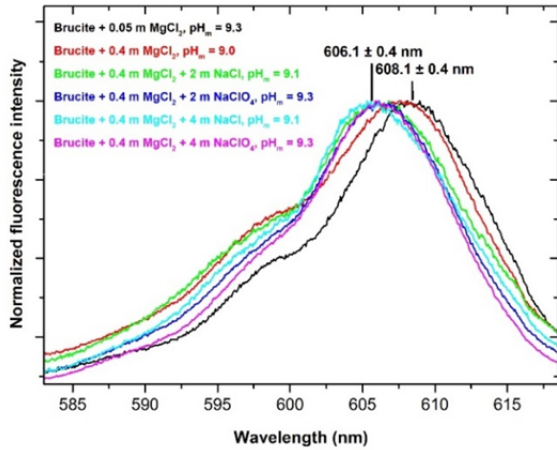


Fig. 1: Normalized Cm(III) emission spectra of brucite /  $MgCl_2 \pm NaCl \pm NaClO_4$  systems and their corresponding  $pH_m$  values.

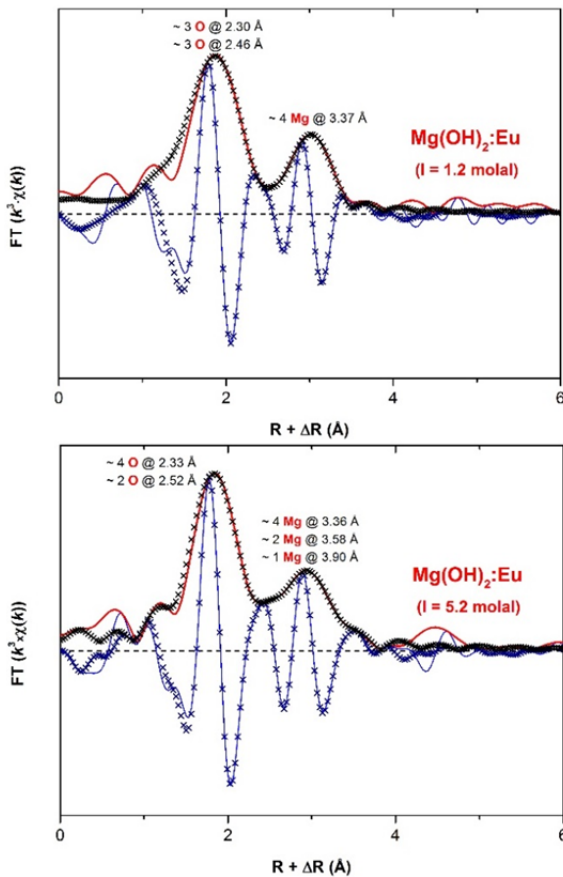


Fig. 2: Fourier transformed EXAFS spectra of  $Mg(OH)_2:Eu$  at ionic strengths of 1.2 and 5.2 molal. The fit results are marked as crosses.

### Modeling long-term leaching experiments of large scale cemented waste simulants: effect of solution composition on diffusion

A common concept for the conditioning of low to medium radioactive wastes is direct cementation in steel drums. Worldwide, such drums are being stored in different facilities below ground, in buildings, or simply at the surface.

This study focused on the release of Cs from such cement monoliths, incorporating homogeneously 10 wt.% of waste simulate which was representative for residues from spent nuclear fuel reprocessing by the Purex process [6]. After hydration, three monoliths with a w/c ratio of 0.24 were leached in tap water and monitored for more than 30 years. Experiments were terminated recently and first analyses of the solid were made.

XRD (Fig. 3) revealed no clinker phase at 2 cm depth, but persistent clinker below  $\sim 4$  cm depth, suggesting that water might not have penetrated the cement monoliths entirely.

The analytically determined effective diffusion coefficient for the release of Cs from the cement monoliths to the leachant solution was determined by plotting the depleted fraction of Cs against the square root of time and solving the diffusion equation for a semi-infinite cylinder. This resulted in a  $D_e$  of  $8.6 \pm 0.6 \cdot 10^{-13} \text{ m}^2/\text{s}$ . A transport model implying diffusion using Phreeqc [7] was set up to (I) test the sensitivity of the diffusion model with regard to the chemical solution composition and (II) estimate the depth profile of Cs leaching from the solid. The motivation for the first point was the criterion of electrical neutrality in each cell of the model which could potentially alter model results. It comes into play when ions of different charge and mobility diffuse.

In the model a fixed porosity of 10% was assumed in all cases. Three distinct solution compositions were used, from pure  $CsNO_3$  solution at pH 7 to the actually measured cement pore water composition at pH 12.6. In all cases the data was satisfactorily reproduced (Fig. 4) with a  $D_e$  of  $3 \cdot 10^{-12} \text{ m}^2/\text{s}$  which was in the same order of magnitude as the analytical solution. It could thus be concluded that in the given conditions the exact solution composition used in the model was not decisive for the diffusive release of Cs.

The computed depth profile (Fig. 5) revealed that the model required mobilization of Cs from the whole cement monolith, even from the center. This contradicted the observations made by XRD analyses which revealed the possibility of a 'dry' core of the cement monolith or at least dry domains within the solid.

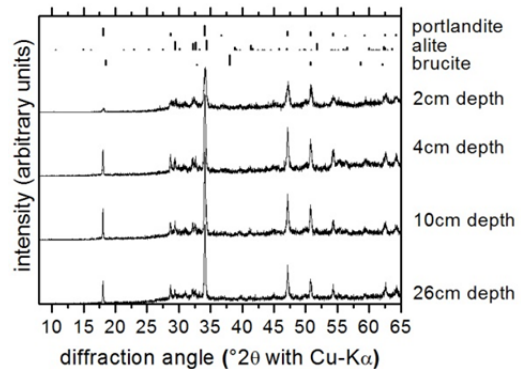


Fig. 3: XRD patterns from powder samples obtained in different depths below the top surface. Above, identified minerals are given with their relative reflection intensities from 0 to 100 %.

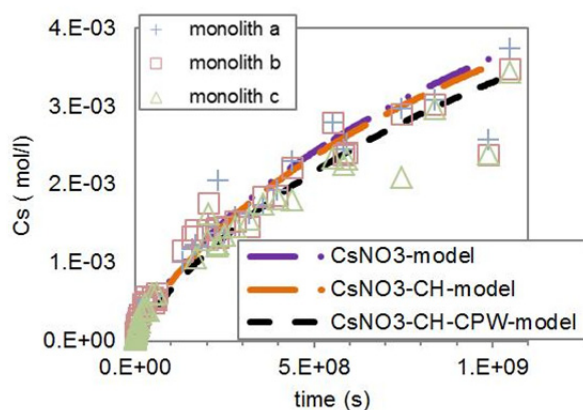


Fig. 4: Cs release from the three cement monoliths over 31 years compared to calculated Cs release according to the Phreeqc model with varying solution compositions

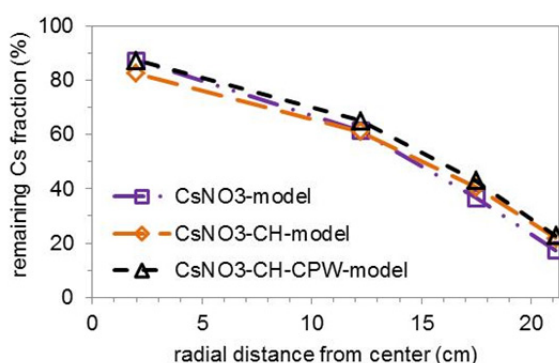


Fig. 5: Profile of the calculated remaining Cs content through the cement monolith from the center to the lateral surface. Results were obtained from the Phreeqc model using varying solution compositions. Only fractions from selected cells 1, 10, 20 and 29 were taken and plotted in the center of the corresponding cell.

Therefore, more detailed analyses of the solid are necessary to identify the mechanisms that did control the release of Cs from the monoliths. For this reason, in the first place the actual depth profiles of remaining Cs and  $\text{NO}_3$  content (Cs was added as  $\text{CsNO}_3$  and additional  $\text{NO}_3$  was included in the waste simulate) in the cement and of the porosity are going to be analyzed. Additionally, possibly formed secondary phases not identified by XRD are going to be identified by Scanning Electron Microscopy.

### Quantification of radionuclide retention in overlying rocks of the Asse salt dome

In 2013 a new law was passed by the Bundestag on “Speeding up the Retrieval of Radioactive Waste and the Decommissioning of the Asse II Mine” (Lex Asse). This law defines the retrieval of the radioactive wastes as the decommissioning option to be pursued as long as it does not pose a radiological and safety-related risk for the staff and the population. For this reason, a new shaft is planned to be sunk for transport of the wastes to the surface. Presently, a shaft pilot drilling is conducted. With respect to emergency

measures – in the case that retrieval is not possible – the sorption of radionuclides and the analysis of the sorption capacity overlying rocks of the Asse salt dome have to be quantified.

The sampling of solids from the overlying rocks followed two lines: (1) Sampling material which is kept under anaerobic conditions (Ar atmosphere) until it is used for the sorption experiments. Materials is available from depth between -15 m down to -415 m, including Triassic Muschelkalk (muS, muW) and Triassic Bunter sandstone (so) from below -130 m. (2) Bunter sandstone kept deeply frozen for the characterization of the pore water with respect to in-situ  $K_d$  values, iron redox speciation and organic matter characterization. Presently, 13 samples of line (1) and 10 samples for (2) are stored and analyzed at INE. Unfortunately, a contact of the sampled material with drilling fluid cannot be excluded which required special attention.

Intensive material characterization was started, including investigations of thin sections, determination of specific surface sizes by BET measurements, mineralogical composition by X-ray powder diffractometry (XRD) and Raman spectrometry, thermal analyses (DTA and DSC) for determination of the water content of the samples as well as crystal water release and phase transformations. Furthermore, element analyses with respect to main and trace elements are going on, and geochemical analyses investigating the equilibrium of water and rock material.

In safety analysis, the Muschelkalk is assumed to be groundwater conducting via fractures, only. This assumption is supported by the low water content of the samples (~ close to the surface, ~1wt.% below -50 m). To provide more insight in the conducting properties of this material and to quantify properties relevant for matrix diffusion, BET measurements were performed using rough crushed limestone samples. BET revealed specific surfaces between  $1.5 - 24 \text{ m}^2 \cdot \text{g}^{-1}$ . These relatively high surface sizes would support radionuclide retention by matrix diffusion processes. It needs to be corroborated by other techniques, such as investigation of thin slices with respect to connected pores.

### References

- [1] Metz, V. et al., *Radiochim. Acta*, **92**:819 (2004).
- [2] Freyer, D., *Proceed. of the International Workshops ABC-Salt (II) and HiTAC 2011. KIT Scientific Reports 7625*, Karlsruhe, p. 29 (2012).
- [3] Altmaier, M. et al., *Geochim. Cosmochim. Acta*, **67**:3595 (2003).
- [4] Rothe, J. et al., *Rev. Sci. Instrum.*, **83** (2012).
- [5] Finck, N. et al, *J. Contam. Hydrol.*, **102**:253 (2008).
- [6] Vejmelka, P. et al., *KfK Bericht 4800*, Kernforschungszentrum Karlsruhe (1990).
- [7] Parkhurst, D.L., Appelo, C.A.J., *U.S. Geological Survey Techniques and Methods, book 6, chap. A43* (2013).

## 5.3 Colloid impact on radionuclide migration

N.L. Banik, M. Bouby, G. Darbha, N. Finck, H. Geckeis, F. Geyer, S. Heck, C. Marquardt, R. Marsac, T. Schäfer  
In co-operation with:

J.V. Kratz<sup>a</sup>

<sup>a</sup> Institute for Nuclear Chemistry, University of Mainz, 55099 Mainz, Germany

### Introduction

Storage in deep geological formation is currently favoured as the safest solution to isolate radioactive wastes from the biosphere. A multi-barrier system is thus designed using technical barriers (waste package, container), geo-engineered barrier (compacted bentonite) and then the host-rock formation itself (volcanic tuff, crystalline rock, rock salt, sedimentary formations). Water is *a priori* the main factor of corrosion and alteration of the different barriers and, in addition, the main vector of radioactive elements potentially released in the natural barrier. Corrosion and alteration processes may lead, *via* the formation of intrinsic colloids and secondary phases and/or *via* the degradation of the engineered barrier system (EBS), to the generation of stable and mobile nanoparticles, acting consequently as potential vectors of especially strong sorbing radionuclides. Furthermore, every aquatic system contains already suspended natural-occurring colloidal particles (like humic substances, iron oxo/hydroxide, silica...) which can interact with radionuclides and might be a carrier towards the biosphere. Consequently, key questions to be answered in the repository near-field and far-field are (a) which colloidal/nanoparticulate phases are present and in which concentration, (b) how do radioelements interact with these phases and (c) under which conditions will these colloidal phases be mobile?

In laboratory experiments, we are currently investigating the potential role of natural organic matter (humic substances) present in porewater, of clay colloids eroded/extracted from various bentonite (planned to be used as buffer backfill material) and of colloidal material naturally present in ground water. Additionally, combined laboratory and in-situ migration experiments give information on the particles interaction with mineral surfaces and their potential impact in the far-field. These investigations require the development and the complementary use of highly sensitive and sophisticated analytical techniques as those presented in this report (see also chapter 9). More specific examples of the investigations follow hereafter to illustrate part of our work.

### Stabilization of polynuclear Pu(IV) species by humic acids

Although Pu(IV) is considered as rather immobile due to its low solubility, it shows a colloid-facilitated transport in presence of humic acids (HA) [1]. Several studies have shown that the interaction of strongly hydrolysable elements with HA (e.g. Fe(III) [2]) can

lead to the stabilization of small polynuclear species, although the experiments were performed below the saturation index of relevant minerals. Pu(IV) has an intrinsic tendency to form a great variety of dissolved polynuclear species [3]. Furthermore, spectroscopic investigations at relatively high concentration demonstrated that HA can inhibit the Pu precipitation by the formation of small polynuclear species [4]. As this fact might significantly impact the apparent solubility of Pu in presence of natural organic matter, this question was addressed in our recent publication [5].

In this fundamental study, Pu(IV) interaction with HA is investigated at 0.1 M ionic strength in NaClO<sub>4</sub> medium, at pH = 1.8, 2.5 and 3, with various [HA] concentrations in the range 0.025-25 mg·L<sup>-1</sup> and for a total Pu concentration ([Pu]<sub>tot</sub>) equals to 6·10<sup>-8</sup> M, which is below the saturation index of PuO<sub>2(am)</sub>. The final Pu(IV) concentrations ([Pu]<sub>eq</sub>) are determined after ultrafiltration at 1 kDa. Pu(IV) sorption to the batch walls and to the filters are measured and taken into account in the calculations.

The results are plotted as binding isotherms (Figure 1). Applying the Freundlich equations, the slopes (not drawn presently) of each isotherm are below 1 (≈ 0.7) for [Pu]<sub>eq</sub> < 10<sup>-8</sup> M, which is characteristic of a heterogeneity in the HA binding sites. The log<sup>HA</sup>β(Pu<sup>4+</sup>) values determined for that [Pu]<sub>eq</sub> concentration range are consistent with values found for other tetravalent actinides (An(IV)) as reviewed in [6]. However, a drastic inflection is observed in all isotherms at ~ [Pu]<sub>eq</sub> = 10<sup>-8</sup> M, leading to slopes approximately equal to 3.5. This suggests the formation

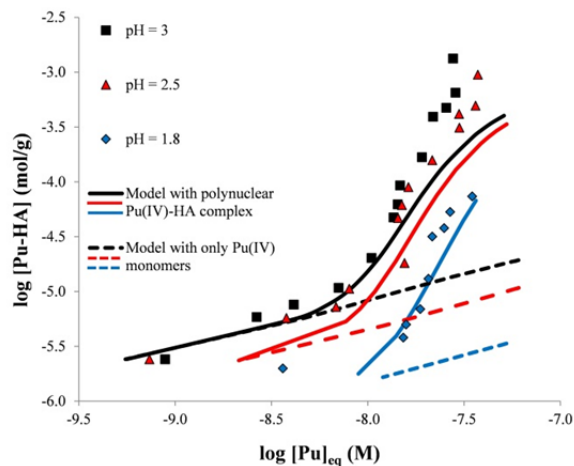


Fig. 1: Experimental Pu-HA binding isotherms compared with Model VII simulation considering or not the formation of polynuclear Pu-HA species.

of polynuclear Pu-HA species with an average Pu:HA stoichiometry of 3.5:1.

The present data are fitted by taking the Pu(IV)-HA complexation parameters considered in the humic-ion binding model, Model VII [7]. If only the data where  $[Pu]_{eq} < 10^{-8}$  M are considered, the fit might be considered as rather satisfactory (dotted lines, Figure 1). However, for  $[Pu]_{eq} > 10^{-8}$  M, the experimental data are strongly underestimated. To better fit the experimental results, a stabilization of Pu tetramer species by HA is proposed, with an average Pu:HA stoichiometry of 3.5:1, as deduced from the slope of the isotherms. This simplified approach allows a description of the experimental results (continuous line, Figure 1), although it still underestimates the extent of Pu-HA interaction for the highest  $[Pu]_{eq}$  and pH values investigated.

Thus, predictive simulations of Pu(IV) apparent solubility in presence of HA with Model VII, show a potential increase by a factor 100 due to the poly-Pu-HA complexes formation compared with simulations considering only monomeric Pu-HA complexes. Therefore, the present study strongly supports a possible transport of An(IV) as humic colloid-borne species in agreement with [1]. Further studies dedicated to more environmental relevant conditions on Pu solubility in presence of HA, in addition to investigations of stability of the “pseudo-colloids” formed are highly required.

### Mobilisation and characterization of nanoparticles from synthetic Yttrium co-precipitated hectorite.

Hectorite, an Mg-rich smectite, has been identified as a phase formed during High Level Waste glass corrosion experiments [8]. Radionuclides can possibly be incorporated in the bulk structure and form a solid solution. If, on one side, the formation of such solid solutions may be seen as an effective long term immobilization of the radionuclides (RNs) incorporated during their formation, on the other side, the release of stable nanoparticles from these solids may be thought, as a potential RNs migration vector. The aim of the present work is to characterize the colloids released from hectorite co-precipitated with element of interest and thus to establish a comparison between the bulk solid and the particles generated.

The nanoparticles analysed are those present in the supernatant obtained after a centrifugation of the initial bulk Y-coprecipitated hectorite suspension prepared as described in the Chapter 5, §5.3 (YcopHec). ICP-OES results suggest the presence of hectorite particles with a mean Si/Mg mol ratio equals to 0.514 (against 0.668 expected from the theoretical structural formula). The colloidal suspension is further analysed by Asymmetric Flow Field-Flow Fractionation (AsFIFFF) coupled to Laser Light Scattering (LLS) and ICP-MS. This hyphenated technique was already successfully tested in the past in similar investigations [9-10] giving information on the size of the nanoparticles released (related to their elution time in s) and on their elemental content (from the ICP-

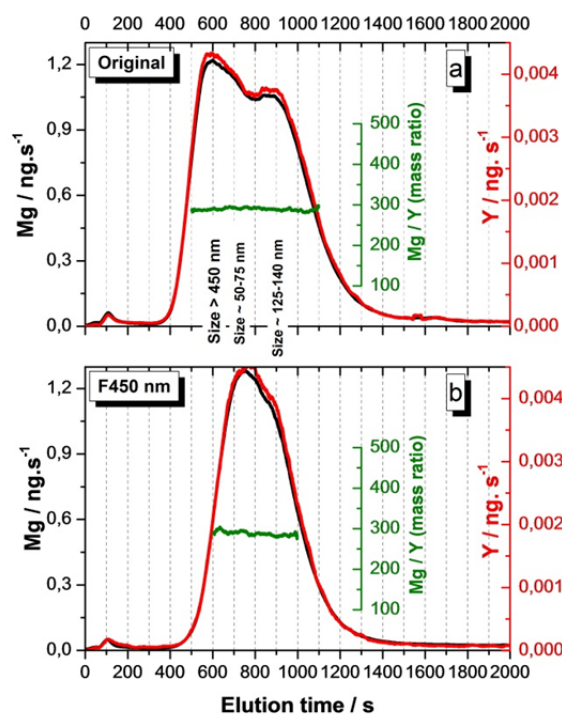


Fig. 2: Mg- and Y-ICP-MS-fractograms obtained after injection of the YcopHec supernatant (100  $\mu$ L). Dilution by 10 prior to the injection, with (b) or without (a) on-line filtration at 450 nm. Mean of two measurements, smoothed data.

MS). In Figure 2, Mg is the fingerprint of the hectorite colloids while Y is followed as element co-precipitated with.

Mg- and Y- ICP-MS fractograms obtained after injection of the supernatant into the AsFIFFF are presented before and after an additional filtration at 450 nm during the sample injection (Figure 2a-b). The results evidence the presence of a multimodal size distribution of hectorite particles with at least three modes as seen by the elution peak maxima at  $\sim 600$  s,  $\sim 750$  s and  $\sim 900$  s (Figure 2a). After filtration at 450 nm, the first peak disappears and the total size distribution is narrower (Figure 2b). This confirms the presence of several particle populations differing by their sizes. According to the operating mode of the AsFIFFF, the results indicate three main size fractions: one at  $\sim 50$ -75 nm, a second at  $\sim 125$ -140 nm and one greater than 450 nm. The hectorite colloids recovery calculated from the Mg recovery is  $61 \pm 1\%$  while the Y recovery is  $64 \pm 3\%$  which is a first strong indication of the association between the Y and the hectorite colloids. After filtration at 450 nm,  $13 \pm 1\%$  of the colloids are removed considering the Mg signal and  $15 \pm 3\%$  considering the Y signal, which is a second indication of a close correlation between the Y and the hectorite particles. The last evidence comes from the examination of the Mg/Y mass ( $289 \pm 33$ ) and molar ( $1057 \pm 120$ ) ratios which are rather constant over the complete multimodal size distribution recorded before and after filtration at 450 nm (resp  $288 \pm 43$  and  $1053 \pm 159$ ). The molar

ratios determined agree well with the expected ones from the synthesis protocol.

In conclusion, as already found with Lu and Eu [9-10], these new results are in favor of a homogeneous incorporation of the Y in the hectorite. This strongly supports the previous conclusions drawn after EXAFS analysis of the bulk solid described in Chapter 5, §5.3. The hectorite particles extracted may be seen as miniatures of the bulk solid. Their mobilization may thus favor the migration of the eventually incorporated radionuclides far away from their production source.

### Probing the interaction forces between $\text{Al}_2\text{O}_3/\text{SiO}_2$ particles and mineral surfaces

Bentonite clay colloids edge sites consist of aluminol and silanol groups. Probing their reactivity towards relevant mineral surfaces in presence of metal ion is a matter of specific research. In this work,  $\text{Al}_2\text{O}_3$  (Figure 3) and  $\text{SiO}_2$  particles are successfully mounted at the end of an AFM cantilever.

This is then used as “colloidal probe” mimicking clay edge sites to estimate adhesion forces against mineral surfaces, at various pH (4 to 9) and trace metal concentration, here Eu(III). Increasing the pH results in a decrease of interaction forces between  $\text{Al}_2\text{O}_3$  and  $\text{SiO}_2$  particles and the mineral surfaces tested (plagioclase, K-feldspar, quartz, biotite).  $\text{Al}_2\text{O}_3$  and  $\text{SiO}_2$  particles have similar adhesion forces towards mineral surfaces with an exception at  $\text{pH} < 6$ , where  $\text{SiO}_2$ -K-feldspar and  $\text{Al}_2\text{O}_3$ -biotite interactions appear higher compared to other colloid-mineral interactions. At pH 5, increasing [Eu(III)] from 0 to  $10^{-5}$  M results in an increase of the adhesion force between the  $\text{SiO}_2$  particle and the mineral surfaces, except for quartz (Figure 4, down part).

No such significant changes are observed when using  $\text{Al}_2\text{O}_3$  particle as a probe (Figure 4 upper part). At [Eu(III)]= $10^{-5}$  M, the ratios  $F_{\text{adh}(\text{SiO}_2)}/F_{\text{adh}(\text{Al}_2\text{O}_3)}$  decrease in the order: 11.3 for biotite > 4.55 for plagioclase > 3.03 for K-feldspar > 0.22 for quartz.

Interestingly, a significant change in the magnitude of adhesion forces (from a factor 1.2 to 2) between  $\text{Al}_2\text{O}_3$  probe and a smooth biotite ( $R_q < 1.2$  nm) is observed (Figure 5) despite almost similar particle size ( $\sim 8.0 \pm 0.1$   $\mu\text{m}$ ).

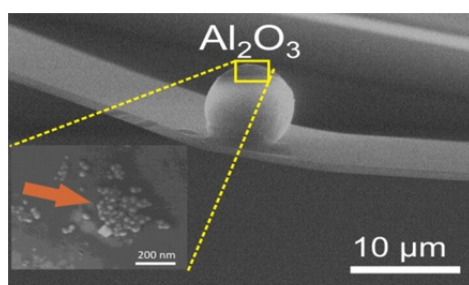


Fig. 3: SEM image of  $\text{Al}_2\text{O}_3$  particle mounted on AFM cantilever

This is a consequence of rough features of  $\sim 10$ – $20$  nm along the colloidal particle surface as determined by SEM and AFM (Fig. 3 and 6), which demonstrates the influence of roughness on particle adhesion forces.

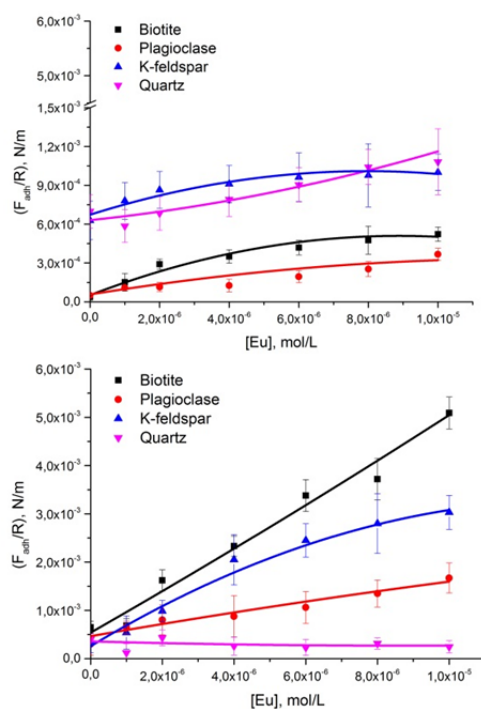


Fig. 4: Comparison of the adhesion forces ( $F_{\text{adh}}$ ) normalized to the colloid radius ( $R$ ) between two colloid probes (up:  $\text{Al}_2\text{O}_3$ , down:  $\text{SiO}_2$ ) vs. mineral surfaces at  $\text{pH} = 5$  and  $I = 1$  mM NaCl ionic strength.

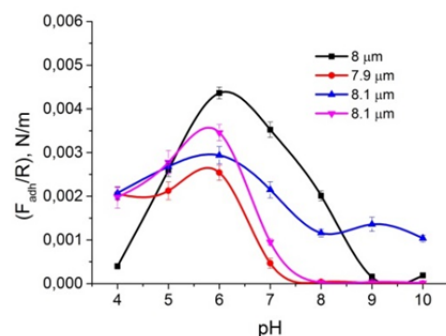


Fig. 5: Adhesion force ( $F_{\text{adh}}$ ) normalized to the colloid radius ( $R$ ) between  $\text{Al}_2\text{O}_3$  microparticles of slightly varying size and smooth biotite.

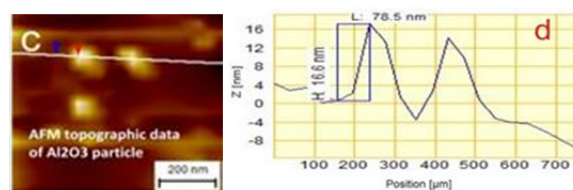


Fig. 6: a) AFM topographic image of  $\text{Al}_2\text{O}_3$  particle b) Height determination of nm-sized rough features on  $\text{Al}_2\text{O}_3$  particle surface.

## References

- [1] Artinger, R. et al., *Radiochim. Acta* **91**, 743-750 (2003).
- [2] Karlsson, T., and Persson, P., *Geochim. Cosmochim. Acta* **74**, 30-40 (2010).
- [3] Walther, C. et al., *Radiochim. Acta* **97**, 199-207 (2009).
- [4] Dardenne, K. et al., *Radiochim. Acta* **97**, 91-97 (2009).
- [5] Marsac, R. et al., *Geochim. Cosmochim. Acta* **131**, 290-300 (2014).
- [6] Reiller, P. et al., *Radiochim. Acta* **96**, 345-358 (2008).
- [7] Tipping, E. et al., *Environ. Chem.* **8**, 225-235 (2011)
- [8] Jollivet, P. et al., *J. Nucl. Mat.* **420**, 508-518 (2012)
- [9] Bouby, M. et al., *Min. Mag.* **76**, 2709-2721 (2012)
- [10] Finck, N. et al., *Min. Mag.* **76**, 2723-2740 (2012)

## 5.4 Thermo-mechanical-hydraulic (TMH) modeling

A. Pudewills

### Evolution of the excavation damage zone in rock salt structures

Between 2010 and 2013, the Federal Ministry of Economics and Technology (BMWi) has funded a joint project within its research program “Improvement of tools for the safety assessment of underground repositories” [1]. The five project partners performed benchmark calculations of an old underground structure, the so-called “Dammjoch” (bulkhead) in a drift at 700 m depth in rock salt at the Asse Mine. The general objectives are to document, check, and compare the advanced models and modeling procedures, to validate their suitability for numerical simulations and reliability, to increase confidence in the results, and to enhance the acceptance of conclusions.

In our institute the finite element program system ADINA ([www.adina.com](http://www.adina.com)) [2] was used to study the mechanical behavior of rock salt. A new viscoplastic constitutive model for rock salt that can describe the volumetric strain (dilatancy and healing/sealing) of the rock has been proposed and implemented in this code. The identification of the model parameters is based on experiments such as creep tests, strength tests and healing tests. For illustration, the Figures 1 and 2 are shown the loading conditions of the sample and the back-calculation of a such healing test performed by TU-Clausthal partner on Asse salt.

Subsequently, the constitutive model was used to calculate the evolution of the excavated damage zone around underground openings such the “Dammjoch” drift in the Asse mine following by healing of previously damaged region due to the construction of bulkhead (i.e. steel tubing and concrete liner) as a sealing system.

The dilatant zones shown in Figure 3 are regions around the drift that are predicted to develop in-

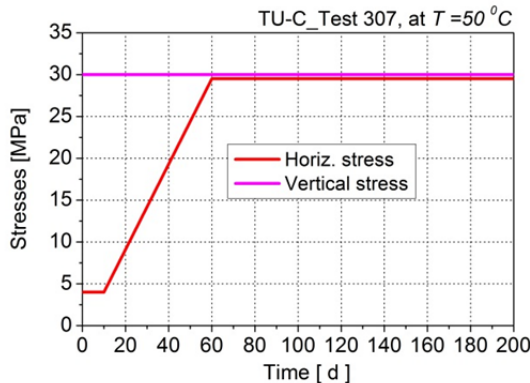


Fig. 1: History of the test loading; during the first 60 days the damage of the sample was induced and in the next 160 days a hydrostatic compaction of the sample at about 30 MPa was performed.

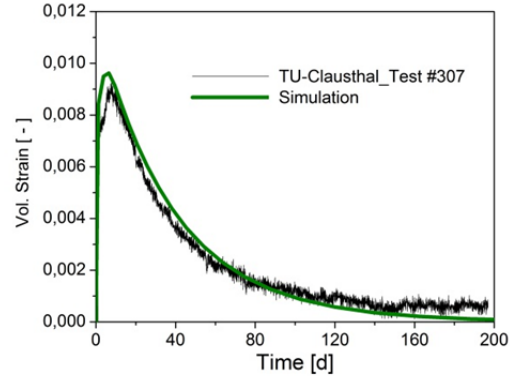


Fig. 2: Comparison of the measured and calculated evolution of volumetric strains in a healing test.

creased permeability as results of damage. It can be seen that the thickness of this zone around the unlined drift extends about one meter behind the drift wall. After 85 years the dilatancy zone around the seal is nearly suppressed.

A comparison of calculation results from all five project partners with in situ measurements will be done by project coordinator and discussed during next project workshop.

In the extension of the current Joint Project III, the thermo-mechanical benchmark calculations will be continued with simulations of an isothermal and a heated drift with quadratic cross sections at the Waste Isolation Pilot Plant (WIPP) in New Mexico, USA. In these calculations, the additional temperature influence on the evolution of damage and dilatancy will be of greater importance.

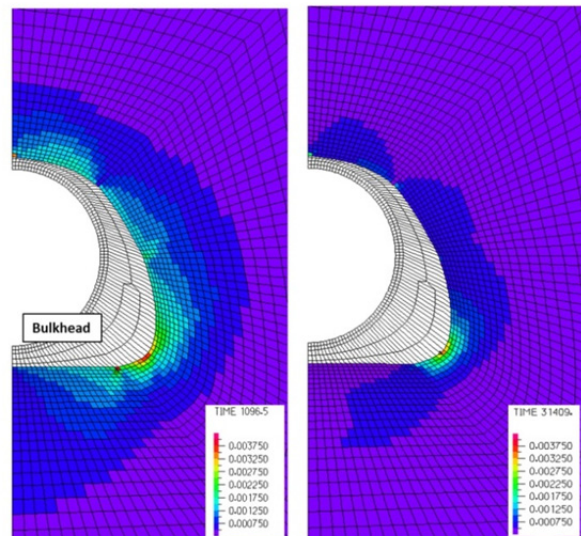


Fig. 3: Development of calculated volumetric strains around the drift 0.5 and 85 years after the bulkhead emplacement.

## Modeling of Flow and Solute Transport in a Shear Zone at the Grimsel Test Site

Crystalline rocks such as granite have been extensively investigated as a potential nuclear waste disposal formation due to the long-term rock mass stability and its favorable hydraulic properties. The granitic rocks are nearly impermeable and the groundwater flows predominantly through discrete fractures or shear zones filled with porous material. Such features provide the primary natural pathway for the migration of radionuclides from the underground repository to the biosphere. In order to predict the movement of radionuclides, the processes involved must be understood and quantified. For this purpose, laboratory tests, field experiments and adequate numerical models are needed.

The Colloid Formation and Migration (CFM) project at the Grimsel Test Site (GTS; <http://www.grimsel.com/gts-phase-vi/cfm-section/cfm-introduction>), [3] aims to investigate and quantify the impact of colloids on the transport of radionuclides in a fracture taking into account the repository relevant spatial and temporal conditions. The in situ experiment is performed at the GTS in a controlled zone. In the second phase of this project, different point dilution tracer tests with uranine and/or amino-G acid as conservative tracers were performed. Prior to the tracer tests, a combination of polymer resin impregnation of the tunnel surface and a steel torus to seal the tunnel surface was constructed. This design gives the opportunity to regulate outflow and thereby adjust the flow velocity in the fracture. At this stage of the project, the development of simple numerical models using the measured far field hydraulic head data were performed. The results obtained provide a fairly consistent picture of the pathway around the CFM location and contributed significantly for further model simulations.

The objectives of the actual numerical modeling are to analyze the conservative tracer data to identify hydraulic and transport processes and effective

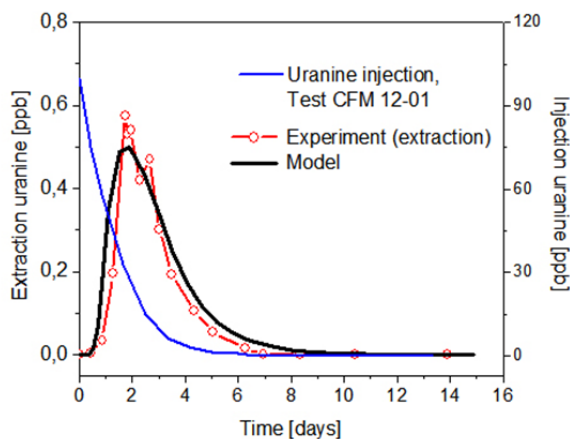


Fig. 4: Comparison of measured and calculated uranine breakthrough curves at the extraction well for test 12-01. The injection concentration (blue curve) is also plotted.

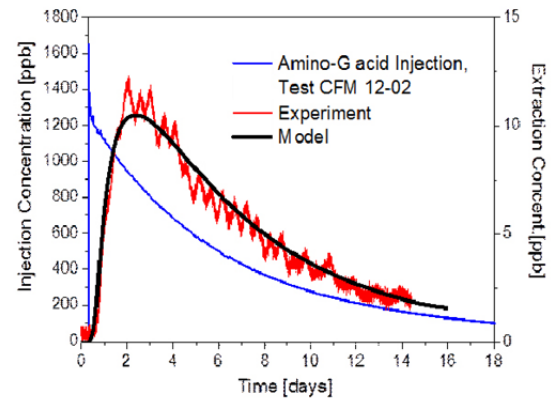


Fig. 5: Comparison of measured and calculated breakthrough curves at the extraction well for test 12-02 with amino-G: (extraction at 25 ml/min and injection velocity  $\sim 0.4$  ml/min).

parameters and also to use the modeling results to predict the outcome of radionuclide migration tests performed in the same geometry and hydraulic conditions.

In this contribution a series of dipole tracer tests was simulated numerically. It was assumed that the groundwater flow and the solute transport take place in fractures filled with porous fault gouge, and the shear zone at the test location is plane which allows a two dimensional approach. The mathematical model is based on the Darcy's law for groundwater flow and the advection-dispersion equations for tracer transport with a linear sorption in the fracture material. However, the model represents a planar confined porous media with a constant porosity and an anisotropic permeability. The analyses were performed with the ADINA-F [2] finite element code ([www.adina.com](http://www.adina.com)). A comparison of the field data and the modelling results is presented as breakthrough curves at the extraction surface packer. As can be seen from Fig-

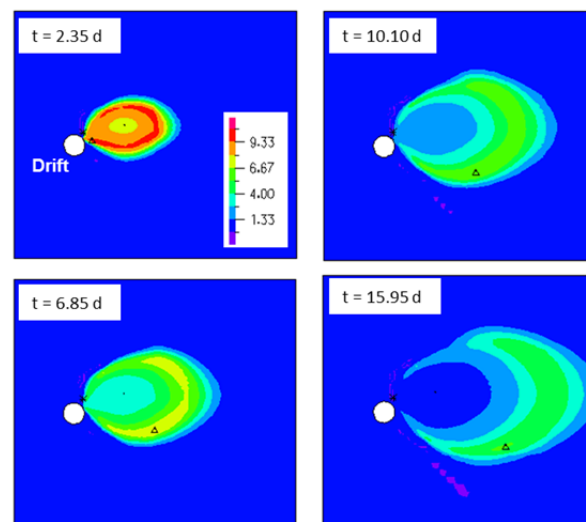


Fig. 6: Calculated distribution of the amino-G concentration (ppb) for test 12-02 at different times after tracer injection.

ures 4 and 5, the model produces a reasonable fit to the experiment. There is clearly a good agreement between both curves regarding in-peak arrival time and the tail. The long tailing seems to be induced by progressive release of the tracer late in the injection interval. The evolution of computed tracer concentration in the shear zone is presented in Figure 6 for different time steps.

The approach used for numerical simulation and the in situ experiments conducted, provide a fairly consistent picture of the flow and transport properties of the shear zone at the location of planned more complex experiments. Therefore, the estimated parameters are an approximation of the real structure which indicates heterogeneities in the distribution of hydraulic conductivity.

## References

- [1] Hampel, A. et al., Benchmark Calculations of the Thermo-Mechanical Behavior of Rock Salt – Results from a US-German Joint Project, 2013. In *Proceedings of the 47th US Rock Mechanics / Geomechanics Symposium 23-26 June 2013*, San Francisco, ISBN: 978-0-894844-0-4.
- [2] Adina R & D Inc., 2012. ADINA (Automatic Dynamic Incremental Nonlinear Analysis), *Report ARD 01-9*, Watertown, MA, USA.
- [3] Blechschmidt, I. et al., *GTS Phase VI: CFM Status Report on Field Work 2004 – 2005. Arbeitsbericht NAB 06-06. Nationale Genossenschaft für die Lagerung radioaktiver Abfälle (NAGRA)*. Wettingen, Schweizerland, 2006.

## 5.5 Impact of fracture heterogeneity on bentonite erosion rates

F. Huber, T. Schäfer

### Introduction

The current concept of a deep geological storage of high level nuclear waste in crystalline rocks (in e.g. Sweden and Finland) foresees a multi-barrier system [1]. The second barrier, the so called geotechnical barrier will consist of bentonite (or a mixture of sand and bentonite). One of the reference scenarios in the safety case deals with the impact of low mineralized glacial melt water intrusion through natural fractures within the crystalline rock down to disposal depths potentially leading to the erosion of the bentonite buffer/backfill. So far, the influence of fracture geometry on bentonite erosion has only been paid little attention. It is well known that heterogeneous flow fields evolve in natural fractures due to the complex fracture geometry leading to flow features like channeling and stagnant flow areas [2, 3]. These fracture flow characteristics will impact the bentonite swelling and erosion behavior. In model calculations on bentonite erosion (rates) using simplified geometries this issue is implicitly not accounted for. The aim of the study in hand which is conducted within the EU project CP BELBaR is to shed light on the influence of flow heterogeneity in natural fractures on the bentonite erosion and derive distributions (and the variability) of bentonite erosion rates as a function of flow rates covering a range of natural flow velocities representative of crystalline ground water environments.

### Material and Methods

One over-cored natural single fracture which has been characterized by means of  $\mu$ -computed tomography ( $\mu$ CT) to obtain parameters like e.g. total porosity and aperture distribution is used. Moreover, the  $\mu$ CT data deliver detailed information on the natural fracture geometry. Based on the digital  $\mu$ CT information, a 3D numerical mesh for computational flow dynamics (CFD) simulations has been produced after threshold segmentation of the  $\mu$ CT to separate the void space (connected porosity = fracture) from the solid material (rock) data. More information on the general segmentation and meshing procedure of the digital dataset to obtain the numerical grids and on the CFD simulations is described in [4].

The most sophisticated model on bentonite swelling and erosion is presented by Neretnieks et al. [5]. Moreno et al. [6] used the model for both rectangular geometry and a more realistic cylindrical geometry of the deposition hole and a constant fracture aperture of 1 mm. A simplified equation based only on the parameters flow velocity and fracture aperture was derived for both cases. The erosion rate  $R_{Erosion}$  [kg/yr] for the latter geometry is given as:

$$R_{Erosion} = A \cdot \delta \cdot v^{0.41} \quad (\text{Eq. 1})$$

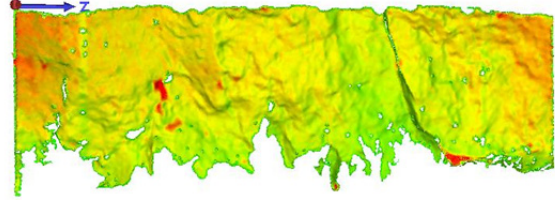


Fig. 1: Rendered visualization of the fracture surface geometry for Core#8 (right). Colors represent the apertures (green: low aperture, yellow: middle apertures and red: high apertures). Length fracture 13.05 cm, fracture width 5.05 cm.

where  $v$  is the flow velocity [m/yr],  $\delta$  is the aperture [m] and the constant  $A = 27.2$ .

The work in hand aims in coupling this simplified approach of calculating bentonite erosion rates to both the complex flow velocity distributions obtained by CFD simulations and the aperture distributions based on the  $\mu$ CT characterization for Core#8. The following three variations of both parameters, aperture distributions and flow velocity distributions, have been realized:

- Case A: Only the mean flow velocity and the mean aperture derived from the 3D dataset is used,
- Case B: The 3D flow velocity distribution and the mean aperture is used,
- Case C: The mean flow velocity and the 3D aperture distribution is used.

All three cases are realized for a range of flow rates, namely, 0.315, 3.15, 31.5 and 315 m/yr according to [6].

### Results

#### Aperture and velocity distributions

Figure 1 shows a rendered visualization of the Core#8 fracture surface colored by the apertures. It can be seen, that the apertures are heterogeneously distributed over the fracture as a consequence of the complex natural fracture geometry. Moreover, areas where both fracture surfaces touch each other (so called asperities) occur, resulting in aperture values of zero. On basis of the  $\mu$ CT dataset, the aperture distribution was determined (Figure 2 left). Core#8 exhibits a maximum aperture of  $\sim 1.53$  mm and a mean aperture of  $\sim 0.45$  mm. The aperture length variation does not follow a simple log-normal aperture distribution which is frequently observed for natural fractures [7]. The distribution is skewed to lower aperture values which may likely be attributed to the very irregular shaped fracture side.

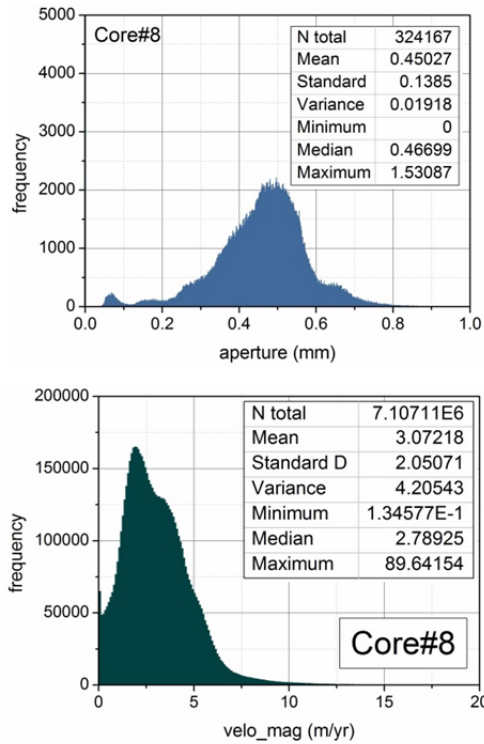


Fig. 2: Aperture (upper) and velocity (lower) distribution for Core#8.

Figure 2 (right) shows the velocity magnitude distributions for Core#8. The velocity distribution shown corresponds to a mean flow rate of 3.15 m/yr. The shape of the histogram shows a rather broad single peak with some minor shoulders for higher velocities indicating different flow regimes (channels). Interestingly, the maximum flow velocity observed is by a factor of  $\sim 29$  higher than the mean velocity clearly having an impact on the calculated erosion rate based on Eq. 1.

**Case A.** The mean aperture of Core#8 is 0.4503 mm as derived from the  $\mu$ CT data. The mean erosion rates determined using the mean values for the aperture and the velocity for the respective specific discharges imposed are depicted in Figure 3. In general, our erosion rates calculated for Case A are always lower than the ones given by Moreno et al. (2010) which is expected due to the higher aperture of 1 mm used in the 2D simulations.

**Case B and C.** Figure 3 depicts histograms for the erosion rates determined in this study for Case B and Case C. Only the results for the maximum flow rate of 315 m/yr and minimum flow rate of 0.315 m/yr. Additionally inserted in the figures are statistics on the results given. Due to the complex flow velocity distribution in the fracture the erosion rate distributions are also quite complex. Since either the 3D velocity or aperture distribution has been used in calculating the erosion rates in Case B and C, the shape of the histograms follow the shape of these distributions. The maximum erosion rates for Case B and Case C are higher than the erosion rates given by [6]. The minimum erosion rates are zero, due to both zero veloci-

ties in the flow at the fracture walls and zero apertures in the aperture distribution. In general, the results clearly reflect the importance of the variability of erosion rates due to the fracture geometry compared to a simplified 2D parallel plate approach to be considered in the assessment of bentonite erosion. Future work tries to couple the erosion model by [5] to our 3D fracture model for fully coupled simulations.

Though, the computational burden of such a transient 3D simulation will be enormous and the general feasibility of this approach needs to be tested.

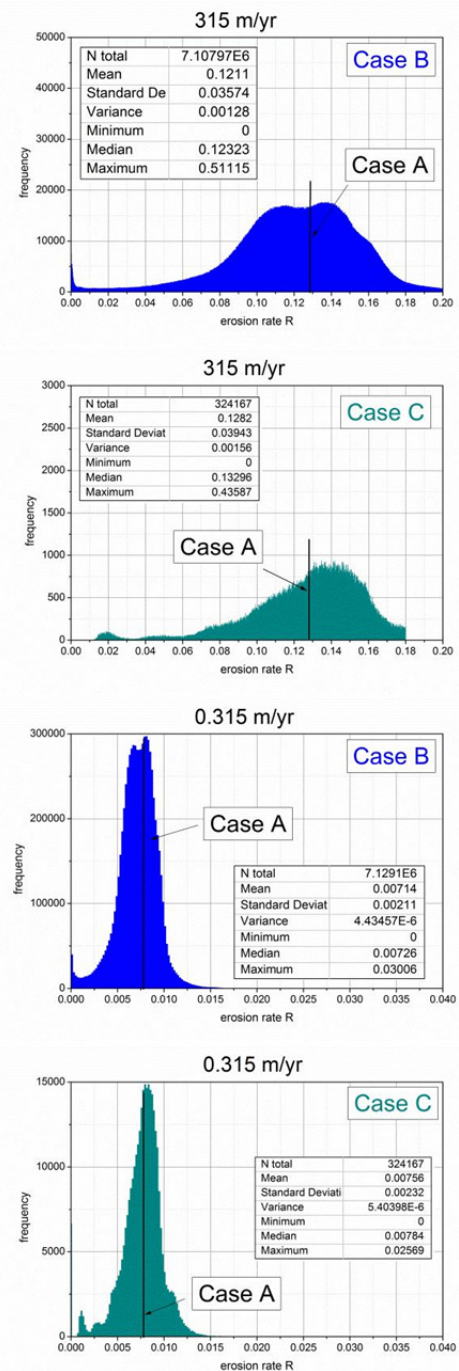


Fig. 3: Histograms of erosion rates determined for cases B and C for 4 different flow rates. Note that scales may vary between

## References

- [1] SKB. TR-06-18. 2006, Stockholm, Sweden.
- [2] Neretnieks, I., Eriksen, T. and Tahtinen, P., *Water Resources Research*, 1982. **18(4)**: p. 849-858.
- [3] Tsang, Y.W., et al., *Water Resources Research*, 1988. **24(12)**: p. 2049-2060.
- [4] Huber, F., et al., *Journal of Contaminant Hydrology*, 2012. **133(0)**: p. 40-52.
- [5] SKB. TR-09-35. 2009, Stockholm, Sweden.
- [6] SKB. TR-10-64. 2010, Stockholm, Sweden.
- [7] Adler, P.M. and J.-F. Thovert, 1999, Dordrecht [u.a.]: Kluwer. XII, 429 S.

## 5.6 Reactive transport modeling

V. Montoya, T. Kupcik, Th. Schäfer, B. Kienzler

### Introduction

Reactive transport models in porous media refers to mathematical and numerical methods integrating chemical reactions with transport processes. The idea of this kind of models is to predict or to describe the distribution in space and time of the chemical reactions occurring along a flow.

In the context of nuclear waste disposal, appropriate reactive transport models, using available codes, are being applied in KIT-INE for modelling radionuclides diffusion/ sorption/ migration processes. Models are tested by comparison to controlled laboratory experiments which will help to understand the evolution of repository subsystems.

Research in this field is focus in all relevant host rock types (rock salt, clay and crystalline rock) in close cooperation with national and international researchers as well as with several waste management organisations. To understand the phenomena governing migration of radionuclides in clay-rocks, sorption and diffusion studies, including experiments and reactive transport modelling have been done in Na-illite.

### Sorption and diffusion processes in heterogeneous porous media

Diffusion experiments with HTO,  $^{36}\text{Cl}^-$  at trace concentrations in a sample of purified Na-illite are modelled with PHREEQC's multicomponent diffusion module. Experiments were carried out in PEEK diffusion cells following an experimental setup described in [1]. A schematic representation of the experimental set-up is shown in Fig 1. In contrast to [1], the stainless steel filters were replaced by a combination of a membrane filter and a perforated PEEK plate, respectively, to (i) sustain a mechanical support of the clay material and (ii) minimize effects of the porous filters on the diffusion properties [2]. Na-illite was compacted to a bulk dry density of  $\sim 1700 \text{ kg}\cdot\text{m}^{-3}$ , attached to two reservoirs containing a  $0.1 \text{ M NaCl} / 10^{-4} \text{ M KCl} / 5\cdot 10^{-3} \text{ M MES}$  solution (pH 5) and pre-equilibrated for one week. Subsequently one solution was spiked with HTO and  $^{36}\text{Cl}^-$ , the other contained the background electrolyte solely (representing the inlet- and outlet-reservoir, respectively). In the experiments, it is observed that the concentrations of the tracers in the inlet reservoir decrease as they diffuse into the clay core, and we want to model how this decrease depends on the properties of the tracers and the clay.

The hydrogeochemical code PHREEQC v.3 [3] has been used with the option to calculate multicomponent diffusion in free pores and in the diffuse double layer (DDL) which allows calculation of diffusion processes with each solute species having its own tracer diffusion coefficient. Solute species can be transported in coexisting charged and uncharged re-

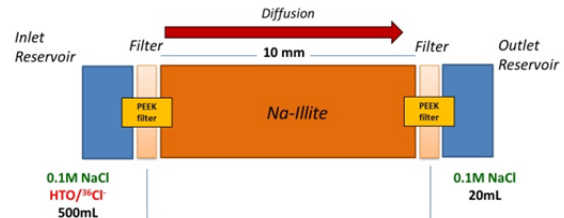


Fig. 1: Schematic representation of the experimental diffusion setup.

gions as may exist in clays. The composition of the DDL is calculated with the Donnan approximation.

HTO gives the accessible porosities and the geometrical factors (the ratio of pore tortuosity and constrictivity,  $\delta/\tau^2$ ) which applies in principle for all the neutral and cationic species. As anions are repelled from the vicinity of the negatively charged clay surfaces, a fraction of the porosity is not accessible for chloride (*anion exclusion*). In the model, half of the porosity is not accessible for chloride due to anion exclusion, and assumed equal to the amount of DDL-water. With this assumptions and taking into account the diffusion coefficient in water  $D_w$  ( $\text{HTO}) = 2.24\cdot 10^{-9}$ ,  $D_w(\text{Cl}^-) = 1.30\cdot 10^{-9} \text{ m}^2/\text{s}$ , experimental results have been modelled as it is shown in Fig. 2. As it can be seen diffusion of  $^{36}\text{Cl}^-$  in the Na-illite are slower attributed to the smaller diffusion coefficient of this tracer and to the less accessible porosity for anions in the clay.

In this case, the understanding of transport processes of cobalt in compacted clay systems can be achieved through the inclusion of sorption models (based on experimental data obtained from dispersed systems) in the reactive transport simulation of diffusion processes in Na-illite.

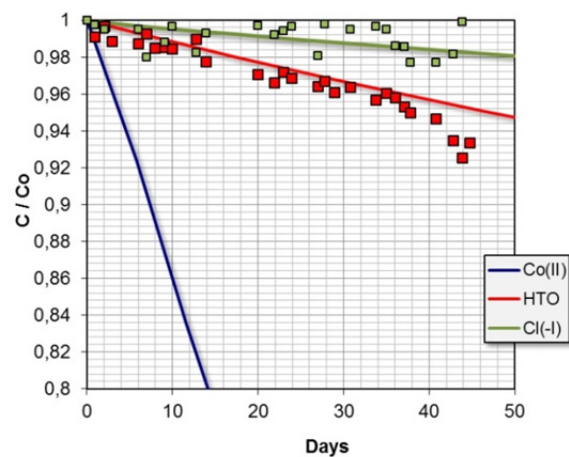


Fig. 2: Calculated decrease of the reservoir concentrations for Co(II) (blue line), HTO (red) and Cl(-) (green) and the related experimental data (squares).

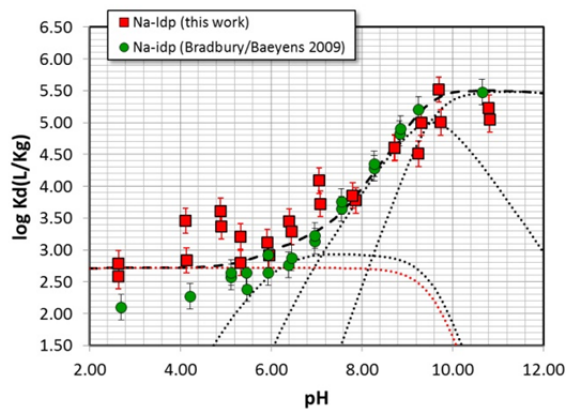


Fig. 3: pH edge of Co(II) in Na-illite at  $I = 0.1 \text{ M NaClO}_4$ . Experiments (squares) and model (lines). Dotted lines represent the different surface species. (In red) the exchange reaction, (in black) the surface complexation species ( $\equiv S^+OCo^+$ ,  $\equiv S^+OCoOH$ ,  $\equiv S^+OCo(OH)_2^-$ ).

New sorption data (both sorption edge and isotherm) for the interaction of Co(II) with purified Na-illite has been obtained in this work and compared with data available in the literature (see Fig 3). A similar site protolysis non-electrostatic surface complexation and cation exchange (2SPNE SC/CE) sorption model like the one described in [4] has been obtained for which the site types, site capacities and protolysis constants were fixed. Thus, surface complexation constants for the strong sites and cation exchange in the 2SPNE SC/CE sorption model for Co(II) has been obtained. In Fig 4, the aqueous (top)

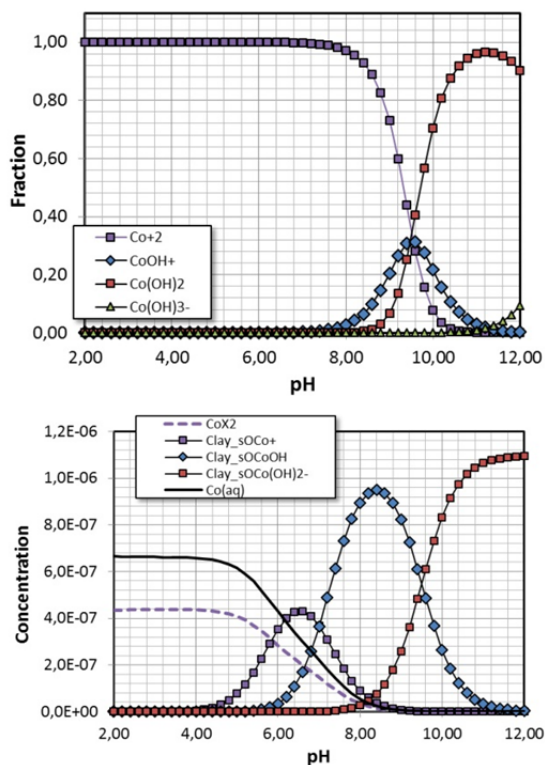


Fig. 4: Top: Aqueous speciation and Bottom: sorption speciation of Co(II) as a function of pH at  $I = 0.1 \text{ M}$ .

and the sorption speciation (bottom) of Co(II) is shown, taking into account the model obtained in this work.

Finally, with the sorption data now available, the 2SPNE SC/CE sorption model has been incorporated into the complete reactive transport models allowing cobalt migration to be calculated/predict. As first approximation, a non-electrostatic sorption model has been incorporated, but for internal consistency, an electrostatic model will be incorporated in the future.

In Fig 2 is illustrated how cobalt concentration in the inlet reservoir is expected to be decreased. A much faster decrease of concentration is observed in comparison to HTO and  $^{36}\text{Cl}^-$ . This difference is mainly attributed to the higher concentration gradient due to sorption processes for cations [5]. Co(II) migration has been modeled using the same accessible porosity than HTO and a  $D_w = 0.8 \cdot 10^{-9} \text{ m}^2/\text{s}$ . If we look to the chemical processes under the conditions where the model is tested ( $\text{pH} = 5$ ), we can observe (see Fig 4) that the most important mechanism for Co(II) retention is the exchange reaction with the Na-illite. taking into account the cation exchange capacity (CEC) determined experimentally and the sorption model described previously. At this moment no competition with other cations of the system has been incorporated in the model, but it is expected that competition between Co(II) and other cations present in the porewater (by the dissolution of the Na-illite) will occur [6]. Future work will be focus in including competition effects in the mobility of Co(II) in Na-illite.

## References

- [1] Van Loon L. R. et al., *J. Contaminant Hydrology* **61**, 73 (2003).
- [2] Glaus, M.A. et al., *Clays Clay Miner.*, **56**, 677 (2008).
- [3] Parkhurst, D. L., Appelo, C. A. J., *U.S. Geological Survey Techniques and Methods*, book 6, chap. A43, 497 p. (2013).
- [4] Bradbury M. H. and Baeyens B. *Geochim. Cosmochim. Acta* **73**, 1004 (2009).
- [5] Appelo et al., *Geochim. Cosmochim. Acta* **74**, 1201 (2010).
- [6] Tournassat C. et al., *American Journal of Science*, **313**, 395 (2013).



## 6 Separation of long-lived minor actinides

B. B. Beele,<sup>a</sup> A. Bremer, A. Geist, D. Magnusson, U. Müllich, P. J. Panak

In co-operation with:

R. Malmbeck,<sup>b</sup> G. Modolo,<sup>c</sup> D. M. Whittaker,<sup>d</sup> A. Wilden<sup>c</sup>

<sup>a</sup> Heidelberg University, Heidelberg, Germany; <sup>b</sup> JRC-ITU, European Commission, Karlsruhe, Germany, <sup>c</sup> Forschungszentrum Jülich, IEK6, Jülich, Germany, <sup>d</sup> The University of Manchester, Manchester, UK

### Background

Recycling transuranium elements (TRU = Np, Pu, Am, Cm) from irradiated nuclear fuel may provide advantages over the direct disposal of used nuclear fuel [1]. This would require separating the actinides from fission products and re-using them as nuclear fuel.

Most separation schemes under development in Europe are based on the PUREX process to remove uranium and plutonium (plus neptunium after slight process modification). Additional processes for Am and Cm are DIAMEX and SANEX but also combinations of these two processes such as 1c-SANEX and i-SANEX [2]. Furthermore, GANEX processes for the co-separation of all TRU have been developed [3-5].

Our contribution to EURATOM projects (ACSEPT, ASGARD, SACSESS) is related to the development and testing of the above processes (except PUREX). Additionally, important fundamental studies regarding the chemistry behind these processes is performed, partly in the framework of a BMBF-funded project (f-Kom, 02NUK020). These studies deal with the complexation of actinides(III) and lanthanides(III) with N-donor ligands such as BTP, BTBP and BTPhen being studied by TRLFS, NMR, XAS and quantum chemistry. Some recent studies are highlighted below; more information is found in other sections of this report.

### BTBP vs. BTPhen

CyMe<sub>4</sub>-BTBP [6, 7] and CyMe<sub>4</sub>-BTPhen [8] (Fig. 1) are efficient agents for the selective extraction of actinides(III) over lanthanides(III). More efficient extraction with better selectivity was found for CyMe<sub>4</sub>-BTPhen compared to CyMe<sub>4</sub>-BTBP. This was reasoned to be due to the locked *cis*-conformation which is necessary for metal ion ligation.

Indeed, TRLFS studies [9] on the complexation of Cm(III) and Eu(III) confirmed a positive impact of this preorganisation on the complexation behaviour. The stability constants of the Cm(III)- and Eu(III)-CyMe<sub>4</sub>-BTPhen 1:2 complexes formed are higher

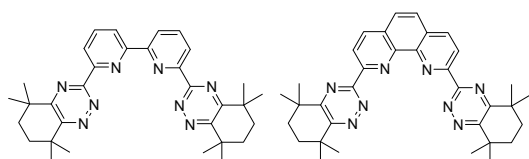


Fig. 1: CyMe<sub>4</sub>-BTBP and CyMe<sub>4</sub>-BTPhen.

Tab. 1: Stability constants  $\log \beta_2$  for the complexation of Cm(III) and Eu(III) with CyMe<sub>4</sub>-BTBP and CyMe<sub>4</sub>-BTPhen in methanol (+ 3.3% H<sub>2</sub>O).

	Cm(III)	Eu(III)	$\Delta$
CyMe <sub>4</sub> -BTBP	12.4±0.2	11.3±0.2	1.1
CyMe <sub>4</sub> -BTPhen	13.8±0.2	11.6±0.2	2.2
$\Delta$	1.4	0.3	

than those of the respective CyMe<sub>4</sub>-BTBP 1:2 complexes, see Tab. 1.

In accordance with extraction data, the stability constants of the 1:2 complexes of Cm(III) are considerably higher than those for Eu(III) for both N-donor ligands. The difference between the two ligands is found to be more pronounced for Cm(III) than for Eu(III), in agreement with the selectivity observed in extraction experiments.

### Solvent effect

It is well known that speciation and complex stability depend on the solvent used. This complicates comparison of literature data on the complexation of actinides(III) and lanthanides(III) with N-donor ligands; different solvents (usually alcohols or alcohol-water mixtures) are used, depending on the solubility of the ligand studied.

The complexation of Cm(III) or Eu(III) with n-Pr-BTP (2,6-bis(5,6-dipropyl-1,2,4-triazin-3-yl)pyridine) was studied [10] in methanol-water and propanol-water mixtures of varied water content (5–50 vol.-% H<sub>2</sub>O). The water content has a strong influence; the stability constant of the Cm(BTP)<sub>3</sub><sup>3+</sup> complex increases by 3.5 and 5 orders of magnitude with decreasing water content in methanol-water and propanol-water mixtures, respectively (see Fig. 2). The stability constants of the Eu(BTP)<sub>3</sub><sup>3+</sup> complex shows a similar trend.

This increase can be explained by a weaker coordination of alcohol molecules to the metal ions compared to water molecules. The evolution of the stability constants with water content is based on the preferential solvation of the metal ion by water in alcohol/water mixtures [11].

The differences between the two solvent mixtures studied are due to several superimposed effects. Additionally to different preferential solvation of water in different alcohol-water mixtures and the different ability of alcohols to ligate the metal ion, a change in the free energy parameters of the complexation reac-

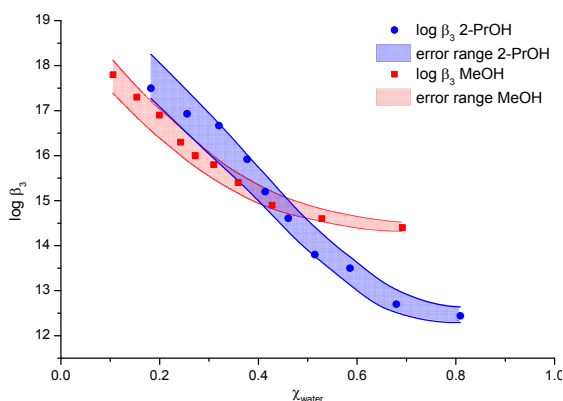


Fig. 2: Stability constants  $\log \beta_3$  of the  $\text{Cm}(\text{BTP})_3^{3+}$  complex as a function of the water mole fraction in different alcohol-water mixtures.

tion (enthalpy vs. entropy driven) is an important factor.

So far we may conclude that use of the same solvent is highly recommended when comparing the complexation properties of ligands. If not possible (e.g. due to solubility issues), these results may help with a reliable estimation of data to compare stability constants measured in different solvents.

$\text{SO}_3\text{-Ph-BTP}$  (Fig. 3), a water soluble bis-triazinyl-pyridine, is an efficient complexing agent for actinides (III) with good selectivity over lanthanides(III) [12]. It could be used to selectively strip actinides (III) from an organic phase loaded with actinides(III) and lanthanides(III). A process for the separation of actinides(III) from PUREX raffinate was developed, combining TODGA as extracting agent and  $\text{SO}_3\text{-Ph-BTP}$  as stripping agent for actinides(III). Based on a flow-sheet previously calculated [13], a spiked so called i-SANEX process test was performed using Jülich's laboratory centrifugal contactor setup [14, 15].

On day one, 16 stages (extraction and scrubbing sections) were used to prepare the organic phase loaded with Am(III), Cm(III) and lanthanides(III), similar to a TODGA-DIAMEX flow-sheet tested earlier [16]. On day two, Am(III) and Cm(III) were stripped from the loaded organic phase, again using 16 stages: 12 stages for stripping actinides and 4 stages for stripping lanthanides(III). A synthetic PUREX raffinate spiked with  $^{241}\text{Am}$ (III),  $^{244}\text{Cm}$ (III) and  $^{152}\text{Eu}$ (III) and containing 50 mmol/L CDTA was used as feed phase. Organic phase was a solution of 0.2 mol/L TODGA +

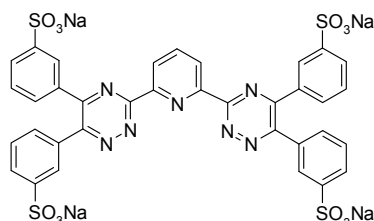


Fig. 3:  $\text{SO}_3\text{-Ph-BTP}$ .

Tab. 2:  $\text{SO}_3\text{-Ph-BTP}$  i-SANEX test, relative fractions of actinides(III) and lanthanides(III) in the effluent solutions.

	An(III)	Ln(III)
Raffinate	$\approx 0.01\%$	$< 0.1\%$
Loaded solvent	$\approx 100\%$	$\approx 100\%$
An(III) product	$> 99.8\%$	$< 0.1\%$
Ln(III) raffinate	0.05%	$> 99.7\%$
Spent solvent	$< 0.1\%$	$< 0.1\%$

5% vol. 1-octanol in kerosene. A solution of 18 mmol/L  $\text{SO}_3\text{-Ph-BTP}$  in 0.35 mol/L  $\text{HNO}_3$  was used to strip Am(III) + Cm(III); Ln(III) were stripped into a 0.5 mol/L citrate solution.

As evident from Tab. 2, Am(III) + Cm(III) were recovered almost quantitatively in the actinide(III) product solution;  $< 0.1\%$  were lost to the raffinate solutions (note that the fraction found in the spent solvent is not lost since the solvent would be recycled in a realistic process). Finally, the product solution's purity was very good; it contained  $< 0.1\%$  of the lanthanides(III), 0.34% Sr and 0.44% Ru.

### Hot EURO-GANEX process test

The GANEX process was developed to co-separate all transuranic (TRU) elements from used nuclear fuel without generating a pure plutonium product [17].

An alternative GANEX 2<sup>nd</sup> cycle process named EURO-GANEX was developed in the ACSEPT project by teams from NNL, Jülich, CEA, JRC-ITU and KIT-INE. A solvent consisting of TODGA + DMDOHEMA in kerosene was developed [4] to co-extract TRU together with the lanthanides. The challenge was to extract rather high concentrations of Pu(IV) (several 10 g/L). A solution containing  $\text{SO}_3\text{-Ph-BTP}$  + acetohydroxamic acid (AHA) in  $\text{HNO}_3$  was found to be suitable for stripping all TRU from the organic phase [18], similarly to the i-SANEX process described above.

Using this system a spiked EURO-GANEX process test was performed at NNL with a feed solution containing 10 g/L Pu(IV) [5]. Based on the results from this spiked test and further flow sheet calculations a hot demonstration test was performed in a 16 + 16 stage centrifugal contactor rig at JRC-ITU.

First a genuine feed solution had to be prepared by dissolving irradiated fast reactor fuel and removing uranium by a GANEX 1<sup>st</sup> cycle process [16]. The raffinate from this process, containing TRU and fission products, was adjusted to 10 g/L Pu and was used as feed for the EURO-GANEX process.

On day one, the loaded organic phase was prepared using 16 stages (12 stages for extraction, four stages for scrubbing). TRU were efficiently extracted from the feed solution; only 0.07% of Np and 0.01% of each Pu, Am and Cm were lost to the raffinate.

The collected organic phase, containing TRU and the lanthanides, was further treated on day two. Again, 16 stages were used (12 stages for TRU strip-

ping + Ln re-extraction and 4 stages for Ln stripping). TRU losses to the Ln raffinate were < 0.1%

The hot EURO-GANEX demonstration test was a full success. The product solution contained  $\approx$  99.9% of the TRU inventory and only 0.06% of the lanthanide inventory.

## References

- [1] *Potential Benefits and Impacts of Advanced Nuclear Fuel Cycles with Actinide Partitioning and Transmutation*; NEA No. 6894, OECD, Nuclear Energy Agency (NEA), Paris: 2011
- [2] Modolo, G. et al., *Radiochim. Acta* 2012, **100**, 715–725.
- [3] Aneheim, E et al., *Solvent Extr. Ion Exch.* 2013, **31**, 237–252.
- [4] Bell, K. et al., *Procedia Chem.* 2012, **7**, 392–397.
- [5] Carrott, M. et al., *Solvent Extr. Ion Exch.* 2014, (accepted).
- [6] Foreman, M.R.S et al., *Dalton Trans.* 2006, 1645–1653.
- [7] Geist, A. et al., *Solvent Extr. Ion Exch.* 2006, **24**, 463–483.
- [8] Lewis, F.W. et al., *J. Am. Chem. Soc.* 2011, **133**, 13093–13102.
- [9] Bremer, A. et al., *Dalton Trans.* 2014, **43**, 2684–2694.
- [10] Bremer, A., *PhD thesis*, Universität Heidelberg, 2014.
- [11] Tanaka, F. et al., *J. Chem. Soc., Faraday Trans. I* 1988, **84**, 1083–1090.
- [12] Geist, A. et al., *Solvent Extr. Ion Exch.* 2012, **30**, 433–444.
- [13] Magnusson, D. et al., *Procedia Chem.* 2012, **7**, 245–250.
- [14] Geist, A. et al., *Proc. GLOBAL 2013*, Salt Lake City, U.S.A., 29 September – 3 October 2013.
- [15] Modolo, G. et al., *Progr. Nucl. Energy* 2014, (in press).
- [16] Magnusson, D. et al., *Solvent Extr. Ion Exch.* 2009, **27**, 26–35.
- [17] Miguiditchian, M. et al., *Proc. Internat. Conf. GLOBAL 2009*, Paris, France, 6–11 September 2009.
- [18] Bell, K. et al., *Procedia Chem.* 2012, **7**, 392–397.



## 7 Vitrification of High-Level Radioactive Waste

*W. Grünewald, K. Hardock, J. Knobloch, K. Meyer, G. Roth, A. Salimi, W. Tobie, S. Weisenburger, K.-H. Weiß, B. Böhland*

### 7.1 VPC Project

The German-Chinese VPC (Vitrification Plant China) project has been established in November 2009 to construct an HLLW vitrification plant in the Sichuan province of China on the basis of the process technology developed by KIT-INE. A second part of the project deals with the construction of an intermediate storage building for the produced waste glass canisters. From German side the project is executed by an industry consortium (STEAG Energy Services, WAK GmbH, Kraftanlagen Heidelberg GmbH) with KIT-INE as nominated subcontractor responsible for design of the core process technique and key components like the waste glass melter and for input of process-chemical and glass-chemical knowhow and expertise. Besides the design work a main part of the contractual deliveries from the German consortium includes the supply of remaining core process components like the glass canister decontamination system as well as mechanical and remote handling equipment.

The Project is divided into three main phases: design (2010-2013), supply (2013/2014) and later technical on-site services, the latter covering supervision of installation, function testing, commissioning of the supplied hardware as well as supervision of the performance of the cold and hot test. In 2010 the main part of the project was dedicated to elaboration of the basic design (BD) of the vitrification plant and the intermediate storage building. The subsequent Detailed Design (DD) of the parts to be supplied by the German side started in 2011 and was finished in 2013.

#### 1. Detailed Design (DD)

The DD documentation included dimensioning calculations, 2D/3D design drawings, data sheets and diverse lists for each part of a component as well as its 3D presentation. The DD documentation serves as detailed information to potential manufacturers as basis for calculation of an offer price as well as for the subsequent manufacturing procedure. All DD documents had to be checked by an independent quality assurance group before release to the manufacturer. The QA procedure followed a well-defined control sequence plan.

In 2013 the DD created by INE comprehended mainly melter parts and subcomponents. The glass melter as the key component of the vitrification plant is composed of 19 subcomponent groups. The DD of the inner ceramic refractory structure of the melter, the stainless steel containment and the firmly inte-

grated components like power electrodes or bottom drain channel had already been finished in 2012. They were required for start of the melter assembly in spring 2013.

One essential DD work in 2013 was addressed to the elaboration of a re-design of the melter off-gas pipe. Such components are - independent on the respective vitrification process - subject to operational problems as they tend to clog by time due to depositing materials emitted from the melter. These deposits consist of entrained dust particles, condensing volatile compounds, and liquid and solid aerosols. Their tendency to stick to the inner wall of the off-gas pipe cannot be avoided. Once the deposition has started, accumulation will proceed. Depending on the process conditions, the off-gas pipe design and the local conditions (off-gas composition, flow rate, wall/gas temperature) the properties of the deposits can vary from a smugdy to a hard consistency. Off-gas pipe cleaning is a key problem of each vitrification process. All strategies applied are directed not to the complete avoidance of deposits but to their periodic removal to counteract accumulation. This is usually achieved by periodic cleaning by various techniques (e.g. brush reamer, water flushing etc.)

Due to the experience of the hot VEK operation a change of the hitherto used design of the off-gas pipe proved to be necessary. The use of the so called blaster technique had not been successful over a longer period of operation. The cleaning method was based on periodic application of air-cannons ('blaster') which release a volume of some liters of compressed air within a few milliseconds. The resulting ultrasonic air wave is to push away potential deposits. The efficiency of these systems was not efficient enough to remove the rigid deposits over a longer operation time period. As a consequence the accumulating deposits tended to clog the pipe. Also additional mechanical cleaning by special tools did not solve the problem. Therefore the off-gas pipe had to be exchanged several times. The exchange of the off-gas pipe as well as the short pressurization of the melter plenum during blaster operation caused spread of contamination in the melter cell. Moreover the remote exchange and mechanical cleaning of the off-gas pipe led to undesired interruption of the vitrification operation.

As a result of the operational experience, modification of the off-gas pipe has been required with respect to minimization of deposits and avoidance of their accumulation. The solution may be achieved by combination of several design and operation features.

The new design of the off-gas pipe is shown in Fig. 1. It is characterized by a vertical and a horizontal part which are connected by an elbow. Both sections are equipped with differential pressure measurements helping to identifying the presence of deposits, potential.

The design combines two independent cleaning methods consisting of a water-flushing technique and the blaster technique. The cleaning strategy is based on the following measures:

- jacket water cooling of the vertical part of the off-gas pipe to keep the inner wall temperature below sintering conditions and to prevent the formation of rigid deposits
- reduction of the inner diameter of the off-gas pipe to increase the off-gas velocity
- continuous supply of pressurized air through the end slit at the lower part of the vertical pipe in order to cool the off-gas from about 400°C to about 250°C, thus counteracting sintering of deposits
- periodic water-cleaning (every 24 h) of the off-gas pipe by injection of water through the end slit of the vertical pipe which, due to the high velocity of the off-gas stream, is entrained through the off-gas pipe into the following dust scrubber
- periodic injection of water through four cleaning nozzles installed at different positions along the horizontal pipe to ensure the cleaning of the inner walls of this section
- the two blasters are kept as additional mean to support the cleaning operation in case of need
- access for mechanical cleaning if required by using e.g. a lance head with pressurized water or other mechanical tools is enabled

The design of the off-gas pipe furthermore enables simple remote maintenance of parts of the off-gas pipe as well as its complete exchange.

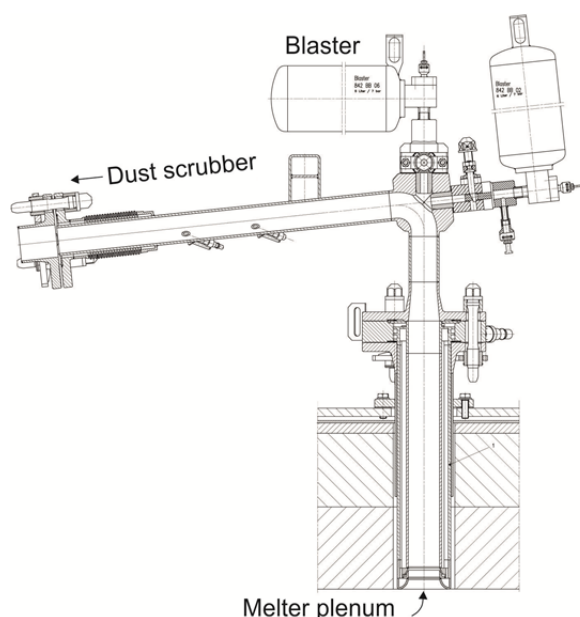


Fig. 1: New design of the melter off-gas pipe.

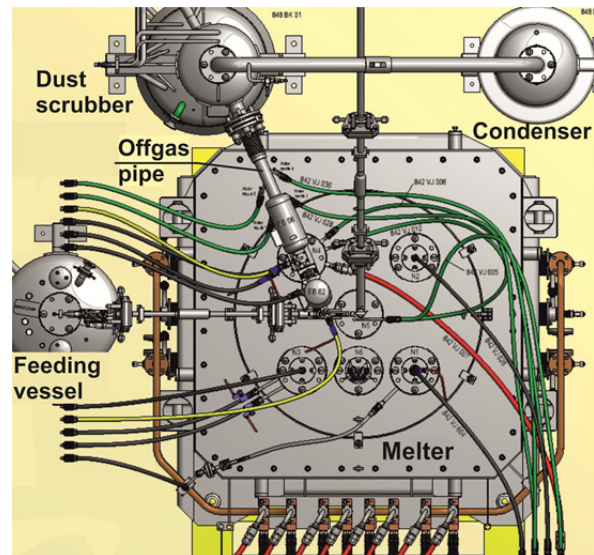


Fig. 2: Arrangement of the media lines and interfaces for the new designed off-gas pipe.

The change in the off-gas pipe design compared to the version laid down in the Basic Design (BD) entailed several modifications related to media supply, interfaces and arrangement. Besides the already existing lines for blaster loading air, purge air for blaster rinsing, instrumental measuring air and cooling water supply/return for melter feeding tube, additional lines were necessary for

- water supply to the 4 cleaning nozzles
- cooling water supply/return for vertical section
- air supply to end slit

The lines partly have to be lockable to avoid potential spread of contamination to the valve galleries. The arrangement of the media lines along with their interfaces are shown in Fig. 2 containing a top view on the melter connected via off-gas pipe to the adjacent dust scrubber. Also the feeding vessel for supply of the waste solution is shown.

## 2. Manufacturing of melter components

The glass melter is composed of 19 subcomponent groups. As shown in Fig. 3 the melter consists of firmly integrated subcomponents (group 1-6) like melt tank ceramic refractories, plenum ceramics, power electrodes, bottom electrode, stainless steel containment and remotely exchangeable subcomponents (group 7-17) like bottom drain housing, HLLW- and glass frit feeding pipe, off-gas pipe, thermo-well for monitoring process temperatures, glass level detection system, and two air bubble. The remaining subcomponent groups (18-19) are composed of service parts and tools for assembly and transportation of the melter.

Based on the DD the bulk of the remotely exchangeable subcomponents were manufactured in 2013 under control and responsibility of KIT-INE. Manufacturer has been the mechanical workshop of KIT Campus North (TID) which has a long experience and expertise in manufacturing of metallic

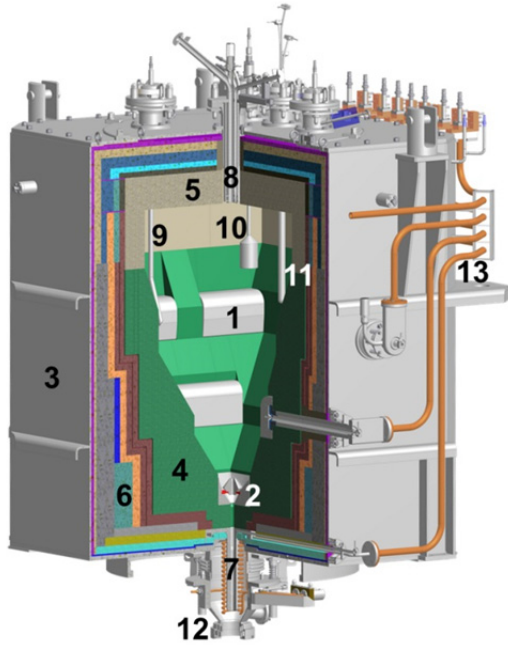


Fig. 3: Main structure of the VPC glass melter. Firmly integrated subcomponents: 1 Power electrodes, 2 bottom electrode, 3 stainless steel containment, 4 melt tank ceramic refractory, 5 melter plenum ceramics, 6 thermal insulation, 7 glass pouring pipe, Remote subcomponents: 8 feed inlet tube, 9 air bubbler, 10 glass level detection system, 11 thermo-well, 12 bottom drain housing, 13 copper tubes for power supply.

melter parts and subcomponents groups as well as their mounting. The list comprehended the feed inlet tube, the bubblers, the thermo-well, the glass level detection system, the bottom drain housing as well as the external SiC heating elements. From all parts multiple copies had to be manufactured as spare parts according to the contract.

### 3. Melter assembly

The melter assembly started in April 2013 after preparation of the assembling place inside the technical hall in the building B714 of KIT-INE under supervision of KIT personnel. Until February 2014 the melter was completed under support of SORG company and TID. Fig. 4 shows stages of the assembly until finalization. For shipment to China the melter will be encased in a special shock-safe containment to minimize the risk of damage during transportation. The remote subcomponents will be packed and sent separately. Transportation of the melter and subcomponents as well as other process components to China via Hamburg and Shanghai is planned to be in June/July 2014. The total transportation distance until destination in Guang Yuan in the Sichuan province covers about 24000 km.

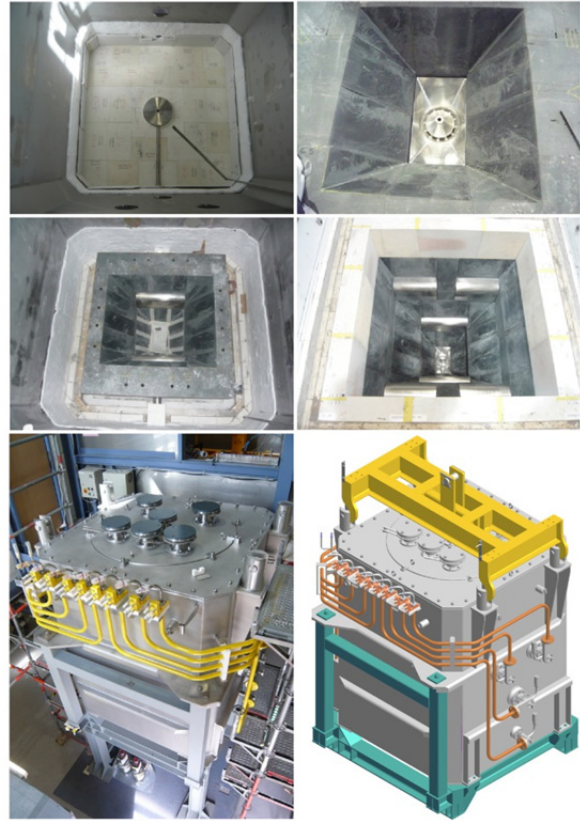


Fig. 4: Stages of the melter assembly at KIT-INE (left to right/downward): melter bottom with pouring channel, lower melt tank with bottom electrode, lower electrode level, upper electrode level, completed melter, 3D-model of the completed melter placed on the assembly console.

## 7.2 Research work for immobilization of high active solid waste

After finishing the vitrification of the WAK-HLLW in 2010 the VEK vitrification plant was rinsed. Now it is subject to decommissioning and dismantling. The remaining rinsing liquid of about 3000 l was stored in equal quantities in VEK's receipt tank 841 BB 02 and in the evaporation concentrate tank 845 BB 03. The analysis of the rinsing solution by ICP-MS revealed high concentrations of Cs and Tc. The liquid was intentionally led self-evaporating (3 l/day) until solid waste was formed on tank bottom in the subsequent years 2012/2013.

Based on considerations regarding solubilities of the different constituents in the aqueous rinsing solution it is assumed that alkali pertechnetates ( $\text{NaTcO}_4$ ,  $\text{CsTcO}_4$ ) have precipitated along with nitrates of Na, Fe, La, etc. during the drying process.

For immobilization of this solid waste different process techniques were evaluated (including sintering, sol-gel process, In-can melting in borosilicate glass). It appeared that In-can melting is one of the most promising candidates to perform the immobilization of the waste which is assumed to be less than 50 kg.

In view of the volatility of Tc and Cs compounds in the solid waste when subjected to high temperatures, a low melting barium borosilicate glass has been preliminary selected for immobilization. The main constituents of this glass matrix are  $\text{SiO}_2$  (38 wt%) and  $\text{BaO}$  (21 wt%). It is required to perform the immobilization process under dry conditions which means dry feeding of the waste and glass forming material into the melting pot and also dry offgas cleaning.

For basic information about the waste to glass conversion, thermogravimetric analysis (TGA) and differential scanning calorimetry (DSC) measurements were performed besides other lab-scale testing. TGA/DSC measurements were performed with waste simulate (with Re as surrogate of Tc) and with individual waste components ( $\text{NaReO}_4$ ,  $\text{CsReO}_4$ ,  $\text{NaNO}_3$ ). Preliminary data are given in Fig. 5.

For lab-scale waste to glass conversion simulated waste and glass frit (premelted at  $1150^\circ\text{C}$ ) were molten together at  $950^\circ\text{C}$  for 1 hour. The waste glass loading was adjusted to 10 wt%. Samples were molten under different conditions regarding melting time, addition of reducing agents, waste precursors and melting cavities. Experiences from these tests are encouraging. An important aspect of dry processing is that easy liberation of the gaseous species is necessary. Simultaneously, removal and recycling of the loss of Cs and Tc compounds into the process is an important challenge as well.

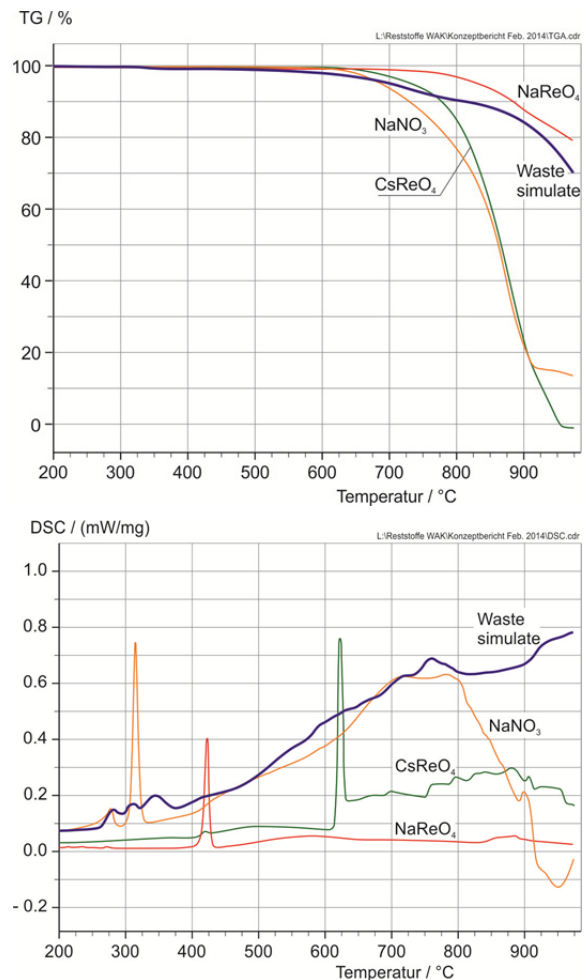


Fig. 5: TGA- and DSC measurements of the waste simulate and of related individual components.

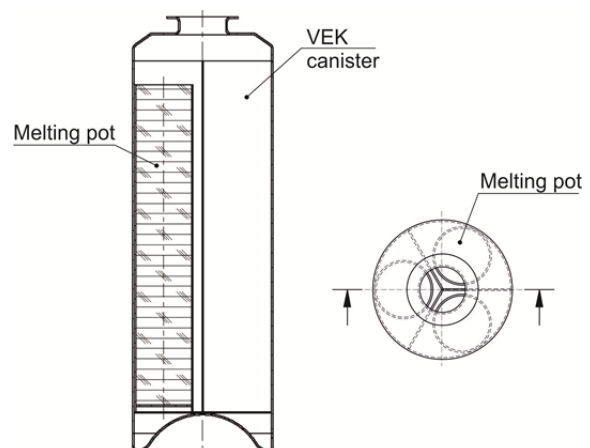


Fig. 6: Simplified scheme of one candidate of In-can melting.

## 8 Development of actinide speciation methods

Maintaining a state-of-the-art portfolio of advanced surface science and spectroscopy methods at INE is an important R&D activity, as these methods are crucial tools for understanding and advancing actinide and radionuclide (geo)chemistry. Radionuclide speciation methods available at INE controlled area laboratories and the KIT synchrotron radiation facility ANKA are continuously adapted to better serve the requirements of the INE in house R&D program. Nevertheless, access is also provided to the radiochemistry and nuclear science community, either through EU funded transnational access initiatives, or through direct cooperation with KIT-INE. The unique methodology offered by INE is in the focus of many national and international collaborations, thus providing training and education for young researchers and helping to maintain a high level of nuclear competence. The long-standing development of LIBD techniques at INE has culminated in 2013 in the manufacturing of the first prototype of a commercial portable system for nanoparticle characterization. The instrument was launched into the market in the framework of a successful technology transfer project. NMR analysis for all BTP and BPP “partitioning” complexes of the whole lanthanide series has been accomplished and compared to results obtained for corresponding Am(III) complexes. Unexpectedly large chemical shift differences have been found for the directly bound nitrogen atoms in the Am(III) complexes, while the non-bonding nitrogens are not affected. This is the first substantial support for the thesis that the extraction selectivity towards trivalent actinide cations originates from covalent interaction between the actinide and the ligands. For the first time ever at a synchrotron radiation experimental station, a genuine glass fragment from a HAWC vitrification process has been investigated at the INE-Beamline at ANKA in 2013. Direct determination of actinide and fission product speciation in a highly active nuclear material has been demonstrated. TEM and high resolution electron diffraction techniques accessible at KIT-IAM have revealed that Ca/Ba rich particles of about 500 nm diameter forming in borosilicate glasses at high Mo loading consist of spatially separated BaMoO<sub>4</sub> and CaMoO<sub>4</sub> crystal phases. TEM and EELS have been also used for the first time in 2013 to characterize nm-sized PuO<sub>2</sub> colloids at atomic resolution. Many of the in house research activities at INE benefit from strong support by quantum chemical calculations, providing molecular structures or thermodynamic data. In 2013 ab initio force field calculations and molecular dynamics simulations have been for the first time successfully combined to model the structure of Cm(III)-BTP complexes in aqueous solution.

### 8.1 R&D projects conducted at the INE-Beamline for Actinide Research at ANKA and at external synchrotron radiation sources

*S. Bahl, N. L. Banik, B. Beele, K. Dardenne, M. A. Denecke, D. Fellhauer, A. Geist, D. Fröhlich, E. González-Robles Corrales, B. Kienzler, P. Lindqvist-Reis, V. Metz, N. Müller, P. Panak, I. Pidchenko, T. Prißmann, J. Rothe, D. Schild, B. Schimmelpfennig, A. Skerencak-Frech, T. Vitova*

#### Introduction

Synchrotron radiation (SR) based techniques have become key speciation methods in actinide and radionuclide research. This development is primarily driven by the need for reliable speciation methods to characterize (geo-)chemical processes determining mobilization or immobilization of long-lived actinide and fission product elements as a prerequisite for the implementation of a repository for highly active, heat producing nuclear waste (HAW) in a deep geological formation. Solving the nuclear disposal safety case requires assessment of a projected repository site on geological time scales, where speciation techniques like XAS (X-ray Absorption Spectroscopy) provide necessary input parameters for modelling geochemical reaction and transport pathways for radionuclides. Nuclear areas profiting from the use of SR based characterization tools include topics in condensed matter physics and material science of the actinides, decommissioning of nuclear facilities, clean-up procedures for contaminated land and sectors of the nuclear fuel cycle including fuel production, reprocessing, waste conditioning and disposal. The INE-

Beamline for actinide science [1] at the KIT synchrotron light source ANKA [2] is operated by KIT-INE since 2005 as a flexible experimental station for spectroscopic investigation of radioactive sample systems. The INE-Beamline is the only facility of its kind in Europe offering access to radiochemistry laboratories with state-of-the-art analytical equipment in direct proximity to a SR experimental station. INE beamline scientists support *in house* and external users in planning, performing and evaluating experiments, including clearance of all relevant radiation safety and personal security issues. INE scientists also conduct various experiments at external SR sources offering capabilities not - or not yet - available at KIT.

#### INE-Beamline user operation in 2013

In 2013 a total of 32 *in house* and external projects were hosted at the INE-Beamline. The time available for INE internal research amounted to ~32% of all available shifts (38 days). Fifteen days were spent for maintenance, development and pilot experiments. As

in the previous years, the majority of beamtime shifts in 2013 was given to external projects with (43 days) and without (9 days) PRC (ANKA Peer Review Committee) evaluation (i.e., through direct cooperation). INE projects at the beamline covered a broad X-ray spectroscopy program for characterization of actinide materials - with an emphasis on initial studies applying advanced high resolution (HR) XANES techniques for actinide speciation studies. Many of these studies are presented in more detail elsewhere in this report or the recent ANKA Annual Report 2012/13 [3]. INE *in house* projects in 2013 included various investigations of the structural incorporation of actinides and chemical homologues in colloids and secondary mineral phases, aqueous speciation of actinides in highly saline solutions, the redox chemistry of Np(VI)/Np(VII), Th(IV) solubility in the presence of fulvic acid and the pH dependency of Am(III) complexation with acetate. For the first time ever at a synchrotron radiation experimental station, a sample derived from a real nuclear process (glass fragment from HAWC vitrification at the WAK reprocessing plant) was investigated at the INE-Beamline in 2013. Direct determination of actinide and fission product speciation in a highly active nuclear material was shown to be in principle feasible.

General user research projects receive beamtime at INE-Beamline following PRC evaluation (biannually in January and June), as approved TALISMAN Joint Research Projects (both together comprising at least 30% of all available shifts) or through direct cooperation with KIT-INE. In 2013 scientists from the 11 German and international research institutions listed below conducted experiments at the INE-Beamline:

- Uppsala University, Department of Physics and Astronomy, Uppsala, Sweden
- JRC - Institute for Transuranium Elements, Karlsruhe, Germany
- Los Alamos National Laboratory, Los Alamos, USA
- Universität Heidelberg, Fakultät für Chemie und Geowissenschaften, Heidelberg, Germany
- University of Manchester, School of Earth, Atmospheric and Environmental Science, Manchester, United Kingdom
- CEA Cadarache, Saint Paul Lez Durance, France
- Bundesanstalt für Geowissenschaften und Rohstoffe, Hannover, Germany
- Leibniz Universität Hannover, Institut für Radioökologie und Strahlenschutz, Hannover, Germany
- Amphos<sup>21</sup>, Barcelona, Spain
- Université Claude Bernard, Institut de Physique Nucléaire de Lyon, Lyon, France
- Lomonosov Moscow State University, Radiochemistry Division, Chemistry Department, Moscow, Russia

Three projects in 2013 received beamtime and were funded through the EU project TALISMAN or its predecessor ACTINET-i3 as Joint Research Projects.

As in previous years, a significant percentage of *in house* and PRC beamtime was used by Master and PhD students to perform experiments in the framework of their theses (a total of 8 projects, corresponding to ~30% of all available shifts).

### High-temperature XAFS

The near-field temperatures in a HAW repository are projected to reach up to 200 °C for deep geological disposal in rock salt formations. Repository failure scenarios generally implicate water intrusion and successive corrosion of waste containers and HAW matrices. In case of disposal in a rock salt formation, chloride will be the most abundant ligand available for complexation reactions with dissolved radionuclides. Due to the elevated temperatures expected in the repository near-field, the chemical properties of radionuclides and potential ligands will change significantly. Nevertheless, there is a general lack of knowledge on actinide complexation by organic and inorganic ligands at elevated temperatures. Am(III) complexation by chloride was investigated in the temperature range 20 - 200 °C applying the custom built high-temperature XAFS cell [4] already used in previous studies of Am(III) complexation by lactate and nitrate.

Fig. 1 shows the experimental  $k^3$ -weighted Am L3-edge EXAFS spectra (left) and corresponding Fourier Transforms (right) of 1 mM Am(III) in the presence of 3 M chloride at 20 - 200 °C together with the fit curves (red symbols). The corresponding structural parameters are summarized in Tab. 1. Details of the fit procedure and errors of the fit parameters can be found elsewhere [4].

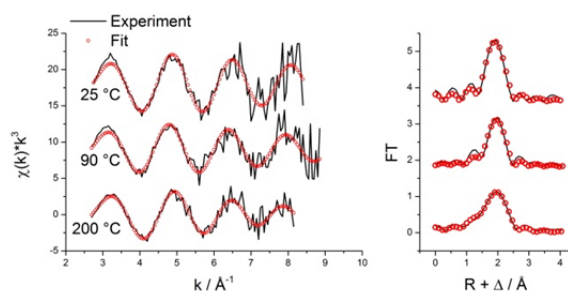


Fig. 1:  $k^3$ -weighted Am L3-edge EXAFS spectra (left) and Fourier Transforms (right) of 1 mM Am(III) in the presence of 3 M chloride at 20, 90, and 200°C.

Tab. 1: Structural parameters related to the fit curves in Fig. 1.

T / °C	Am-O			Am-Cl		$\Delta E_0$ / eV
	N	R / Å	$\sigma^2$ / Å <sup>2</sup>	N	R / Å	
20	9.6	2.45	0.007	-	-	-4.9
90	9.0	2.48	0.009	-	-	-5.0
200	6.3	2.44	0.015	2.4	2.78	-5.0

Whereas room temperature studies did not indicate any complexation of trivalent actinides by chloride at  $[Cl^-] < 8\text{ M}$  [5], the present work unambiguously proved Am-Cl interaction at  $T = 200\text{ }^\circ\text{C}$  at the relatively low chloride concentration of 3 M. Thus one has to assume that the impact of chloride complexation on the speciation of trivalent actinides will increase significantly at elevated temperatures. This finding emphasizes the necessity to derive high temperature thermodynamic and structural data for a reliable assessment of actinide solubility and mobility under repository near-field conditions.

### XAFS investigation of a HAWC glass fragment

The Karlsruhe Reprocessing Plant (WAK) was operated from 1971 to 1991 as a pilot facility for the reprocessing of spent nuclear fuels from German pilot reactors and commercial power plants. Reprocessing activities resulted in  $\sim 60\text{ m}^3$  of highly radioactive waste concentrates (HAWC) stored on-site in liquid form. An important step in the current decommissioning of the WAK was the HAWC vitrification in the Karlsruhe Vitrification Plant (VEK) constructed close to the HAWC storage facilities [6] (cf. chapter 8). Sections of genuine HAWC glass rods were retained during the vitrification process and transferred to the INE shielded box line for later glass product characterization. In 2013 a mm sized fragment (Fig. 2, left) with a contact dose rate of  $\sim 590\text{ }\mu\text{Sv/h}$  was selected and mounted in a specially designed sample holder (Fig. 2, right) for pilot XAS/XRF investigations at the INE-Beamline. The experiment was aimed at elucidating the potential of direct actinide / radionuclide speciation (with an emphasis on fission products) in highly active nuclear materials (e.g., waste glass, spent fuel) and at assessing the possible influence of the  $\gamma$ -radiation field surrounding highly active samples on the XAS detection electronics.

While the influence of the  $\gamma$ -radiation field turned out to be negligible, initial radionuclide speciation studies by XAS were most promising. Exemplarily, Fig. 3 depicts normalized Se K- (top) and Tc K-edge XANES measurements (bottom) of the HAWC glass fragment and corresponding Se and Tc reference samples, respectively. Edge position and simple spectral fingerprint analysis point to the presence of Se in the glass as selenite as in  $\text{Na}_2\text{SeO}_3$ . Pronounced dampening of the near-edge fine structure indicates dispersion of the  $\text{SeO}_3^{2-}$  oxoanions in the glass matrix, where the crystalline ordering such as in the

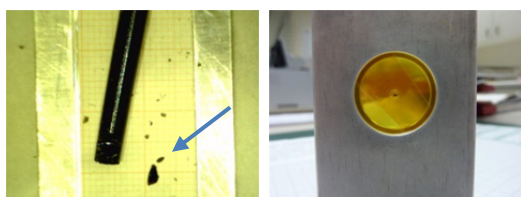


Fig. 2: HAWC glass fragment (arrow) selected for investigation at INE-Beamline (left) and glass fragment inside a double containment mounted in the sample holder (right) prior to the transport to ANKA.

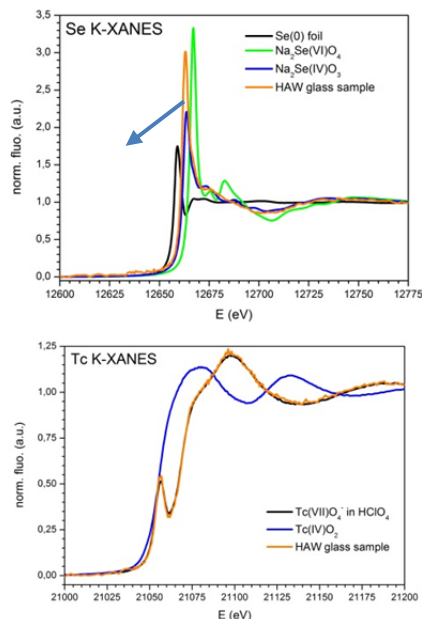


Fig. 3: Se K- (top) and Tc K-edge XANES (bottom) of a HAW glass fragment and corresponding reference spectra.

$\text{Na}_2\text{SeO}_3$  reference is lost. Tc is dispersed as pertechnetate anion ( $\text{TcO}_4^-$ ) in the glass matrix as in the aqueous Tc(VII)/ $\text{HClO}_4$  reference sample, which is unequivocally proven by the edge shift relative to  $\text{Tc(IV)O}_2$  and the pronounced pre-edge feature at  $\sim 21056\text{ eV}$  indicative of tetrahedral oxygen coordination.

### High energy resolution X-ray emission spectroscopy (HRXES)

Installation and commissioning of the multi-analyzer crystal (MAC) spectrometer for high energy resolution X-ray emission spectroscopy (HRXES) was completed at the INE-Beamline in 2013 (Fig. 4).

Fig. 5 compares conventional Pu L3-edge XANES spectra measured in conventional fluorescence detection mode (a) and Pu L3-edge high energy resolution XANES (HR-XANES) spectra recorded with the MAC-spectrometer (b) of aqueous Pu species in perchloric acid at oxidation states III, IV, V and VI [3].

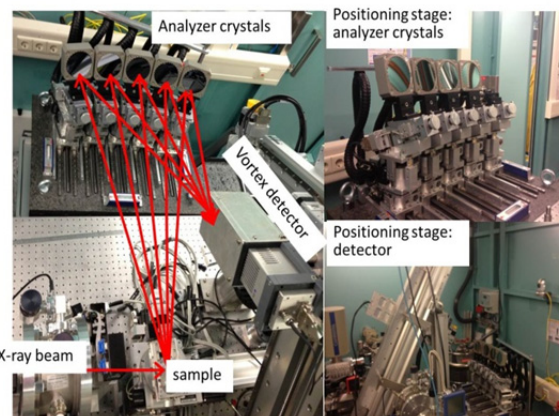


Fig. 4: The MAC spectrometer during initial experiments at INE-Beamline.

The most intense absorption resonance (white line, B) has higher intensity and is better separated from the post edge feature C in the Pu(V) and Pu(VI) HR-XANES spectra compared to the conventional spectra. The energy distance ( $\Delta E$ ) between features B and C is roughly a measure of the bond length ( $R$ ) between Pu and the axial oxygen atoms ( $O_{ax}$ ):  $\Delta E \cdot R^2 = \text{constant}$ . The HR-XANES spectra allow for more precise evaluation of these distances due to the better resolution. In addition, the reduced width of spectral features facilitates detection of minor contributions in spectra of samples containing Pu oxidation state mixtures.

Quantum chemical calculations of the Pu(VI) HR-XANES spectrum performed with the *FEFF9.5* code are depicted in Fig. 5c. The Pu  $d$  and  $f$  density of states ( $d$ -,  $f$ -DOS) are plotted along with calculated Pu L3-edge HR-XANES spectra, including either only dipole ( $2p_{3/2} \rightarrow 6d$ ) or dipole and quadrupole ( $2p_{3/2} \rightarrow 5f$ ) electronic transitions. The overall shape of the experimental spectrum resembles the Pu  $d$ -DOS, implying predominance of dipole transitions. Additionally, a pre-edge feature A, similar to that observed for U(VI) [7], might be present in the Pu(VI) HR-XANES spectrum as well. *FEFF9.5* calculations implicate transitions to unoccupied Pu  $f$  states as origin of this feature. In 2014 the MAC-spectrometer will be upgraded with a slit system designed and built in 2013, which will improve the experimental energy resolution and thereby facilitate detection of these kind of spectral features.

In addition to actinide L3-edge HR-XANES measurements, pilot experiments at the U M4-edge (3728 eV) were performed in 2013. One major re-

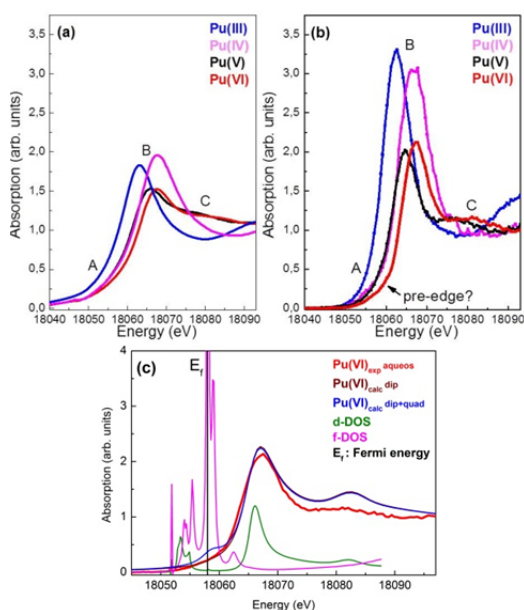


Fig. 5: (a) conventional Pu L3-edge XANES and (b) HR-XANES spectra of Pu(III), Pu(IV), Pu(V) and Pu(VI) in perchloric acid. (c) FEFF9.5 calculation of the Pu(VI) HR-XANES spectrum and corresponding density of states (DOS).

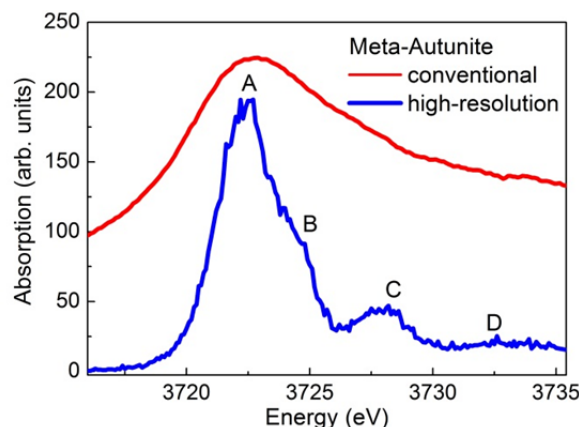


Fig. 6: U M4-edge XANES (top) and HR-XANES (bottom) of the U mineral Meta-Autunite.

quirement in this energy range was to minimize the path length of the incident beam and the U  $M\beta$  fluorescence photons (3339.8 eV) in air in order to increase the efficiency of the experiment. A He filled polyethylene bag based on an original ESRF design was purchased and tested as a preliminary concept. An optimized He enclosure of the whole spectrometer setup will be developed and tested in 2014. Despite the persisting  $\sim 90\%$  intensity loss due to remaining air gaps and necessary polymer windows in front of sample, analyzer crystals and detector, the U M4-edge HR-XANES spectrum of the mineral meta-autunite was successfully measured (Fig. 6). The energy resolution of the U M4-edge HR-XANES spectrum is significantly improved compared to the conventional measurement. The absorption resonances A, B and C of the high-resolution spectrum have been assigned to electronic transitions of U  $3d_{3/2}$  electrons to  $\phi/\delta$  (A),  $\pi^*$  (B) or  $\sigma^*$  (C) molecular orbitals [8]. The  $\phi/\delta$  orbitals have major U  $5f$  and minor ( $<15\%$ ) O  $2p$  valence orbital character derived from O neighbors in the equatorial plane ( $O_{eq}$ ), whereas  $\pi^*$  and  $\sigma^*$  have about 24% and 64% O  $2p$  contributions from  $O_{ax}$  neighbors, respectively. The U M4 HR-XANES spectrum probes the relative energies of the lowest unoccupied molecular orbitals (LUMO) and the level of U  $5f$  and  $O_{eq}/O_{ax}$   $2p$  valence orbital hybridization, thereby providing insight into the nature of the U-ligand bonding previously not available in such detail.

## N K-edge investigations of partitioning complexes

One of the major steps in the partitioning and transmutation (P&T) strategy for the reduction of the long-term radiotoxicity and heat-load of spent nuclear fuel is the separation of  $5f$  elements from their chemically similar  $4f$  counterparts (cf. chapter 7). Selective liquid-liquid extraction of An(III) from Ln(III) has been demonstrated using heterocyclic N-donor ligands, e.g., bistriazinylpyridines (BTP) and bistriazinylbipyridines (BTBP). However, these ligands do not yet fulfill all necessary criteria for application in an industrial process. Further ligand optimization requires a sound understanding of the chemical and

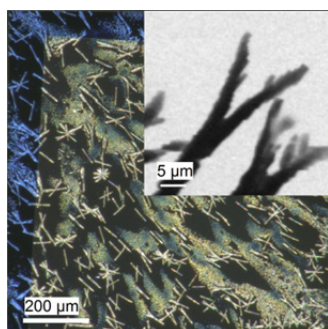


Fig. 7: Optical and X-ray microscopy (STXM, inset) images of  $\text{Am}(\text{BTP})_3(\text{OTf})_3$  crystals.

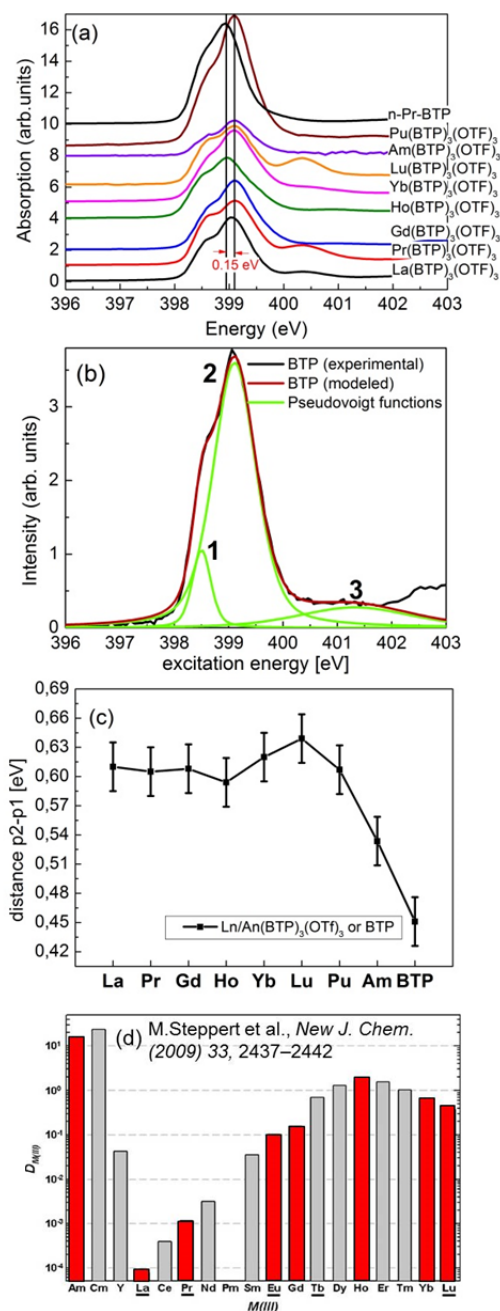


Fig. 8: (a) N K-edge XANES pre-edge region of  $[\text{Ln}/\text{An}(\text{BTP})_3](\text{OTf})_3$ ,  $[\text{Am}/\text{Pu}(\text{BTP})_3](\text{OTf})_3$  and  $n\text{-Pr-BTP}$ ; (b) Pre-edge region modeled with Pseudo-Voigt profiles; (c) Energy differences between peak 1 and 2 for Ln/An complexes and the free BTP ligand; (d) Distribution ratios ( $D_{M(III)}$ ) for Ln/An extraction to the organic phase.

physical properties responsible for their selectivity towards  $\text{An}(\text{III})$ . Systematic comparative N K-edge XANES investigations complemented by quantum chemical calculations can help to differentiate between subtle bonding differences in  $\text{An-BTP}$  and  $\text{Ln-BTP}$  complexes looking from the point of view of the organic ligand. Bonding characteristics like molecular orbital energy differences and relative electronic populations can be extracted.

N K-edge XANES investigations of  $[\text{Pu}(\text{BTP})_3](\text{OTf})_3$ ,  $[\text{Ln}(\text{BTP})_3](\text{OTf})_3$  ( $\text{Ln}=\text{La}, \text{Pr}, \text{Gd}, \text{Ho}, \text{Lu}$  or  $\text{Yb}$ ) complexes and 2,6-Bis(5,6-dipropyl-1,2,4-triazin-3-yl)-pyridine ( $n\text{-Pr-BTP}$ ) were performed in fluorescence mode at the soft X-ray spectroscopy beamline WERA at ANKA. The samples were prepared by drying  $\sim 2 \mu\text{l}$  of the solved complexes on Al foil. N K-edge spectra of  $[\text{Am}(\text{BTP})_3](\text{OTf})_3$  were measured by scanning transmission X-ray microscopy (STXM) at beamline 11.0.2 at the Advanced Light Source (ALS), Berkeley Natl. Laboratory, USA. One  $\mu\text{l}$  of a 30 mmol/L  $\text{Am}(\text{BTP})_3(\text{OTf})_3$  solution was dried on a 100 nm thick  $\text{Si}_3\text{N}_4$  window. A second window was glued on top to provide containment. The optical microscopy image and a STXM micrograph of the  $\text{Am}(\text{BTP})_3(\text{OTf})_3$  crystals obtained above the N K-edge (inset) are depicted in Fig. 7.

All N K-edge XANES spectra have a distinct pre-edge feature at about 399 eV arising from excitations of the N 1s electron to antibonding  $\pi^*$  molecular orbitals (Fig. 8a). This feature can be successfully mod-

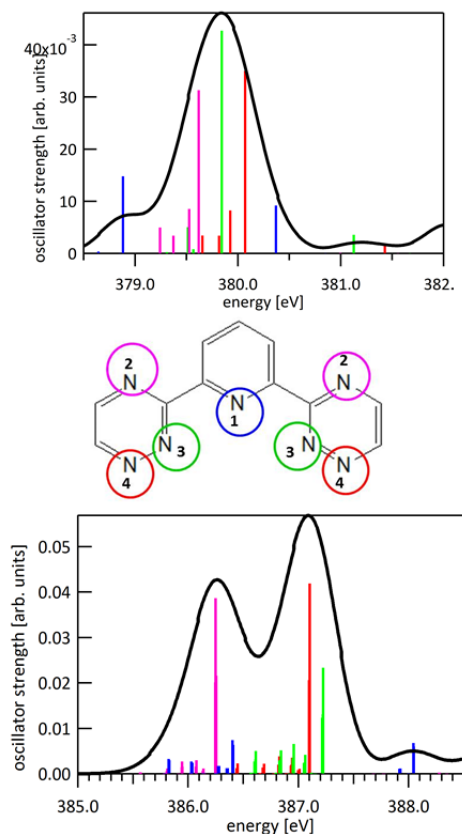


Fig. 9: ORCA calculations of N K-edge XANES pre-edge region and corresponding N 1s excitations (color-coded to the BTP structure shown in the middle) for H-BTP (top) and  $\text{La}(\text{BTP})_3$  (bottom).

eled by fitting three Pseudo-Voigt (PV) functions to the experimental spectrum (Fig. 8b) [9]. The energy difference between the main peaks **1** and **2** (Fig. 8c) shows a weak anti-correlation with respect to the trend of the ligand selectivity (Fig. 8d). This difference is the smallest for the free BTP ligand, indicating distinct differences in molecular orbital energies between free ligand and complexes. These differences can be partially explained by quantum chemical calculations. The theoretical N 1s spectra of H-BTP calculated with the ORCA [10] program reproduces the number of peaks observed in the experimental spectra (Fig. 9, top). Analyzing the origin of the 1s electronic transitions (marked with color-coded sticks) allows identification of contributions of non-equivalent N atoms of the BTP molecule (Fig. 9, center) to the spectra. Calculations of the La(BTP)<sub>3</sub> complex show a different transition sequence (Fig. 9, bottom), suggesting higher charge density in the vicinity of the bonding N atoms. The lower oscillatory strength of transitions from bonding N atoms compared to non-bonding N atoms for the complex compared to the free ligand might be interpreted as evidence for lower contributions of N *p* states to the π\* molecular orbitals, suggesting strong admixtures of metal orbitals in the complex. The calculation of the Am(BTP)<sub>3</sub> complex is discussed in more detail in section 9.5.

### Acknowledgement

Many thanks to H. Blank (Bonn University), A. Neumann, V. Krepper, J. Thomas, A. Bauer and Ch. Marquardt (all KIT-INE), T. Hoffmann and G. Christill (both KIT-SUM) for invaluable technical and logistic support. Support of the WERA (KIT-ANKA) and 11.0.2 (ALS/LBNL) beamline teams is thankfully acknowledged. We also thank Christos Apostolidis (JRC-ITU) for synthesizing and providing the [Am(BTP)<sub>3</sub>](OTf)<sub>3</sub> complex.

### References

- [1] Rothe, J. et al., *Rev. Sci. Instrum.* **83**, 043105 (2012)
- [2] [www.anka.kit.edu](http://www.anka.kit.edu)
- [3] ANKA Annual Report 2012/2013, KIT Scientific Publishing 2014
- [4] Skerencak-Frech, A. et al., *Inorg. Chem.* **53**, 1062-1069 (2014)
- [5] Allen, P. G. et al., *Inorg. Chem.* **39**, 595-601 (2000)
- [6] Roth, G. et al., *Nucl. Engineering and Design* **202**, 197-207 (2000)
- [7] Vitova, T. et al., *Phys. Rev. B* **82**, 235118 (2010); Walshe, A. et al., *Dalton Trans.* **43**, 4400 (2014)
- [8] Fillaux, C. et al., *C. R. Chimie* **10**, 859 (2007)
- [9] Prüßmann, T. et al., *J. Physics: Conference Series* **430**, 012115 (2013)
- [10] Becker U, et al., ORCA - an ab initio, DFT and semiempirical electronic structure package

## 8.2 Laser spectroscopy

S. Büchner, C. García, K. Gompper, R. Götz, W. Hauser, J. Laber, P. Lindqvist-Reis

In co-operation with:

A.T. Wagner<sup>a</sup>, P.W. Roesky<sup>a</sup>, M. Löble<sup>a</sup>, F. Breher<sup>a</sup>, P. Nagtegale<sup>b</sup>

<sup>a</sup> Institut für Anorganische Chemie, Karlsruher Institut für Technologie (KIT), Karlsruhe, Germany.

<sup>b</sup> Cordouan Technologies, Bordeaux, France.

### Introduction

Continuous development of laser-based speciation techniques is one of the most important tasks performed at INE, providing efficient tools for the analysis of nuclear waste forms and their possible interaction with the surrounding environment. The main advantages of techniques like Laser Induced Breakdown Detection (LIBD) or Time-Resolved Laser Fluorescence Spectroscopy (TRLFS) are the minimal efforts required for sample preparation in combination with an extremely high sensitivity. These advantages are quite important when analysing the behaviour of lanthanides and actinides under nuclear repository far-field conditions. The long-standing development of LIBD techniques at INE has culminated in 2013 in the design and manufacturing of the first prototype of a commercial portable system for nanoparticle characterization. The instrument was launched into the market under the name “MAGELLAN”. Basic research applying TRLFS has been carried out in 2013 with a focus on Eu(III) luminescence quenching by water and hydroxide ligands in different host compounds. Finally, an initial feasibility study has been finished in 2013, assessing the implementation of remote Laser Induced Breakdown Spectroscopy (LIBS) instrumentation for the analysis of highly radioactive nuclear waste or residues left over from HAWC vitrification.

### Launch of the first commercial portable LIBD system (collaboration with Cordouan Technologies)

The success of a recent technology transfer project executed by KIT-INE in collaboration with an industrial partner, the French company Cordouan Technologies, has been demonstrated with the market launch of the “MAGELLAN” in 2013. This instrument (Fig. 1) is the first mobile nanoparticle analyzer based on the LIBD technique which is able to determine size distributions of particles (in the size range 10 nm – 1 µm) in liquid media [1]. The project has been finalized in 2013 by instrumental optimization, calibration of the system and the development of a specific software for instrument control and data analysis.

As a proof of its success, the “NPA/LIBD” project has been awarded in 2013 with the first prize in the category for technology transfer projects within the 1<sup>st</sup> edition of the “NEULAND Innovation Award” donated by KIT [2].



Fig. 1: View of the new “Magellan” instrument and its analysis software shown by Cordouan Technologies on their webpage [1].

### Luminescence quenching by water and hydroxide

Eu(III) and Cm(III) are frequently used as luminescence probes in time-resolved laser fluorescence spectroscopy (TRLFS) experiments. Because of the high sensitivity of the method, the concentration of these ions may be as low as  $10^{-7}$ - $10^{-8}$  mol/L. In general, the luminescence spectra probe the ions’ local (coordination) structure, while the luminescence lifetimes ( $\tau$ ) contain information about the number of coordinated water and/or hydroxide ligands. If no water or hydroxide ligands are coordinated to the ions, the lifetimes may reach several milliseconds. If the ions are fully hydrated, as in the case of the nonhydrated lanthanide(III) and actinide(III) triflate salts or in aqueous solution, the lifetimes are reduced to about 105 and 65  $\mu$ s, respectively [3,4]. This luminescence quenching takes place through multi-phonon energy transfer by coupling with ligand OH stretch vibrational overtones, a process that bridges the energy gap between the excited state and the ground state.

The effective (observed) emission decay rate constant,  $k_{\text{obs}} (= \tau^{-1})$ , is composed of a radiative and a nonradiative part. The latter contains contributions due to the decay by  $n$  water molecules or hydroxide ions ( $n \cdot k_{\text{H}_2\text{O},\text{OH}^-}$ ) and other nonradiative decay pathways ( $k_{\text{nr}}$ )

$$k_{\text{obs}}(\text{H}_2\text{O},\text{OH}^-) = k_r + k_{\text{nr}} + n \cdot k_{\text{H}_2\text{O},\text{OH}^-} \quad (1)$$

Since  $k_r$  and  $k_{\text{nr}}$  are independent of  $\text{H}_2\text{O}$ ,  $\text{D}_2\text{O}$ ,  $\text{OH}^-$  and  $\text{OD}^-$ , and  $k_{\text{D}_2\text{O}} \ll k_{\text{H}_2\text{O}}$  and  $k_{\text{OD}^-} \ll k_{\text{OH}^-}$ ,

$$n = (k_{\text{obs}}(\text{H}_2\text{O},\text{OH}^-) - k_{\text{obs}}(\text{D}_2\text{O}))/k_{\text{H}_2\text{O},\text{OH}^-} \quad (2)$$

Eq. 2 is the basis for the ‘‘Horrocks equation’’, in which the number of water molecules coordinated to an Eu(III) ion can be obtained [5]. More recently, Supkowski et al. published an extended equation allowing calculation of the number of water, alcohol, amine, and amide ligands in Eu(III) complexes [6]. Although hydroxo complexes were not investigated, we may expect the nonradiative decay rate constant of a hydroxide ion,  $k_{\text{OH}^-}$ , to be similar to that of an alcohol molecule,  $k_{\text{alcohol}} \approx 450 \text{ s}^{-1}$ , a value about half that of a water molecule,  $k_{\text{H}_2\text{O}} \approx 900 \text{ s}^{-1}$ . In the following, we will estimate the values of  $k_{\text{H}_2\text{O}}$  and  $k_{\text{OH}^-}$  in aqua and hydroxo compounds with known structures. To simplify we shall assume that  $k_r + k_{\text{nr}} \approx 0.579 \text{ s}^{-1}$  in all of the studied compounds. This value is obtained by inspection of eqs. 1 and 3, the latter being an empirical equation by Kimura et al. [7] for the calculation of the number of water ligands in Eu(III) complexes without measuring the corresponding deuterated complexes

$$n = 1.07k_{\text{obs}} - 0.62 \quad (3)$$

Combining and rearranging eqs. 1 and 3 gives

$$n \cdot k_{\text{H}_2\text{O},\text{OH}^-} \approx k_{\text{obs}} - 0.579 \quad (4)$$

This means that the decay rate constants for water and hydroxide ions can be compared, at least approximately. Here, we present selected data from an ongoing study on the luminescence quenching of Eu(III) by aqua and hydroxide ligands in five different host compounds (**1-5**).

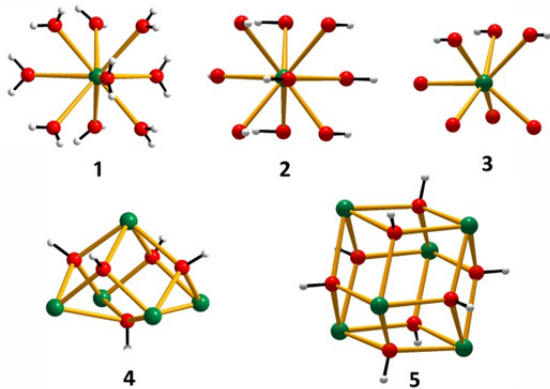


Fig. 2:  $M(\text{H}_2\text{O})_9$ ,  $M(\text{OH})_3$ ,  $\text{MO}_4(\text{OH})_3$ ,  $\text{Y}_5(\text{OH})_5$ , and  $\text{La}_6(\text{OH})_8$  entities in **1-5** obtained from X-ray diffraction.

Tab. 1: Luminescence quenching of  $\text{Eu}^{3+}$  by  $\text{H}_2\text{O}$  and  $\text{OH}^-$  ligands in **1-5** at room temperature.

Coordination entity in host	Quench entity	$\tau$ [ $\mu\text{s}$ ]	$k_{\text{H}_2\text{O},\text{OH}^-}$ [ $\text{s}^{-1}$ ]
<b>1</b>	$9 \times \text{H}_2\text{O}$	105(5)	994(50)
<b>2</b>	$9 \times \text{OH}^-$	287(5)	323(10)
<b>3</b>	$3 \times \text{OH}^-$	435(5)	573(10)
<b>4</b>	$4 \times \text{OH}^-$	350(5)	570(10)
<b>5</b>	$4 \times \text{OH}^-$	374(5)	524(10)

TRLFS spectra were recorded on the compounds of  $[\text{M}(\text{H}_2\text{O})_9](\text{CF}_3\text{SO}_3)_3$  ( $\text{M} = \text{La}, \text{Gd}, \text{Y}, \text{Lu}$ ; (**1**)),  $\text{M}(\text{OH})_3$  ( $\text{M} = \text{La}, \text{Gd}, \text{Y}$ ; (**2**)),  $\text{MOOH}$  ( $\text{M} = \text{La}, \text{Gd}, \text{Y}, \text{Lu}$ ; (**3**)),  $[\text{Y}_5(\text{OH})_5](\text{D-PhGly})_4(\text{Ph}_2\text{acac})_6$  (**4**), and  $[\text{La}_6(\text{OH})_8(\text{N-MeIm})_6(\text{CF}_3\text{SO}_3)_{12}](\text{HN-MeIm})_2$  (**5**), each containing a small amount of Eu(III). In **2** and **3**  $\text{M}(\text{OH})_9$  and  $\text{MO}_4(\text{OH})_3$  entities, respectively, form 3D networks, whereas in **4** and **5**  $\text{Y}_5(\text{OH})_5$  and  $\text{La}_6(\text{OH})_8$  clusters, respectively, are incorporated in large metal organic frameworks (Fig. 2).

Table 1 lists the luminescence lifetimes of Eu(III) in **1-5** together with the corresponding  $k_{\text{H}_2\text{O}}$  and  $k_{\text{OH}^-}$  values as obtained from eq. 4. The lifetimes in **1-3** were found to be slightly longer for the lanthanum hosts than for the yttrium and lutetium hosts owing to differences in the ionic radii between  $\text{Eu}^{3+}$  and the host metal ions. Therefore, the listed values represent gadolinium hosts since the ionic radii of  $\text{Gd}^{3+}$  and  $\text{Eu}^{3+}$  are similar; however, **4** is a yttrium host and **5** is a lanthanum host. Despite these inconsistencies, the values of  $k_{\text{OH}^-}$  are significantly lower, on the average about 50%, than the value of  $k_{\text{H}_2\text{O}}$ . Although this study is far from complete, the results suggest that for photoexcited Eu(III) complexes  $k_{\text{OH}^-} \approx k_{\text{alcohol}} \approx \frac{1}{2} k_{\text{H}_2\text{O}}$ . Further studies are underway, including luminescence studies of complexes doped with Cm(III).

### Feasibility studies for the development of LIBS analytical systems for remote analysis

Laser Induced Breakdown Spectroscopy (LIBS) is an optical emission spectroscopy (OES) technique used for the spectroscopic analysis of a laser induced plasma. After focusing a laser beam onto the sample surface, a dielectric breakdown is produced which leads to the plasma formation. Due to multiple collision processes, atoms and ions inside the plasma are electronically excited, emitting light at element or even isotope specific discrete frequencies. The spectral information is then collected and analysed, allowing the identification of the elements present in the sample, thus giving a ‘‘fingerprint’’ of the chemical composition of the sample [8]. Main advantages of LIBS are: little or no sample preparation, nearly negligible sample consumption, simultaneous multi-elemental analysis and a sensitivity in the ppm range for most elements. An additional feature of the technique is its capability of providing spatially resolved information, correlating the coordinates of the samp-

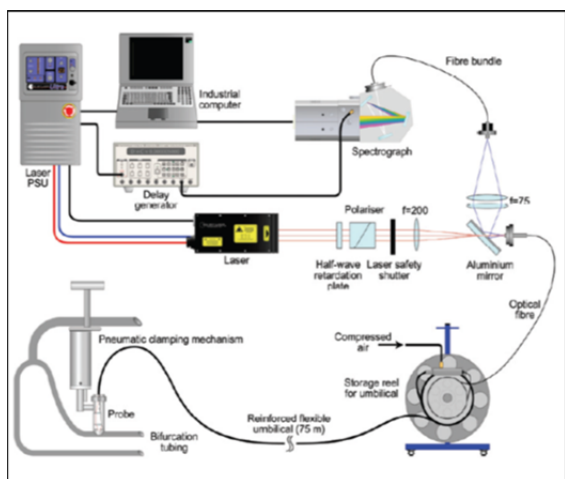


Fig. 3: Typical LIBS setup with a fiber-optic configuration for remote analysis inside nuclear installations [10].

led position to the obtained spectroscopic data. All these advantages make LIBS a suitable technique for in-situ and remote analysis, mainly in those applications with restricted access to the sample or where close-by analysis might pose a serious hazard to the operator [9].

In 2013 initial steps have been undertaken at INE to exploit the applicability of LIBS as a chemical sensor for the elemental and spatial characterization of highly radioactive waste forms (e.g., HAWC glass, vitrification residues or spent fuel). The use of LIBS as a remote technique is expected to minimize the problems associated with sampling and handling of highly active materials or the risk for additional contamination posed by the necessary sample pre-treatment and conditioning steps associated with regular in-lab analytical procedures. Installation of a bench-top LIBS set-up is currently in progress at INE controlled area laboratories. This system will be applied for preliminary investigations of the elemental composition of radioactive samples and for additional feasibility studies of a fiber-optic configuration for remote LIBS measurements (cf. Fig. 3).

## References

- [1] Technical notes and Magellan datasheet at <http://www.cordouan-tech.com>.
- [2] 1<sup>st</sup> NEULAND Award to the „NPA/LIBD“ transfer project, Geckeis, H., Walther, C., Hauser, W., Büchner, S., Götz, R. Information available at <http://www.innovation.kit.edu/971.php>.
- [3] Lindqvist-Reis, P. et al., unpublished results.
- [4] Lindqvist-Reis, P. et al., *J. Phys. Chem. C*, **113**: 449 (2009).
- [5] Horrocks, W. et al., *J. Am. Chem. Soc.*, **101**: 334 (1979).
- [6] Supkowski, R.M. et al., *Inorg. Chim. Acta*, **340**: 44 (2002).
- [7] Kimura, T. et al., *J. Alloys Comp.*, **213/214**: 313 (1994).
- [8] Cremers, D. and Radziemski, L., 2013, “*Handbook of Laser-Induced Breakdown Spectroscopy*”, John Wiley & Sons, Ltd.
- [9] Fortes, F. J. and Laserna, J. J., *Spectrochim. Acta B*, **65**: 975 (2010).
- [10] Whitehouse, A.I. et al., *Spectrochim. Acta B* **56**: 821 (2001).

## 8.3 Characterisation at the nanoscale by TEM and XPS

T. Yokosawa, E. Soballa, S. Bahl, D. Fellhauer, U. Kaplan, D. Schild

### Introduction

Chemical and morphological analysis at the nanometer scale is essential to elucidate composition and structure of precipitates, secondary phases and colloids formed in solubility studies - either in aqueous solution or in a glass melt. Different complementary analytical techniques are applied to achieve a comprehensive characterisation of samples and the assessment of processes involved in their formation: Raman spectroscopy, atomic force microscopy (AFM), X-ray photoelectron spectroscopy (XPS), environmental scanning electron microscopy (ESEM), and analytical transmission electron microscopy (TEM).

### TEM study on Ba/Ca-molybdate particles formed in a borosilicate glass

For the vitrification of High Level Waste Concentrates (HAWC) with high molybdenum contents (as fission product) a borosilicate glass composition able to incorporate high molybdenum loadings is requested. Presently, formation of crystalline  $\text{CaMoO}_4$  and  $\text{BaMoO}_4$  phases above 4 wt-%  $\text{MoO}_3$  loading is detected by Raman spectroscopy and powder X-ray diffraction (XRD). Spherically shaped particles composed of Ba, Ca, Mo, and O are observed by SEM-EDX. TEM is applied to investigate glass samples with  $\text{MoO}_3$  loadings above and below 4 wt-% in order to study composition and structure of these particles depending on the molybdenum content.

### High $\text{MoO}_3$ concentration

Figure 1a depicts a backscattered electron image of a borosilicate glass with 12.28 wt-% of  $\text{MoO}_3$  taken by ESEM. Bright image areas denote the presence of heavier elements compared to surrounding regions. The particles marked by arrows with an average diameter of 500 nm are rich in Ba and Ca as confirmed by SEM-EDX analysis. In order to analyze the crystallinity of these particles and the possible presence of different internal crystal phases, TEM measurements are performed employing a FEI Tecnai G2 F20 X-TWIN operated at 200 kV, located at IAM-WBM-FML (KIT).

Figure 1b shows a bright-field (BF) image taken from the glass sample. Relatively darker areas indicated by arrows correspond to the particles seen as brighter spots in the SEM image. Figure 1c shows a view zoomed into the area indicated by the dotted square in Fig. 1b. Relatively darker and brighter contrast seen in the area of the particle is just due to a typical diffraction effect. Figure 1d depicts selected-area electron diffraction (SAED) pattern taken from an area indicated by a dotted circle in Fig. 1c. The SAED pattern is indexed in terms of the tetra-

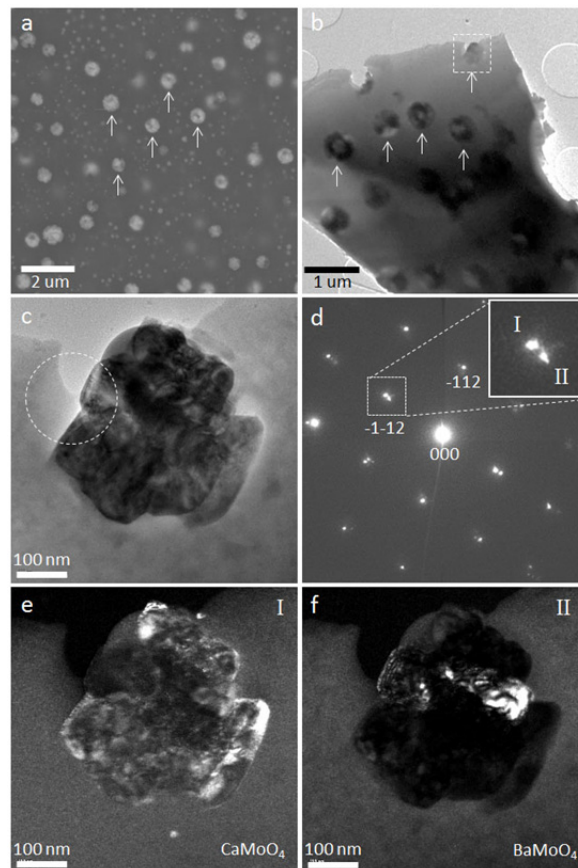


Fig. 1: Microscopy analysis of a glass sample with high  $\text{MoO}_3$  loading: (a) backscattered electron image taken by ESEM; (b) BF-TEM image; (c) zoom into the dotted square depicted in (b); (d) SAED pattern taken from the particle; (e) and (f) DF-TEM images taken using reflections I and II depicted in (d), respectively.

gonal lattice of either  $\text{CaMoO}_4$  ( $a = 0.5222$  nm,  $c = 1.1452$  nm),  $I4_1/a$  [1]) or  $\text{BaMoO}_4$  ( $a = 0.5548$  nm,  $c = 1.274$  nm,  $I4_1/a$  [2]). The crystalline zone axis of the SAED pattern is  $[201]$ . In the SAED pattern, the splitting of the reflections is clearly seen. The inset in Fig. 1d is a magnified depiction of the  $-1-12$  reflection. Reflection I appears at a 7% larger angle than reflection II. This difference of the  $-1-12$  reflection corresponds to the crystal lattice difference between  $\text{BaMoO}_4$  and  $\text{CaMoO}_4$ , indicating that  $\text{BaMoO}_4$  and  $\text{CaMoO}_4$  are formed as separate phases in the particle. In order to elucidate how the two phases are distributed in the particle, dark-field (DF) TEM images are taken for both reflections I and II.  $\text{CaMoO}_4$  and  $\text{BaMoO}_4$  phases appear in Figs. 1e and 1f as relatively bright areas, respectively, clearly indicating spatial separation. It was also confirmed by EDX that the brighter areas in Figs. 1e and 1f contain more Ca and Ba, respectively, which is consistent with the results

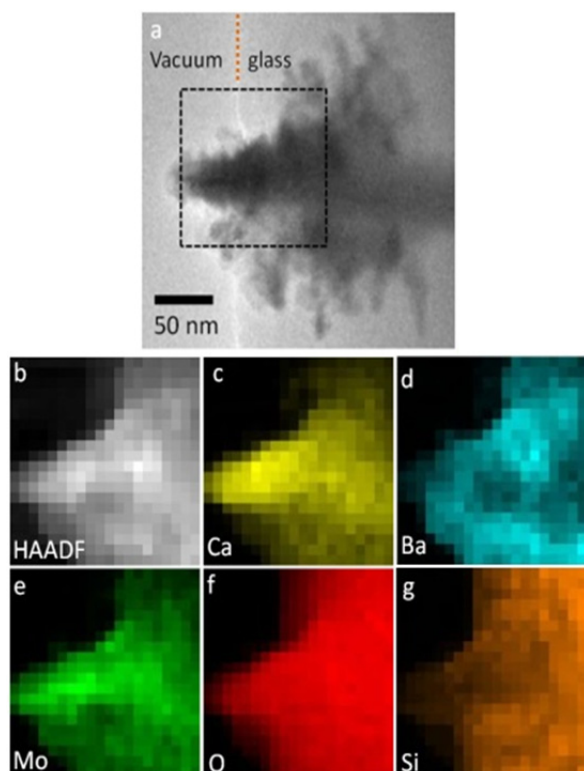


Fig. 2: TEM investigation of low  $\text{MoO}_3$  concentration sample: (a) BF-TEM image; (b) HAADF-STEM image; (c-g) STEM-EDX mapping images for Ca, Ba, Mo, O and Si, respectively.

obtained by SAED. Hence, it was revealed by applying TEM-based techniques that the Ca/Ba rich particles of about 500 nm diameter forming in the borosilicate glass at high Mo loading consist of separated crystalline  $\text{BaMoO}_4$  and  $\text{CaMoO}_4$  phases.

### Low $\text{MoO}_3$ concentration

In the case of the low  $\text{MoO}_3$  concentration sample (3.38 wt-%), the number and the average size of the molybdate phase particles forming in the glass is reduced compared to the high concentration sample. Nevertheless, it is still possible to perform structural and elemental analysis of these particles down to the sub-nanometer scale by using TEM-based methods. The BF-TEM image depicted in Fig. 2a exhibits a dendrite-like morphology of such a particle, which is typically occurring under supercooling conditions. Figure 2b depicts a High Angle Annular Dark Field (HAADF) image representing the sample morphology based on the thickness and atomic numbers ( $Z$ ) of the probed elements. Figures 2c-g show the results of Scanning Transmission Electron Microscopy–Energy Dispersive X-ray Spectroscopy (STEM-EDX) elemental mapping. Ca, Ba and Mo locations in the particle and Si in the glass matrix are clearly visualized at nanometer scale (pixel size corresponds to 7.75 nm).

Furthermore, a clear phase separation between Ca- and Ba-molybdates is observed in Figs. 2c and 2d. Detailed investigation of crystal lattice fringes on the

sub-nanometer scale ( $< 0.2$  nm) revealed the existence of nm-sized Ca- and Ba-molybdate phases in the particle.

### TEM study on plutonium nanocolloids

Plutonium colloids are obtained from a 4 mM  $^{242}\text{Pu}$  solution in 1 M  $\text{HClO}_4$  (pH = 0), equilibrated during 9 months. The greenish color of the solution indicated the presence of Pu(IV)-colloids. Dilution and ultrafiltration (10 kDa) are used to obtain a filter cake which is resuspended with 0.01 M  $\text{HClO}_4$ . An amount of ca. 0.5  $\mu\text{L}$  of the resulting 0.4 mM  $^{242}\text{Pu}$  suspension is deposited onto a copper TEM grid with a holey carbon film, corresponding to a total amount of 0.2 nM  $^{242}\text{Pu}$ .

A combination of High Resolution–TEM (HR-TEM), STEM-EDX and STEM–Electron Energy Loss Spectroscopy (STEM-EELS) is ideal to investigate nm-sized colloidal particles, providing structural data (both geometric and electronic) as well as elemental composition information. Figure 3 shows a HR-TEM image taken from Pu colloids dispersed on the carbon film. The average size of the colloids is less than 5 nm, which is consistent with results reported in [4]. The inset on the top of Fig. 3 depicts a zoom into the area marked by a black rectangle. The crystal lattice fringes with  $d \sim 0.31$  nm and  $d \sim 0.27$  nm are clearly resolved. Based on the assumption that the nano-sized colloids are of  $\text{PuO}_2$  ( $a = 0.5398$  nm, Fm-3m [3]) fluorite type crystal structure, the fringes correspond to  $\{002\}$  ( $d = 0.3117$  nm) and  $\{111\}$  ( $d = 0.2699$  nm) atomic planes, respectively.

It is also possible to characterize individual nanocolloids by STEM-EDX and STEM-EELS for detection of the elemental composition and electronic structure, respectively (see the insets in the bottom of Fig. 3). Core-loss EELS in STEM mode provides electronic structure information similar to X-ray based XANES, but at sub-nanometer spatial resolution [6].

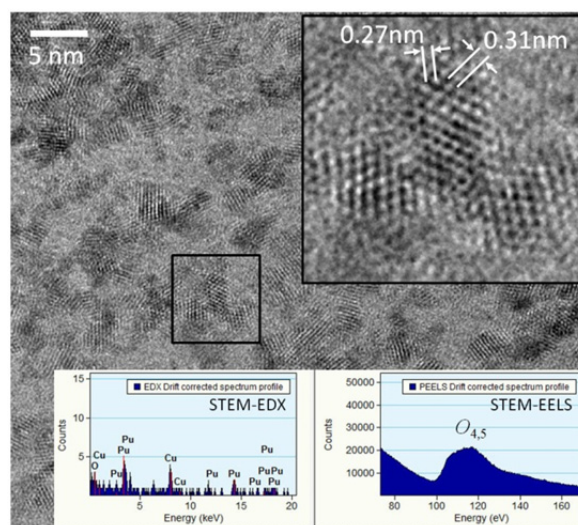


Fig. 3: HR-TEM image, STEM-EDX and EELS spectra of nanometer-sized  $\text{PuO}_2$  colloids. The EELS spectrum shows the  $O_{4,5}$  edge of Pu [5].

## Investigation of natural organic matter derived from Boom Clay by XPS

Dissolved and mobile natural organic material (NOM) may facilitate migration of radionuclides by complexation. XPS is applied to characterize size fractions of NOM extracted from Boom Clay [7] to analyze size dependent functionality. Filter cakes from ultra-filtration are rinsed with water to remove  $\text{NaHCO}_3$ . About 2  $\mu\text{L}$  of resuspended filter cake are deposited and dried on aluminum foil for XPS analysis. Survey spectra and narrow scans of the elemental lines (Fig. 4) are acquired using monochromatic  $\text{Al K}\alpha$  X-ray excitation ( $h\nu = 1486.6 \text{ eV}$ ) for the determination of C, N, and S atomic concentrations and species present in the NOM.

Size fractions of (1-10) kDa, (10-100) kDa, and  $> 100$  kDa corresponding to a Stokes radius of about (0.8-2) nm, (2-7) nm, and  $> 7$  nm were analyzed by XPS, respectively (sample EG/BS bulk).

Small colloids show increased concentration ratios of  $[\text{N}]/[\text{C}_{\text{tot}}]$ ,  $[\text{COO}]/[\text{C}_{\text{tot}}]$ , and  $[\text{SO}_4]/[\text{S}_{\text{tot}}]$  but a concurrent decrease of  $[\text{S}]/[\text{C}]$  compared to larger colloids, indicating that smaller colloids are more oxidized. The sodium concentration is higher for small colloids than for larger colloids, consistent with the low isoelectric point,  $\text{pH} = 3$ , reported for the 10 kDa macromolecules [8].

In conclusion, nano-scale characterization of a borosilicate glass, plutonium colloids and Boom Clay NOM is demonstrated by applying several microscopy and spectroscopy techniques (TEM, SEM and XPS). TEM experiments at IAM-WBM-FML (KIT) are currently performed with a spatial resolution down to  $\sim 0.2 \text{ nm}$  under high vacuum ( $\sim 10^{-5} \text{ Pa}$ ) with a standard instrument. Nowadays, the spatial resolution can be improved to be better than  $0.1 \text{ nm}$  by using an aberration corrector, and in-situ TEM in gas or liquid phase at atmospheric pressure is becoming feasible [9,10]. By applying such techniques to study environmental and actinide samples, the crystal and electronic structures are expected to become accessible at the nanoscale under realistic environmental conditions.

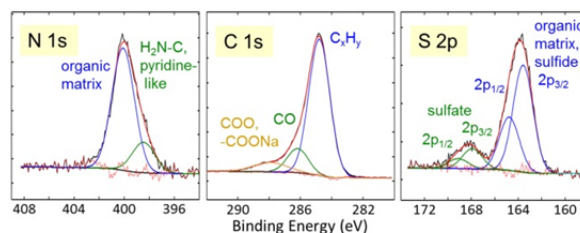


Fig. 3: Narrow scans of elemental lines with result of curve fits (Sample: EG/BS bulk,  $> 100$  kDa). Charge reference: C 1s ( $\text{C}_x\text{H}_y$ ) 284.8 eV.

## References

- [1] Hazen, R.M. et al., *J. Phys. Chem. Solids* **46(2)**: 253 (1985).
- [2] Nassif, V. et al., *J. Solid State Chem.* **146**: 266 (1999).
- [3] Belin, R.C. et al, *J. Appl. Crystallogr.* **37(6)**: 1034 (2004).
- [4] Delegard, C.H., *Radiochim. Acta* **101**: 313 (2013).
- [5] Moore, K.T. and Van der Laan, G., *Ultramicroscopy* **107(12)**: 1201 (2007).
- [6] Egerton, R.F., *Electron Energy-Loss Spectroscopy in the Electron Microscope*, 3<sup>rd</sup> Ed., Springer (New York): 15 (2011).
- [7] Bruggeman, C. and De Craen, M., *SCK•CEN Report Number. ER-206* (2012).
- [8] Guo, L. and Santschi, P.H., *Environmental Colloids and Particles*, (Eds.: Wilkinson, K.J. and Lead, J.R.) IUPAC: 205 (2007).
- [9] De Jonge, N. and Ross, F.M., *Nat. Nanotechnol.* **6(11)**: 695 (2011).
- [10] Yokosawa, T. et al., *Ultramicroscopy* **112(1)**: 47 (2012).

## 8.4 NMR spectroscopy – covalence in actinide complexes

*P. Kaden, C. Adam, B.B. Beele, U. Müllich, J. Schäfer, L. Böringer, P.J. Panak, A. Geist*

### Introduction

The extent of covalence in the metal-ligand bond of nitrogen-donor ligands for the separation of minor actinides has received much attention in recent years.<sup>[1-4]</sup> In a number of studies the reason for the ligands' extraction behaviour and the origin of the observed selectivity of actinides over lanthanides in certain ligand systems was addressed.<sup>[5-8]</sup> NMR spectroscopy measuring the effect of electron density distribution on the evolution of spins of ligand nuclei appears to be very promising to investigate bonding interactions.

### Covalence in metal-organic complexes – the NMR view

Electron density distribution in organic molecules in general has a significant influence on the observed nuclear spins, as electron density in close proximity to the nuclear spins is the major contributor to all NMR parameters (chemical shift, relaxation rates, etc.). Thus, any change of the electron distribution on the ligands, e.g., in complexes with elements of the lanthanide or actinide series will be detected. Such a change can be due to different influences: an ionic interaction disturbing the distribution by Coulomb attraction or repulsion or the exchange of electron density between metal ion and complexing ligand.

In addition to this general electronic description of the ligands, the electronic configuration of the metal ions involved in metal-organic complexes often has an influence on the measured parameters that is orders of magnitude higher than the described diamagnetic interactions. For f-elements two general electronic configurations of the metal ions can be distinguished: diamagnetic and paramagnetic metal ions. Diamagnetic metal ions with a magnetic permeability that is less than  $\mu_0$  (the permeability of free space) exhibit only a weak magnetic field in opposition to the externally applied magnetic field, which is often negligible in NMR measurements. Paramagnetic metal ions, in contrast, possess a permanent magnetic moment (magnetic permeability greater than or equal to 1) due to the spin and angular momentum of unpaired electron density. The net magnetic momentum induced by

the applied external magnetic field is linear in the field strength in paramagnetic ions and can cause drastic effects in NMR measurements of nuclei in surrounding molecules.

### Probing covalence – the paramagnetic approach

Unpaired electron density is a common physical property of most lanthanide and actinide ions. Employing known mathematical treatments on observed paramagnetically induced chemical shifts (KNIGHT shift) in the lanthanide series allows the separation of the different chemical shift contributions. The two main contributions are commonly interpreted in terms of a non-covalent (dipolar) bonding interaction and a covalently transferred interaction (FERMI contact contribution). The desired transfer of these well-known mathematical treatments to the actinide series, however, suffers from uncertainties in the determination of different physical constants. Extensive research at KIT-INE addressing these open questions is performed.

### Probing covalence – the diamagnetic approach

A qualitative approach to address the extent of covalence in actinide complexes can be performed in a diamagnetic approach by simply comparing the observed effects of the electronic spin density on ligand nuclei in diamagnetic complexes. In general, one would expect only a minor influence on the electron distribution on the ligand upon ionic complexation with a metal ion. Thus the resulting shifts should be comparable with those observed in solutions of the pure ligand. Drastic changes of these observed chemical shifts are only expected if the electron density distribution is disturbed by a delocalisation along a covalent bond. Generally, covalence is characterized as an exchange of electron density between the bonding partners.

Of course the real bonding situation in actinide as well as in lanthanide complexes is a combination of these two limiting cases (dipolar vs. covalent interaction). NMR can only qualitatively compare sets of measurements on complexes of different diamagnetic metal ions. Only if significant differences are discovered, general trends can be derived.

### <sup>15</sup>N – a sensitive sensor

From an NMR spectroscopy point of view the BxP systems are ideal systems to investigate the bonding mode in N-donor complexes of the f-elements. The high symmetry of their complexes leads to the observation of only one signal for each nucleus in the respective position for all three involved ligands and, furthermore, to only one signal in symmetric positions

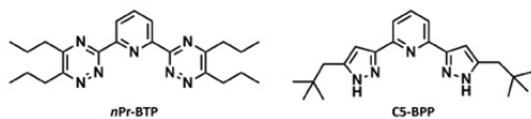


*Fig. 1: Chemical structures of two classes of ligands for the separation of actinides(III) from lanthanides(III). left: 2,6-bis(5,6-dipropyl-1,2,4-triazin-3-yl)pyridine (nPr-BTP); right: 2,6-bis(5-(2,2-dimethylpropyl)-1H-pyrazol-3-yl)pyridine (C5-BPP).*

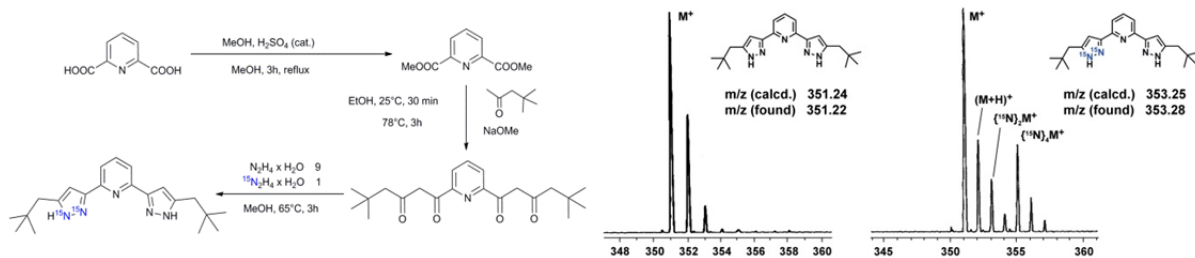


Fig. 2: left: Modified protocol for the synthesis of  $^{15}\text{N}$  labelled C5-BPP. right: LIFDI-MS results for unlabelled and  $^{15}\text{N}$  enriched C5-BPP clearly indicating a 10% enrichment of both nitrogen atoms of one or both lateral rings.

in the single ligand. Even in this rather ideal situation the  $^{15}\text{N}$  nuclei that should be most affected by any change in the bonding mode are not observable in a direct excitation experiment due to their low natural abundance. Employing magnetization transfer techniques in 2D experiments that heavily depend on the proximity of protons to the  $^{15}\text{N}$  nuclei, some but not all  $^{15}\text{N}$  resonances are observable. However, the resulting resolution is limited by experimental restrictions.

### Synthesis of $^{15}\text{N}$ enriched ligands

Thus it appears desirable to enrich the nitrogen bearing moieties of the ligand with the NMR active isotope  $^{15}\text{N}$ . This is only possible by introducing the  $^{15}\text{N}$  isotopes during the synthesis of the ligand. Following an optimised synthesis route we were able to  $^{15}\text{N}$  enrich the two lateral heteroaromatic rings both in BTP and BPP type ligands. The synthesis is showcased for C5-BPP in Figure 2. Analysis by LIFDI-MS spectroscopy<sup>[9-10]</sup> shows evidence for approx. 10%  $^{15}\text{N}$  enrichment in one or both lateral rings (Figure 2). Following a protocol with a similar modification for BTP resulted as well in a  $^{15}\text{N}$  enriched *n*Pr-BTP with excellent yields.<sup>[11]</sup> All intermediates and both ligands were purified and characterised by NMR and LIFDI-MS.<sup>[9-10]</sup>

Generally, uniform  $^{15}\text{N}$  enrichment in both BTP and BPP ligands would be desirable. However,  $^{15}\text{N}$  enrichment especially in the pyridine moiety remains a

challenge. Efforts to establish a synthesis for a uniform  $^{15}\text{N}$  isotopic labelling are currently progressing.

### Results

NMR analysis for all BTP and BPP complexes of the whole lanthanide series was performed to compare the results to spectra of the Am(III) complexes. Identification and assignment of all  $^1\text{H}$  and  $^{13}\text{C}$  resonances was accomplished by 1D direct excitation spectra and 2D spectra (gHSQC, gHMBC) following standard protocols. Unambiguous assignment of all  $^{15}\text{N}$  resonances is possible by measurement of 2D gHMQC spectra correlating the known  $^1\text{H}$  resonances with the  $^{15}\text{N}$  resonances over three or four chemical bonds. The collection of high resolution direct excitation spectra as well as high resolution 2D NMR spectra, however, was only possible for complexes with  $^{15}\text{N}$  enriched ligands in a reasonable time.

Comparing the results obtained for the diamagnetic lanthanides La(III) and Lu(III), the diamagnetic lanthanide surrogate Y(III) and the almost diamagnetic Sm(III) cation with those obtained for the actinide Am(III), unexpectedly large differences of chemical shifts are found for the bonding nitrogens, while the non-bonding nitrogens are not affected.<sup>[11]</sup> This is a strong indication for exchanged electron density and, thus, for the existence of covalent interactions between Am(III) and the ligands. Taking into account that both ligands are excellent systems for separating actinide ions from their lanthanide counterparts and

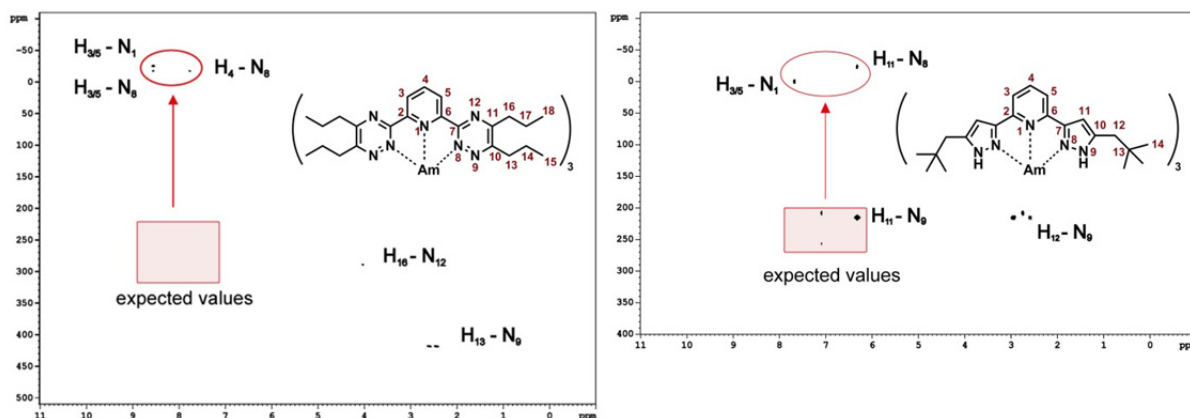


Fig. 3: An overlay of  $^1\text{H},^{15}\text{N}$ -gHMQC spectra of  $\text{Am}(n\text{Pr-BTP})_3$  is shown in the 2D spectrum on the left. The spectrum on the right shows the same type of experiment for  $\text{Am}(\text{C5-BPP})_3$ . In both cases the expected range for cross-peaks of the directly bound  $^{15}\text{N}$  to the respective  $^1\text{H}$  is indicated by a red rectangle. One can clearly see that for the Am(III) complexes a large shift is only observed for the coordinating nitrogen nuclei. This is a strong indication for exchanged electron density and thus for the existence of covalent interactions between Am(III) and the ligands.

considering the long-standing notion that covalence maybe the decisive cause for the ligand selectivity, these experiments present the first substantial support for this hypothesis.

### Acknowledgements

This work is supported by the German Federal Ministry of Education and Research (BMBF) under contract numbers 02NUK020A and 02NUK020D.

### References

- [1] Choppin, G. R., *J. Alloys Compd.* **223**(2): 174 (1995).
- [2] Trumm, S., et al., *Eur. J. Inorg. Chem.* **2010** (19)(19): 3022 (2010).
- [3] Trumm, S., et al., *Dalton Trans.* **39**(3): 923 (2010).
- [4] Kaltsoyannis, N., *Inorg. Chem.* **52**(7): 3407 (2012).
- [5] Kolarik, Z., et al., *Solvent Extr. Ion Exch.* **17**(1): 23 (1999).
- [6] Kolarik, Z., et al., *Solvent Extr. Ion Exch.* **17**(5): 1155 (1999).
- [7] Trumm, S., et al., *Solvent Extr. Ion Exch.* **29**(2): 213 (2011).
- [8] Bremer, A., et al., *Inorg. Chem.* **51**(9): 5199 (2012).
- [9] Linden, H. B. and J. H. Gross, *Rapid Commun. Mass Spectrom.* **26**(3): 336 (2012).
- [10] Linden, H. and J. Gross, *J. Am. Soc. Mass Spectrom.* **22**(12): 2137 (2011).
- [11] Adam, C., et al., *Dalton Trans.* **42**(39): 14068 (2013).

## 8.5 Computational Chemistry

B. Schimmelpfennig, R. Polly, M. Trumm, T. Stumpf, P. Lindqvist-Reis, X. Gaona, E. Yalcintas, T. Prüssmann, T. Vitova, M. Altmaier

In co-operation with:

M. Skripkin<sup>a</sup>, C. Apostolidis<sup>b</sup>, O. Walter<sup>b</sup>

<sup>a</sup> Department of Chemistry, St. Petersburg State University, St. Petersburg, Russia; <sup>b</sup> JRC-ITU, European Commission, Karlsruhe, Germany

### Computational Chemistry

There is a wide range of applications for Computational Chemistry at INE - from providing molecular structure or thermodynamic data to reproducing experimental EXAFS and XANES spectra as an alternative for the extraction of structural data via fit procedures. The systems under investigation vary from small complexes in solution to crystals or interfaces. New algorithms and the constantly improving computer hardware allow to get an increasingly exact and detailed description of actinide systems at the electronic structure level.

#### Incorporation of Cm(III) into the calcite bulk

Sorption and incorporation reactions with mineral phases may have an essential impact on the mobility and bioavailability of radionuclides in soils and sediments. Both incorporation and surface sorption are regarded as efficient retardation mechanisms affecting the transport of radionuclides in groundwater [1].

Calcite ( $\text{CaCO}_3$ ) represents an important mineral phase occurring in the engineered or geological barriers enclosing an underground nuclear waste repository, first of all as mineral constituent in clay formations. The incorporation of Cm(III) into calcite and the corresponding formation of a solid solution is of high relevance in this context. A sound theoretical description of the local structure at Cm(III) sites provides additional support for the interpretation of experimental EXAFS data.

For reasons of charge compensation we regarded the substitution  $2\text{Ca}^{2+} \rightarrow \text{Cm}^{3+} + \text{Na}^+$  and studied the local

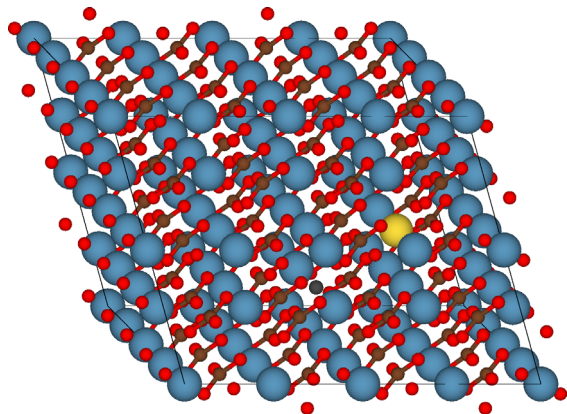


Fig. 1: Hexagonal  $2 \times 4 \times 2$  supercell used for the study of the incorporation of  $\text{Cm}^{3+}$  into calcite. Blue spheres: calcium, red spheres: oxygen, brown spheres: carbon, yellow sphere: sodium, black sphere: curium.

deformation of the calcite crystal structure.

We used a  $2 \times 4 \times 2$  super cell for the calculations consisting of 64 Ca, 192 O and 64 C atoms. All three ions have similar ionic radii ( $\text{Ca}^{2+}$ : 100 pm,  $\text{Cm}^{3+}$ : 97 pm,  $\text{Na}^+$ : 102 pm). Therefore, incorporation of  $\text{Cm}^{3+}$  cations in the calcite structure is expected.

The DFT calculations are carried out with periodic boundary conditions and plane-wave basis sets as implemented in the Vienna Ab initio Simulation Package (VASP). Electron exchange and correlation are described using the Perdew-Burke-Ernzerhof (PBE) functional. The ion cores are dealt with by the projector augmented wave (PAW) method. We employed an energy cut-off of 550 eV for the kinetic energy of the plane waves for all calculations.

In pure calcite the  $\text{Ca}^{2+}$ - $\text{Ca}^{2+}$  distance is 409 pm. The calculated  $\text{Cm}^{3+}$ - $\text{Ca}^{2+}$  distances are increased to 412-422 (average value: 414) pm and the  $\text{Na}^+$ - $\text{Ca}^{2+}$  distances are decreased to 396-409 (average value: 405) pm. These structural changes are due to electrostatics and not to the different ionic radii.

For the  $\text{Ca}^{2+}$ - $\text{C}^{4+}$  distances we find an increase from 325 pm in the pure mineral to 320-332 (average value 326) pm for  $\text{Cm}^{3+}$ - $\text{C}^{4+}$  and 325-333 (average value 329) pm for  $\text{Na}^+$ - $\text{C}^{4+}$ . The  $\text{Ca}^{2+}$ - $\text{O}^{2-}$  distances are 239 pm in the pure mineral.  $\text{Cm}^{3+}$ - $\text{O}^{2-}$  distances remain almost unchanged: 232-243 (average value: 239) pm, but increase for the  $\text{Na}^+$ - $\text{O}^{2-}$  distances: 241-252 (average value: 246) pm.

The calculated  $\text{Cm}^{3+}$ - $\text{O}^{2-}$  distance of 239 is well in agreement with the available experimental Am  $L_3$ -EXAFS data by Stumpf *et al.* [2]. The authors reported an  $\text{Am}^{3+}$ -O distance of 240 pm.

#### Structure and bonding in $\text{AnO}_2(\text{NO}_3)_2(\text{H}_2\text{O})_2$ (An = U, Np, Pu) complexes

The design of efficient and selective extraction ligands for separation of uranium and transuranium elements from spent nuclear fuel by liquid-liquid extraction requires detailed information on the ligand properties and the actinide-ligand bonding interaction. In the feed solutions of the PUREX, DIAMEX and SANEX processes actinides are provided in an aqueous nitric acid phase originating from the dissolution of the spent fuel. Therefore, detailed knowledge on the coordination chemistry of actinides in nitric acid solutions is essential for improving these processes. Spectroscopic studies have shown that uranyl(VI) is coordinated by 2-3 nitrate ions in concentrated nitric acid [3]. Furthermore, there is convincing evidence

that neptunyl(VI) is coordinated by two nitrate ions and two water molecules in the equatorial plane [4-5]. Coordination by two nitrate ions and two water molecules in the equatorial plane is reported for  $[\text{AnO}_2(\text{NO}_3)_2(\text{H}_2\text{O})_2] \cdot n\text{H}_2\text{O}$  ( $\text{An} = \text{U}, \text{Np}, \text{Pu}$ , **1-3**) complexes in [5-7], respectively. These isotopic compounds, which crystallize from concentrated nitric acid solutions, are ideal model structures for actinyl(VI)-dinitrate complexes in nitric acid solution. We are currently studying their vibrational spectra, aiming to determine to which extent the actinide electronic structure and the ligands influence the bond strength of the actinyl moiety,  $\text{O}=\text{An}^{\text{VI}}=\text{O}$ . An important question is whether the bond length and stretching force constant follow the actinide ionic radii or if other effects contribute as well.

To answer these questions we have initiated a program using quantum chemical methods on clusters and periodic crystal lattices of the  $[\text{AnO}_2(\text{NO}_3)_2(\text{H}_2\text{O})_2]$  complex. Preliminary results from these calculations are presented here.

Fig. 2 shows the DFT-optimized (in TURBOMOLE) structures of the  $[\text{AnO}_2(\text{NO}_3)_2(\text{H}_2\text{O})_2] \cdot n\text{H}_2\text{O}$  ( $n = 0, 6, 8$ ) and  $5 \times [\text{AnO}_2(\text{NO}_3)_2(\text{H}_2\text{O})_2] \cdot 2\text{H}_2\text{O}$  clusters, the latter is a relaxed molecular cluster with initial coordinates from the corresponding crystal structures of **1-3**. It is clear that the hydrogen bonding between the first and second sphere water molecules results in a shortening of the  $\text{An}-\text{OH}_2$  bonds as well as a shift of

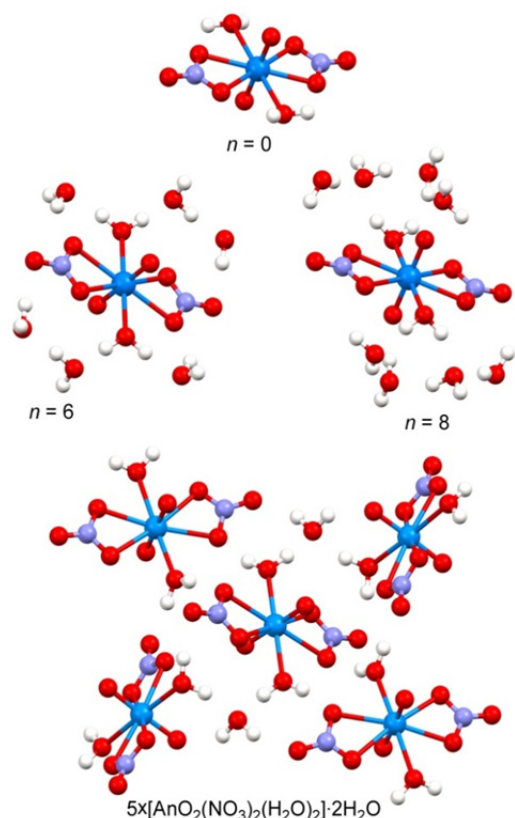


Fig. 2: Molecular structures of  $[\text{AnO}_2(\text{NO}_3)_2(\text{H}_2\text{O})_2] \cdot n\text{H}_2\text{O}$  ( $n = 0, 6, 8$ ) and  $5 \times [\text{AnO}_2(\text{NO}_3)_2(\text{H}_2\text{O})_2] \cdot 2\text{H}_2\text{O}$ , optimized with BP86-DFT using TURBOMOLE.

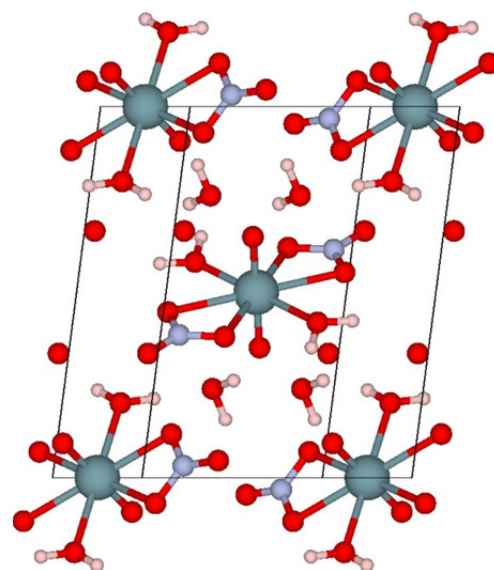


Fig. 3: Unit cell ( $P-1$  space group) content of the DFT optimized crystal structure of **1-3** obtained with VASP.

several vibrational frequencies compared to the cluster without a second water sphere. This effect is also evident in the pentanuclear complex.

Although the ‘central’ complex of the pentanuclear cluster mimics well the structure and the vibrational spectrum of the corresponding crystal (see below), DFT calculations (in VASP) of periodic structures of **1-3** were performed in addition. Fig. 3 shows the unit cell of the optimized  $[\text{AnO}_2(\text{NO}_3)_2(\text{H}_2\text{O})_2] \cdot \text{H}_2\text{O}$  structure.

Fig. 4 compares the experimentally determined and the DFT-calculated actinyl  $\text{An}=\text{O}$  distances in **1-3** and the corresponding DFT-calculated distances in  $5 \times [\text{AnO}_2(\text{NO}_3)_2(\text{H}_2\text{O})_2] \cdot 2\text{H}_2\text{O}$ . Also plotted are the symmetric ( $\nu_s$ ) and antisymmetric ( $\nu_{as}$ ) stretch frequencies of the actinyl entities. We note that both the experimental and calculated  $\nu_s$  values decrease when

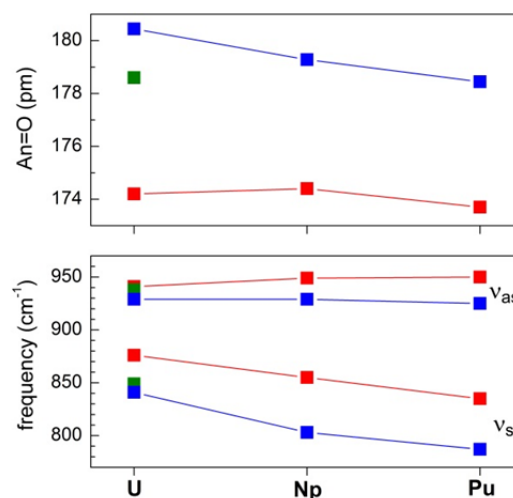


Fig. 4: Comparison of  $\text{An}=\text{O}$  bond distances and symmetric ( $\nu_s$ ) and antisymmetric ( $\nu_{as}$ ) stretch frequencies in **1-3** and  $5 \times [\text{AnO}_2(\text{NO}_3)_2(\text{H}_2\text{O})_2] \cdot 2\text{H}_2\text{O}$ . Legends:  $\blacksquare$  experiment;  $\blacksquare$  DFT-VASP;  $\blacksquare$  DFT-TURBOMOLE.

going from U to Pu. This is consistent with a larger force constant of the U=O stretching mode, which may be due to a stronger bond. This is peculiar since the An=O bond shows a contraction when going from U to Pu. In contrast to that, there is virtually no change in  $\nu_{as}$  going from U to Pu. Additional work, including force field analysis, is needed in order to understand the influence of the actinide electronic structure on the An=O bonds and trends in the vibrational spectra.

### Tc(IV) hydrolysis species and ternary Mg/Ca-Tc<sup>IV</sup>-OH complexes in alkaline MgCl<sub>2</sub> and CaCl<sub>2</sub> solutions

Tc-99 is a redox-sensitive  $\beta$ -emitting fission product with very long half-life ( $T_{1/2} \sim 211,000$  a). Tc is expected to prevail as tetravalent Tc(IV) cation in the very reducing conditions expected under repository conditions.

Tc(IV) hydrolyzes very strongly. The anionic species  $\text{TcO}(\text{OH})_3^-$  has been shown to dominate the aqueous chemistry of Tc(IV) in dilute alkaline conditions of  $\text{pH} \geq 11$  [8]. In concentrated alkaline  $\text{MgCl}_2$  and  $\text{CaCl}_2$  solutions, solubility experiments conducted at KIT-INE (see section 5.1) hint towards the formation of ternary hydrolysis species of the type  $\text{Mg}_x[\text{TcO}(\text{OH})_4]^{2x-2}$  and  $\text{Ca}_x[\text{TcO}(\text{OH})_4]^{2x-2}$ . Quantum chemical calculations are well suited to identify possible Tc(IV) solvation species in alkaline solution. Since there are no ab initio calculations on  $[\text{TcO}(\text{OH})_4]^{2-}$  or  $[\text{TcO}]^{2+}$  available up to now, we performed pilot studies of these two species with high level Complete Active Space Self Consistent Field (CASSCF) and Multi Reference Configuration Interaction (MRCI) calculations to determine the ground states of these species.

These calculations - carried out with MOLPRO - showed that the ground states of both species,  $[\text{TcO}(\text{OH})_4]^{2-}$  and  $[\text{TcO}]^{2+}$ , are single reference states and, thus, the application of Density Functional Theory (DFT) calculations is permitted in this case. This opens the door for the future application of large DFT

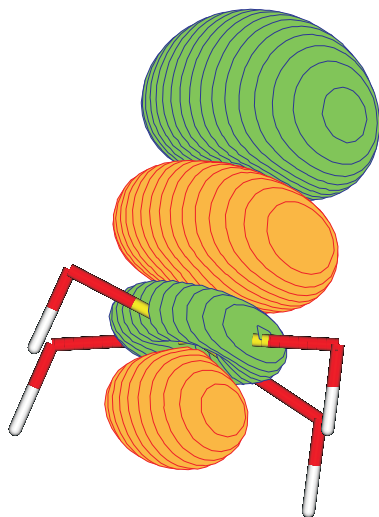


Fig. 5: Bonding orbital in  $[\text{TcO}(\text{OH})_4]^{2-}$ .

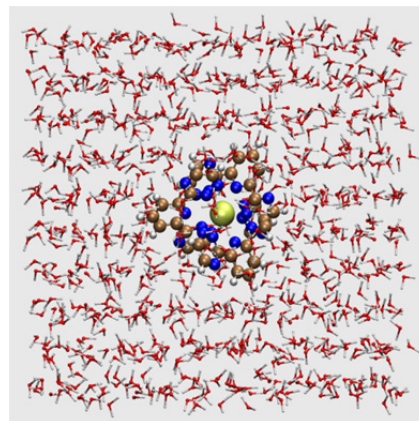


Fig. 6: Bonding orbital in  $[\text{TcO}(\text{OH})_4]^{2-}$ .

calculations to determine the structure of various species involving Tc(IV) in alkaline solutions.

### Force Field calculations on An(III)/Ln(III) complexes with BTP-type ligands

The investigation of Ln(III)/An(III) partitioning complexes in bulk solutions is a challenge task for theoretical methods, because the systems at hand are much larger in size than corresponding aquo-complexes of the metal ions. Hence, Molecular Dynamics (MD) simulations have been performed to complement the data obtained by quantum chemical methods. Especially for the An(III) bistriazinylpyridine (BTP) system the applicability of MD has never been explored, as existing force fields are not accurate enough to correctly describe the interactions involved in An(III) complexation.

The force fields describing the interactions between all atoms and molecules in the system must be built carefully to assure a realistic description of the system's dynamics. To remain as independent of the experiments as possible, we adjusted our force fields to state-of-the-art quantum chemical ab initio reference data on the MP2 or CCSD(T) level, using large diffuse basis sets of aug-cc-pVTZ quality. Relativistic effects, necessary to correctly describe heavy metals, are accounted for by either pseudo-potentials - implicitly including those effects - or by a second order Douglas-Kroll-Hess Hamiltonian.

MD simulations have been performed on  $[\text{Cm}(\text{BTP})_n]^{3+}$  ( $n = 1, 2, 3$ ) in aqueous solvent, explicitly modelled by 1000 water molecules in the cubic simulation box (Fig. 6). The 10 ns time-scale allows for a good statistics of the configuration space. The resulting trajectories are in good agreement with radial distribution functions obtained by Cm L<sub>3</sub>-EXAFS [9] - showing a Cm-N distance of 2.57 Å for the coordinating nitrogen atoms compared to 2.56 Å obtained from the measurement. Using the FEFF code, EXAFS spectra can be directly calculated from the trajectories (Fig. 7).

In future projects these force fields will be used to shed further light on the complexation reactions of An(III)/Ln(III) with BTP-ligands. We will use alchemy reaction techniques to transmute different ligands or metal ions in order to investigate the origins of the

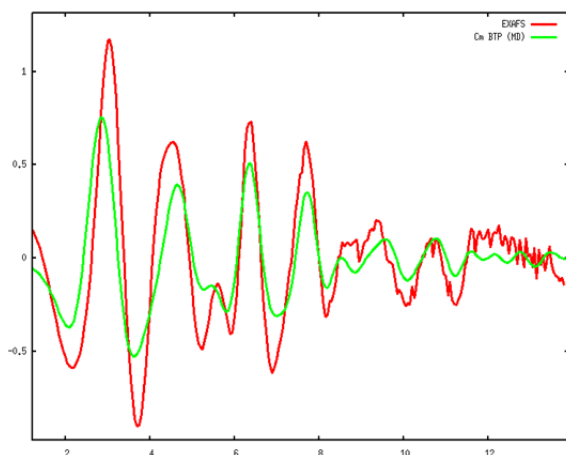


Fig. 7: Calculated (green) and measured (red) EXAFS spectra of the Cm-BTP 1:3 complex.

different bonding behavior in terms of structure and thermodynamics.

### N K-edge investigations of BTP partitioning complexes

In close collaboration with the HYIG led by T. Vitova we have investigated the N(1s) excitation spectra of Ln(III) and An(III) complexes with BTP ligands. As one of the major questions is related to the energy position and intensity for excitation to the metal-centered f-manifold, the computational methods suitable for such a task are limited. After pilot studies on the BTP ligand with the RI-ADC(2)-approach (TURBOMOLE software) and TD-DFT (ORCA software) the Amsterdam Density Functional software package (ADF) was employed, as it allows all-electron calculations including scalar-relativistic and spin-orbit effects within the ZORA approximation already at the DFT level for the ground state and for the excited states. Due to the lack of multi-configuration contributions, this approach is only suitable for closed-shell systems - in the present context  $J=0$ . This restricts applications to La(III), Eu(III) and Am(III). Although experimental data for the Ac(III) complexes will most likely not be available in the near future, the theoretical data could be interesting in comparison to the Ln(III) system.

As the calculations are computationally demanding, basis sets on the ligand were chosen to be of DZP quality only in combination with TZP-quality sets for the metal centres. The computational effort was further reduced by limiting the available virtual orbitals to those with negative energy only and by performing separate calculations for the symmetry distinct nitrogen atoms (cf. Fig. 9 in section 9.1). Still, several hundred excited states and their oscillator strengths were calculated at the TD-DFT level.

One can clearly see the benefits of such first principles calculations, as they allow to separate the contributions from different coordinating and non-coordinating BTP nitrogen atoms (in contrast to the experiment) and to assign the antibonding BTP orbit-

als involved in the N(1s) excitation (cf. section 9.1 for a more detailed discussion of the results).

### Structure and vibrational spectra of the Cm(III)-HClO<sub>4</sub> system.

A number of researchers have previously reported that the luminescence lifetime of Eu(III) in aqueous solution decreases substantially with increasing concentration of perchlorate ions (which may be added in the form of HClO<sub>4</sub> or NaClO<sub>4</sub>) [10-13]. We have recently shown that this is also true for Cm(III) [14]. The reason for this luminescence quenching is still a matter of controversy. In contrast to water molecules or hydroxide ions, both of which quench the luminescence lifetime of Eu(III) through multi-phonon coupling with OH vibrational overtones, the corresponding mechanism for perchlorate is unfavorable and does not result in quenching. It has even been proposed that the reduced Eu(III) lifetime is a consequence of an increased hydration number [10-12]. Considering that the hydration number of Eu(III) may change between eight and nine depending on the chemical environment, an increase of the hydration number from nine to eleven, corresponding to a reduction of the lifetime from about 110 to 90  $\mu\text{s}$  [12], is not realistic. Therefore, other mechanisms should account for the quenching. TRLFS and vibronic sideband spectroscopic measurements at INE suggest that perchlorate ions in the second hydration spheres of the hydrated metal ions form weak hydrogen bonds to the water molecules of the first hydration sphere, effecting their OH-vibrational manifolds [14]. MD simulations suggest two possible geometries with either two or three perchlorate ions in the second hydration sphere (Fig. 8).

Vibrational modes calculated with DFT and RIC2 techniques concur with experimental findings. For both structures, the OH-vibrations of first shell water molecules are blue-shifted in the presence of the perchlorate ion by 100  $\text{cm}^{-1}$  in average.

Additional MD and ab initio MD simulations in the NVE ensemble are currently being performed. The resulting trajectories will be used to obtain IR- and power-spectra from the velocity-autocorrelation function of the atoms.

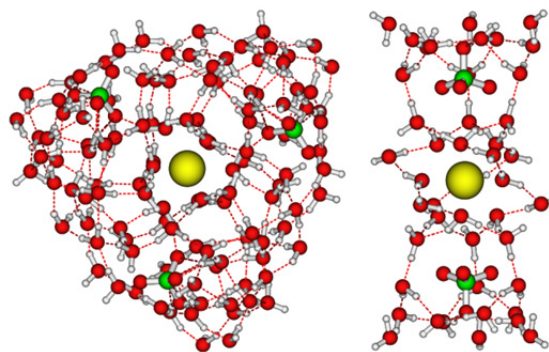


Fig. 8: Optimized structure of the Cm(III) aquo ion with two (right) and three (left) second shell perchlorate ions.

### Acknowledgements

This work was supported by the European FP7 TALISMAN project TAL-C01-07 under contract with the European Commission.

### References

- [1] Geckeis, H. et al., *Chem. Rev.*, **113**: 1016 (2013)
- [2] Stumpf, T. et al., *J. Colloid Interface Sci.*, **302**: 240 (2006)
- [3] Ikeda-Ohno, A. et al., *Inorg. Chem.*, **48**: 7201 (2009)
- [4] Ikeda-Ohno, A. et al., *Inorg. Chem.*, **47**: 8294 (2008)
- [5] Lindqvist-Reis, P. et al., *Dalton Trans*, **42**: 15275 (2013)
- [6] Hughes K.-A. et al., *Acta Cryst.*, C59: i7 (2003)
- [7] Gaunt, A.J. et al, *Inorg. Chem.*, **50**: 4244 (2011)
- [8] R. Guillaumont, T. Fanghänel, J. Fuger, I. Grenthe, V. Neck, D. A. Palmer, M. H. Rand, *Update on the Chemical Thermodynamics of Uranium, Neptunium, Plutonium, Americium and Technetium 2003*, Vol. 5 (Elsevier: Amsterdam).
- [9] Denecke, M.A. et al, *Inorg. Chem.*, **44**: 8418 (2005)
- [10] Breen, P.J. et al, *Inorg. Chem.*, **22**: 536 (1983)
- [11] Tanaka, F. et al, *Inorg. Chem.*, **23**: 2044 (1984)
- [12] Lis, S. et al, *Materials Chem. Phys.*, **31**: 159 (1992)
- [13] Nehlig, A. et al, *Radiochim. Acta*, **91**: 37 (2003)
- [14] KIT-INE, unpublished results

## 9 Radiochemical and Elemental Analysis

*M. Plaschke, C.-H. Graser, M. Lagos, F. Quinto, N. Banik, K. Bender, M. Böttle, M. Fuss, F.W. Geyer, K. Gompper, S. Heck, S. Hilpp, A. Kaufmann, T. Kisely, Ch. Marquardt, S. Moisei-Rabung, T. Schäfer, A. Seither, C. Walschburger, and H. Geckeis*

In co-operation with:

*P. Steier<sup>1</sup>, T. Shinonaga<sup>2</sup>*

<sup>1</sup> Institut für Isotopenforschung und Kernphysik der Universität Wien, Währinger Straße 17, A-1090 Wien, Austria

<sup>2</sup> Helmholtzzentrum München, German Research Center for Environmental Health, Institute of Radiation Protection, D-85764 Neuherberg, Germany

At KIT-INE a pool of advanced analytical techniques, well-developed procedures and competences in the fields of radiochemical sample handling and preparation, element and isotope analysis, chromatography and nuclear spectroscopy is available and applied for the R&D projects of the institute. Commercial analytical service is provided in the context of nuclear waste management, i.e., for nuclear waste treatment facilities, High Level Liquid Waste (HLLW) vitrification or decommissioning of nuclear installations. Analytical services are as well offered for the quality control of radio-analytical separation resins and radiopharmaceuticals. For all these purposes analytical methods and procedures are developed. Mass spectrometry techniques are especially adapted and improved for trace element analysis and speciation studies of actinides. Sector Field (SF)-ICP-MS and collision cell quadrupole CC-Q-ICP-MS are coupled to species sensitive methods, i.e. to capillary electrophoresis (CE-SF-ICP-MS) and field-flow field fractionation (FFF-Q-ICP-MS). Accelerator Mass Spectrometry (AMS) is introduced at INE for the sensitive determination of isotopic fingerprints and concentrations of actinides at levels far below the detection limits of the aforementioned mass spectrometric techniques. In addition, the analytical group supports the infrastructure of the institute, is involved in various educational activities and is responsible for teaching of chemical laboratory assistants.

### Routine Analysis

Over twenty thousands of samples are routinely analysed each year providing the data for the INE R&D projects and external clients. For this purpose a pool of advanced analytical techniques, well-developed procedures, competence in the fields of radiochemical sample preparation and separation techniques, elemental and isotope analysis, chromatographic methods and nuclear spectroscopic techniques is available. Our personnel is trained in handling of nuclear samples and in the operation and maintenance of instruments adapted to glove boxes. Several analytical techniques listed in Table 1 are available both in inactive and radio-analytical labs.

### Commercial Analytical Services

Commercial analytical service is offered for various clients on the basis of formal contract agreements. Data are recorded, documented and quality controlled according to the requirements of the clients.

### Nuclear Waste Treatment and Decommissioning of Nuclear Facilities (WAK-HDB)

Samples from the WAK-HDB (Wiederaufarbeitungsanlage Karlsruhe GmbH, Hauptabteilung Dekontaminationsbetriebe) can be classified according to their origin in samples from the HDB incineration (ashes) or LAW evaporation plants (liquid concentrates), annually averaged samples from the different facilities, samples from decommissioning of nuclear facilities etc..

Samples are processed by radio-analytical separation methods and then analysed using elemental, isotope and nuclear spectroscopic techniques. The nuclides routinely determined include (but are not limited to): <sup>238,239,240,241,242</sup>Pu, <sup>233,234,235,236,238</sup>U, <sup>55</sup>Fe, <sup>63</sup>Ni, <sup>90</sup>Sr, <sup>242,243+244</sup>Cm, <sup>241</sup>Am. In 2013 all analytical procedures and documentations have been successfully evaluated in the course of a client audit.

### Quality Control of Separation Resins

INE is the first quality control lab of the TRISKEM Sr separation resin and the secondary lab for actinide separating TRU and TEVA resins. The analytical service comprise the determination of the capacity of the Sr resin, column tests (loading, washing, elution), determination of possible interferences and the determination of eluted organic material by carbon analysis. Around one sample batch of Sr resin is analyzed each month.

### Quality Control of Radiopharmaceuticals

A Ra-223 containing alpha-radiopharmaceutical developed by Algeta was successfully launched to the U.S. and European market in 2013. During the last years this preparation is regularly analyzed with regard to the content of toxic heavy metal trace impurities at INE. Ra-223 acts as a calcium mimic and is indicated for patients suffering from bone metastases. Due to the short penetration of the alpha emitter a highly-localized tumor cell killing is achieved with minimal damage to surrounding normal tissue. A method validation procedure adopting the guidelines

Tab. 1: Analytical techniques available at INE.

<b>Elemental and Isotope Analysis</b>
Quadrupole Inductively Coupled Mass Spectrometry (Q-ICP-MS)
Collision Cell Q-ICP-MS (CC-Q-ICP-MS)
Sector Field ICP-MS (SF-ICP-MS)
Inductively Coupled Optical Emission Spectrometry (ICP-OES)
Atomic Absorption Spectrometry (AAS)
Flame Atomic Emission Spectrometry (F-AES)
X-Ray Fluorescence Spectrometry (XRF)
<b>Nuclear Spectroscopic Methods</b>
Alphaspectrometry
Liquid Scintillation Counting (LSC, conventional and high sensitivity)
Gammaspectrometry (with auto-sampler)
<b>Other Methods</b>
Ion Chromatography (IC) for cations and anions
Gas Chromatography (GC)
Carbon Analysis (TOC, DOC, TIC, NPOC)
Specific Surface Area Analysis (BET)
Differential Thermal Analysis (DTA)
Dilatometry
Fusion and Microwave Digestions
Gravimetry and Titrations

of the U.S. Pharmacopodia [USP 233] for the determination of ten specified heavy metals by ICP-MS was performed. A batch of the preparation (plus extra samples from the drug development) is analyzed weekly in our lab.

## Projects

Direct contributions to INE research projects are provided by the analytical group, e.g.:

*FIRST Nuclides and CAST:* An experimental setup for the collection of the volatile radionuclide  $^{14}\text{C}$ , which is part of the inventory of instant release fractions and of zircaloy claddings of nuclear spent fuel, is designed, installed and tested in the controlled area (as part of a technical thesis).  $^{14}\text{C}$ -recoveries have been determined by low-level LSC using standard materials ( $^{14}\text{C}$  Na-carbonate and  $^{14}\text{C}$  Na-acetate for the inorganic and organic carbon, respectively).

*Vitrification projects:* Immobilization of HLLW containing high amounts of a  $\text{Cs}_3\text{PMo}_{12}\text{O}_{40}$  containing solid is a challenge for the vitrification process. The effectiveness of the radionuclide retention (i.e., with respect to Cs) on the one hand side and the final stability of the glass product on the other hand side are affected by the high Cs volatility and the formation of Mo-rich separated phases, respectively. In the frame of a technical thesis, different glass simulants with increasing amounts of Cs-P-Mo-rich solids have been produced and characterized by a multi-method approach. Alkaline melting digestions are used for sample preparation and F-AES, ICP-OES, XRF and IC for the elemental and anion analysis.

*WAK – HAW residues:* The conditioning of HAW residues from WAK storage tanks is a challenge for the decommissioning of the facility. For this purpose a conceptual approach for the elemental analysis of

the residues was developed, including sampling, sample transport to INE, sample preparation in hot cells and radiochemical analysis.

## Mass Spectrometry Techniques

At INE several mass spectrometers are currently in operation including two Quadrupole ICP-MS instruments (one equipped with a reaction/collision cell) and since 2010 Sector Field ICP-MS (SF-ICP-MS, Element XR/2, Thermo Scientific, Bremen) adopted to a glove box. The latter is installed at the INE radioactive laboratories. SF-ICP-MS provides 1) detection limits for transuranium elements as low as  $\sim 10^{-14}$  mol/L (lower ppq range) and 2) elevated mass resolution (up to 10.000) which is crucial for accurate determinations of elements such as Fe, Se, but also lanthanides which can severely suffer from interfering species at low mass resolution. Apart from the determination of trace element contents and isotope ratio measurements the instrument is also extensively used in combination with capillary electrophoresis (CE) to study actinide speciation in aqueous solution.

To expand the INE analytical capabilities especially in terms of enhanced sensitivity and lower detection limits Acceleration Mass Spectrometry (AMS) has been recently introduced at INE. Measurements are performed in cooperation with the VERA AMS facility at Vienna.

### SF-ICP-MS

SF-ICP-MS (Sector Field Inductively Coupled Plasma Mass Spectrometry) has been recently used in different scientific projects taking advantage of the aforementioned high sensitivity and the possibility of high mass resolution.

Applications are, e.g., solubility studies of actinides (e.g., Np) and Fe in aqueous solution, sorption experiments on Al- and Fe-oxides, leaching experiments, experiments on the formation of sulfate-solid solutions in aqueous systems, analysis of samples from radionuclide migration experiments at the Grimsel test site (GTS) and also the analysis of filter samples from Japan in the context of the Fukushima Daiichi Nuclear Power Plant accident.

In Fig. 1 the results obtained in a combined  $\gamma$ -spectrometry, AMS and SF-ICP-MS study on filter samples collected during the time period of the Fukushima event at Tokaimura 120 km south of the reactor accident are shown. The data indicate that  $^{137}\text{Cs}$ , Pu and also U were released into the atmosphere and transported directly over 120 km distance by aerosol and wind within a few days after the reactor hydrogen explosions [1].

Fig. 2 depicts the breakthrough curves for various radionuclides ( $^{232}\text{Th}$ ,  $^{233}\text{U}$ ,  $^{237}\text{Np}$ ,  $^{242}\text{Pu}$ , and  $^{243}\text{Am}$ ) which were injected together with Ni doped montmorillonites in June 2013 at the GTS. Compared to an earlier run (02-12) the recent experiment was conducted with a lower - near natural - flow rate. This results in longer residence times of radionuclides in the fracture and, therefore, a larger retention of Np and U which are not primarily controlled by colloidal

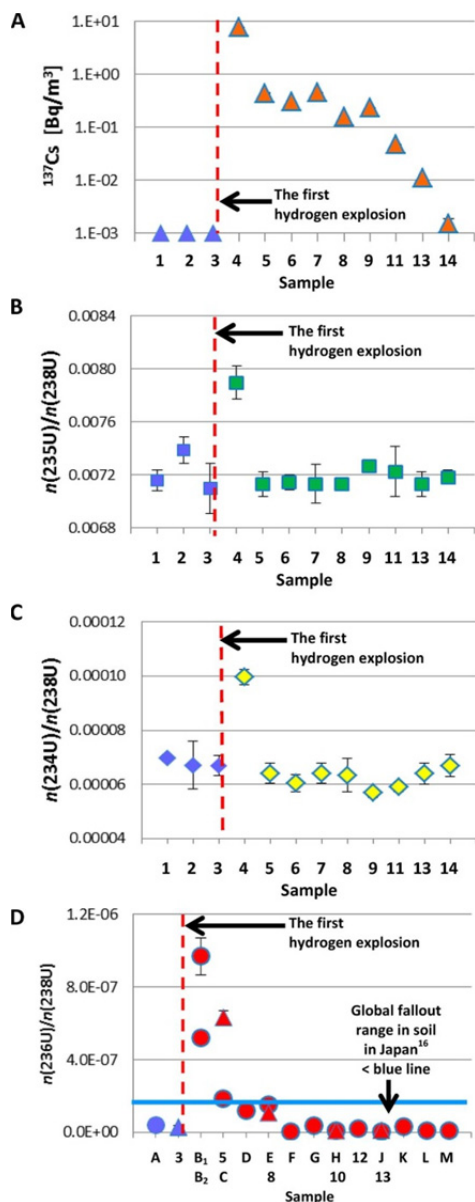


Fig. 1: (A): Activity concentration of  $^{137}\text{Cs}$ , (B):  $n(^{235}\text{U})/n(^{238}\text{U})$ , (C):  $n(^{234}\text{U})/n(^{238}\text{U})$  and (D):  $n(^{236}\text{U})/n(^{238}\text{U})$  in aerosol samples collected at 120 km south-southwest of the FDNPP (reprinted with permission from T. Shinonaga et al., *Environ. Sci. Technol.*, 48 (2014), DOI: 10.1021/es404961w, Copyright 2014, American Chemical Society).

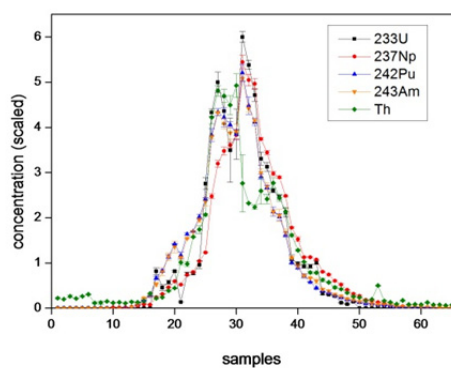


Fig. 2: Breakthrough curves from the 07-2013 radionuclide migration experiment at the GTS. Concentrations are scaled to the corresponding mean value.

transport. Samples from the tailing of the breakthrough curves (from runs 02-12 and 07-13) which could not be analyzed for  $^{237}\text{Np}$ ,  $^{242}\text{Pu}$ , and  $^{243}\text{Am}$  by SF-ICP-MS due to concentrations below the detection limits will be analyzed by AMS and RIMS in the near future (cf. AMS section of this chapter).

#### CE-SF-ICP-MS

The long-term safety assessment for nuclear waste repositories requires a detailed understanding of actinide aqueous (geo)chemistry. The Pu redox chemistry system of aqueous solutions is quite complex with up to four different oxidation states stable in one solution. The properties of these species vary considerably. Therefore, knowledge of their behavior under natural conditions is a vital issue in nuclear waste disposal.

In order to study actinide speciation in aqueous solution we used Capillary Electrophoresis (CE) hyphenated to SF-ICP-MS to measure the redox speciation of Pu(III, IV, V, VI) and Np(IV, V) at concentration levels below  $10^{-9}$  M. In previous studies it was shown that 1 M acetic acid does not significantly disturb the Pu(III)/Pu(V) equilibrium of the original solution [2]. Therefore, it was chosen as the background electrolyte (BGE) for the separations of Pu and Np redox species.

Tab. 2: Limits of detection and electrophoretic mobilities of Pu and Np oxidation states.

Species	Limit of detection [mol/L]	Electrophoretic mobility [ $\times 10^{-4} \text{ cm}^2 \text{ V}^{-1} \text{ s}^{-1}$ ]
$\text{Pu}^{3+}$	$2 \times 10^{-12}$	$4.0 \pm 0.07$
$\text{Pu}^{4+}$	$5 \times 10^{-12}$	$1.2 \pm 0.08$
$\text{PuO}_2^+$	$6 \times 10^{-12}$	$1.6 \pm 0.06$
$\text{PuO}_2^{2+}$	$2 \times 10^{-12}$	$2.4 \pm 0.05$
$\text{Np}^{4+}$	$6 \times 10^{-12}$	$1.8 \pm 0.03$
$\text{NpO}_2^+$	$8 \times 10^{-12}$	$2.4 \pm 0.02$

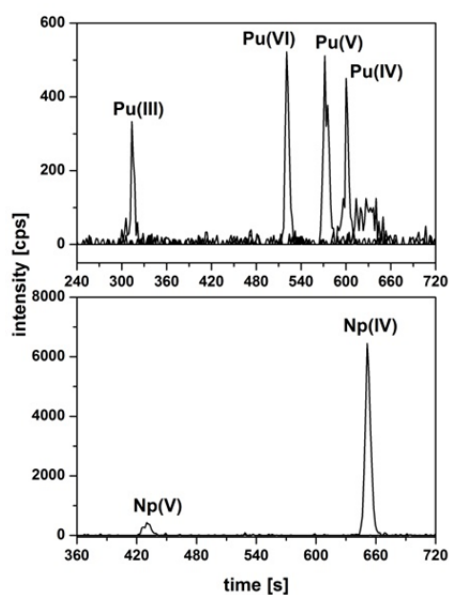


Fig. 3: Electropherogram of four Pu oxidation states (above) and two Np oxidation states (below);  $[\text{Pu}]_{\text{total}}$  and  $[\text{Np}]_{\text{total}}$  each  $1 \times 10^{-10}$  M, hydrodynamic injection: 10s/2psi; voltage: 30 kV; BGE: 1 M HAc; pH = 2.4.



Fig. 4: Argon box with the CE instrument (right) hyphenated to SF-ICP-MS (left).

The limits of detection and the electrophoretic mobilities determined during the CE measurements are listed in Tab. 2. The electropherogram in Fig. 3 was obtained under aerobic conditions. Therefore, it was crucial to stabilize the redox sensitive species e.g. Pu(III), Pu(V), Pu(VI) and Np(IV). The lower oxidation states were treated with a holding reductant (i.e. sodium hydroxymethanesulfinate). The total concentration of Np and Pu in solution was  $1 \times 10^{-10}$  mol/L each and the pH of the solution was 2.4. The tailing of the Pu(IV) peak at 600 s probably indicates the formation of colloidal Pu(IV) polyspecies. In order to minimize redox processes during analysis the CE instrument is now placed inside an argon glove box (Fig. 4). It is planned to use this arrangement to carry out speciation experiments without stabilizing agents. Furthermore it is intended to investigate the Se speciation under reducing conditions in collaboration with the Paul Scherrer Institute (PSI, Switzerland).

In the near future CE-SF-ICP-MS under argon atmosphere will also be used to determine stability constants between actinides and carboxylate ligands in water/methanol systems.

#### AMS

Trace analysis with AMS (Accelerator Mass Spectrometry) represents a valuable tool for the isotopic fingerprint determination of actinides in the environment below ppq levels. Actinide contamination of



Fig. 5: The vessel filled with SF<sub>6</sub> at a pressure of about 6 bar which contains the +3-MV tandem accelerator of VERA (Pelletron type, model 9SDH-2).

groundwater may occur as consequence of effluents of nuclear facilities, releases from nuclear accidents, as well as leakages from nuclear waste repositories. We are developing an analytical protocol for the determination of U, Np, Pu, Am and Cm in groundwater samples without previous chemical separation from each other. A challenge is the availability of suitable isotopic tracers for quantitative mass spectrometric measurements, e.g., for the determination of <sup>237</sup>Np and <sup>243</sup>Am. For this purpose <sup>239</sup>Pu and <sup>248</sup>Cm are used as non-isotopic tracers for <sup>237</sup>Np and <sup>243</sup>Am, respectively. AMS measurements are performed at the VERA Laboratory (Vienna, Austria) employing stripping with helium to the 3+ charge state at 1.65 MV terminal voltage (Fig. 5).

#### First AMS Results

Groundwater (250 ml) and MilliQ water samples are spiked with Np, Pu, Am and Cm isotopes, their concentrations spanning from  $\sim 3 \cdot 10^2$  to  $\sim 4 \cdot 10^6$  atoms/ml. The actinides are co-precipitated with 2 mg Fe(OH)<sub>3</sub> which is then converted to Fe-oxide used as cathode material in AMS.

In Fig. 6 it is shown that a reliable determination of up to seven actinide nuclides with concentrations from  $\sim 2$  ppq down to  $\sim 0.0001$  ppq is possible without previous chemical separation of the actinides from each other and with a total measurement time of  $\sim 32$  min. The <sup>237</sup>Np/<sup>239</sup>Pu atom ratios measured in several kinds of groundwater samples scatter to a larger extend with respect to the corresponding ratios measured from MilliQ water samples. However, the average values of  $12.0 \pm 1.6$  for the groundwater samples, and  $11.7 \pm 0.4$  for the MilliQ water samples, are consistent to each other. The ratios are lower than their nominal value of  $14.2 \pm 0.4$ , indicating a higher ionization yield in the AMS ion source of PuO<sup>-</sup> relative to NpO<sup>-</sup>, in agreement with previous observations [3]. Similar results were obtained for <sup>248</sup>Cm and <sup>243</sup>Am, in fact the measured <sup>248</sup>Cm/<sup>243</sup>Am atom ratios are higher than their nominal value of  $1.38 \pm 0.02$ , indicating a higher ionization yield of CmO<sup>-</sup> relative to AmO<sup>-</sup>, again in agreement with recent observations [4]. The <sup>248</sup>Cm/<sup>243</sup>Am ratios measured in

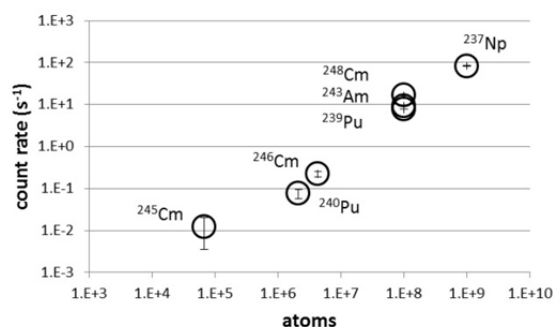


Fig. 6: Count rates (s<sup>-1</sup>) of <sup>245</sup>Cm ( $\sim 0.03$  fg), <sup>240</sup>Pu ( $\sim 0.8$  fg), <sup>246</sup>Cm ( $\sim 2$  fg), <sup>239</sup>Pu ( $\sim 40$  fg), <sup>243</sup>Am ( $\sim 40$  fg), <sup>248</sup>Cm ( $\sim 40$  fg) and <sup>237</sup>Np ( $\sim 400$  fg) from the same cathode produced from a 250 ml groundwater sample.

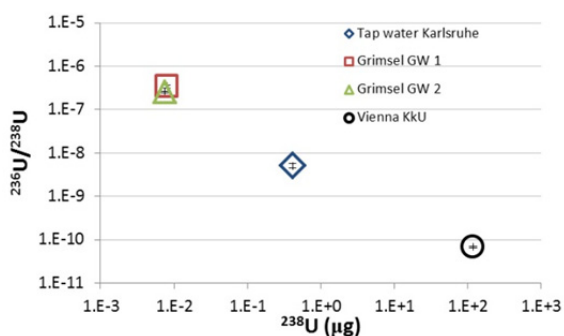


Fig. 7: Measurement of  $^{236}\text{U}/^{238}\text{U}$  isotopic ratio in two groundwater samples from the GTS, in a tap water sample from Karlsruhe and in the in-house standard Vienna KkU.

groundwater samples, with an average of  $1.6 \pm 0.1$ , are consistent with the corresponding ratios measured in MilliQ water samples, with an average of  $1.4 \pm 0.1$ . These preliminary results indicate a dependency of the ionization yield of the actinides on the sample matrix. We conclude that the use of  $^{239}\text{Pu}$  and  $^{248}\text{Cm}$  as non-isotopic tracers for  $^{237}\text{Np}$  and  $^{243}\text{Am}$ , respectively, is possible in groundwater samples by AMS when an accurate estimate of the relative ionization yields of the various actinides is carried out.

In order to test the performances of the method when analysing an existing nuclear contamination in groundwater samples, measurements of  $^{236}\text{U}/^{238}\text{U}$  isotopic ratios were carried out. Fig. 7 shows that from a 250 ml groundwater sample (blue rhombus, red square and green triangle) the signal of anthropogenic  $^{236}\text{U}$  is detectable relative to the pre-nuclear age Vienna KkU in-house standard (black dot). The  $^{236}\text{U}/^{238}\text{U}$  isotopic ratios measured in the groundwater samples from the GTS  $(2.5 \pm 0.1) \times 10^{-7}$  and  $(3.4 \pm 0.3) \times 10^{-7}$ , as well as the ratio detected in the

tap water samples from Karlsruhe  $(5.0 \pm 0.6) \times 10^{-9}$  are consistent with the global fallout origin [5]. These findings indicate the mobility of global fallout  $^{236}\text{U}$  which apparently is able to migrate together with meteoric water from the surface to depths down to the level of the GTS groundwater at 450 m. Interestingly, fallout Pu could not be detected indicating a much lower mobility under given conditions. The measured  $^{236}\text{U}$  levels do not constitute, however, any radiological concern.

It is intended to develop an analytical protocol which can be used for ultra-trace analysis of actinides in groundwater (and seawater) samples in general. A first application will be the 12-02 run of the GTS field experiments. From the gradient of the injected tracers ( $^{233}\text{U}$ ,  $^{237}\text{Np}$ ,  $^{242}\text{Pu}$ , and  $^{243}\text{Am}$ ) at the tailing edge of the breakthrough curves important information about retention of actinides in a granite fracture and the reversibility of the corresponding processes is expected.

## References

- [1] T. Shinonaga, P. Steier, M. Lagos, T. Ohkura, *Environ. Sci. Technol.*, **48** (2014), DOI: 10.1021/es404961w.
- [2] B. Kuczewski, et al., *Anal. Chem.*, **75**: 6769 (2003).
- [3] L.K. Fifield et al., *Nucl. Instr. Meth. Phys. Res., Sect. B* **123**: 400 (1997).
- [4] M. Christl et al., *Nucl. Instr. Meth. Phys. Res., Sect. B* (2014), DOI: 10.1016/j.nimb.2013.11.045
- [5] F. Quinto et al., *Environ. Sci. Technol.*, **47**: 5243 (2013).



## 10 Radiation Protection Research

*B. Breustedt, P. Panak, F. Becker, Ch. Blunck, J.S. Eberhardt, M.A. Harrendorf, B. Heide, W. Klein, D. Leone, O. Marzocchi, S. Pözl*

### Introduction

Radiation Protection Research at INE is focusing on assessing radiation exposures by estimation of doses either from external radiation fields or from intakes of radionuclides. Besides measurements, the modeling and simulation of radiation fields and their interaction with tissues of the human body or detectors measuring the field are the techniques applied in the work of the group. Basic vision of the work is to provide techniques and models for an individualized dosimetry, which goes beyond the current approach of applying reference models in the dose assessments. The exposed individual with his or her anatomical and physiological properties as well as the radiation fields – properly characterized – are taken into account in an individualized dosimetry. In 2013 we again focused on the three main topics

- Dosimetry in external radiation fields
- Dosimetry after intakes of radionuclides
- Modeling and simulation of radiation protection scenarios

The ASF group is collaborating with national and international partners in several research projects funded by BMBF (e.g. Projects “Strahlung und Umwelt 2” in Competence Alliance Radiation Research KVVSF) or EC (e.g. project “BOOSTER” in FP7Sec). Our group is also engaged in the European Radiation Dosimetry Group (EURADOS e.V., <http://www.eurados.org>), which promotes and develops research and European collaboration in radiation dosimetry.

Selected results from the 2013 work of the radiation protection research group at INE are presented in this chapter.

### Personalised body counter calibration using anthropometric parameters

Body counting is a method for in vivo activity assessment applied to the monitoring of people with risk of radionuclide incorporation. Energy-sensitive radiation detectors are arranged relative to the body to quantify the activity of radionuclide deposits in anatomical structures, such as lungs, liver and skeleton. This method is sensitive to the common interindividual anatomical variation in the measured persons. Accurate activity estimates, which are the basis for dose calculation [1], require extensive calibration procedures typically involving experimental measurements of anthropomorphic phantoms conforming to a reference person. Current calibration methods [2] offer personalisation for lung and liver counting only with respect to ratios of body mass and height and do not specify uncertainties.

This work [3] revises and extends the currently applied personalisation methods using radiation transport simulation in combination with computational phantoms, allowing a large range of individual anatomies and incorporation scenarios. It is applied to the calibration of the In Vivo Measurement Laboratory (IVM) at Karlsruhe Institute of Technology (KIT), which comprises four freely arrangeable high-purity germanium detectors in lung, liver, knee and head measurement setups. The XCAT computational phantom series [4] was selected for the calibration. The advantage of this series is that each phantom is directly derived from tomographic imaging data of a medical patient.

The detectors of the IVM have been individually modelled [5] including their kinematics for realistic positioning. A selection of 30 voxelized phantoms of the XCAT series was applied to body counter calibration for standard measurement setups including lungs, liver, knee, and head, and 26 samples of photon energies in the range of 25 keV to 2 MeV. The integration of each phantom into a body counting scenario with according detector arrangement using anatomic landmarks, preprocessing for the Monte Carlo code MCNPX [6] and subsequent peak identification and peak area computation was done with Voxel2MCNP [7]. The results of this virtual calibration method are comparable to experimental measurements. This was tested on physical torso phantoms.

In addition, 19 anthropometric parameters, partially based on standard body measures for clothing sizes defined by EN 13402-1 [8], were specified and computed on all phantoms using geometric algorithms with regard to actual measurement on persons during in vivo monitoring from the perspective of the performing technicians. The computed parameter values are comparable to those of persons measured at the IVM.

Statistical analysis was applied to the generated samples consisting of photon energy, anthropometric parameters and counting efficiency for each pair of source organ and detector to determine subsets of sensitive anthropometric parameters. Those were then used to estimate mean and variance of counting efficiencies among the population of phantoms. Meta optimization was performed to reduce overfitting to the available training data and to guarantee generalization of the estimators.

The results show largest deviations in the computed counting efficiencies of the available phantoms for lungs, followed by liver, knee and head (Fig. 1). They generally increase with a reduction in photon energy and can triple from 2 MeV to 25 keV. These deviations can be reduced by creating estimators related to

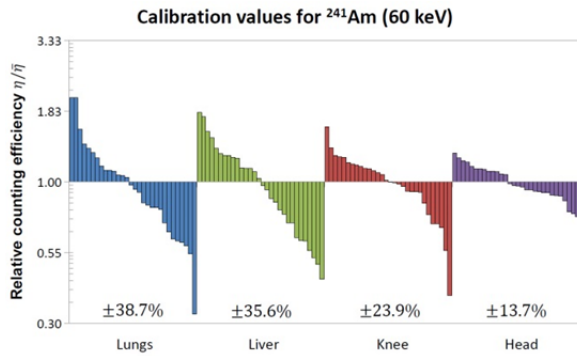


Fig. 1: Calibration values  $\eta$  at 60 keV normalized to their mean  $\bar{\eta}$  for 30 XCAT phantoms in different measurement setups of the IVM body counter. The percentages show the according standard deviations.

body circumferences close to the source structures. These are bust circumference for lungs, waist circumference for liver, thigh circumference for knee, and head circumference for head. The relative reduction generally increases with photon energy. Whole-body measures, such as body mass and its derivatives, have a lower impact. An explanation for this effect could be that body circumferences at the vicinity of the source structure are positively correlated to local tissue thickness, which has a considerable impact on photon attenuation.

An extension of the presented method can easily be achieved by applying the same workflow to additional phantoms of the XCAT series or other phantom series, and defining additional specific anthropometric parameters. The method can also be applied to different body counters by replacing the associated models and implemented measurement setups.

This work is funded by the BMBF under project no. 02NUK015A.

### EURADOS intercomparison exercise on Monte Carlo modeling for the in vivo monitoring of $^{241}\text{Am}$ in skull phantom

An intercomparison exercise on the topic of in vivo monitoring of  $^{241}\text{Am}$  was launched by EURADOS at the end of 2011. The project focused on the measurements of three human skull phantoms, which circulated among the participants. In September 2012 a Monte Carlo (MC) exercise using the voxel representations of the real phantoms was proposed. The full MC exercise consists of three tasks. In the first one the participants simulate a given detector and a defined semi-skull phantom. In the second one they model their own detector and compare their simulated response with the measurement. In the third task the participants simulate the detector geometry they use for routine measurement with a provided skull as subject. The first task is described in the following [9].

A detector from Helmholtz Zentrum München was used for the reference measurement. It consists of a germanium crystal with 50 mm diameter and 10 mm thickness, encapsulated in an aluminium alloy end-cap with a carbon-epoxy window. The participants

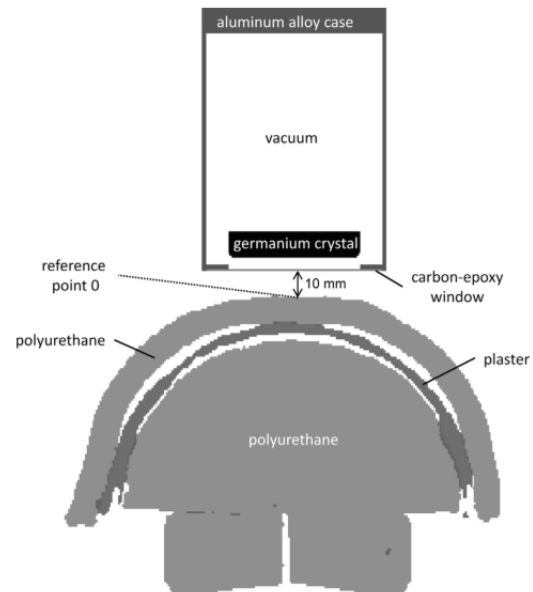


Fig. 2: Experimental setup of the measurement of the physical phantom with the Helmholtz Zentrum München detector.

modelled this detector using their MC software. The technical drawings were provided to uniform the simulated geometry that, in this case included also the inactive part of the detector.

The voxel model of the phantom was created from CT measurement of the physical phantom and was distributed among the participants as a fully segmented and labelled phantom with the material description. The labels were necessary in order to orient it correctly.

All surface voxels of bone equivalent material were treated as source region, with  $^{241}\text{Am}$  as source, whose emission spectrum, containing 31 energy lines from 10 to 60 keV, was distributed to the participants as input data. The experimental measurement setup is shown in Fig. 2. Each participant returned a simulated

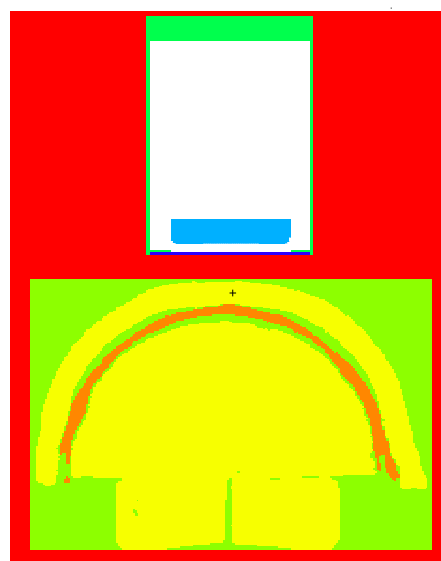


Fig. 3: Sketch of the simulated geometry.

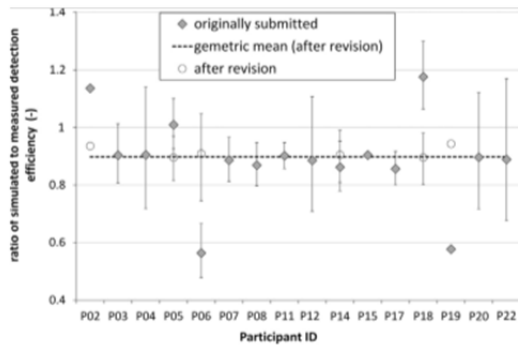


Fig. 4: Relative detection efficiencies.

spectrum including its statistical uncertainties, the detection efficiency for the 59.54 keV peak (in unit counts  $\text{Bq}^{-1} \text{s}^{-1}$ ) and all the relevant information about the simulation.

There were 16 responses, 13 of them obtained with different versions of the MCNP/MCNPX family [10], one with GEANT4 [11], one with EGS4 [12] and one with VNC [13].

We used the version 2.7 of MCNPX; our results have been accepted without need of revision. In Fig. 3 a sketch of the simulated experimental setup is shown, while Fig. 4 shows the relative detection efficiency for the several participants. The geometric mean of the simulated detection efficiencies (after revision for some participants) underestimate the experimental value of about 10%, while the variation among the simulated results is relatively small. Our result (participant ID P07) follows this tendency. Since an experiment with another detector and the same physical phantom compared with the corresponding simulation did not exhibit this large discrepancy, there is the hypothesis that the difference between the average of the simulations and the measurement is due to a mistake in the detector/phantom positioning.

### The BOOSTER project: Development of tools for triage of a large group of individuals exposed to radioactive material

The BOOSTER (BiO-dOSimetric Tools for triage to Responders) project, founded by the European Union under the Seventh Framework Programme, focuses on developing new biosimetric tools and the effective management of an event involving the exposure of a large number of people to radioactive material, either accidentally or following a malevolent use of radioactive material. This includes a mechanism for fast triage of exposed individuals, for an efficient and fast categorization of potentially affected victims, and to provide medical staff crucial information for further treatment in the longer term following the event.

New measurement tools allow securing the first responder from the radiation exposure as these tools do not only check the affected people but also provide clear and comprehensive information on the existing contamination level which is far beyond existing radiation equipment available so far. KIT-INE activi-



Fig. 5: A picture of the field exercise scenario simulating a terrorist attack with dirty bombs in a stadium. The event started with sounds of explosions, smoke coming from smoke machines, and stroboscopic lights simulating the explosion.



Fig. 6: A picture of the gamma camera as employed in the field exercise.

ties in 2013 are related to a gamma camera developed by CEA and Canberra. This device is a radiation measurement instrument that creates two images of a scenario: gamma radiation and video pictures of a scene are superimposed.

It allows for quasi real-time visualization and localization of radioactive spots. The contribution of KIT-INE was the calibration of the prototypes in well-defined reference radiation fields of X-rays and Cs-137.

The BOOSTER system was successfully presented during a field exercise in May 2013, on the KFKI Campus, Budapest (examples are shown in Fig. 5 and 6). This project dissemination event showed the functionality of all devices and the applicability of the BOOSTER system to intended crisis management. KIT-INE was involved in the preparation and demonstration of the Decision Support System (DSS) (developed by KIT-IKET). The DSS collects all data from measurements taken in the field as well as the victims' radiological and status data. It informs a crisis manager on the location of radioactivity and allows for evaluating the situation of each victim and elaborates detailed reports from the results

of the different tests in order to help the medical staff in performing a triage of victims.

## References

- [1] ICRP (2007). 'ICRP Publication 103: The 2007 recommendations of the international commission on radiological protection'. In: *Annals of the ICRP* **37** (2-4). doi: 10.1016/j.icrp.2007.11.001.
- [2] Pierrat, N., G. Prulhiere, L. de Carlan and D. Franck (2007). 'Determination of new European biometric equations for the calibration of in vivo lung counting systems using the Livermore phantom'. In: *Radiation Protection Dosimetry* **125** (1-4): 449–455. doi: 10.1093/rpd/ncm150.
- [3] Pölz, S. (2014). 'Personalised body counter calibration using anthropometric parameters'. PhD thesis. KIT Scientific Publishing, doi: 10.5445/KSP/1000038415.
- [4] Segars, W. P. and G. M. Sturgeon (2010). 'The new XCAT series of digital phantoms for multimodality imaging'. In: *Nuclear Science Symposium Conference Record (NSS/MIC)*, 2010 IEEE: 2392–2395.
- [5] Marzocchi, O., B. Breustedt and M. Urban (2010). 'Characterisation, modelling and optimisation of the model of a HPGe detector with the aid of point sources'. In: *Applied Radiation and Isotopes* **68** (7-8): 1438–1440. doi: 10.1016/j.apradiso.2009.11.022.
- [6] Pelowitz, D. B. (2007). *MCNPX user's manual*. Tech. rep. LA-CP-07-1473. Los Alamos, NM: Los Alamos National Laboratory.
- [7] Pölz, S., S. Laubersheimer, J. S. Eberhardt, M. A. Harrendorf, T. Keck, A. Benzler and B. Breustedt (2013). 'Voxel2MCNP: A framework for modeling, simulation and evaluation of radiation transport scenarios for Monte Carlo codes'. In: *Physics in Medicine and Biology* **58** (16): 5381–5400. doi: 10.1088/0031-9155/58/16/5381.
- [8] *European Committee for Standardization (2001). Size designation of clothes — Part 1: Terms, definitions and body measurement procedure. Tech. rep. EN 13402-1:2001 (ISO 3635:1981 modified)*. Brussels: European Committee for Standardization.
- [9] Vrba T. et al, *EURADOS intercomparison exercise on MC modeling for the in-vivo monitoring of AM-241 in skull phantoms (Part I)*, *Radiat. Phys. Chem.* (2014), doi: 10.1016/j.radphyschem.2013.12.010.
- [10] Pelowitz D., 2005, *MCNOX Users's Manual, Los Alamos National Laboratory Report, LA-CP-05-0368*.
- [11] Agostinelli et al., 2003, *Geant4 a simulation toolkit, Nucl. Instrum. Methods Phys. Res., Sect A* **506**(3), 250-303.
- [12] Nelson W.R. et al., 1985, *The EGS code system, SLAC Report 265*.
- [13] Hunt J.G. et al., 2003, *Voxel phantom and Monte Carlo methods applied to in vivo measurements for simultaneous <sup>241</sup>Am contamination in four body regions, Radiat. Prot. Dosim.* **105** (1-4), 549-55.
- [14] [www.booster-project.org](http://www.booster-project.org) (Feb 2014).

## 11 Publications

### ISI/SCOPUS:

- [1] Adam, C.; Kaden, P.; Beele, B. B.; Muellich, U.; Trumm, S.; Geist, A.; Panak, P. J.; Denecke, M. A., *Evidence for covalence in a N-donor complex of americium(III)*, *Dalton Transactions* 2013, 42, 14068-14074.
- [2] Afsar, A.; Laventine, D. M.; Harwood, L. M.; Hudson, M. J.; Geist, A., *Utilizing electronic effects in the modulation of BTPPhen ligands with respect to the partitioning of minor actinides from lanthanides*, *Chemical Communications* 2013, 49, 8534-8536.
- [3] Altmaier, M.; Gaona, X.; Fanghanel, T., *Recent Advances in Aqueous Actinide Chemistry and Thermodynamics*, *Chem Rev* 2013, 113, 901-943.
- [4] Baillieux, P.; Schill, E.; Edel, J. B.; Mauri, G., *Localization of temperature anomalies in the Upper Rhine Graben: insights from geophysics and neotectonic activity*, *Int Geol Rev* 2013, 55, 1744-1762.
- [5] Ballhaus, C.; Laurenz, V.; Munker, C.; Fonseca, R. O. C.; Albarede, F.; Rohrbach, A.; Lagos, M.; Schmidt, M. W.; Jochum, K. P.; Stoll, B.; Weis, U.; Helmy, H. M., *The U/Pb ratio of the Earth's mantle-A signature of late volatile addition*, *Earth and Planetary Science Letters* 2013, 362, 237-245.
- [6] Banik, N. L.; Denecke, M. A.; Geist, A.; Modolo, G.; Panak, P. J.; Rothe, J., *2,6-Bis(5,6-dipropyl-1,2,4-triazin-3-yl)-pyridine: Structures of An(III) and Ln(III) 1:3 complexes and selectivity*, *Inorg Chem Commun* 2013, 29, 172-174.
- [7] Batuk, O. N.; Szabo, D. V.; Denecke, M. A.; Vitova, T.; Kalmykov, S. N., *Synthesis and characterization of thorium, uranium and cerium oxide nanoparticles*, *Radiochim Acta* 2013, 101, 233-239.
- [8] Beele, B. B.; Rudiger, E.; Schworer, F.; Mullich, U.; Geist, A.; Panak, P. J., *A TRLFS study on the complexation of novel BTP type ligands with Cm(III)*, *Dalton Transactions* 2013, 42, 12139-12147.
- [9] Bremer, A.; Geist, A.; Panak, P. J., *Complexation of Cm(III) and Eu(III) with 2,6-bis(5-(2,2-dimethylpropyl)-1H-pyrazol-3-yl)pyridine and 2-bromohexanoic acid studied by time-resolved laser fluorescence spectroscopy*, *Radiochim Acta* 2013, 101, 285-291.
- [10] Bube, C.; Metz, V.; Bohnert, E.; Garbev, K.; Schild, D.; Kienzler, B., *Long-term cement corrosion in chloride-rich solutions relevant to radioactive waste disposal in rock salt - Leaching experiments and thermodynamic simulations*, *Phys Chem Earth* 2013, 64, 87-94.
- [11] Carvajal Nuñez, U.; Martel, L.; Prieur, D.; Lopez Honorato, E.; Eloirdi, R.; Farnan, I.; Vitova, T.; Somers, J., *Coupling XRD, EXAFS, and <sup>13</sup>C NMR to Study the Effect of the Carbon Stoichiometry on the Local Structure of UCl<sub>4</sub>x* *Inorg Chem* 2013, 52, 11669-11676.
- [12] Curtius, H.; Kaiser, G.; Rozov, K.; Neumann, A.; Dardenne, K.; Bosbach, D., *Preparation and characterization of Fe-, Co-, and Ni-containing Mg-Al-layered double hydroxides*, *Clay Clay Miner* 2013, 61, 424-439.
- [13] Denecke, M. A.; Petersmann, T.; Marsac, R.; Dardenne, K.; Vitova, T.; Prüssmann, T.; Borchert, M.; Bösenberg, U.; Falkenberg, G.; Wellenreuther, G., *XANES characterization of UO<sub>2</sub>/Mo(Pd) thin films as models for ε-particles in spent nuclear fuel*, *Journal of Physics: Conference Series* 2013, 430.
- [14] Farah, J.; Marzocchi, O.; Leone, D.; Breustedt, B.; Franck, D.; Broggio, D., *Coupling in vivo measurements and Monte-Carlo simulations to assess organ Specific activity*, *Radiation Measurements* 2013, 51-52, 55-61.
- [15] Figueira, C.; Becker, F.; Blunck, C.; DiMaria, S.; Baptista, M.; Esteves, B.; Paulo, G.; Santos, J.; Teles, P.; Vaz, P., *Medical staff extremity dosimetry in CT fluoroscopy: an anthropomorphic hand voxel phantom study*, *Physics in Medicine and Biology* 2013, 58, 5433-5448.
- [16] Fischer, C.; Aurin, P.; Darbha, G. K.; Arp, G., *Experimental approaches to the formation of early-diagenetic grain coats on quartz surfaces*, *Zeitschrift Der Deutschen Gesellschaft Fur Geowissenschaften* 2013, 164, 225-236.

- [17] Fröhlich, D. R.; Skerencak-Frech, A.; Morkos, M. L. K.; Panak, P. J., *A spectroscopic study of Cm(III) complexation with propionate in saline solutions at variable temperatures*, *New Journal of Chemistry* 2013, 37, 1520-1528.
- [18] Gaona, X.; Fellhauer, D.; Altmaier, M., *Thermodynamic description of Np(VI) solubility, hydrolysis, and redox behavior in dilute to concentrated alkaline NaCl solutions*, *Pure and Applied Chemistry* 2013, 85, 2027-2049.
- [19] Gaona, X.; Wieland, E.; Tits, J.; Scheinost, A. C.; Dahn, R., *Np(V/VI) redox chemistry in cementitious systems: XAFS investigations on the speciation under anoxic and oxidizing conditions*, *Applied Geochemistry* 2013, 28, 109-118.
- [20] Geckeis, H.; Lützenkirchen, J.; Polly, R.; Rabung, T.; Schmidt, M., *Mineral-Water Interface Reactions of Actinides*, *Chem Rev* 2013, 113, 1016-1062.
- [21] Goettlicher, J.; Kotelnikov, A.; Suk, N.; Kovalski, A.; Vitova, T.; Steininger, R., *Sulfur K X-ray absorption near edge structure spectroscopy on the photochrome sodalite variety hackmanite*, *Z Kristallogr* 2013, 228, 157-171.
- [22] Guglielmetti, L.; Comina, C.; Abdelfettah, Y.; Schill, E.; Mandrone, G., *Integration of 3D geological modeling and gravity surveys for geothermal prospection in an Alpine region*, *Tectonophysics* 2013, 608, 1025-1036.
- [23] Heide, B., *Assessment of doses caused by electrons in thin layers of tissue-equivalent materials, using MCNP*, *Radiat Prot Dosim* 2013, 156, 495-505.
- [24] Holliday, K.; Dardenne, K.; Walther, C.; Stumpf, T., *The incorporation of europium into apatite: a new explanation*, *Radiochim Acta* 2013, 101, 267-272.
- [25] Kobayashi, T.; Bach, D.; Altmaier, M.; Sasaki, T.; Moriyama, H., *Effect of temperature on the solubility and solid phase stability of zirconium hydroxide*, *Radiochim Acta* 2013, 101, 645-651.
- [26] Kobayashi, T.; Scheinost, A. C.; Fellhauer, D.; Gaona, X.; Altmaier, M., *Redox behavior of Tc(VII)/Tc(IV) under various reducing conditions in 0.1 M NaCl solutions*, *Radiochim Acta* 2013, 101, 323-332.
- [27] Lindqvist-Reis, P.; Apostolidis, C.; Walter, O.; Marsac, R.; Banik, N. L.; Skripkin, M. Y.; Rothe, J.; Morgenstern, A., *Structure and spectroscopy of hydrated neptunyl(VI) nitrate complexes*, *Dalton Transactions* 2013, 42, 15275-15279.
- [28] Lindqvist-Reis, P.; Klenze, R.; Loeble, M.; Finck, N.; Geckeis, H., *Influence of chemical pressure on various luminescence properties of curium(III) and europium(III) ions in rare-earth hydroxides: A time-resolved laser fluorescence spectroscopy (TRLFS) study*, *Abstr Pap Am Chem S* 2013, 245.
- [29] Löble, M. W.; Ona-Burgos, P.; Fernandez, I.; Apostolidis, C.; Morgenstern, A.; Walter, O.; Bruchertseifer, F.; Kaden, P.; Vitova, T.; Rothe, J.; Dardenne, K.; Banik, N. L.; Geist, A.; Denecke, M. A.; Breher, F., *Exploring the solution behavior of f-element coordination compounds: a case study on some trivalent rare earth and plutonium complexes*, *Chem Sci* 2013, 4, 3717-3724.
- [30] Lützenkirchen, J., *Specific Ion Effects at Two Single-Crystal Planes of Sapphire*, *Langmuir* 2013, 29, 7726-7734.
- [31] Lützenkirchen, J.; Preocanin, T.; Stipic, F.; Heberling, F.; Rosenqvist, J.; Kallay, N., *Surface potential at the hematite (001) crystal plane in aqueous environments and the effects of prolonged aging in water*, *Geochim Cosmochim Acta* 2013, 120, 479-486.
- [32] Lützenkirchen, J.; Richter, C., *Zeta-potential measurements of OTS-covered silica samples*, *Adsorption* 2013, 19, 217-224.
- [33] Maczka, E.; Lützenkirchen, J.; Kosmulski, M., *The significance of the solid-to-liquid ratio in the electrokinetic studies of the effect of ionic surfactants on mineral oxides*, *J Colloid Interf Sci* 2013, 393, 228-233.
- [34] Magnusson, D.; Geist, A.; Malmbeck, R., *SX process-A code for solvent extraction processes in centrifugal contactors simulation*, *Chemical Engineering Science* 2013, 99, 292-297.
- [35] Magnusson, D.; Geist, A.; Malmbeck, R.; Müllich, U., *Study of the Mass Transfer Behavior in a Centrifugal Contactor and Verification of the Solvent Extraction Model for the SX Process Program*, *Solvent Extraction and Ion Exchange* 2013, 31, 578-589.

- [36] Magnusson, D.; Geist, A.; Wilden, A.; Modolo, G., *Direct Selective Extraction of Actinides(III) from PUREX Raffinate Using a Mixture of CyMe4-BTBP and TODGA as 1-cycle SANEX Solvent PART II: Flow-sheet Design for a Counter-Current Centrifugal Contactor Demonstration Process, Solvent Extraction and Ion Exchange* 2013, *31*, 1-11.
- [37] Panak, P. J.; Geist, A., *Complexation and Extraction of Trivalent Actinides and Lanthanides by Triazinylpyridine N-Donor Ligands, Chem Rev* 2013, *113*, 1199-1236.
- [38] Payne, T. E.; Brendler, V.; Ochs, M.; Baeyens, B.; Brown, P. L.; Davis, J. A.; Ekberg, C.; Kulik, D. A.; Lützenkirchen, J.; Missana, T.; Tachi, Y.; Van Loon, L. R.; Altmann, S., *Guidelines for thermodynamic sorption modelling in the context of radioactive waste disposal, Environ Modell Softw* 2013, *42*, 143-156.
- [39] Pekov, I. V.; Chukanov, N. V.; Filinchuk, Y. E.; Zadov, A. E.; Kononkova, N. N.; Epanchintsev, S. G.; Kaden, P.; Kutzer, A.; Gottlicher, J., *Kasatkinite, Ba<sub>2</sub>Ca<sub>8</sub>B<sub>5</sub>Si<sub>8</sub>O<sub>32</sub>(OH)<sub>(3)</sub> \* 6H<sub>2</sub>O, a new mineral from the Bazhenovskoe deposit, the Central Urals, Russia, Geol Ore Deposit+* 2013, *55*, 558-566.
- [40] Pidchenko, I.; Salminen-Paatero, S.; Rothe, J.; Suksi, J., *Study of uranium oxidation states in geological material, Journal of Environmental Radioactivity* 2013, *124*, 141-146.
- [41] Polly, R.; Schimmelpfennig, B.; Flörsheimer, M.; Rabungi, T.; Kupcik, T.; Klenze, R.; Geckeis, H., *Quantum chemical study of inner-sphere complexes of trivalent lanthanide and actinide ions on the corundum (110) surface, Radiochim Acta* 2013, *101*, 561-570.
- [42] Pölz, S.; Laubersheimer, S.; Eberhardt, J. S.; Harrendorf, M. A.; Keck, T.; Benzler, A.; Breustedt, B., *Voxel2MCNP: a framework for modeling, simulation and evaluation of radiation transport scenarios for Monte Carlo codes, Physics in Medicine and Biology* 2013, *58*, 5381-5400.
- [43] Prieur, D.; Carvajal-Nunez, U.; Vitova, T.; Somers, J., *Local and Electronic Structure of Americium-Bearing PuO<sub>2</sub>, Eur J Inorg Chem* 2013, 1518-1524.
- [44] Prüßmann, T.; Denecke, M. A.; Geist, A.; Rothe, J.; Lindqvist-Reis, P.; Loble, M.; Breher, F.; Batchelor, D. R.; Apostolidis, C.; Walter, O.; Caliebe, W.; Kvashnina, K.; Jorissen, K.; Kas, J. J.; Rehr, J. J.; Vitova, T., *Comparative investigation of N donor ligand-lanthanide complexes from the metal and ligand point of view, Journal of Physics: Conference Series* 2013, *430*.
- [45] Quinto, F.; Hrncsek, E.; Krachler, M.; Shotyk, W.; Steier, P.; Winkler, S. R., *Measurements of U-236 in Ancient and Modern Peat Samples and Implications for Postdepositional Migration of Fallout Radionuclides, Environ Sci Technol* 2013, *47*, 5243-5250.
- [46] Quinto, F.; Hrncsek, E.; Krachler, M.; Shotyk, W.; Steier, P.; Winkler, S. R., *Determination of Pu-239, Pu-240, Pu-241 and Pu-242 at femtogram and attogram levels - evidence for the migration of fallout plutonium in an ombrotrophic peat bog profile, Environmental Science-Processes & Impacts* 2013, *15*, 839-847.
- [47] Réal, F.; Trumm, M.; Schimmelpfennig, B.; Masella, M.; Vallet, V., *Further insights in the ability of classical nonadditive potentials to model actinide ion-water interactions, Journal of Computational Chemistry* 2013, *34*, 707-719.
- [48] Rojo, H.; Tits, J.; Gaona, X.; Garcia-Gutierrez, M.; Missana, T.; Wieland, E., *Thermodynamics of Np(IV) complexes with gluconic acid under alkaline conditions: sorption studies, Radiochim Acta* 2013, *101*, 133-138.
- [49] Rosenberg, Y. O.; Metz, V.; Ganor, J., *Radium removal in a large scale evaporitic system, Geochim Cosmochim Acta* 2013, *103*, 121-137.
- [50] Rothe, J.; Brendebach, B.; Bube, C.; Dardenne, K.; Denecke, M. A.; Kienzler, B.; Metz, V.; Prüßmann, T.; Rickers-Appel, K.; Schild, D.; Soballa, E.; Vitova, T., *Characterization of U(VI)-phases in corroded cement products by micro( $\mu$ )-spectroscopic methods, Journal of Physics: Conference Series* 2013, *430*.
- [51] Serrano-Purroy, D.; Casas, I.; Gonzalez-Robles, E.; Glatz, J. P.; Wegen, D. H.; Clarens, F.; Gimenez, J.; de Pablo, J.; Martinez-Esparza, A., *Dynamic leaching studies of 48 MWd/kgU UO<sub>2</sub> commercial spent nuclear fuel under oxic conditions, J Nucl Mater* 2013, *434*, 451-460.
- [52] Skerencak, A.; Hohne, S.; Hofmann, S.; Marquardt, C. M.; Panak, P. J., *Spectroscopic Studies on the Thermodynamics of the Complexation of Trivalent Curium with Propionate in the Temperature Range from 20 to 90°C, Journal of Solution Chemistry* 2013, *42*, 1-17.

- [53] Skerencak, A.; Panak, P. J.; Fanghänel, T., *Complexation and thermodynamics of Cm(III) at high temperatures: the formation of  $[Cm(SO_4)(n)](3-2n)$  ( $n=1, 2, 3$ ) complexes at  $T=25$  to  $200^\circ\text{C}$* , *Dalton Transactions* 2013, 42, 542-549.
- [54] Skerencak-Frech, A.; Fröhlich, D. R.; Rothe, J.; Dardenne, K.; Panak, P. J., *Combined Time-Resolved Laser Fluorescence Spectroscopy and Extended X-ray Absorption Fine Structure Spectroscopy Study on the Complexation of Trivalent Actinides with Chloride at  $T = 25-200^\circ\text{C}$* , *Inorg. Chem.* 2013, 53, 1062-1069.
- [55] Steier, P.; Hrnccek, E.; Priller, A.; Quinto, F.; Srcnik, M.; Wallner, A.; Wallner, G.; Winkler, S., *AMS of the Minor Plutonium Isotopes, Nuclear Instruments & Methods in Physics Research Section B-Beam Interactions with Materials and Atoms* 2013, 294, 160-164.
- [56] Vitova, T.; Denecke, M. A.; Göttlicher, J.; Jorissen, K.; Kas, J. J.; Kvashnina, K.; Prüßmann, T.; Rehr, J. J.; Rothe, J., *Actinide and lanthanide speciation with high-energy resolution X-ray techniques*, *Journal of Physics: Conference Series* 2013, 430.
- [57] Walshe, A.; Prüßmann, T.; Vitova, T.; Baker, R. J., *An EXAFS and HR-XANES study of the uranyl peroxides  $[UO_2\eta^2-O_2](H_2O)_2 \cdot nH_2O$  ( $n = 0, 2$ ) and uranyl (oxy)hydroxide  $[(UO_2)_4O(OH)_6] \cdot 6H_2O$* , *Dalton Transactions* 2013, 43.

#### **Other referred publications:**

- [58] Geckeis, H.; Altmaier, M.; Kaden, P., *Annual Report 2012 : Institute for Nuclear Waste Disposal, Vol. 7655*, KIT Scientific Reports, 2013.
- [59] Kienzler, B.; Altmaier, M.; Bube, C.; Metz, V., *Radionuclide source term for irradiated fuel from prototype, research and education reactors, for waste forms with negligible heat generation and for uranium tails*, KIT Scientific Reports, 2013.
- [60] Wieland, E.; Dähn, R.; Gaona, X.; Mace, N.; Tits, J., in *Cement-Based Materials for Nuclear Waste Storage, Micro- and Macroscopic Investigations of Actinide Binding in Cementitious Materials*, 2013, pp. 93-101.
- [61] Vitova, T.; Rothe, J.; Denecke, M.; Kutzer, A.; Prüßmann, T.; Pidchenko, I.; Kvashnina, K., in *ESRF user report*, 2013.

#### **Invited oral presentations:**

- [62] Altmaier, M., *Actinides in environment - overview of what is done through European Projects in Europe, Second ACTINET I3 Plenary Meeting*, Avignon, France, 2013
- [63] Altmaier, M., *Recent Advances in Aqueous Neptunium Chemistry and Thermodynamics, Actinides 2013*, Karlsruhe, Germany, 2013
- [64] Altmaier, M., *Solubility, speciation and thermodynamics of actinides and fission products, 14th International Conference on the Chemistry and Migration Behaviour of Actinides and Fission Products in the Geosphere (Migration)*, Brighton, U.K., 2013
- [65] Altmaier, M.; Duro, L.; Grive, M.; Montoya, V.; Buckau, G.; Kienzler, B., *ReCoSy: "Understanding of redox phenomena controlling the long-term release/retention of radionuclides in nuclear waste disposal"*, *EURADWASTE - 8th EC Conference on the Management of Radioactive Waste Community Policy and Research on Disposal*, Vilnius, Lithuania, 2013
- [66] Altmaier, M.; Fellhauer, D.; Gaona, X., *Actinide solubility and speciation in alkaline  $CaCl_2$  brine solutions, 3rd International Workshop – Mechanisms and Modeling of Cement/Waste Interactions*, Ghent, Belgium, 2013
- [67] Altmaier, M.; Gaona, X.; Fellhauer, D.; Neck, V., *Recent Studies on Aqueous Neptunium Chemistry and Thermodynamics at KIT-INE, Seaborg Institute, Los Alamos National Laboratories*, Los Alamos, USA, 2013
- [68] Beele, B., *Complexation and Separation Performance of N- and O- Donor Ligands Used in Actinide Separation, Department of Nuclear Chemistry, Czech Technical University, Prag, Czeck Republic*, 2013

- [69] Bremer, A.; Geist, A.; Panak, P. J., *Selective complexation of f-elements – Partitioning & Transmutation, 1. Projektstatusgespräch zur BMBF-geförderten Nuklearen Sicherheitsforschung*, Karlsruhe, Germany, 2013
- [70] Breustedt, B.; Blanchardon, E.; Berard, P.; Fritsch, P.; Gremy, O.; Giussani, A.; Kastl, M.; Nosske, D.; M.A., L., *Towards a model of DTPA decorporation therapy The Fifth International MELODI Workshop*, Brussels, Belgium, 2013
- [71] Gaona, X., *Aquatic chemistry and thermodynamics of actinides: solubility, redox processes and complexation with organics ligands*, Hungarian Chemical Society Seminar, University of Szeged Szeged, Hungary, 2013
- [72] Gaona, X.; Altmaier, M.; Dardenne, K.; Rothe, J.; Denecke, M. A.; Petrov, V.; Kalmykov, S.; Tits, J.; Wieland, E.; Fellhauer, D., *Redox chemistry and solubility of Np(V/VI in NaCl-NaOH and TMA-OH solutions*, Second ACTINET-i3 plenary meeting, Avignon, France, 2013
- [73] Gaona, X.; Fellhauer, D.; Altmaier, M., *Solubility, hydrolysis and redox chemistry of neptunium*, Institutseminar, Johannes Gutenberg-Universität Mainz, Institut für Kernchemie, Mainz, Germany, 2013
- [74] Geckeis, H., *Endlagerung radioaktiver Abfälle: technisch gelöst oder Herausforderung an die Wissenschaft, 77. Jahrestagung der DPG und DPG Frühjahrstagung, Arbeitskreis Energie*, Dresden, Germany, 2013
- [75] Geckeis, H., *Nuclear waste disposal: a technically resolved problem or a scientific challenge*, ABC-Salt Workshop, Santa Fe, USA, 2013
- [76] Geckeis, H., *Radionuclide analysis by ICP-MS*, IAEA-KIT Interregional Advanced Training Course on Marine Radioactivity, Karlsruhe, Germany, 2013
- [77] Geckeis, H., *Disposal of high level nuclear waste - Facts and perspectives*, Summer School on Actinide Science and Applications, Karlsruhe, Germany, 2013
- [78] Geckeis, H., *Future challenges in radioactive waste disposal research in Germany*, Farewell Symposium Dr. Michael Bradbury, Villigen, Switzerland, 2013
- [79] Geist, A., *Hydrometallurgical TRU Separations*, Internal ASGARD School, Warschau, Poland, 2013
- [80] Geist, A., *An(III)/Ln(III) separation: N-donors do the job — but how?*, 9th International Conference on the Chemistry and Physics of the Actinide Elements - ACTINIDES 2013, Karlsruhe, Germany, 2013
- [81] Geist, A., *Hydrometallurgische Abtrennung von Actiniden aus bestrahlten Kernbrennstoffen*, Leibnitz-Universität Hannover, Institut für Radioökologie und Strahlenschutz, Hannover, Germany, 2013
- [82] Geist, A., *Hydrometallurgical actinide separation processes for advanced nuclear fuel cycles*, European Summer Campus “Energy on all Scales“, Strasbourg, France, 2013
- [83] Geist, A.; Beele, B.; Bremer, A.; Denecke, M. A.; Müllich, U.; Panak, P. J.; Rothe, J.; Ruff, C., *Actinide Separations Using N-Donor Compounds*, ACTINET-13 Theoretical User Lab (ThUL), Karlsruhe, Germany, 2013
- [84] Grünewald, W.; Roth, G.; Weisenburger, S., *German vitrification technology and control measures applied by the VEK plant for the production of qualified highly radioactive waste glass*, E-MRS 2013 Spring Meeting, Strasbourg, France, 2013
- [85] Hampel, A.; Argüello, L.; Hansen, F.; Günther, R.-M.; Salzer, K.; Herchen, K.; Wolters, R.; Düsterloh, U.; Pudewills, A.; Yildirim, S.; Gährken, A.; Missal, C.; Stahlmann, J., *Benchmark Calculations of the Thermo-Mechanical Behavior of Rock Salt – Results from a US-German Joint Project*, 4th US-German Workshop on Salt Repository Research, Design and Operations Berlin, Germany, 2013
- [86] Heide, B., *Avoiding Uncertainties Due to the Multiple Scattering Model Applied in MCNP Which Occur in Thin Tissue-Equivalent Layers During Electron Transport*, Technische Universität Dresden, Institut für Kern- und Teilchenphysik, Dresden, Germany, 2013
- [87] Hofmann, A.; Hiemstra, T.; Lützenkirchen, J., *CD-MUSIC to Interpret Drifting Primary Charge of Ferrihydrite*, Goldschmidt, Florence, Italy, 2013
- [88] Kienzler, B.; González-Robles, E.; Metz, V.; Valls, A.; Duro, L., *FIRST-Nuclides: European Project on Radionuclide Release from Spent Fuel*, 14th Int. High Level Waste Management Conference, Albuquerque, USA 2013

- [89] Kienzler, B.; Loida, A.; González-Robles, E.; Müller, N.; Metz, V., *Fast/Instant Radionuclide Release: Effects inherent to the experiment, Scientific Basis of Nuclear Waste Management XXXVII*, Barcelona, Spain, 2013
- [90] Kienzler, B.; Metz, V.; González-Robles, E.; Duro, L.; Valls, A.; Wegen, D.; Carbol, P.; Serrano-Purroy, D.; Curtius, H.; Günther-Leopold, I.; Zumbiehl, A. F.; Curti, E.; Lemmens, K.; Vandenborre, J.; Pablo, J. d.; Casas, I.; Clarens, F.; Hózer, Z.; Roth, O., *CP FIRST-Nuclides: "Fast / Instant Release of Safety Relevant Radionuclides from Spent Nuclear Fuel"*, EURADWASTE'13 - 8th EC Conference on the Management of Radioactive Waste, Community Policy and Research on Disposal, Vilnius, Lithuania, 2013
- [91] Law, G.; Thorpe, C.; Bots, P.; Shaw, S.; Lloyd, J.; Livens, F.; Denecke, M. A.; Rothe, J.; Dardenne, K.; Brookshaw, D.; Morris, K., *Neptunium Biogeochemistry in Systems Representative of the Nuclear Legacy, 9th International Conference on the Chemistry and Physics of the Actinide Elements - ACTINIDES 2013*, Karlsruhe, Germany, 2013
- [92] Lindqvist-Reis, P.; Klenze, R.; Löble, M.; Finck, N.; Geckeis, H., *Influence of chemical pressure on various luminescence properties of curium(III) and europium(III) ions in rare-earth hydroxides: A time-resolved laser fluorescence spectroscopy (TRLFS) study*, 245th ACS National Meeting & Exposition, New Orleans, USA, 2013
- [93] Lützenkirchen, J., *Some experimental observations at electrolyte/mineral interfaces - more or less controlled laboratory model systems*, Cecam-Workshop, Liquid/Solid interfaces: Structure and dynamics from spectroscopy and simulations, Lausanne, Switzerland, 2013
- [94] Lützenkirchen, J., *The MUSIC Model over the Years from a Personal Point of View*, Goldschmidt Florence, Italy, 2013
- [95] Lützenkirchen, J., *Water on hydroxylated oxides: some counter-intuitive observations and attempts to explain them*, Cecam-Workshop, Approche moléculaire expérimentale et théorique des interfaces oxyde/eau, Paris, France 2013
- [96] Lützenkirchen, J., *Charging of solid water interfaces*, KIT-IMK Karlsruhe, Germany, 2013
- [97] Marquardt, C. M., *Investigations of actinides in the context of final disposal of high-level radioactive waste*, NUCAR-2013, Jabalpur, India, 2013
- [98] Marsac, R.; Schnurr, A.; Kupcik, T.; Rabung, T.; Schäfer, T.; Banik, N. L.; Marquardt, C.; Marques Fernandes, M.; Baeyens, B.; Bradbury, M. H.; Geckeis, H., *Eu(III) and Np(V) sorption to illite*, Royal Institute of Technology, department of applied physico-chemistry Stockholm, Schweden, 2013
- [99] Marsac, R.; Schnurr, A.; Kupcik, T.; Rabung, T.; Schäfer, T.; Banik, N. L.; Marquardt, C.; Marques Fernandes, M.; Baeyens, B.; Bradbury, M. H.; Geckeis, H., *Competitive effect of Al(III) on Eu(III) sorption to illite*, Institut Polytechnique, LaSalle Beauvais, France, 2013
- [100] Panak, P. J., *Spectroscopic characterization of actinides*, Summer School on Actinide Science & Applications, Karlsruhe, Germany 2013
- [101] Panak, P. J., *Time-resolved Laser Fluorescence Spectroscopy – A Valuable Tool for Actinide Speciation*, Seminarvortrag Tschechische Technische Universität, Prag, Czech Republic, 2013
- [102] Rabung, T., *CROCK: Investigations of uncertainties in radionuclide transport processes in the far-field of a repository in crystalline rock*, EURADWASTE'13 - 8th EC Conference on the Management of Radioactive Waste, Community Policy and Research on Disposal, Vilnius, Lithuania, 2013
- [103] Schäfer, T., *Sorption processes on clays*, 5th DTTG Workshop, Karlsruhe, Germany, 2013
- [104] Schäfer, T., *Mineral stability affecting contaminant transport in argillaceous and fractured media*, Berufungskommission "Joint Professor of Mineralogy" at the University of Bern and Laboratory Head at the Paul Scherrer Institute, Bern, Switzerland, 2013
- [105] Schäfer, T., *The role of colloids/nanoparticles on radionuclide migration in the geosphere*, Korean Advanced Institute of Science and Technology (KAIST), Department of Nuclear & Quantum Engineering, Daejeon, South Korea, 2013
- [106] Schäfer, T., *Radionuclide Migration and Retention Processes in Deep Geological Formations*, Lawrence Livermore National Laboratory (LLNL), Glenn T. Seaborg Institute, Livermore, USA, 2013
- [107] Schill, E., *Enhancement of the Soutz EGS site by Hydraulic and Chemical Stimulation*, ICEGS, Potsdam, Germany, 2013

- [108] Schill, E.; Genter, A.; Jung, R., *Stimulation and Fluid Circulation in the EGS Project Soultz-sous-Forêt (F): Results of > 20 Years Research*, ZLG Geothermie, ETH, Zürich, Switzerland, 2013
- [109] Vallet, V.; Réal, F.; Trumm, M.; Schimmelpfennig, B.; Masella, M., *How to build accurate macroscopic models of actinide ions in aqueous solvents?*, 9th International Conference on the Chemistry and Physics of the Actinide Elements - ACTINIDES 2013, Karlsruhe, Germany, 2013
- [110] Vitova, T., *Structural investigations of actinides with advanced X-ray spectroscopy techniques*, 9th International Conference on the Chemistry and Physics of the Actinide Elements - ACTINIDES 2013, Karlsruhe, Germany, 2013
- [111] Yokosawa, T., *In-situ TEM on (de)hydrogenation of Palladium*, School of Materials, Manchester University, Manchester, U.K., 2013

### Oral presentations

- [112] Abdelfettah, Y.; Schill, E.; Kuhn, P., *Delimitation and characterization of geothermally relevant Permo-Carboniferous graben in the Swiss Crystalline basement*, Swiss Geoscience Meeting 2013, Lausanne, Switzerland, 2013
- [113] Adam, C.; Kaden, P.; Beele, B.; Geist, A.; Denecke, M. A.; Panak, P. J., *Probing Bonding Modes in Actinide and Lanthanide Complexes by NMR Spectroscopy*, Euract-NMR Workshop, Karlsruhe, Germany, 2013
- [114] Adam, C.; Kaden, P.; Beele, B.; Müllich, U.; Geist, A.; Denecke, M. A.; Panak, P. J., *NMR Reveals Unexpected Paramagnetism in Am(III) Complexes*, EUFEN2 Conference, Dublin, Ireland, 2013
- [115] Adam, C.; Kaden, P.; Beele, B.; Müllich, U.; Trumm, S.; Geist, A.; Panak, P. J.; Denecke, M. A., *NMR Investigations at KIT-INE, ThUL Spring School 2013*, Karlsruhe, Germany, 2013
- [116] Adam, C.; Kaden, P.; Beele, B. B.; Geist, A.; Denecke, M. A.; Panak, P. J., *Implications of Metal-Ligand Bonding from Unexpected Paramagnetism in NMR Spectra of Am(n-Pr-BTP)<sub>3</sub>(NO<sub>3</sub>)<sub>3</sub>*, GDCh Wissenschaftsforum, Darmstadt, Germany, 2013
- [117] Altmaier, M., *Aquatic chemistry and thermodynamics of actinides and fission products*, CEA-INE Exchange Meeting, Saclay, France, 2013
- [118] Altmaier, M., *Radionuclide Retention and Redox Conditions*, IGD-TP 4th Exchange Forum, Prague, Czech Republic, 2013
- [119] Altmaier, M.; Bourg, S.; Bryan, N.; Collings, P.; Dacheaux, N.; Duplantier, B.; Ekberg, C.; Grolimund, D.; Natranjan, L.; Poinssot, C.; Raison, P.; Schäfer, T.; Scheinost, A. C.; Schimmelpfennig, B., *TALISMAN - Transnational Access to Large Infrastructures for a Safe Management of Actinides, Actinides 2013*, Karlsruhe, Germany, 2013
- [120] Altmaier, M.; Gaona, X.; Fellhauer, D.; Buckau, G., *RECOSY Intercomparison Exercise on Redox Determination Methods*, EURADWASTE - 8th EC Conference on the Management of Radioactive Waste Community Policy and Research on Disposal, Vilnius, Lithuania, 2013
- [121] Altmaier, M.; Geckeis, H., *The Institute for Nuclear Waste Disposal (INE) at KIT*, Technical meeting at Nuclear Waste Management Organisation, Canada, Toronto, 2013
- [122] Altmaier, M.; Geckeis, H., *Actinide chemistry and thermodynamics – a key contribution to nuclear waste disposal safety*, 44th IUPAC World Chemistry Congress, Istanbul, Turkey, 2013
- [123] Altmaier, M.; Kienzler, B.; Bube, C.; Metz, V.; Geckeis, H., *Radionuclide source term estimations for the Preliminary Safety Assessment Gorleben (VSG)*, 14th International Conference on the Chemistry and Migration Behaviour of Actinides and Fission Products in the Geosphere, Brighton, U.K., 2013
- [124] Altmaier, M.; Kienzler, B.; Metz, V.; Bube, C.; Geckeis, H., *Vorläufige Sicherheitsanalyse Gorleben – Quellterm für wärmeproduzierende radioaktive Abfälle*, GDCh-Wissenschaftsforum Chemie 2013, Darmstadt, Germany, 2013
- [125] Altmaier, M.; Reed, D., *State-of-Art-Report on Pitzer modeling in nuclear waste disposal*, 4th US/German Workshop on Salt Repository Research, Design and Operation, Berlin, Germany, 2013
- [126] Altmaier, M.; Reed, D., *ABC-SALT Workshop Series*, OECD-NEA Salt Club Annual Meeting, Berlin, Germany, 2013

- [127] Autillo, M.; Kaden, P.; Geist, A.; Berthon, C.; Guerin, L.; Moisy, P., *Americium (III) paramagnetism in solution: Radicals effects on magnetic susceptibility measurements*, Euract-NMR Workshop, Karlsruhe, Germany, 2013
- [128] Bauer, N.; Fröhlich, D. R.; Panak, P. J., *Interaction of Human Serum Transferrin with Cm(III) using Time-Resolved Laser Fluorescence Spectroscopy*, GDCh Wissenschaftsforum, Darmstadt, Germany, 2013
- [129] Bauer, N.; Fröhlich, D. R.; Panak, P. J., *Interaction of Human Serum Transferrin with Cm(III) using Time-Resolved Laser Fluorescence Spectroscopy*, Actinides 2013, Karlsruhe, Germany 2013
- [130] Becker, F., *CT-Fluoroscopy staff dosimetry*, EURADOS Annual Meeting AM2012, Barcelona, Spain, 2013
- [131] Becker, F., *Vorstellung des INE-Arbeitspakets 3.4.5: Individuelle Dosimetrie für Beschäftigte in Entsorgungsanlagen*, ENTRIA Kick-Off-Meeting, Goslar, Germany, 2013
- [132] Becker, F.; Pang, B., *ENTRIA und Individuelle Dosimetrie für Beschäftigte in Entsorgungsanlagen*, 79. Sitzung des Arbeitskreises Dosimetrie (AKD) Kernkraftwerk Isar, Germany, 2013
- [133] Beele, B. B., *Complexation and Separation Performance of N- and O-donor ligands used in Actinide Separation*, Seminarvortrag Tschechische Technische Universität, Prag, Czech Republic, 2013
- [134] Bouby, M., *Colloid(al size) characterization methods available at KIT-INE*, Ondraf-Niras/SCK-CEN/KIT-INE Kick-Off Meeting, Common project: „Characterization of Natural Organic Matter derived from Boom Clay“, Brussels, Belgium, 2013
- [135] Bouby, M.; Heck, S.; Huber, F.; Schäfer, T., *Erosion /destabilisation of compacted FEBEX bentonite with glacial melt type water under quasi-stagnant flow conditions*, First CP-BelBar Workshop, Helsinki, Finland, 2013
- [136] Bourg, S.; Geist, A., *SACSESS — a new FP7 EURATOM collaborative project on the safety of actinide separation processes*, GLOBAL 2013 (Nuclear Energy at a Crossroads), Salt Lake City, USA, 2013
- [137] Bremer, A.; Whittaker, D. M.; Geist, A.; Panak, P. J., *Complexation of Cm(III) and Eu(III) with CyMe<sub>4</sub>-BTBP and CyMe<sub>4</sub>-BTPPhen studied by time resolved laser fluorescence spectroscopy*, EUFEN 2 (European F-Element Network), Dublin, Ireland, 2013
- [138] Brendler, V.; Bok, F.; Marquardt, C.; Altmaier, M., *THEREDA revisited – what happened so far*, 14th International Conference on the Chemistry and Migration Behaviour of Actinides and Fission Products in the Geosphere, Brighton, U.K., 2013
- [139] Breustedt, B.; Mohr, U.; Marzocchi, O.; Biegard, N.; Cordes, G.; Frank, G., *Messungen im KIT in-vivo Messlabor im Zusammenhang mit der Reaktorkatastrophe in Fukushima* Global Conference on Radiation Topics, Preparedness, Response, Protection, Research, Munich, Germany, 2013
- [140] Dumas, T.; Fellhauer, D.; Gaona, X.; Altmaier, M.; Scheinost, A. C., *Is plutonium being incorporated by magnetite under anoxic conditions?*, Goldschmidt 2013, Florence, Italy, 2013
- [141] Duro, L.; Bruno, J.; Grive, M.; Montoya, V.; Kienzler, B.; Altmaier, M.; Buckau, G., *Redox processes in the safety case of deep geological repositories of radioactive wastes: contribution of the European RECOSY Collaborative Project*, EURADWASTE - 8th EC Conference on the Management of Radioactive Waste Community Policy and Research on Disposal, Vilnius, Lithuania, 2013
- [142] Duro, L.; García, D.; Colàs, E.; Montoya, V., *Geochemical modeling in highly saline conditions*, ABC Salt (III) Workshop, Santa Fe, USA, 2013
- [143] Fellhauer, D.; Altmaier, M.; Neck, V.; Gaona, X.; Wiss, T.; Lagos, M.; Runke, J.; Fanghänel, T., *Thermodynamic evaluation of Np redox processes in dilute aqueous solutions at pH 4 – 10 under reducing conditions*, ACTINIDES 2013, Karlsruhe, Germany, 2013
- [144] Finck, N.; Bouby, M.; Dardenne, K.; Geckeis, H., *Tetravalent cation coprecipitation with clay minerals*, Migration 2013 Brighton, UK, 2013
- [145] Fröhlich, D. R.; Skerencak-Frech, A.; Panak, P. J., *A combined EXAFS and TRFLS spectroscopic study to determine the thermodynamic and structural properties of trivalent actinide complexes with organic and inorganic ligands at elevated temperatures*, Migration 2013, Brighton, UK, 2013

- [146] Froideval Zumbiehl, A.; Bullemer, A.; Curti, E.; Günther-Leopold, I.; Martin, M.; Borca, C. N.; Grolimund, D.; Dardenne, K.; Rothe, J., *Selenium speciation in a spent UO<sub>2</sub> fuel and in non-irradiated UO<sub>2</sub> reference samples: a synchrotron-based (micro-)XRF/XAS feasibility study*, E-MRS 2013 Spring Meeting, Strasbourg, France, 2013
- [147] Gamaletsos, P.; Godelitsas, A.; Kuzmin, A.; Lagos, M.; Xanthos, S.; Mertzimekis, T. J.; Goettlicher, J.; Steininger, R.; Zarkadas, C.; Komelkov, A.; Pontikes, Y.; Angelopoulos, G. N., *New insights into environmental characterization of bauxite residues (red mud) from Greece*, Goldschmidt 2013, Florence, Italy, 2013
- [148] Gaona, X., *Aquatic chemistry and thermodynamics of actinides and fission products*, Technical meeting at Nuclear Waste Management Organisation Canada, Toronto, Canada, 2013
- [149] Gaona, X.; Adam, C.; Rojo, H.; Böttle, M.; Kaden, P.; Altmaier, M., *Complexation of Np(IV) with gluconate in dilute to concentrated CaCl<sub>2</sub> solutions: solubility and NMR studies*, ABC-Salt Workshop '13, Santa Fe, USA, 2013
- [150] Gaona, X.; Adam, C.; Rojo, H.; Böttle, M.; Kaden, P.; Altmaier, M., *Solubility and NMR Studies of Ca-gluconate and Na-Np(IV)-gluconate Systems in Dilute to Concentrated Alkaline CaCl<sub>2</sub> Solutions*, Migration 2013 Conference, Brighton, UK, 2013
- [151] Gaona, X.; Fellhauer, D.; Altmaier, M., *Solubility, hydrolysis and redox behaviour of Np(VI) under alkaline NaCl solutions*, 3rd International Workshop Mechanisms and Modelling of Waste/Cement Interactions, Ghent, Belgium, 2013
- [152] Gaona, X.; Marques Fernandes, M.; Baeyens, B.; Altmaier, M., *Solubility and hydrolysis of U(VI) at 80°C under acidic to hyperalkaline conditions*, Migration 2013, Brighton, UK, 2013
- [153] Gaona, X.; Roja, H.; Adam, C.; Böttle, M.; Garcia, M.; Missana, T.; Kaden, P.; Altmaier, M., *Effect of Ca in the Np(IV)-gluconate system under hyperalkaline conditions*, 3rd International Workshop Mechanisms and Modelling of Waste/Cement Interactions, Ghent, Belgium, 2013
- [154] Gaona, X.; Skerencak-Frech, A.; Marques, M.; Fröhlich, D. R.; Rothe, J.; Dardenne, K.; Panak, P. J.; Altmaier, M., *Aquatic chemistry of actinides at elevated temperatures: solubility and spectroscopic studies at KIT-INE, Actinide and Brine Chemistry in a Salt Repository (ABC Salt III) Workshop*, Santa Fe, USA, 2013
- [155] García, D.; Duro, L.; Colàs, E.; Montoya, V., *Radionuclide solubility calculations in crystalline and sedimentary groundwaters from the Canadian Shield*, Migration 2013, Brighton, UK, 2013
- [156] Geist, A.; Modolo, G.; Wilden, A.; Kaufholz, P., *Minor actinide separation: simplification of the DIAMEX-SANEX strategy by means of novel SANEX processes*, GLOBAL 2013 (Nuclear Energy at a Crossroads), Salt Lake City, USA, 2013
- [157] González-Robles, E.; Bohnert, E.; Müller, N.; Herm, M.; Metz, V.; Kienzler, B., *Determination of the fission gas release in the segment N0204 and gas phase results of anoxic leaching experiment*, 2nd Annual Workshop of the FIRST-Nuclide Project Antwerpen, Belgium, 2013
- [158] González-Robles, E.; Wegen, D. H.; Bohnert, E.; Papaioannou, D.; Müller, N.; Nasyrow, R.; Kienzler, B.; Metz, V., *Physico-chemical characterization of a spent UO<sub>2</sub> fuel with respect to its stability under final disposal conditions.*, Proceedings of MRS 2013 - 37th Int'l Symposium on the Scientific Basis for Nuclear Waste Management, Barcelona, Spain, 2013
- [159] González-Robles, E.; Wegen, D. H.; Papaioannou, D.; Kienzler, B.; Nasyrow, R.; Metz, V., *Physical characterisation of spent nuclear fuel: First steps to further Instant Release Fractions investigations*, EURADWASTE '13, Vilnius, Lithuania, 2013
- [160] Graser, C.-H.; Banik, N. L.; Lagos, M.; Marquardt, C. M.; Geckeis, H., *Speciation of elements relevant to nuclear waste disposal by capillary electrophoresis hyphenated to inductively coupled plasma sector field mass spectrometer (CE-ICP-SFMS)*, GDCh-Wissenschaftsforum CHEMIE 2013, Darmstadt, Germany, 2013
- [161] Griffiths, T. L.; Tucker, K. L.; Sharrad, C. A.; Livens, F.; Martin, L. R.; Sarsfield, M. R.; Kaden, P., *Spectroscopic investigations of Lanthanide and Actinide complexes relevant to the nuclear fuel cycle*, Euract-NMR Workshop, Karlsruhe, Germany, 2013
- [162] Griffiths, T. L.; Tucker, K. L.; Sharrad, C. A.; Martin, L. R.; Kaden, P., *Understanding molecular speciation of actinides in solvent extraction processes*, Global 2013 Conference, Salt Lake City, USA, 2013

- [163] Hampel, A.; Argüello, L.; Hansen, F.; Günther, R.-M.; Salzer, K.; Herchen, K.; Wolters, R.; Düsterloh, U.; Pudewills, A.; Yildirim, S.; Rokahr, R.; Gährken, A.; Missal, C.; Stahlmann, J., *Benchmark Calculations of the Thermo-Mechanical Behavior of Rock Salt – Results from a US-German Joint Project, Proceedings of the 47th US Rock Mechanics / Geomechanics Symposium* San Francisco, USA, 2013
- [164] Heberling, F.; Vinograd, V. L.; Polly, R., *A Thermodynamic Entrapment Model for the Quantitative Description of Selenite Coprecipitation with Calcite, Goldschmidt Conference 2013*, Florence, Italy, 2013
- [165] Herm, M.; Bohnert, E.; Böttle, M.; González-Robles, E.; Lagos, M.; Müller, N.; Altmaier, M.; Kienzler, B.; Metz, V.; Geckeis, H., *Experimental approach to quantify and specify 14C mobilized from HLW materials, VESPA project meeting*, Jülich, Germany, 2013
- [166] Herm, M.; Gaona, X.; Rabung, T.; Crepin, C.; Metz, V.; Altmaier, M.; Geckeis, H., *The effect of nitrate on trivalent actinide and lanthanide solubility in dilute to concentrated brine solutions, ABC-Salt Workshop '13*, Santa Fe, Germany, 2013
- [167] Herm, M.; Gaona, X.; Rabung, T.; Crepin, C.; Metz, V.; Altmaier, M.; Geckeis, H., *Löslichkeit und Speziation von trivalenten Actiniden in NaCl–NaNO<sub>3</sub> und MgCl<sub>2</sub>–Mg(NO<sub>3</sub>)<sub>2</sub> Lösungen unter endlagerrelevanten Bedingungen, GDCh Wissenschaftsforum Chemie 2013*, Darmstadt, Germany, 2013
- [168] Herm, M.; Gaona, X.; Rabung, T.; Crepin, C.; Metz, V.; Altmaier, M.; Geckeis, H., *Solubility and TRLFS study of Nd(III) and Cm(III) in dilute to concentrated alkaline NaCl–NaNO<sub>3</sub> and MgCl<sub>2</sub>–Mg(NO<sub>3</sub>)<sub>2</sub> solutions, 14th International Conference on the Chemistry and Migration Behaviour of Actinides and Fission Products in the Geosphere (MIGRATION)*, Brighton, UK, 2013
- [169] Hinz, K.; Altmaier, M.; Gaona, X.; Rabung, T.; Schild, D.; Adam, C.; Geckeis, H., *Complexation of Nd(III)/Cm(III) with borate in dilute to concentrated alkaline NaCl, MgCl<sub>2</sub> and CaCl<sub>2</sub> solutions: solubility and TRLFS studies, 14th International Conference on the Chemistry and Migration Behaviour of Actinides and Fission Products in the Geosphere (MIGRATION)*, Brighton, UK, 2013
- [170] Hinz, K.; Altmaier, M.; Rabung, T.; Geckeis, H., *Complexation of An(III/IV) with borate in dilute to concentrated alkaline NaCl, CaCl<sub>2</sub> and MgCl<sub>2</sub> solutions, ABC-Salt Workshop '13*, Santa Fe, USA, 2013
- [171] Hinz, K.; Altmaier, M.; Rabung, T.; Geckeis, H., *Boratkomplexierung drei- und vierwertiger Actiniden in alkalischen NaCl, CaCl<sub>2</sub> und MgCl<sub>2</sub> Lösungen, GDCh Wissenschaftsforum Chemie 2013*, Darmstadt, Germany, 2013
- [172] Ho Mer Lin, D.; Varga, Z.; Manara, D.; Lindqvist-Reis, P.; Schild, D.; Fanghänel, T.; Mayer, K., *Characterization of Uranium Ore Concentrates by Raman Spectroscopy for Nuclear Forensic Purposes, GDCh-Wissenschaftsforum Chemie 2013*, Darmstadt, Germany, 2013
- [173] Jahn, M.; Schill, E.; Breunig, M., *Towards a 4D database management system for geothermal projects: an example of the hydraulic data of Soultz, Second European Geothermal Workshop*, Strasbourg, France, 2013
- [174] Kaden, P.; Adam, C.; Beele, B.; Müllich, U.; Trumm, S.; Geist, A.; Panak, P. J.; Denecke, M. A., *Evidence for covalence in a N-donor complex of americium(III), Euract-NMR Workshop*, Karlsruhe, Germany, 2013
- [175] Kienzler, B.; Finck, N.; Hilpp, S.; Metz, V.; Plaschke, M.; Cron, T.; Miassoedov, A., *Radionuclide retention onto heat treated concrete under sea water conditions, 3rd International Workshop on Mechanisms and Modelling of Waste/Cement Interactions*, Ghent, Belgium, 2013
- [176] Kienzler, B.; González-Robles, E., *State-of-the-art on instant release of fission products from spent nuclear fuel, 15th International Conference on Environmental Remediation and Radioactive Waste Management (ICEM2013). ASME*, Brussels, Belgium, 2013
- [177] Kuhn, P.; Abdelfettah, Y.; Schill, E., *3D geological modelling of the Northern Swiss Permo-Carboniferous basin using gravity forward modelling, Second European Geothermal Workshop*, Strasbourg, France, 2013
- [178] Lebreton, F.; Martin, P. M.; Belin, R. C.; Horlait, D.; Dardenne, K.; Rothe, J.; Rossberg, A.; Scheinost, A. C.; Delahaye, T.; Blanchart, P., *U<sub>1-x</sub>Am<sub>x</sub>O<sub>2±δ</sub> Solid Solution Study, E-MRS Spring Meeting*, Strasbourg, France, 2013

- [179] Loeble, M. W.; Keith, J.; Tobash, P. H.; Scott, B. L.; Olson, A. C.; Minasian, S. G.; Daly, S. R.; Boland, K. S.; Bauer, E.; Dardenne, K.; Rothe, J.; Vitova, T.; Weng, T.-C.; Sokaras, D.; Freibert, F. J.; Martin, R. L.; Batista, E. R.; Clark, D. L.; Kozimor, S. A., *Probing and Quantifying Orbital Mixing in f-Element Molecular Bonding, ACTINIDES 2013*, Karlsruhe, Germany, 2013
- [180] Marsac, R.; Banik, N. L.; Marquardt, C. M.; Schild, D.; Rothe, J.; Schäfer, T.; Geckeis, H., *Neptunium and plutonium sorption to illite-batch and spectroscopy study, HATT-workshop*, Potsdam, Germany, 2013
- [181] Marsac, R.; Schnurr, A.; Kupcik, T.; Rabung, T.; Schäfer, T.; Banik, N. L.; Marquardt, C. M.; Marques-Fernandez, M.; Baeyens, B.; Bradbury, M. H.; Geckeis, H., *Aluminium competitive effect on Eu(III) sorption to illite, Goldschmidt 2013*, Florence, Italy, 2013
- [182] Marsac, R.; Schnurr, A.; Kupcik, T.; Rabung, T.; Schäfer, T.; Banik, N. L.; Marquardt, C. M.; Marques-Fernandez, M.; Baeyens, B.; Bradbury, M. H.; Geckeis, H., *Eu(III) and Np(V) sorption to illite, Royal Institute of Technology, department of applied physico-chemistry (Sweden)*, 2013
- [183] Marsac, R.; Schnurr, A.; Kupcik, T.; Rabung, T.; Schäfer, T.; Banik, N. L.; Marquardt, C. M.; Marques-Fernandez, M.; Baeyens, B.; Bradbury, M. H.; Geckeis, H., *Competitive effect of Al(III) on Eu(III) sorption to illite, Institut Polytechnique, LaSalle Beauvais (France)*, 2013
- [184] Meixner, J.; Gaucher, E.; Kohl, T.; Grimmer, J.; Schill, E., *Slip-and dilation tendency analysis: Implications for geothermal exploration in the Upper Rhine Graben, Second European Geothermal Workshop*, Strasbourg, France, 2013
- [185] Metz, V., *Overview of Activities within WPI "Samples and Tools", FIRST-Nuclides 2nd Annual Workshop*, Antwerpen, Belgium, 2013
- [186] Metz, V., *WP5 – training activities summary, FIRST-Nuclides 2nd Annual Workshop*, Antwerpen, Belgium, 2013
- [187] Metz, V., *Radiolysis Enhanced Corrosion of Spent Nuclear Fuel, FIRST-Nuclides Training Course*, Karlsruhe, Germany (INE), 2013
- [188] Metz, V., *Interactions of americium with cement alteration products in brines, 3rd International Workshop Mechanisms and Modelling of Waste/Cement Interactions*, Gent, Belgium, 2013
- [189] Metz, V., *Combining thermodynamic simulations, element and surface analytics to study U(VI) retention in a corroded cement monolith upon >20 years of leaching, 3rd International Workshop Mechanisms and Modelling of Waste/Cement Interactions*, Gent, Belgium, 2013
- [190] Metz, V., *Radionuklidquellterme für verschiedene Entsorgungsoptionen, Auftakttreffen Projekt ENTRIA „Entsorgungsoptionen für radioaktive Reststoffe – interdisziplinäre Analysen und Entwicklung von Bewertungsgrundlagen*, Goslar, Germany, 2013
- [191] Metz, V., *Beiträge des KIT-INE in der ENTRIA Forschungsplattform -Radionuklidquellterme für verschieden Entsorgungsoptionen, ITAS – INE Fachgespräch*, Karlsruhe, Germany (ITAS), 2013
- [192] Natrajan, L. S.; Woodall, S. D.; Swinburne, A. N.; McDouall, J. J.; Kaden, P.; Adam, C.; Geist, A.; Banik, N. L.; Ruff, C.; Beele, B. B.; Denecke, M. A.; Panak, P. J., *Elucidating Structure and Speciation of Paramagnetic Actinide Complexes, Euract-NMR Workshop*, Karlsruhe, Germany, 2013
- [193] Norrfors, K.; Bouby, M.; Heck, S.; Finck, N.; Marsac, R.; Schäfer, T.; Wold, S., *Montmorillonite colloid size heterogeneity - Impact on stability in suspension and radionuclide sorption capacities First CP-BelBar Workshop*, Helsinki, Finland, 2013
- [194] Norrfors, K.; Bouby, M.; Heck, S.; Finck, N.; Marsac, R.; Schäfer, T.; Wold, S., *Montmorillonite colloid size heterogeneity – Summary of the radionuclide sorption studies, First CP-BelBar Workpackage 3 Workshop*, Brighton, UK, 2013
- [195] Petrov, V.; Gaona, X.; Fellhauer, D.; Rothe, J.; Dardenne, K.; Kalmykov, S.; Altmaier, M., *Np(V) solubility in dilute to concentrated MgCl<sub>2</sub> solutions, Migration 2013*, Brighton, UK, 2013
- [196] Plaschke, M.; Stollenwerk, A.; Lemmer, D.; Schild, D., *Versuch zur Dekontamination von Metalloberflächen durch Laserablation (Clean-Laser-Versuch), 7. Workshop RCA (VKTA)*, Dresden, Germany, 2013
- [197] Pözl, S.; Breustedt, B., *Calibration of partial body counters using Voxel2MCNP and the XCAT phantom series, 4th International Workshop on Computational Phantoms for Radiation Protection, Imaging and Radiotherapy*, Zurich, Switzerland, 2013

- [198] Pudewills, A., *Simulation of thermo-mechanical behavior of rock salt in the vicinity of a disposal drift and the interaction with technical barriers, Proceedings of the ARMA's 47th US Rock Mechanics / Geomechanics Symposium*, San Francisco, USA, 2013
- [199] Quinto, F.; Hrneck, E.; Krachler, M.; Shotyk, W.; Steier, P.; Winkler, S. R., *Investigating the migration of trace levels of fallout plutonium and uranium in an ombrotrophic peat bog profile, ACTINIDES 2013*, Karlsruhe, Germany, 2013
- [200] Rojo, H.; Gaona, X.; Rabung, T.; Garcia, M.; Missana, T.; Altmaier, M., *Complexation of Nd(III)/Cm(III) with gluconate in dilute NaCl and CaCl<sub>2</sub> alkaline solutions: solubility and TRLFS studies, 3rd International Workshop Mechanisms and Modelling of Waste/Cement Interactions*, Ghent, Belgium, 2013
- [201] Rojo, H.; Gaona, X.; Rabung, T.; Garcia, M.; Missana, T.; Altmaier, M., *Solubility and TRLFS studies on Nd(III)/Cm(III) complexation with gluconate in NaCl and CaCl<sub>2</sub> media, Goldschmidt 2013*, Florence, Italy, 2013
- [202] Rojo, H.; Gaona, X.; Rabung, T.; Garcia, M.; Missana, T.; Altmaier, M., *Complexation of Nd(III)/Cm(III) with gluconate in alkaline NaCl and CaCl<sub>2</sub> solutions: solubility and TRLFS studies, Migration 2013*, Brighton, UK, 2013
- [203] Rolker, J.; Schill, E.; Neumann, T.; Kohl, T., *Geochemical analysis and thermo-hydraulic modeling of a thermal spring system in the southern Black Forest, Second European Geothermal Workshop*, Strasbourg, France, 2013
- [204] Sailhac, P.; Larnier, H.; Matthey, P. D.; Schill, E.; Chambodut, A., *Testing geothermal monitoring using MT and SP at Rittershoffen, Second European Geothermal Workshop*, Strasbourg, France, 2013
- [205] Schäfer, T.; Huber, F.; Blechschmidt, I.; Bouby, M.; Büchner, S.; Brendlé, J.; Darbha, G.; Geckeis, H.; Kupcik, T.; Götz, R.; Hauser, W.; Heck, S.; Lagos, M.; Martin, A., *The latest results on colloid associated radionuclide mobility from the CFM project, Grimsel (Switzerland), Migration 2013*, Brighton, UK, 2013
- [206] Schill, E., *EGS geothermal challenges within the Upper Rhine Valley based on the Soultz experience, Third Geothermal Review*, Mainz, Germany, 2013
- [207] Schnurr, A.; Marsac, R.; Rabung, T.; Lützenkirchen, J.; Geckeis, H., *Sorption investigations of actinides and lanthanides onto clay minerals at highly saline conditions, BMWi-Workshop „Radionuklid-Rückhaltung in Ton und salinaren Systemen“*, Karlsruhe, Germany, 2013
- [208] Schnurr, A.; Marsac, R.; Rabung, T.; Lützenkirchen, J.; Geckeis, H., *Investigations of actinide and lanthanide sorption on clay minerals under saline conditions, ABC-Salt Workshop III Santa Fe*, USA, 2013
- [209] Schoepff, V.; Alamsi, I.; Amgarou, K.; Becker, F.; Carrel, F.; Carvajal, F.; Gaboriau, D. C.; Gmar, M.; Kovacs, A.; Lemaire, H.; Mena, N.; Morat, L.; Morrison, C. G.; Perez-Ilopis, I.; Raskob, W.; Szabo, S.; Szeles, E.; Testard, I.; Trybushnyi, D.; Ugolin, N.; Viau, M.; Vincze, A., *BOOSTER: Development of a Toolbox for Triage of a Large Group of Individuals Exposed to Radioactive Material, ANNIMA 2013 Conference* Marseille, France, 2013
- [210] Shinonaga, T.; Steier, P.; Lagos, M.; Ohkura, T., *Isotopic Composition of Uranium and Activity Concentration of <sup>134,137</sup>Cs in Aerosol Samples Collected at 120 km from Fukushima before and after the Reactor Accidents, ACTINIDES 2013*, Karlsruhe, Germany, 2013
- [211] Tucker, K. L.; Griffiths, T. L.; Sharrad, C. A.; Heath, S. L.; Kaden, P.; Taylor, R., *Heavy Metal extraction using advanced PUREX style partitioning systems, Euract-NMR Workshop*, Karlsruhe, Germany, 2013
- [212] Wilden, A.; Modolo, G.; Lange, S.; Sadowski, F.; Beele, B. B.; Skerencak-Frech, A.; Panak, P. J.; Geist, A.; Iqbal, M.; Verboom, W., *Modifizierte Diglycolamide für die Actinidenabtrennung: Untersuchungen zur Komplexierung durch Flüssig-Flüssig-Extraktion und zeitaufgelöste Laserfluoreszenzspektroskopie, GDCh Wissenschaftsforum*, Darmstadt, Germany, 2013
- [213] Woodall, S. D.; Kaden, P.; Adam, C.; Geist, A.; Banik, N. L.; Ruff, C.; Beele, B. B.; Denecke, M. A.; Panak, P. J.; Natrajan, L. S., *Complexing Imidophosphinates and Bulky Pyridines on Transuranics, Euract-NMR Workshop*, Karlsruhe, Germany, 2013

### **Proceedings:**

- [214] Abdelfettah, Y.; Schill, E., *Exploration of geothermally relevant structures in the crystalline basement of Switzerland using gravity constrained by seismic data, Proceedings European Geothermal Congress (EGC), Pisa, Italy, 2013*
- [215] Altmaier, M.; Bourg, S.; Bryan, N.; Collings, P.; Dacheaux, N.; Duplantier, B.; Ekberg, C.; Grolimund, D.; Natranjan, L.; Poinssot, C.; Raison, P.; Schäfer, T.; Scheinost, A. C.; Schimmelpfennig, B., *TALISMAN - Transnational Access to Large Infrastructures for a Safe Management of Actinides, Actinides 2013, Karlsruhe, Germany, 2013*
- [216] Altmaier, M.; Gaona, X.; Fellhauer, D.; Buckau, G., *RECOSY Intercomparison Exercise on Redox Determination Methods, EURADWASTE, 8th EC Conference on the Management of Radioactive Waste Community Policy and Research on Disposal, Vilnius, Lithuania, 2013*
- [217] Bahl, S.; Vitova, T.; Kutzer, A.; Prüßmann, T.; Pidchenko, I.; Soballa, E.; Roth, G.; Geckeis, H., *Impact of increasing Cs<sub>3</sub>PMo<sub>12</sub>O<sub>40</sub> loading on vitrification properties of multicomponent borosilicate glass, 22nd International Congress on X-ray Optics and Microanalysis (ICXOM22), Hamburg, Germany, 2013*
- [218] Banik, N. L.; Marquardt, C. M.; Altmaier, M.; Walther, C.; Rothe, J.; Denecke, M. A.; Schimmelpfennig, B.; Real, F.; Vallet, V., *Preparation, stabilization, spectroscopic, computational studies of tetravalent protactinium in aqueous solution, Abstracts of the 9th International Conference on the Chemistry and Physics of the Actinide Elements - ACTINIDES 2013, Karlsruhe, Germany, 2013*
- [219] Bouby, M.; Finck, N.; Truche, L.; Brendlé, J.; Schäfer, T.; Geckeis, H., *Characterization of Colloids Extracted from Two Synthetic Clay Materials by Flow Field Flow Fractionation (FFFF) Coupled to ICP-MS Detector, NEA CLAY CLUB, Workshop Proceedings, Karlsruhe, Germany, 2013*
- [220] Bube, C.; Dardenne, K.; Denecke, M. A.; Metz, V.; Rothe, J.; Schild, D.; Soballa, E.; Vitova, T.; Kienzler, B., *Combining thermodynamic simulations, element and surface analytics to study U(VI) retention in a corroded cement monolith upon >20 years of leaching, 3rd Internat. Workshop Mechanisms and Modelling of Waste/Cement Interactions, Ghent, Belgium, 2013*
- [221] Chagneau, A.; Claret, F.; Madé, B.; Wolf, M.; Enzmann, F.; Schäfer, T., *Applicability of a geometrical model coupled to computed tomography to characterize the transport properties of porous materials: comparison with through diffusion experiments, Book of Abstracts, 5th International Conference on Porous Media & Annual Meeting (InterPore), Prag, Czech Republic 2013*
- [222] Chagneau, A.; Claret, F.; Madé, B.; Wolf, M.; Enzmann, F.; Schäfer, T., *Coupling HTO tracer experiments and tomography imaging to monitor the effects of celestite porosity clogging on diffusion properties in porous media, Book of Abstracts, Goldschmidt, Florence, Italy, 2013*
- [223] Claret, F.; Lerouge, C.; Grangeon, S.; Sato, T.; Schäfer, T.; Giffaut, E.; Tournassat, C., *Chemical homologue speciation in natural systems: A key to understand the anthropogenic RN fate, Book of Abstracts, Goldschmidt, Florence, Italy, 2013*
- [224] Dardenne, K.; Rothe, J.; Fernandez, T.; Schild, D.; Soballa, E.; Metz, V.; Bube, C.; Kienzler, B.; Denecke, M. A.; Geckeis, H., *μ-focus capabilities at the INE-Beamline for actinide science at ANKA, Abstracts of the 9th International Conference on the Chemistry and Physics of the Actinide Elements - ACTINIDES 2013, Karlsruhe, Germany, 2013*
- [225] Delavernhe, L.; Steudel, A.; Schäfer, T.; Darbha, G. K.; Schuhmann, R.; Wöll, C.; Geckeis, H.; Emmerich, K., *Surface properties of montmorillonite and influences on bentonite properties. Part I: Baseline study of seven particle size fractions, 50th Anniversary Annual Meeting of The Clay Minerals Society, Urbana-Champaign, USA, 2013*
- [226] Fernandes, T.; Duro, L.; Masque, P.; Delos, A.; Flinois, J. S.; Videau, G.; Schäfer, T., *Uranium retention and migration in the process waste of a conversion facility (France), Book of abstracts, 14th International Conference on the Chemistry and Migration Behaviour of Actinides and Fission Products in the Geosphere (Migration), Brighton, U.K., 2013*
- [227] Fernandes, T.; Duro, L.; Masque, P.; Schäfer, T.; Delos, A.; Flinois, J. S.; Videau, G., *Characterisation of the Waste of a Uranium Conversion Facility, Book of Abstracts, Goldschmidt, Florence, Italy, 2013*
- [228] Finck, N.; Bouby, M.; Dardenne, K.; Geckeis, H., *Tetravalent cation coprecipitation with clay minerals, Migration 2013, book of abstracts, Brighton, U.K., 2013*

- [229] Gaona, X.; Adam, C.; Rojo, H.; Böttle, M.; Kaden, P.; Altmaier, M., *Complexation of Np(IV) with gluconate in dilute to concentrated CaCl<sub>2</sub> solutions: solubility and NMR studies, Actinide and Brine Chemistry in a Salt Repository (ABC Salt III) Workshop*, Santa Fe, USA, 2013
- [230] Gaona, X.; Adam, C.; Rojo, H.; Böttle, M.; Kaden, P.; Altmaier, M., *Complexation of Np(IV) with gluconate in dilute to concentrated CaCl<sub>2</sub> solutions: solubility and NMR studies, Migration 2013*, Brighton, UK, 2013
- [231] Gaona, X.; Rojo, H.; Adam, C.; Böttle, M.; Garcia, M.; Missana, T.; Kaden, P.; Altmaier, M., *Effect of Ca in the Np(IV)-gluconate system under hyperalkaline conditions, 3rd International Workshop Mechanisms and Modelling of Waste/Cement Interactions*, Ghent, Belgium, 2013
- [232] Gaona, X.; Skrerencak-Frech, A.; Marques, M.; Fröhlich, D. R.; Rothe, J.; Dardenne, K.; Panak, P. J.; Altmaier, M., *Aquatic chemistry of actinides at elevated temperatures: solubility and spectroscopic studies at KIT-INE, Actinide and Brine Chemistry in a Salt Repository (ABC Salt III) Workshop*, Santa Fe, USA, 2013
- [233] Geist, A.; Beele, B.; Bremer, A.; Denecke, M. A.; Müllich, U.; Panak, P. J.; Rothe, J.; Ruff, C., *Actinide separation using N-donor compounds, book of abstracts, ACTINET-13 ThUL School 2013*, Karlsruhe, Germany, 2013
- [234] Geist, A.; Modolo, G.; Wilden, A.; Kaufholz, P., *Minor actinide separation: simplification of the DIAMEX-SANEX strategy by means of novel SANEX processes, Proc. Internat. Conf. GLOBAL (Nuclear Energy at a Crossroads)*, Salt Lake City, USA, 2013
- [235] González-Robles, E.; Bohnert, E.; Loida, A.; Müller, N.; Lagos, M.; Metz, V.; Kienzler, B., *Fission gas measurements and description of leaching experiments with of KIT's irradiated PWR fuel rod segment (50.4 GWd/tHM), 1st Annual Workshop Proceedings of the Collaborative Project "Fast / Instant Release of Safety Relevant Radionuclides from Spent Nuclear Fuel" (7th EC FP CP FIRST-Nuclides)*, Budapest, Hungary 2013
- [236] González-Robles, E.; Wegen, D. H.; Bohnert, E.; D., P.; Müller, N.; Nasyrow, R.; Kienzler, B.; Metz, V., *Physico-chemical characterization of a spent UO<sub>2</sub> fuel with respect to its stability under final disposal conditions, Proceedings of MRS 2013 - 37th Int'l Symposium on the Scientific Basis for Nuclear Waste Management*, Barcelona, Spain, 2013
- [237] Graser, C.-H.; Banik, N. L.; Lagos, M.; Marquardt, C. M.; Geckeis, H., *Speciation of elements relevant to nuclear waste disposal by capillary electrophoresis hyphenated to inductively coupled plasma mass spectrometer (CE-ICPMS), Book of Abstracts GDCh Tagung 2013*, Darmstadt, Germany, 2013
- [238] Griffiths, T. L.; Tucker, K. L.; Sharrad, C. A.; Martin, L. R.; Kaden, P., *Understanding molecular speciation of actinides in solvent extraction processes, Abstr Pap Am Chem S*, 2013
- [239] Guglielmetti, L.; Negro, F.; Mauri, G.; Vuataz, F.-D.; Abdelfettah, Y.; Clerc, N.; Giroud, N.; Marguet, L.; Schill, E., *GeoNE: an integrated project for the exploration of low enthalpy deep aquifers in the canton of Neuchatel, western Switzerland, Proceedings European Geothermal Congress (EGC) Pisa, Italy*, 2013
- [240] Herm, M.; Gaona, X.; Rabung, T.; Crepin, C.; Metz, V.; Altmaier, M.; Geckeis, H., *The effect of nitrate on trivalent actinide and lanthanide solubility in dilute to concentrated brine solutions, Book of Abstracts, ABC-Salt Workshop*, Santa Fe, USA, 2013
- [241] Herm, M.; Gaona, X.; Rabung, T.; Crepin, C.; Metz, V.; Altmaier, M.; Geckeis, H., *Löslichkeit und Speziation von trivalenten Actiniden in NaCl-NaNO<sub>3</sub> und MgCl<sub>2</sub>-Mg(NO<sub>3</sub>)<sub>2</sub> Lösungen unter endlagerrelevanten Bedingungen, CD of Abstracts, GDCh Wissenschaftsforum Chemie*, Darmstadt, Germany, 2013
- [242] Herm, M.; Gaona, X.; Rabung, T.; Crepin, C.; Metz, V.; Altmaier, M.; H., G., *Solubility and TRLFS study of Nd(III) and Cm(III) in dilute to concentrated alkaline NaCl-NaNO<sub>3</sub> and MgCl<sub>2</sub>-Mg(NO<sub>3</sub>)<sub>2</sub> solutions, Book of Abstracts, 14th International Conference on the Chemistry and Migration Behaviour of Actinides and Fission Products in the Geosphere (MIGRATION)*, Brighton, UK, 2013
- [243] Hinz, K.; Altmaier, M.; Gaona, X.; Rabung, T.; Schild, D.; Adam, C.; Geckeis, H., *Complexation of Nd(III)/Cm(III) with borate in dilute to concentrated alkaline NaCl, MgCl<sub>2</sub> and CaCl<sub>2</sub> solutions: solubility and TRLFS studies, Migration 2013, Book of Abstracts*, Brighton, UK 2013
- [244] Hinz, K.; Altmaier, M.; Rabung, T.; Geckeis, H., *Complexation of An(III/IV) with borate in dilute to concentrated alkaline NaCl, CaCl<sub>2</sub> and MgCl<sub>2</sub> solutions, Book of Abstracts, ABC-Salt Workshop* Santa Fe, USA, 2013

- [245] Hinz, K.; Altmaier, M.; Rabung, T.; Geckeis, H., *Boratkomplexierung drei- und vierwertiger Actiniden in alkalischen NaCl, CaCl<sub>2</sub> und MgCl<sub>2</sub> Lösungen*, CD of Abstracts, GDCh Wissenschaftsforum Chemie, Darmstadt, Germany, 2013
- [246] Huber, F.; Trinchero, P.; Molinero, J.; Schäfer, T., *RN migration in a single fracture from Äspö, Sweden: Experiments and reactive transport modelling*, CP CROCK, Final Workshop, Karlsruhe, Germany, 2013
- [247] Huber, F.; Trinchero, P.; Molinero, J.; Schäfer, T., *Np(V) Migration in a Single Fracture from Äspö, Sweden: Experiments and Reactive Transport Modelling*, 8th EC Conference on the Management of Radioactive Waste (Euradwaste), Vilnius, Lithuania, 2013
- [248] Kienzler, B.; Altmaier, M.; Bube, C.; Metz, V., *Preliminary Safety Analysis Gorleben: Source Terms for Heat-Producing Wastes*, Society, A.N. (Ed.), 14th Int. High Level Waste Management Conference, Albuquerque, USA, 2013
- [249] Kienzler, B.; Bube, C.; González-Robles, E.; Metz, V., *Modelling of boundary conditions for upscaling migration / retention processes of fission products in the spent nuclear fuel structure*, 1st Annual Workshop Proceedings of the Collaborative Project "Fast / Instant Release of Safety Relevant Radionuclides from Spent Nuclear Fuel" (7th EC FP CP FIRST-Nuclides), Budapest, Hungary 2013
- [250] Kienzler, B.; Finck, N.; Hilpp, S.; Metz, V.; Plaschke, M.; Cron, T.; Miassoedov, A., *Radionuclide retention onto heat treated concrete under sea water conditions*, Book of Abstracts, 3rd Internat. Workshop Mechanisms and Modelling of Waste/Cement Interactions, Ghent, Belgium, 2013
- [251] Kienzler, B.; González-Robles, E., *State-of-the-Art on instant release of fission products from spent nuclear fuel*, ASME 2013 15th International Conference on Environmental Remediation and Radioactive Waste Management, Brussels, Belgium, 2013
- [252] Kienzler, B.; González-Robles, E.; Metz, V.; Valls, A.; Duro, L., *FIRST-Nuclides: European Project on Radionuclide Release from Spent Fuel*, Society, A.N. (Ed.), 14th Int. High Level Waste Management Conference, Albuquerque, USA 2013
- [253] Kienzler, B.; Loida, A.; González-Robles, E.; Metz, V., *Rapid Radionuclide Release: Effect of Solution Compositions*, Proceedings of MRS 2013 - 37th Int'l Symposium on the Scientific Basis for Nuclear Waste Management, Barcelona, Spain, 2013
- [254] Kienzler, B.; Metz, V.; González-Robles, E.; Bohnert, E.; Loida, A.; Müller, N., *Recent activities on HLW and Spent Nuclear Fuel related research at KIT-INE*, Book of Abstracts, International Workshop on Actinide and Brine Chemistry in a Salt-Based Repository (ABC-Salt III), Santa Fe, USA, 2013
- [255] Kupcik, T.; Marsac, R.; Hedde, M.; Rabung, T.; Schäfer, T.; Marques, M.; Baeyens, B.; Geckeis, H., *Eu and Cm sorption onto un-purified illite: batch-type experiments and time resolved laser fluorescence spectroscopy (TRLFS)*, Book of abstracts, 14th International Conference on the Chemistry and Migration Behaviour of Actinides and Fission Products in the Geosphere (Migration), Brighton, U.K., 2013
- [256] Kutzer, A.; Vitova, T.; Kvashnina, K.; Prüßmann, T.; Rothe, J.; Soballa, E.; Adam, C.; Kaden, P.; Denecke, M. A.; Weisenburger, S.; Roth, G.; Geckeis, H., *Impact of increasing MoO<sub>3</sub> loading on incorporation properties of multi-component borosilicate glass*, Goldschmidt 2013, Florence, Italy, 2013
- [257] Lindqvist-Reis, P.; Apostolidis, C.; Walter, O.; Marsac, R.; Banik, N. L.; Skripkin, M. Y.; Rothe, J.; Morgenstern, A., *Structure and spectroscopic evidence of hexavalent neptunyl and plutonyl mono- and dintrate complexes in aqueous nitric acid*, Book of Abstracts, 9th International Conference on the Chemistry and Physics of the Actinide Elements - ACTINIDES 2013, Karlsruhe, Germany, 2013
- [258] Marsac, R.; Schnurr, A.; Kupcik, T.; Rabung, T.; Schäfer, T.; Banik, N. L.; Marquardt, C. M.; Marques-Fernandez, M.; Baeyens, B.; Bradbury, M. H.; Geckeis, H., *Aluminium competitive effect on Eu(III) sorption to illite*, Book of Abstracts Goldschmidt 2013, Florence, Italy, 2013
- [259] Martínez-Torrents, A.; González-Robles, E.; Bohnert, E.; Casas, I.; de Pablo, J.; Metz, V.,  *$\alpha$ -Radiolysis under alkaline conditions in 0.05 and 5.0 molar NaCl*, Book of Abstracts, International Workshop on Actinide and Brine Chemistry in a Salt-Based Repository (ABC-Salt III), Santa Fe, USA, 2013
- [260] Metz, V., *Overview WPI –Sample and Tools*, 1st Annual Workshop Proceedings of the Collaborative Project "Fast / Instant Release of Safety Relevant Radionuclides from Spent Nuclear Fuel" (7th EC FP CP FIRST-Nuclides), Budapest, Hungary 2013

- [261] Metz, V.; Bohnert, E.; Bube, C.; Garbev, K.; Schlieker, M.; Kienzler, B., *Interactions of americium with cement alteration products in brines, Book of Abstracts, 3rd International Workshop Mechanisms and Modelling of Waste/Cement Interactions*, Ghent, Belgium, 2013
- [262] Metz, V.; Loida, A.; González-Robles, E.; Bohnert, E.; Kienzler, B., *Characterization of irradiated PWR UO<sub>x</sub> fuel (50.4 Gwd/tHM) used for leaching experiments, 1st Annual Workshop Proceedings of the Collaborative Project "Fast / Instant Release of Safety Relevant Radionuclides from Spent Nuclear Fuel" (7th EC FP CP FIRST-Nuclides)*, Budapest, Hungary 2013
- [263] Norrfor, K.; Bouby, M.; Heck, S.; Finck, N.; Marsac, R.; Schäfer, T.; Geckeis, H.; Wold, S., *Montmorillonite Colloid Size Heterogeneity – Fractionation and Characterization, Mineralogical Magazine, Goldschmidt Conference, Florence, Italy, 2013*
- [264] Norrfor, K.; Bouby, M.; Heck, S.; Finck, N.; Marsac, R.; Schäfer, T.; Geckeis, H.; Wold, S., *Montmorillonite Colloids Size Heterogeneity-Impact on stability in suspension, Book of Abstracts, 14th International Conference on the Chemistry and Migration Behaviour of Actinides and Fission Products in the Geosphere (Migration)*, Brighton, U.K., 2013
- [265] Norrfor, K. K.; Bouby, M.; Heck, S.; Finck, N.; Marsac, R.; Schäfer, T.; Geckeis, H.; Wold, S., *Montmorillonite colloid size heterogeneity- Fractionation and characterization, Goldschmidt 2013, Mineralogical Magazine, Florence, Italy, 2013*
- [266] Petrov, V.; Gaona, X.; Fellhauer, D.; Rothe, J.; Dardenne K.; Kalmykov, S.; Altmaier, M., *Np(V) solubility in dilute to concentrated MgCl<sub>2</sub> solutions, Migration 2013*, Brighton, UK, 2013
- [267] Prüßmann, T.; Denecke, M. A.; Geist, A.; Rothe, J.; Lindqvist-Reis, P.; Banik, N. L.; Schimmelpfennig, B.; Fellhauer, D.; Apostolidis, C.; Walter, O.; Batchelor, D. R.; Nagel, P.; Schuppler, S.; Kvashnina, K.; Jorissen, K.; Kas, J. J.; Rehr, J. J.; Vitova, T., *Structural investigation of N donor ligand-Ln/An complexes from the metal and ligand point of view, CD of Abstracts, GDCh Wissenschaftsforum Chemie, Darmstadt, Germany, 2013*
- [268] Rojo, H.; Gaona, X.; Rabung, T.; Garcia, M.; Missana, T.; Altmaier, M., *Complexation of Nd(III)/Cm(III) with gluconate in dilute NaCl and CaCl<sub>2</sub> alkaline solutions: solubility and TRLFS studies, 3rd International Workshop Mechanisms and Modelling of Waste/Cement Interactions Ghent, Belgium, 2013*
- [269] Rojo, H.; Gaona, X.; Rabung, T.; Garcia, M.; Missana, T.; Altmaier, M., *Complexation of Nd(III)/Cm(III) with gluconate in alkaline NaCl and CaCl<sub>2</sub> solutions: solubility and TRLFS studies, Migration 2013, book of abstracts, Brighton, UK, 2013*
- [270] Rothe, J.; Dardenne, K.; Fellhauer, D.; Gaona, X.; Altmaier, M.; Fanghänel, T., *XAFS and solubility investigations of penta- and hexavalent actinides in dilute to concentrated salt brines, Abstracts of the 9th International Conference on the Chemistry and Physics of the Actinide Elements - ACTINIDES 2013*, Karlsruhe, Germany, 2013
- [271] Schäfer, T.; Blechschmidt, I.; Bouby, M.; Büchner, S.; Brendlé, J.; Darbha, G.; Geckeis, H.; Kupcik, T.; Götz, R.; Hauser, W.; Heck, S.; Huber, F.; Lagos, M.; Martin, A., *The latest results on colloid associated radionuclide mobility from the CFM project, Grimsel (Switzerland), Book of abstracts, 14th International Conference on the Chemistry and Migration Behaviour of Actinides and Fission Products in the Geosphere (Migration)*, 2013
- [272] Schäfer, T.; Blechschmidt, I.; Bouby, M.; Büchner, S.; Brendlé, J.; Darbha, G.; Geckeis, H.; Kupcik, T.; Götz, R.; Hauser, W.; Heck, S.; Huber, F.; Lagos, M.; Martin, A., *The latest results on colloid associated radionuclide mobility from the CFM project, Grimsel (Switzerland), Book of abstracts, AGU Fall meeting*, 2013
- [273] Schoepff, V.; Alamsi, I.; Amgarou, K.; Becker, F.; Carrel, F.; Carvajal, F.; Gaboriau, D. C.; Gmar, M.; Kovacs, A.; Lemaire, H.; Mena, N.; Morat, L.; Morrison, C. G.; Perez-Ilopis, I.; Raskob, W.; Szabo, S.; Szeles, E.; Testard, I.; Trybushnyi, D.; Ugolin, N.; Viau, M.; Vincze, A., *BOOSTER: Development of a Toolbox for Triage of a Large Group of Individuals Exposed to Radioactive Material, proceedings of International conference on Advancements in Nuclear Instrumentation Measurement Methods and their Applications (ANIMMA)*, Marseille, France, 2013
- [274] Serrano-Purroy, D.; Aldave de las Heras, L.; Glatz, J.-P.; Benes, O.; Colle, J.-Y.; Sureda, R.; González-Robles, E.; de Pablo, J.; Casas, I.; Barrachin, M.; Dubourg, R.; Martínez-Esparza, A., *Interpretation of Knudsen Cell Experiments to determine the Instant Release Fraction in Spent fuel Corrosion Scenarios by using a mechanistic approach: the Caesium Case, Proceedings of MRS 2013 - 37th Int'l Symposium on the Scientific Basis for Nuclear Waste Management*, Barcelona, Spain, 2013

- [275] Skripkin, M.; Lindqvist-Reis, P.; Apostolidis, C.; Klenze, R.; Mink, J., *Vibrational spectroscopic study of some rare-earth metals trifluoromethylsulfonates enneahydrates and of corresponding salts of U(III) and Cm(III)*, *Book of Abstracts, ACTINIDES* Karlsruhe, Germany, 2013
- [276] Temgoua, L.; Chagneau, A.; Geckeis, H.; Schäfer, T., *Effect of solution supersaturation and presence/absence of seeding crystals on the precipitation kinetics of celestite and strontianite*, *Book of Abstracts, Goldschmidt*, Florence, Italy, 2013
- [277] Totksiy, Y.; Huber, F.; Schäfer, T.; Geckeis, H., *Tc(VII) immobilization on granotoid rocks from Äspö (Sweden)*, *Book of abstracts, 14th International Conference on the Chemistry and Migration Behaviour of Actinides and Fission Products in the Geosphere (Migration)*, Brighton, U.K., 2013
- [278] Valls, A.; Riba, O.; Duro, L.; González-Robles, E.; Kienzler, B.; Metz, V., *Previous investigations on the instant release fraction and general description of the project, 1st Annual Workshop Proceedings of the Collaborative Project "Fast / Instant Release of Safety Relevant Radionuclides from Spent Nuclear Fuel" (7th EC FP CP FIRST-Nuclides)*, Budapest, Hungary 2013
- [279] van Laer, L.; Kupcik, T.; Bruggeman, C.; Maes, N.; Schäfer, T., *Sorption and diffusion of Zn onto Na-illite under a wide variety of conditions*, *Book of abstracts, 14th International Conference on the Chemistry and Migration Behaviour of Actinides and Fission Products in the Geosphere (Migration)*, Brighton, U.K., 2013
- [280] Vitova, T., *Structural investigations of actinides with advanced X-ray spectroscopy techniques*, *Abstracts of the 9th International Conference on the Chemistry and Physics of the Actinide Elements - ACTINIDES 2013*, Karlsruhe, Germany, 2013
- [281] Wiedemann, M.; Metz, V.; Rabung, T.; Geckeis, H., *Retention of Cm(III) and Eu(III) on Stable Solid Phases in the System Mg-Na-Cl-H<sub>2</sub>O at Room Temperature*, *Book of Abstracts, International Workshop on Actinide and Brine Chemistry in a Salt-Based Repository (ABC-Salt III)*, Santa Fe, USA, 2013
- [282] Wiedemann, M.; Metz, V.; Rabung, T.; Geckeis, H., *Rückhaltung von trivalenten Curium und Europium an Mg(OH)<sub>2</sub>-haltigen Feststoffen im System Mg<sup>2+</sup>-Na<sup>+</sup>-OH-Cl-H<sub>2</sub>O*, *Kurzreferatband Nuklearchemie, Gesellschaft Deutscher Chemiker Jahrestagung*, Darmstadt, Germany, 2013
- [283] Wilden, A.; Modolo, G.; Lange, S.; Sadowski, F.; Beele, B. B.; Skerencak-Frech, A.; Panak, P. J.; Iqbal, M.; Verboom, W.; Geist, A.; Bosbach, D., *Modified Diglycolamides for Actinide Separation: Solvent Extraction and Time-Resolved Laser Fluorescence Spectroscopy Complexation Studies*, *Proceedings Global*, Salt Lake City, USA, 2013

#### **Posters:**

- [284] Adam, C.; Kaden, P.; Geist, A.; Panak, P. J.; Denecke, M. A., *Unexpected Paramagnetic Effects in NMR Spectra of Am(n-Pr-BTP)<sup>33+</sup> Complexes Reveal Covalent Bonding*, *ThUL Spring School 2013*, Karlsruhe, Germany, 2013
- [285] Banik, N. L.; Marquardt, C. M.; Altmaier, M.; Walther, C.; Rothe, J.; Denecke, M. A.; Schimmelpfennig, B.; Real, F.; Vallet, V., *Preparation, stabilization, spectroscopic, computational studies of tetravalent protactinium in aqueous solution*, *Actinides 2013*, Karlsruhe, Germany, 2013
- [286] Beele, B. B.; Wilden, A.; Skerencak-Frech, A.; Lange, S.; Sadowski, F.; Modolo, G.; Geist, A.; Panak, P. J., *TRLFS Study on the Complexation of Cm(III) and Eu(III) with methyl-substituted Diglycolamides*, *Actinides 2013*, Karlsruhe, Germany, 2013
- [287] Bots, P.; Shaw, S.; Law, G. T. W.; Marshall, T.; Mosselmans, J. F. W.; Livens, F. R.; Denecke, M. A.; Rothe, J.; Dardenne, K.; Morris, K., *The BIGRAD consortium - the influence of iron oxide crystallization on the mobility of neptunium*, *Migration*, Brighton, UK, 2013
- [288] Bremer, A.; Geist, A.; Panak, P. J., *Influence of the solvent on the complexation of Cm(III) with nPr-BTP studied by time-resolved laser fluorescence spectroscopy*, *ACTINIDES 2013*, Karlsruhe, Germany, 2013
- [289] Dardenne, K.; Rothe, J.; Fernandes, T.; Schild, D.; Soballa, E.; Bube, C.; Kienzler, B.; Denecke, M. A.; Geckeis, H.,  *$\mu$ -focus capabilities at the INE-Beamline for actinide science at ANKA*, *Actinides 2013*, Karlsruhe, Germany, 2013

- [290] Dardenne, K.; Rothe, J.; Fernandes, T.; Schild, D.; Soballa, E.; Bube, C.; Kienzler, B.; Denecke, M. A.; Geckeis, H.,  *$\mu$ -focus capabilities at the INE-Beamline for actinide science at ANKA*, ANKA User Meeting, Karlsruhe, Germany, 2013
- [291] Dardenne, K.; Rothe, J.; Fernandez, T.; Schild, D.; Soballa, E.; Metz, V.; Bube, C.; Kienzler, B.; Denecke, M. A.; Geckeis, H.,  *$\mu$ -focus capabilities at the INE-Beamline for actinide science at ANKA*, ANKA User Meeting 2013, Bruchsals, Germany, 2013
- [292] Quinto, F.; Hrncsek, E.; Krachler, M.; Shoty, W.; Steier, P.; Winkler, S. R., *Determination of U and Pu isotopes in an ombrotrophic peat core and implications for post-depositional migration of fallout radionuclides*, The 29th International conference for the Society for Environmental Geochemistry and Health, Toulouse, France, 2013
- [293] Quinto, F.; Hrncsek, E.; Krachler, M.; Shoty, W.; Steier, P.; Winkler, S. R., *Analysis of actinides in an ombrotrophic peat core - evidence of post-depositional migration of fallout radionuclides*, European Geosciences Union General Assembly 2013, Vienna, Austria, 2013
- [294] Fröhlich, D. R.; Skerencak-Frech, A.; Panak, P. J., *Spektroskopische Untersuchungen zur Komplexbildung von Am(III)/Cm(III) mit einfachen organischen Liganden bei erhöhten Temperaturen*, Wissenschaftsforum Chemie, Darmstadt, Germany, 2013
- [295] Gaona, X.; Adam, C.; Rojo, H.; Böttle, M.; Kaden, P.; Altmaier, M., *Complexation of Np(IV) with gluconate in dilute to concentrated CaCl<sub>2</sub> solutions: solubility and NMR studies*, 3rd US-German workshop on actinide and brine chemistry in a salt repository (ABC Salt III), Santa Fe, USA, 2013
- [296] González-Robles, E.; Bohnert, E.; Müller, N.; Herm, M.; Metz, V.; Kienzler, B., *Determination of the fission gas release in the segment N0204 and gas phase results of anoxic leaching experiment*, 2nd Annual Workshop of the FIRST-Nuclide Project, Antwerpen, Belgium, 2013
- [297] González-Robles, E.; Wegen, D. H.; Papaioannou, D.; Kienzler, B.; Nasyrow, R.; Metz, V., *Physical characterisation of spent nuclear fuel: First steps to further Instant Release Fractions investigations*, 8th EC Conference on the Management of Radioactive Waste Community Policy and Research on Disposal, Vilnius, Lithuania, 2013
- [298] Graser, C.-H.; Banik, N. L.; Lagos, M.; Marquardt, C. M.; Geckeis, H., *Speciation of elements relevant to nuclear waste disposal by capillary electrophoresis hyphenated to inductively coupled plasma mass spectrometer (CE-ICPMS)*, GDCH Tagung 2013, Darmstadt, Germany 2013
- [299] Griffiths, T. L.; Tucker, K. L.; Sharrad, C. A.; Livens, F.; Martin, L. R.; Sarsfield, M. R.; Kaden, P., *Understanding molecular speciation of actinides in the PUREX process*, ACTINIDES 2013 Conference, Karlsruhe, Germany, 2013
- [300] Huber, F.; Trincherio, P.; Molinero, J.; Schäfer, T., *Np(V) Migration in a Single Fracture from Äspö, Sweden: Experiments and Reactive Transport Modelling*, Euradwaste'13, 8th EC Conference on the Management of Radioactive Waste, Vilnius, Lithuania, 2013
- [301] Kaden, P.; Adam, C.; Beele, B.; Müllich, U.; Trumm, S.; Geist, A.; Panak, P. J.; Denecke, M. A., *Evidence for covalence in a N-donor complex of americium(III)*, ACTINIDES 2013 Conference, Karlsruhe, Germany, 2013
- [302] Kaden, P.; Adam, C.; Gaona, X.; Lützenkirchen, J.; Metz, V.; Bauer, A.; Löble, M.; Kutzer, A., *Multinuclear NMR Investigations at KIT-INE*, Euract-NMR Workshop, Karlsruhe, Germany, 2013
- [303] Kienzler, B.; Metz, V.; González-Robles, E.; Duro, L.; Valls, A.; Wegen, D. H.; Carbol, P.; Curtius, H.; Günther-Leopold, I.; Curti, E.; Froideval-Zumbiehl, A.; Lemmens, K.; Vandenborre, J.; De Pablo, J.; Clarens, F.; Hózer, Z.; Roth, O., *CP FIRST-Nuclides: "Fast / Instant Release of Safety Relevant Radionuclides from Spent Nuclear Fuel"*, 8th EC Conference on the Management of Radioactive Waste Community Policy and Research on Disposal, Vilnius, Lithuania, 2013
- [304] Kupcik, T.; Marsac, R.; Finck, N.; Rabung, T.; Schäfer, T.; Marques Fernandes, M.; Baeyens, B.; Geckeis, H., *Eu and Cm sorption onto unpurified illite. Batch-type experiments and time resolved laser fluorescence spectroscopy (TRLFS)*, Migration 2013 Brighton, UK, 2013
- [305] Law, G. T. W.; Thorpe, C. L.; Bots, P.; Shaw, S.; Law, K.; Marshall, T.; Livens, F. R.; Lloyd, J. R.; Denecke, M. A.; Rothe, J.; Dardenne, K.; Morris, K., *The Bigrad Consortium - Neptunium biogeochemical interactions with the manganese cycle*, Migration, Brighton, UK, 2013

- [306] Norrfors, K. K.; Bouby, M.; Heck, S.; Finck, N.; Marsac, R.; Schäfer, T.; Geckeis, H.; Wold, S., *Montmorillonite colloid size heterogeneity: Impact on radionuclide sorption capacities*, Migration 2013, Brighton, UK, 2013
- [307] Norrfors, K. K.; Bouby, M.; Heck, S.; Finck, N.; Marsac, R.; Schäfer, T.; Geckeis, H.; Wold, S., *Montmorillonite colloid size heterogeneity: Impact on stability in suspension*, Migration 2013 Brighton, UK, 2013
- [308] Petrov, V. G.; Gaona, X.; Fellhauer, D.; Rothe, J.; Dardenne, K.; Kalmykov, S. N.; Altmaier, M., *Np(V) Solubility in dilute to concentrated MgCl<sub>2</sub> solutions* Migration, Brighton, UK, 2013
- [309] Polly, R.; Heberling, F.; Schimmelpfennig, B.; Geckeis, H., *Quantum chemical investigation of the sorption of selenite on the calcite (104) surface and incorporation into the bulk*, STC 2013, Erlangen, Germany, 2013
- [310] Rabung, T.; Garcia, D.; Molinero, J., *CROCK: crystalline rock retention processes – a 7th framework programme collaborative project (2011-2013)*, Migration, Brighton, UK, 2013
- [311] Schimmelpfennig, B.; Trumm, M.; Réal, F.; Vallet, V.; Masella, M., *Investigating the hydration of Ln(III) and An(III) ions by quantum chemistry and molecular dynamics*, STC 2013, Erlangen, Germany, 2013
- [312] Schnurr, A.; Marsac, R.; Rabung, T.; Lützenkirchen, J.; Geckeis, H., *Investigations of actinide and lanthanide sorption on clay minerals under saline conditions*, Migration, Brighton, UK, 2013
- [313] Schnurr, A.; Rabung, T.; Lützenkirchen, J.; Geckeis, H., *Sorptionsuntersuchungen von dreiwertigen Actiniden an Tonmineralien in hochsalinaren Systemen*, GDCh Wissenschaftsforum Chemie, Darmstadt, Germany, 2013
- [314] Skerencak-Frech, A.; Fröhlich, D. R.; Panak, P. J., *The thermodynamics of the complexation of Cm(III) with small organic ligands under saline conditions and increased temperatures*, Migration 2013, Brighton, UK, 2013
- [315] Thien, B.; Heberling, F.; Kulik, D., *Modeling Non-Equilibrium Uptake of Se(IV) Upon Calcite Precipitation*, Goldschmidt Conference 2013, Florence, Italy, 2013
- [316] Trumm, M.; Trumm, S.; Schimmelpfennig, B.; Masella, M., *Quantum chemical and molecular dynamics study of aqueous Ln(III) / An(III) solutions interacting with BTP-based ligands*, STC 2013, Erlangen, Germany, 2013
- [317] Tucker, K.; Griffiths, T.; Sharrad, C.; Heath, S.; Kaden, P., *Actinide extraction using advanced PUREX style ligands in mixed acid systems*, Gobaal 2013 Conference, Salt Lake City, USA, 2013
- [318] Tucker, K. L.; Griffiths, T. L.; Sharrad, C. A.; Heath, S. L.; Kaden, P.; Taylor, R., *Heavy Metal extraction using advanced PUREX style partitioning systems*, ACTINIDES 2013 Conference, Karlsruhe, Germany, 2013

